NSWCDD/TR-93/91

IMPROVED AEROPREDICTION CODE: PART I–SUMMARY OF NEW METHODS AND COMPARISON WITH EXPERIMENT

BY FRANK G. MOORE THOMAS C. HYMER ROY M. MCINVILLE
WEAPONS SYSTEMS DEPARTMENT

MAY 1993

Approved for public release, distribution is unlimited.

NAVAL SURFACE WARFARE CENTER
DAHLGREN DIVISION
Dahlgren, Virginia 22448-5000

Transition of the 1993 Version of the Aeroprediction Code (AP93)

The AP93 code has recently been completed and is now available for transition to requesting users. Users of the 1981 version of the code included approximately 60 DOD contractors, DOD or other government agencies, universities and several foreign countries. A small charge was incurred by the requester to alleviate administrative costs of the transition. In an effort to promote dual use technology between government and industry, transition of the AP93 will be done free of charge to requesting users. This includes either a 9 track tape or disk along with a users guide. For DOD contractors or other government agencies, the attached form must be filled out completely and signed by appropriate authorities. For foreign countries or companies owned by foreign countries, the request must go from the foreign embassy to the U.S. Embassy for approval since the code is for limited distribution. The U.S. Embassy will then forward the request to the Office of Naval Technology for implementation at NSWCDD. Since we are sending out a copy of the new code free of charge, we will not be able to provide the level of consulting that we would like to. However, we do request several things from the users. First, if you find an error in the code, we would appreciate you bringing it to either my attention at (703) 663-8141, to Mr. Tom Hymer at (703) 663-4164, or to Dr. Roy McInville at (703) 663-4760. Secondly, if you find areas of success or areas of weakness, we would appreciate hearing from you. We use information such as this to help guide any future modifications. Thirdly, if you find areas where additional code capability would be desirable, again we would like to hear from you. In all cases, a written letter is preferred but a phone call is better than no communication at all. Also, if you use the code for the purpose of comparing the results to other computations within the external literature, we would like you to use the terminology AP93. If you modify the AP93 to suit your own needs you could refer to the code as modified AP93. Finally, we request that you not send any copies of the code to other agencies or even other activities in your company if it is at a different location. Please refer them to us so that we can keep track of copies of the code.

DR. FRANK MOORE
Dahlgren Division
Naval Surface Warfare Center
Dahlgren, VA 22448

AP93 Transition Request

NAME: _____

COMPANY NAME: _____

ADDRESS: _____

_____

_____

PHONE NUMBER: _____

GOVT CONTRACT NUMBER: _____

MEANS OF TRANSITION: 9 Track Tape ___ 5.25" Diskette ___
3.5" Diskette ___ E-Mail ___

Please supply E-Mail address if
E-Mail is desired_____

We agree to not give a copy of the AP93 to any other agency. We will refer them to NSWCDD at the address below for a copy.

Your Signature _____

Supervisor Signature _____

Please send this form completely filled out to:

Commander
Attn Dr. Frank Moore (G04)
Dahlgren Division
Naval Surface Warfare Center
Dahlgren, VA 22448

We will try to get you a copy of the AP93 along with a users guide within a month.

NSWCDD/TR-93/91

IMPROVED AEROPREDICTION CODE: PART I–SUMMARY OF NEW METHODS AND COMPARISON WITH EXPERIMENT

BY FRANK G. MOORE THOMAS C. HYMER ROY M. MCINVILLE
WEAPONS SYSTEMS DEPARTMENT

MAY 1993

NAVAL SURFACE WARFARE CENTER
DAHLGREN DIVISION
Dahlgren, Virginia 22448-5000

FOREWORD

The effort described in this report is the culmination of a three-and-half-year effort to upgrade the Naval Surface Warfare Center, Dahlgren Division (NSWCDD) aeroprediction code (AP93) to meet the needs that have arisen over the past 10 years. These needs included high Mach numbers, accurate nonlinear aerodynamics for low-aspect ratio missile configurations, and improved base-drag prediction. This report summarizes all the new technology developed and shows example comparisons of the new AP93 code to the former 1981 version. A user's guide and program listing will be included in Part II of this report, which will have a more limited distribution.

Other personnel who participated in this effort are Fred DeJarnette of North Carolina State University, Frank Baltakis of Advanced Technology Associates, Floyd Wilcox of the National Aeronautics and Space Administration/Langley Research Center, and Mike Armistead , Steve Rowles, and Leroy Devan from NSWCDD. Appreciation is expressed to each of these individuals for their roles, which have been documented in previous technical reports.

The work described in this report was supported through the Office of Naval Research (Dave Siegel) and, more specifically, the Surface-Launched Weapons Technology Block Program managed at NSWCDD by Robin Staton. The authors express their appreciation to these individuals for their support in this work.

Approved by:

David Malyevac

DAVID S. MALYEVAC, Deputy Department Head
Weapons Systems Department

ABSTRACT

A new and improved version of the Naval Surface Warfare Center, Dahlgren Division aeroprediction code (AP93) has been developed. The new code contains new technology that allows planar aerodynamics of axisymmetric solid rocket-type weapons to be computed with engineering accuracy over the entire Mach number range and for angles of attack to 30 deg. New technology developed and included in the AP93 includes

- A new engineering method to compute aeroheating information at a high Mach number
- Extension of the second-order shock-expansion theory to include real-gas effects, including several new pressure prediction techniques
- An improved body-alone nonlinear normal-force method
- New methods for computing nonlinear aerodynamics of wing alone, wing body, and body wing due to angle of attack, and wing body due to control deflection
- A new base-drag database and improved empirical base-drag estimation technique

Comparison of the AP93 code to the former aeroprediction code (AP81) and experimental data on many configurations and test conditions showed the following:

- The AP93 code reduces the normal-force and center-of-pressure errors of the AP81 code considerably for most configurations.
- The AP93 code is more robust in terms of accuracy over a broad range of Mach numbers, angles of attack, and configuration geometries.
- The AP93 code gave slightly improved axial-force coefficients on average.
- Computational time and ease of use were about the same.

Comparison of the AP93 code to available computations of other state-of-the-art codes shows the AP93 to be as good or superior to these codes for planar aerodynamics.

The new code and associated technology will be available for transition to legitimate requesting users by September 1993 at no charge to the user.

CONTENTS

ILLUSTRATIONS

ILLUSTRATIONS (CONTINUED)

ILLUSTRATIONS (CONTINUED)

ILLUSTRATIONS (CONTINUED)

TABLES

1.0 INTRODUCTION AND BACKGROUND

For the past 20 years, the Naval Surface Warfare Center, Dahlgren Division (NSWCDD) has been involved in developing codes to calculate aerodynamics on tactical weapons. These codes have attempted to meet the changing needs of the Tactical Weapons Community and keep pace with aerodynamic requirements. A recent effort[1] was undertaken to look at where we have been, where we are, and where we need to go in the future with respect to aerodynamic codes. One of the primary needs identified in Reference 1 was an upgrade of the NSWCDD aeroprediction code (APC) to allow Mach numbers up to 20 (including the effects of real gases), improved lift prediction with particular emphasis on low-aspect ratio lifting surfaces, and improved base-drag prediction. All three of these efforts were undertaken and have now been completed. In addition, other minor modifications to the 1981 version of the APC have been made, including options for boundary layer transition and generating aerodynamic heat transfer coefficients. This report serves as a summary theoretical document of the new APC; i.e., aeroprediction 1993 (AP93). The new technology developed will be summarized, and the technology available in the 1981 version of the APC; i.e., aeroprediction 1981 (AP81), that remains in the AP93 will also be discussed. Finally, a new technology, a new nonlinear wing-body interference factor for control deflections, until now not documented, will be discussed in more detail. In addition, some other minor modifications to the new nonlinear theory will be introduced.

The four former versions of APC were documented[2-8] and transitioned to users in 1972, 1974, 1977, and 1981. Each of these versions attempted to meet the requirements as seen by the tactical weapons community. The first version[2] was for general-shaped bodies alone. It was the first such code known that combined a good mix of accuracy in aerodynamic computations, ease of use and computational time. It is believed that this mix led to the code's initial popularity and requests for additional capability. In 1974,[3,4] the code was extended to allow up to two sets of lifting surfaces in the computational process. In 1977,[5,6] dynamic aerodynamic derivatives were added to the code's capability. Finally, the last version of the code[7,8] extended the Mach number range up to eight and added high angle-of-attack capability for a narrow range of configurations.

Over the past 10 years, the AP81 has been used to compile aerodynamics on configurations at conditions where the accuracy is not good. This includes angles of attack greater than about 15 deg on missiles with two sets of lifting surfaces and Mach numbers greater than eight where real-gas effects become important in the aerothermal environment. Furthermore, the base-drag estimation, while including

angle of attack and first-order fin effects, needed additional wind tunnel data for more accurate computations. As a result of these known shortcomings, a desire to still use the APC and the fact that there is no accurate engineering code available to accomplish the objectives of angle of attack, Mach number, and base-drag prediction capability, an effort was begun in 1990 to extend the APC to meet these requirements.

The extension of the code to hypersonic Mach numbers, including real-gas effects, was completed and documented.[9,10] In the development of this new technology, three new pressure prediction methods were derived along with a method for accurately estimating inviscid surface temperatures. The inviscid surface temperatures were then used to develop an engineering method for boundary layer heating.[11] The new method thus provides engineering estimates of adiabatic wall temperature and heat transfer coefficients for configurations flying at hypersonic Mach numbers and at angle of attack.

New methods for nonlinear wing-alone, wing-body, and body-wing normal force were recently developed.[12,13] In addition, an improved body-alone nonlinear normal force prediction capability was developed. Improved center-of-pressure estimates were added that gave improved pitching moments. The code's angle-of-attack range is now 0 to 30 deg in the planar or ($\phi = 0$) roll position.

Wind tunnel tests were conducted to measure base pressure as a function of Mach number, angle of attack, fin thickness, fin location, and fin deflection. Using this data, an improved empirical base-drag prediction methodology has been developed.[14,15]

A new nonlinear method for wing-body interference due to control deflection has recently been developed. This new technology, along with options for skin friction drag computation, will be discussed in this report.

Thus, a summary of the new technology developed, a review of the technology used in the AP81 that will remain in AP93, along with results and discussion on several missile configurations will be given in this report. Where results of other state-of-the-art aerodynamics codes are available, these results will also be presented for comparison purposes. The second volume of this report, which has a limited distribution statement, contains the computer code listing, along with guidelines on how to use the code.

2.0 SUMMARY OF NEW METHODS IN AP93

2.1 HYPERSONIC MACH NUMBER METHODOLOGY

The hypersonic Mach number methodology, which in the AP93 is taken to be $M_\infty \geq 6$, is based on the use of the second-order shock-expansion theory (SOSET) with inclusion of real-gas effects. The details of the new technology are reported in Reference 9 and summarized in Reference 10. An even briefer summary follows.

SOSET defines the pressure at any point on a pointed body of revolution as

$$p = p_c - (p_c - p_2)e^{-\eta} \tag{1}$$

where η is an exponential decay term given by

$$\eta = \frac{\left(\frac{\partial p}{\partial s}\right)_2 (s - s_2)}{p_c - p_2} \tag{2}$$

Refer to Figure 1 for the nomenclature.

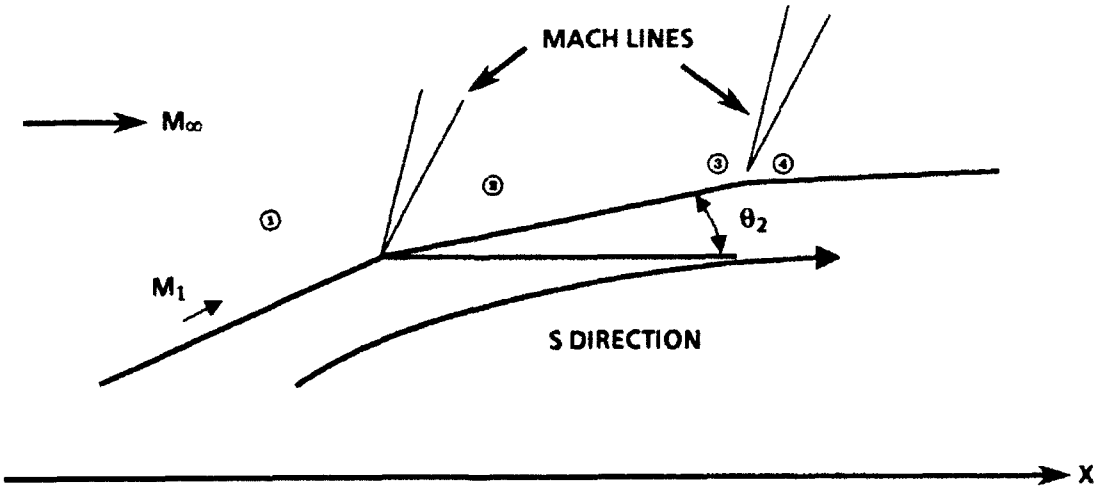

FIGURE 1. FLOW ABOUT A FRUSTUM ELEMENT

Here η is positive. If conditions are such that η becomes negative, then Equation 1 does not satisfy the boundary conditions of $p = p_c$ as $s \rightarrow \infty$ and therefore η must be defined by an equation different from Equation 2. A value of $\eta = 0$ causes the SOSET to revert back to the generalized shock-expansion theory (GSET); a value of η between $\eta = 0$ and $\eta = \infty$ allows a blend of these two theories. To extend SOSET to real gases requires several things: (1) a cone solution for real gases (p_c); (2) a Prandtl-Meyer Expansion (PME) for real gases (p_2); (3) a derivation of a new pressure derivative $(\partial p/\partial s)_2$, where the perfect-gas assumption has not been made; and (4) a way to compute temperature given values of pressure. After the real-gas pressure derivative $(\partial p/\partial s)_2$ was derived and checked, it was found that $(\partial p/\partial s)_2$ became negative for many cases causing one to choose between the GSET ($\eta = 0$) and the tangent cone theory ($\eta = \infty$). In comparisons of the pressure prediction to full Euler computations, it was found that a better way to implement the shock expansion theory for $M \geq 6$ was to redefine Equation 1 as

$$p = p_c - (p_c - p_2)\,\eta_1 \tag{3}$$

with η_1 being an input parameter chosen by the user. It was found that a value of $\eta_1 = 0$ gave slightly better pressure predictions for slightly blunt configurations, whereas a value of $\eta_1 = 1$ gave better accuracy where bluntness was large. The final implementation of SOSET in AP93 is thus Equation 3 allowing η_1 as an input, p_c is the real-gas tanget cone pressure, and p_2 is the real-gas value of pressure computed from a Prandtl-Meyer expansion.

To compute inviscid temperatures (and other properties) along the surface of a pointed or blunt body, use is made of the constancy of entropy along the surface for perfect, frozen, or equilibrium chemically reacting flows. Knowing the value of entropy and pressure from the pointed cone solution of Reference 16 or the normal shock solution of Reference 17 for a blunt body, one can then use the thermofit equations of References 18 and 19 to determine other properties; i.e.,

$$T = T(p,S) \tag{4a}$$

$$\rho = \rho(p,S) \tag{4b}$$

$$a = a(p,S) \tag{4c}$$

$$e = e(p,S) \tag{4d}$$

The remaining properties at the body surface can be found from standard thermodynamic relationships; i.e.,

$$h = e + p/\rho \tag{5a}$$

$$H_o = \left(\frac{\gamma_r R}{\gamma_r - 1}\right) T_{0_r} = \text{constant} \tag{5b}$$

$$V = \sqrt{2(H_o - h)} \tag{5c}$$

$$M = V / a \tag{5d}$$

$$\gamma = \frac{a^2 \rho}{p} \tag{5e}$$

$$Z = \frac{p}{\rho RT} \tag{5f}$$

In the process of computing surface properties, three new pressure prediction methods were derived. The first of these was to give an improved pressure coefficient prediction on the blunt nose of a missile configuration over that provided by the modified Newtonian theory (MNT). If the pressure coefficient of MNT is defined as

$$\left(C_p\right)_{MNT} = C_{p_o} \sin^2 \delta_{eq} \tag{6}$$

then the new pressure on the blunt nose part of a missile is given by

$$C_p = \left(C_p\right)_{MNT} - \Delta C_p \tag{7}$$

ΔC_p of Equation 7 is defined by

$$\Delta C_p = k \cos^m(\delta\, eq) \left[\cos \delta\, eq - \cos(\delta\, eq)_m\right] \tag{8}$$

where $(\delta\, eq)_m = 25.95$ deg, $m = 2.78$, and

$$k = 2.416 C_{p_o} + 4.606 \left[0.1507\, C_{p_o}^2 + \frac{1.124}{M_\infty^2} C_{p_o}\right]^{1/2}$$

Figure 2 shows the results of the improved modified Newtonian theory (IMNT) of Equations 7 and 8, compared to Equation 6 alone and a full numerical solution of the Euler equations[20] for a hemispherical forebody at $M_\infty = 10$. The IMNT gives up to 7-percent improvement in pressure compared to the MNT. Even past the match point ($\delta\, eq < 25.95$ deg), the IMNT gives good agreement with the numerical solution down to δeq values of 10 deg. This level of accuracy in pressure prediction will also translate into more accurate drag computations, particularly on bodies with large bluntness.

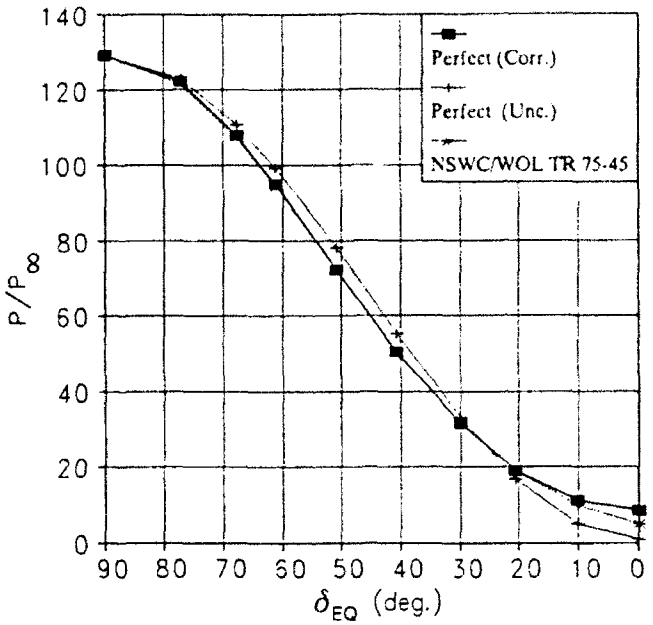

FIGURE 2. SURFACE PRESSURE DISTRIBUTION OVER A HEMISPHERICAL FOREBODY AT $M_\infty = 10$

The other two pressure prediction formulas have to do with calculating the pressure on a point behind the blunt nose portion of the body but at an angle of attack. These are

$$C_p(\alpha,\phi) = C_{p_{\alpha=0}} - (2\alpha)\sin(2\theta)\cos(\phi) + (F\cos^2\theta)\alpha^2 + (4/3\sin(2\theta)\cos(\phi))\alpha^3 \quad (9)$$

where

$$F = \left(2 - \frac{1}{\beta}\right)(1 - \tan^2\theta_c) - \left(2 + \frac{2}{\beta}\right)\sin^2\phi$$

and

$$C_p(\alpha,\phi) = C_{p_{\alpha=0}} - \frac{(2\alpha)\sin(2\theta)\cos(\phi)}{3} \quad (10)$$

Equation 9 is used for pointed body configurations, as well as for blunt body configurations in the windward plane area ($60° < \phi \leq 180°$). Equation 10 is used in the leeward plane ($\phi \leq 60°$) for configurations with blunt noses. In Equation 9, $(C_p)_{\alpha=0}$ is the pressure coefficient at $\alpha = 0$, which comes from Equation 3. Figure 3 is an example of the application of Equation 9 to a cone along with the associated inviscid surface temperatures. The approximate results are close to the exact cone solution of Reference 21.

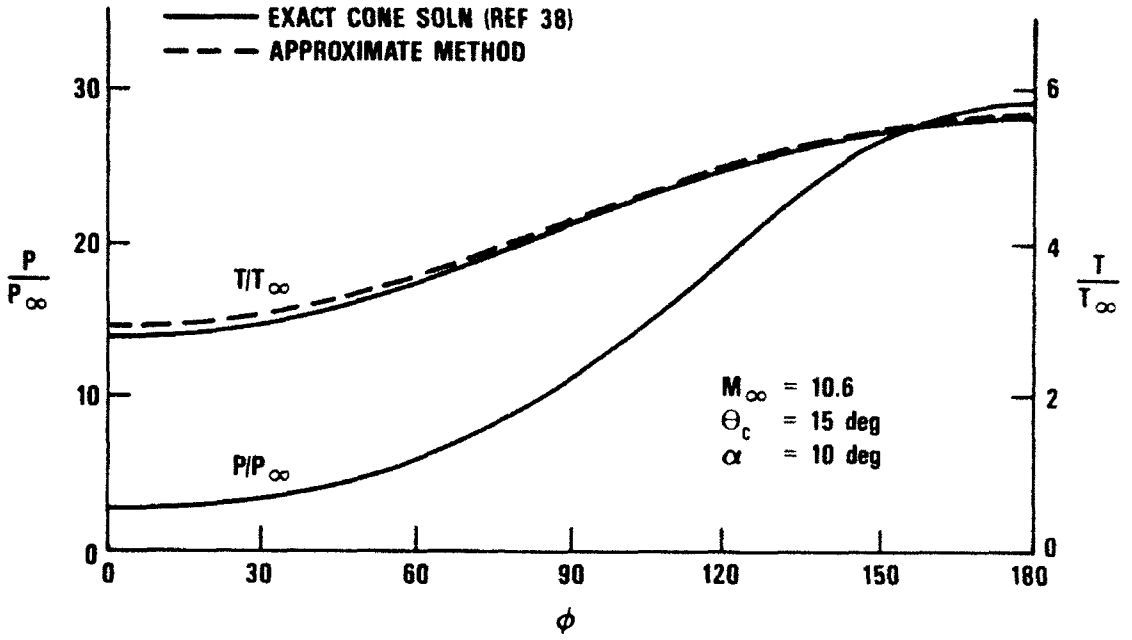

FIGURE 3. PERFECT-GAS COMPARISON OF EXACT AND APPROXIMATE CONE SOLUTIONS

Figure 4 presents the comparison of the present methodology for predicting inviscid surface temperatures on a 20-percent blunt cone at $\alpha = 10$ deg and $M_\infty = 15$. These results are compared to a full numerical solution of the Euler equations (ZEUS)[22] for both perfect and real gases. The real-gas temperatures are substantially lower than the perfect-gas results and also agree with the full Euler solution except in the vicinity of the overexpansion region past the blunt tip. Figure 4 uses most of the theory developed for the approximate methodology in Equations 3 through 10, along with the assumptions used in computing temperature.

2.2 AEROHEATING

The AP93 output presents boundary layer heating information in the form of a heat transfer rate, $\dot{q}_w$; a heat transfer coefficient, H; and a recovery temperature (adiabatic wall temperature), T_{aw}, at each computational point. These variables are related in the following manner.

$$H = \frac{\dot{q}_w}{T_{aw} - T_w} \tag{11}$$

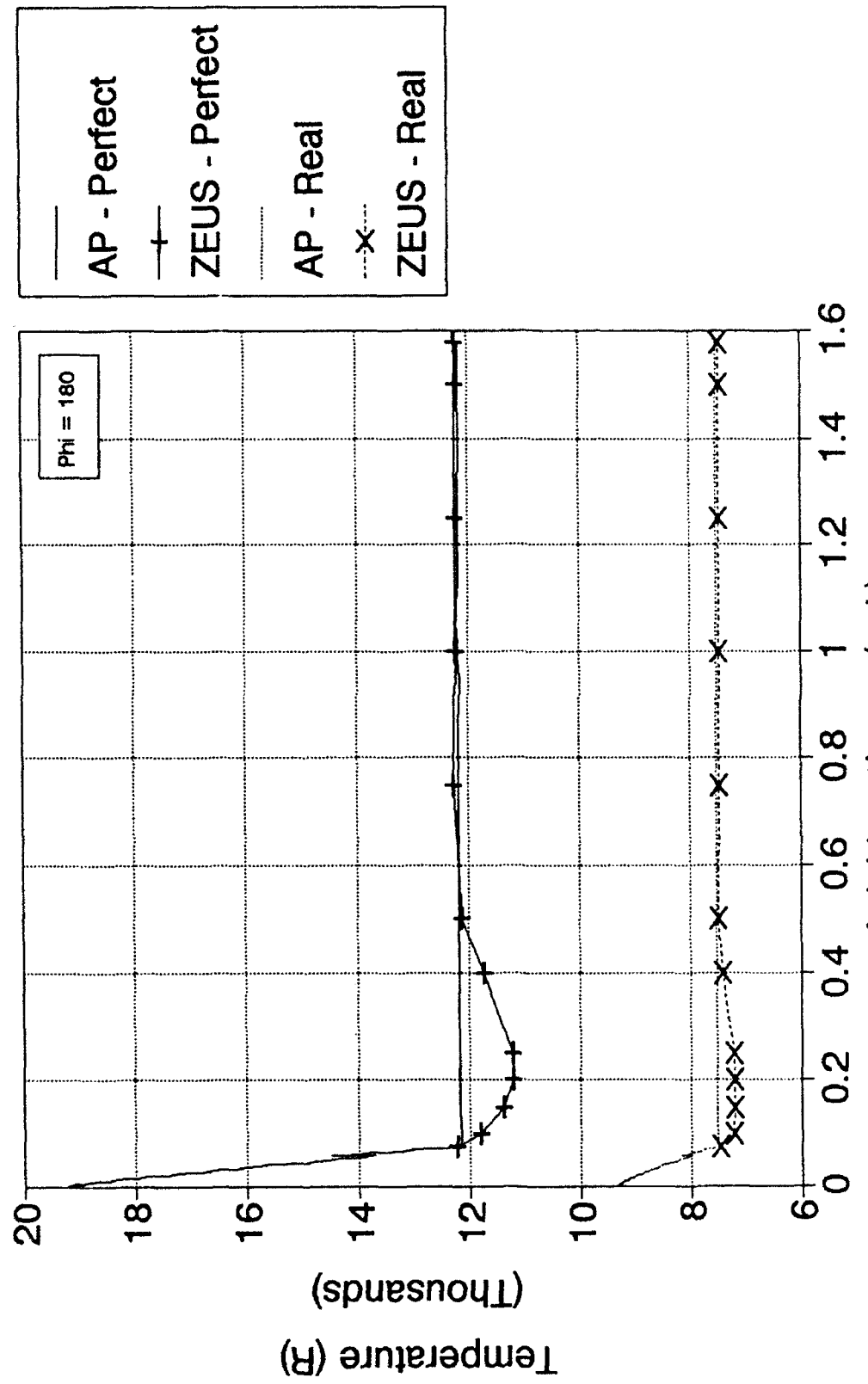

FIGURE 4. COMPARISON OF APPROXIMATE AND EXACT TEMPERAURE IN WINDWARD PLANE OF A 20 PERCENT BLUNT CONE ($M_\infty = 15$, $\alpha = 10$ DEG)

T_w is the wall temperature. For high-temperature flows, the heat transfer coefficient is often expressed in terms of enthalpies.

$$H_1 = \frac{\dot{q}_w}{h_{aw} - h_w} \tag{12}$$

At temperatures above about 1500 °R, this enthalpy formulation is the more rigorously correct of the two. Within the code, all real-gas, high-temperature computations are performed using the enthalpy as the basic variable; but to maintain consistency with other codes in use at NSWCDD, the results are converted to the temperature form for output. The heat transfer is normalized as shown in Equations 11 and 12 because the coefficients H and H_1 remain fairly constant over a wide range of wall temperatures, even though the actual heat transfer rate, $\dot{q}_w$, may vary significantly. Thus, since T_{aw} and h_{aw} are not functions of wall temperature, once a heating computation is performed for a given Mach number/altitude combination, it need not be repeated simply because of changes in wall conditions. This weak coupling greatly simplifies the problem of tracking the time-dependent thermal response of a surface exposed to boundary layer heating. The aerodynamic solution may be obtained first with a code such as AP93 and the results stored in tabular form as functions of Mach number, altitude, and angle of attack. This information can then be accessed by an independent algorithm to compute the time-varying heat transfer rates and the resulting integrated surface temperature history along any given trajectory that lies within the limits of the data matrix.

The AP93 user has the option, specified in the input file, of using either perfect- or real-gas relations in the computation of the inviscid solution for the geometric configuration and flight conditions of interest.[9] In the former case, the familiar analytical thermodynamic relations are employed to generate the necessary fluid properties. In the latter instance, real-gas properties are determined by the use of a series of curve fit relations.[18,19] This procedure is carried over into the routines that compute the boundary layer heating. Some additional work is required to generate the full complement of variables needed as input to this section of the code, and these additions are described in full in Reference 11. The only departure from the use of true inviscid surface conditions as boundary layer edge properties occurs in the case of blunt bodies. The curvature of the detached bow shocks associated with these configurations creates an entropy layer near the body surface. The inviscid solution would give a uniform boundary layer edge entropy over the entire body equal to that behind a normal shock at the free-stream Mach number, since this is the entropy along the inviscid streamline that wets the body surface. In reality, because of the finite thickness of the boundary layer, the true edge entropy is that which exists at some point in the entropy layer located at a distance above the surface equal to the local boundary layer thickness. This entropy value is determined by an iterative mass balance technique as described in Reference 11.

Once appropriate boundary layer edge conditions are determined, a series of specialized analytical relations is used to determine the aerodynamic heating at various locations. At the nose tip stagnation point, a simplified version of the Fay-Riddell formula gives[23]

$$\dot{q}_w = 0.763\,Pr^{-0.6}\sqrt{\rho_0\mu_0}\,\sqrt{\frac{dV_e}{dx}}\,(h_{aw} - h_w) \tag{13}$$

The stagnation point velocity gradient, dV_e/dx, is determined from the Newtonian theory, assuming a spherical nose tip. At the nose tip, the flow will always be laminar.

If control surfaces are present, the viscous heating along their leading edge stagnation lines is determined by the Beckwith and Gallagher swept-cylinder relations[24] modified to include real-gas effects.[25] For the laminar case,

$$\dot{q}_{w,l} = 0.57\,Pr^{-0.6}\sqrt{\rho_0\mu_0}\,\sqrt{\frac{dV_e}{dx}}\,(h_{aw} - h_w)(\cos\Lambda)^{1.1} \tag{14}$$

where Λ is the leading edge sweep angle and dV_e/dx is the stagnation line velocity gradient derived from Newtonian theory assuming, in this instance, a cylindrical leading edge. For turbulent flow,

$$\dot{q}_{w,t} = 1.04\,Pr^{-0.6}\,\frac{(\rho^*\mu^*)^{0.8}}{(\mu_0)^{0.6}}\,(V_p\sin\Lambda)^{0.6}\left(\frac{du_e}{dx}\right)^{0.2}(h_{aw} - h_w) \tag{15}$$

where V_p is the flow velocity parallel to the leading edge stagnation line and the (*) superscript denotes evaluation at a reference enthalpy given by[26]

$$h^* = 0.5\,(h_w + h_e) + 0.22\,(h_{aw} - h_e) \tag{16}$$

The (e) subscript denotes evaluation at the boundary layer edge. The laminar or turbulent status of the flow is determined by comparison of the Reynolds number, based on the leading edge diameter, to user-specified upper and lower limits. If Re_D is below the lower limit, laminar values are used. If Re_D is above the upper limit, fully turbulent flow is assumed. For intermediate values of Re_D, a linear combination of laminar and turbulent values is output.

For points on the body, the Eckert reference enthalpy flat plate formulation is used.[27] For laminar flow,

$$\dot{q}_{w,l} = 0.332\,(Pr^*)^{-0.667}\,\frac{\rho^* V_e}{\sqrt{\frac{Re^*}{N_l}}} \tag{17}$$

and for the turbulent case,

$$\dot{q}_{w,t} = 0.185\,(Pr^*)^{-0.667}\,\frac{\rho^* V_e}{\left|\ln \frac{Re^*}{N_t}\right|^{2.584}} \tag{18}$$

N_l and N_t are transformation factors that allow for the approximation of three-dimensional (3-D) effects. They are equal to three and two, respectively. The laminar or turbulent flow character is determined as before by comparing the local Reynolds number, based on boundary layer running length, to user-specified upper and lower limits.

Heating rates on the surfaces of wings, fins, or canards are determined by using Equations 17 and 19, but in this case, N_l and N_t are both equal to one because of the two-dimensional (2-D) nature of the flow. The degree of turbulence is determined in the same manner as for the body.

Validation of the new heat transfer methodology was carried out in two steps. The first involved comparing results for stagnation point and stagnation line flows from AP93 with those from the MINIVER code, an approximate engineering design tool that was developed to model primarily 2-D and axisymmetric configurations. MINIVER handles these specialized situations quite well, providing a good check for both heat transfer and inviscid boundary layer edge conditions. The latter comparisons served as further validation of the real-gas model previously incorporated into the AP93 code. These computations covered a range of Mach numbers from 7.73 to 15. The results are detailed in Reference 11 and will not be repeated here. In summary, agreement of all computer variables, including heat transfer, was generally good with variations of well under 5 percent being typical. Where larger differences occurred, the underlying reason was readily apparent, and the AP93 results were concluded to be the better of the two. (A typical case in point would be the use of curve fits in AP93 to determine Prandtl number and viscosity, whereas MINIVER relies on constant Prandtl numbers and Sutherland's law for viscosity. At high temperatures, the curve fits should be superior.)

The second set of computations in the validation process was done for spherically blunted cones at angle of attack. Results from two of these examples are shown in Figures 5 and 6. In both instances, free-stream pressure and temperature were 2.66 lb/ft^2 and 89.971 °R, respectively, and the cone half angle was 15 deg. The Mach number was 10.6, and the wall temperature was 540 °R. The results shown in Figure 5 represent the heating rates along the symmetry line of a cone with nose radius of 0.375 in. at 20-deg angle of attack. For comparison purposes, analytical results are shown from Reference 28 that uses a more advanced engineering design code involving complex streamline tracking methods and the axisymmetric analog technique to model 3-D effects. Experimental data from Reference 29 are also shown, along with results from the MINIVER code used in a tangent cone mode. AP93 and MINIVER tend to underpredict the experimental data and the more sophisticated computational results by 10 to 15 percent, a performance that is creditable considering the simplified solution approach. Figures 6 and 7 show similar results for a cone with a 1.1-in. nose radius at angles of attack of 5 and 10 deg. In this instance, comparisons are shown from AEROHEAT, an engineering design code similar to the one described and from a second approximate code[30] that uses more sophisticated streamline tracking, as well as a more exact boundary layer formulation. MINIVER results are also shown along with experimental data from Reference 29. AP93 does well beyond about five nose radii downstream but tends to overpredict heating rates near the nose tip. This discrepancy is believed to be caused by the use of heating expressions that are based on flat plate theory and are thus incapable of modeling the effects of the rapidly changing boundary layer edge conditions in this region. The AP93 results are slightly better than those from MINIVER because of the inclusion of variable entropy effects. AP93 has the added advantage over MINIVER of being able to compute a more realistic 3-D distribution of heating rates over the entire surface at angle of attack.

2.3 SKIN FRICTION DRAG

The AP81 uses Van Driest II for computing skin friction drag on both the body and fins. The code assumes a critical Reynolds number (Re_c), where the flow transitions from laminar to turbulent of $1X10^6$ on the body and $0.5X10^6$ on the fins. This methodology is described in Reference 2.

Two changes were made in the AP81 methodology. These changes both had to do with the assumptions of that work. The AP81 methodology was associated with typical flight conditions of vehicles manufactured with a certain level of surface roughness and at zero angle of attack. Hence, when comparing the AP81 drag results to those of wind tunnel data (which may or may not have a boundary layer trip) from a smooth model, mixed results were obtained. As a result, three additional alternatives are included for Re_c. The first is associated with a boundary layer trip on a wind tunnel model. In this case, a small value for Re_c is assumed so that the boundary layer is turbulent over the entire model. A second alternative is to assume a high Re_c so that laminar flow occurs over the entire model. A third alternative is for the case of a wind tunnel model with no boundary layer trip. For that case, a Re_c of $4X10^6$ and $2X10^6$, respectively, is assumed for the body and wing or tail.

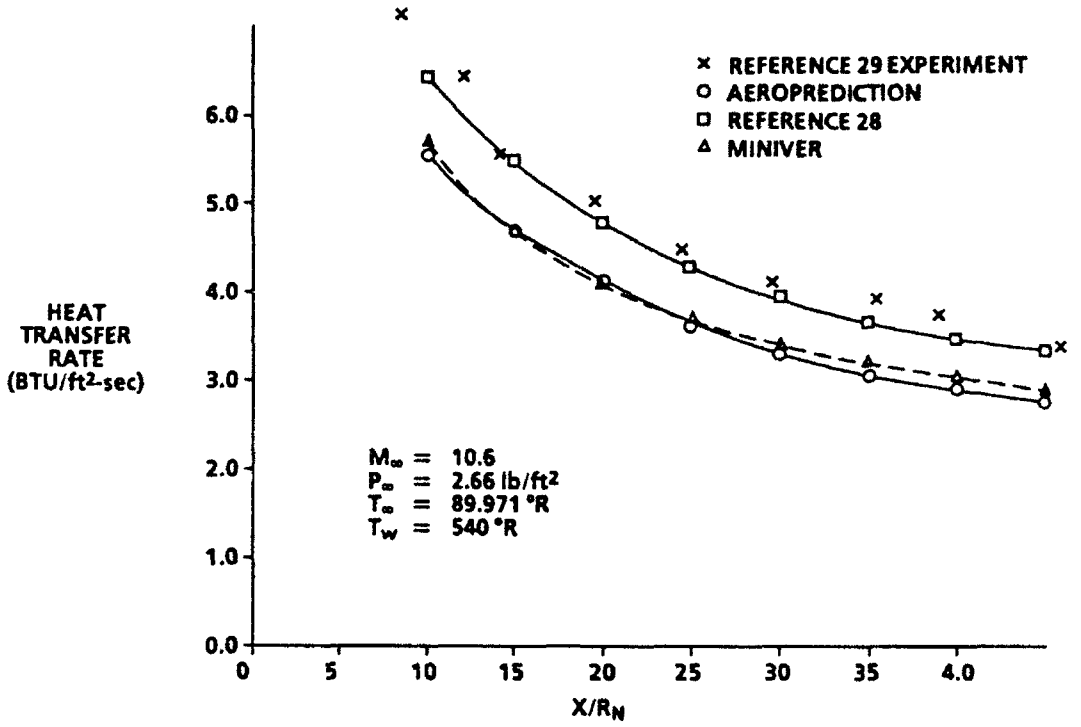

FIGURE 5. WINDWARD PLANE HEAT TRANSFER RATES FOR 0.375-IN. NOSE RADIUS, 15-DEG HALF-ANGLE CONE AT $\alpha = 20$ DEG

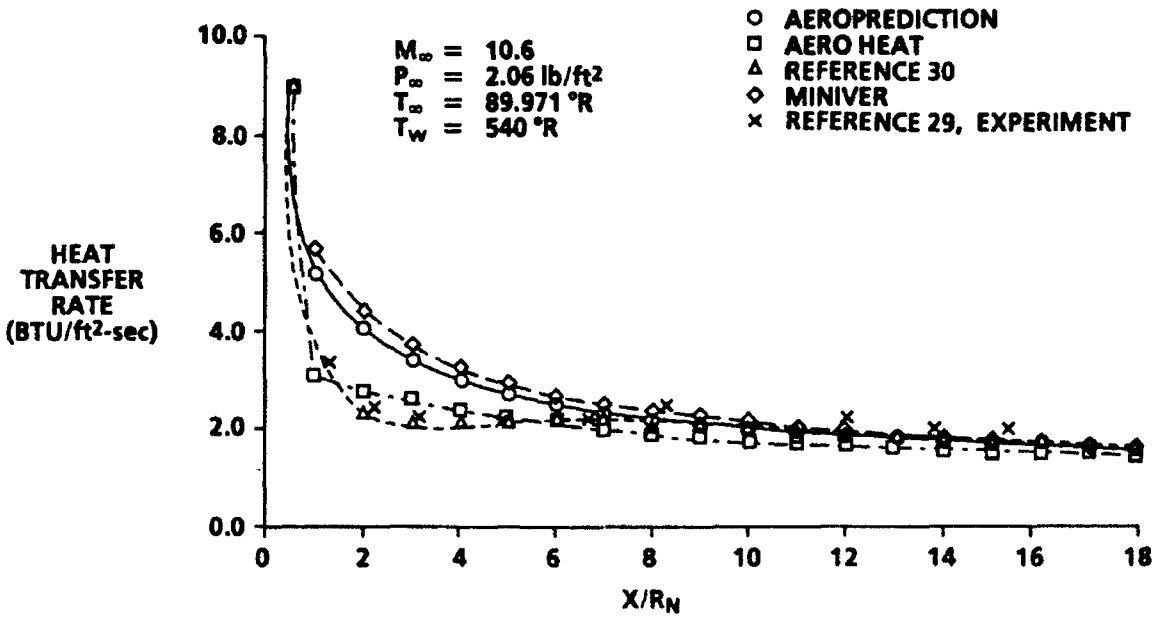

FIGURE 6. WINDWARD PLANE HEAT TRANSFER RATES FOR 1.1-IN. NOSE RADIUS, 15-DEG HALF-ANGLE CONE AT $\alpha = 5$ DEG

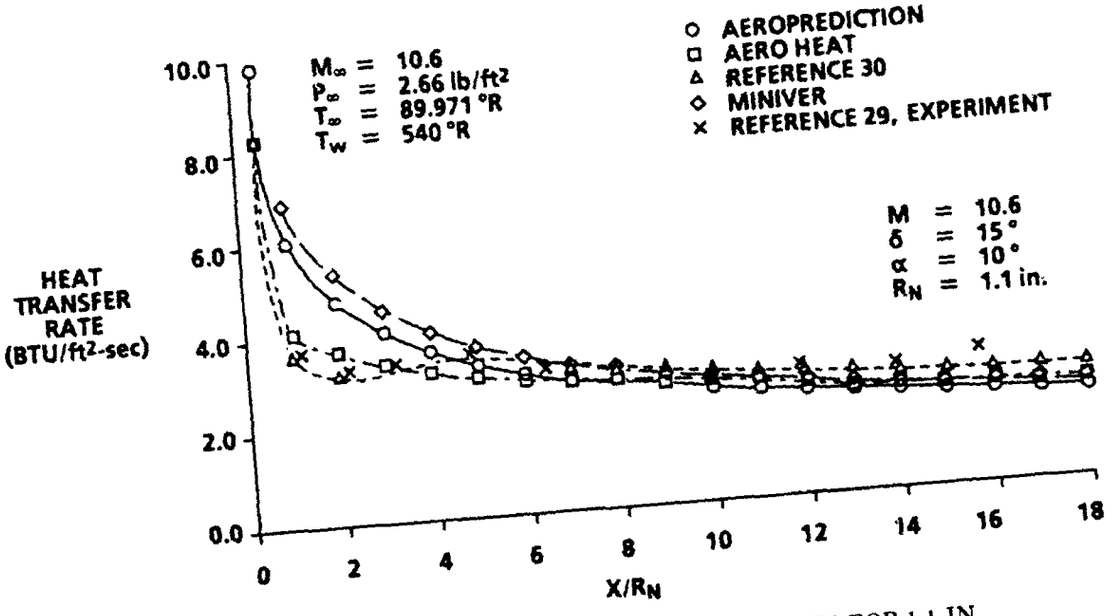

FIGURE 7. WINDWARD PLANE HEAT TRANSFER RATES FOR 1.1-IN. NOSE RADIUS, 15-DEG HALF-ANGLE CONE AT $\alpha = 10$ DEG

A second change introduced into AP93 is angle-of-attack effect on Re_c. For both the options where the boundary layer transition is allowed to occur on the body or lifting surface (flight or wind tunnel model with no trip), the Re_c is assumed to vary from the values specified as previously discussed at $\alpha = 0$ to a value small enough at $\alpha = 30$ deg so that fully turbulent flow occurs over the entire missile surface. This assumption occurs in a linear fashion with angle of attack from $\alpha = 0$ deg to $\alpha = 30$ deg.

2.4 BASE DRAG

The AP81 estimated base drag using a composite of empirical data for the body alone. Also, an approximation was made for the effect of angle-of-attack, fin location, and fin thickness effects as a function of Mach number based on a limited amount of data. As a result, a request was made to the National Aeronautics and Space Administration at the Langley Research Center (NASA/LRC) to perform additional wind tunnel tests, where additional base pressure measurements could be taken to try and quantify the effects mentioned plus those due to control deflection.

Floyd Wilcox, coauthor of References 14 and 15, was the chief engineer for the tests that were conducted and reported in those references. Eighty-nine base pressure taps were placed around a 7.2-caliber, 5-in. diameter body with a side-mounted sting. These taps were placed every 22.5 deg in circumferential location and at several radii from the body centroid toward the outer edge. The configuration matrix of data taken is shown in Table 1. The base pressure measured at each of the 89 orifice locations was then averaged over its incremental base area to get the average base pressure at each condition of Table 1. Based on these average base pressure measurements at each test condition, changes in base pressure, and hence, base drag because of a particular physical model change or flight condition change could be readily computed by simply substracting the two data points.

TABLE 1. CONFIGURATION INDEX

Config	t/c				x/c					δ				α (M_∞=2.0)	α ($M_\infty \geq 2.5$)
	Fins Off	0.05	0.10	0.15	0.5	1.0	1.5	2.0	2.5	0	5	10	15	20	
1	X														Sweep	Sweep
2				X	X					X					0,5,10	0
3				X	X							X			0,5,10	0
4				X	X									X	0,5,10	0
5			X		X					X					0,5,10	0
6			X		X							X			0,5,10	0
7			X		X									X	0,5,10	0
8		X			X					X					0,5,10	0
9		X			X							X			0,5,10	0
10		X			X									X	0,5,10	0
11		X					X			X					0,5,10	0
12			X				X			X					0,5,10	0
13				X			X			X					0,5,10	0
14				X					X	X					0,5,10	0
15			X						X	X					0,5,10	0
16		X							X	X					0,5,10	No data

Using the process described, along with a wind tunnel database not available when AP81 was developed,[31] a new empirical estimate of base pressure coefficient (C_{p_B}) was derived. This new estimate is shown in Figure 8 and compared to the AP81 value of C_{p_B}. The two curves are similar, with the AP93 slightly higher than AP81 for $M_\infty \leq 1.5$ and slightly lower than AP81 for $M_\infty \geq 3.0$. Body-alone angle-of-attack effects on base pressure are then estimated by

$$\left(C_{p_B}\right)_{NF,\alpha} = \left(C_{p_B}\right)_{NF,\alpha=0} \left|1 + 0.01F_1\right| \tag{19}$$

Here, $(C_{p_B})_{NF,\alpha=0}$ comes from Figure 8 and F_1, the increase due to angle of attack from Figure 9a or 9b, depending on the Mach number. Boattail and power-on effects on base drag are estimated as present in AP81.

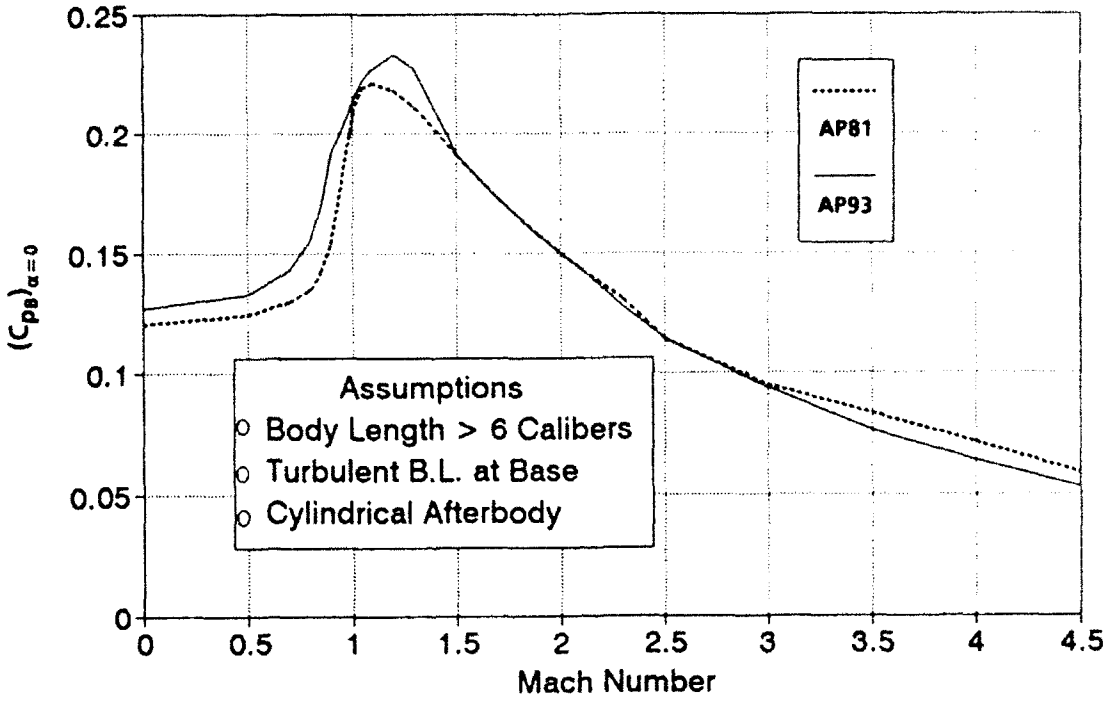

FIGURE 8. MEAN BODY-ALONE BASE PRESSURE COEFFICIENT USED IN AP81 AND AP93

At this point, it is worth noting that, while the databases of References 14, 15, and 31 helped to improve the estimate of base pressure as a function of Mach number and angle of attack for the body alone, additional data are still needed for $\alpha \geq 15$ deg at all Mach numbers. This need is indicated by the dotted lines in Figures 9a and 9b, which are extrapolations from data available for $\alpha \leq 15$ deg and engineering judgment. This same statement will also be even more true for fin effects due to control deflection and angle of attack, as will be discussed in the following paragraphs.

The total body base pressure coefficient for fins located flush with the base is

$$\left(C_{p_B}\right)_{\alpha,\delta,t/c,x/c=0} = \left|1+0.01F_2\right|\left(C_{p_B}\right)_{NF,\alpha=0} + 0.01\,F_3\,(t/d) \tag{20}$$

where $(C_{p_B})_{NF,\alpha=0}$, F_2, and F_3 come from the AP93 curve of Figures 8, 10, and 11, respectively.

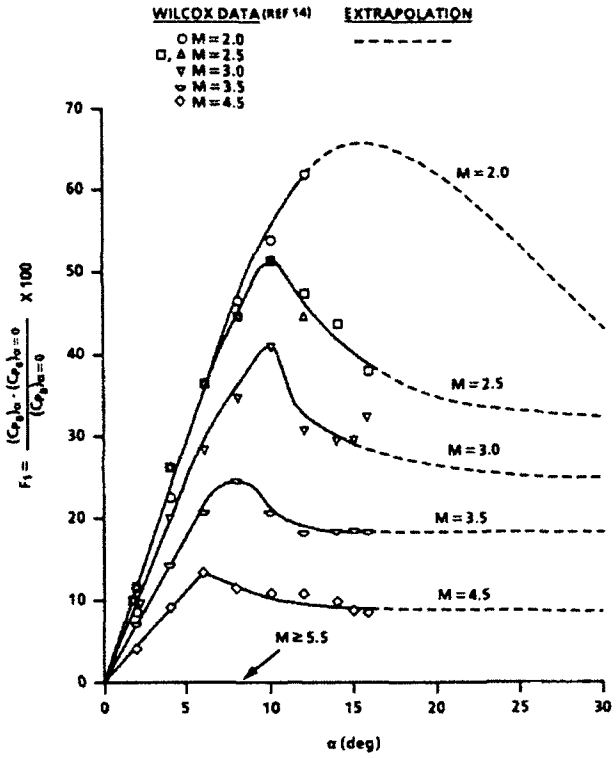

a. ($M_\infty \geq 2$)

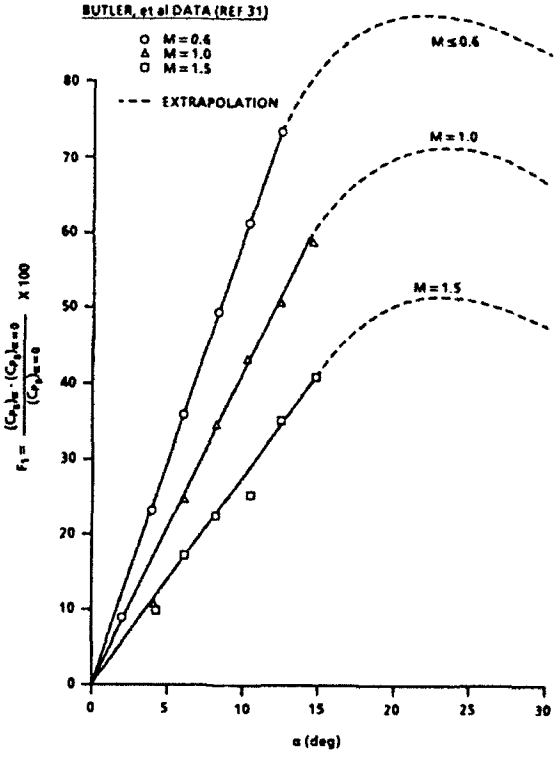

b. ($M_\infty < 2$)

FIGURE 9. PERCENT INCREASE IN BODY-ALONE BASE PRESSURE COEFFICIENT DUE TO ANGLE OF ATTACK

In Figure 10, no data were taken for $M_\infty < 2$ in the test of References 14 and 15, and none could be found in the literature. Hence, the data for $M_\infty = 2$ are assumed to apply for $M_\infty < 2$ as well. While this is a big assumption, it is believed to be better than neglecting the base pressure effect due to control deflection and angle of attack, which other engineering aerodynamics codes do. It is also worth noting that Figure 11 indicates what is intuitively obvious; i.e., for small control deflections and angles of attack, fin thickness effects are important in base pressure estimation, whereas for large values of α and δ, the additional change in C_{P_B} due to fin thickness is minimal.

The final parameter to define the effect on base pressure is fin location relative to the body base. This is done through Equation 21, where

$$\left(C_{P_B}\right)_{\alpha,\delta,t/c,x/c} = \left(C_{P_B}\right)_{NF,\alpha} + 0.01\left(\Delta C_{P_B}\right)_{\alpha,\delta,t/c,x/c} \tag{21}$$

Here $(C_{P_B})_{NF,\alpha}$ is the body-alone base pressure coefficient at a given angle of attack given by Equation 19 and $(\Delta C_{P_B})_{\alpha,\delta,t/c,x/c}$ is the total change due to the presence of fins at a given α, δ, t/c, and x/c. An example of $(\Delta C_{P_B})_{\alpha,\delta,t/c,x/c}$ is given in Figure 12 for $M_\infty = 2.0$ and $|\alpha + \delta| = 10$ deg. Reference 14 shows other curves for this parameter. Figure 12 shows that the change in base pressure due to all variables present varies from that at $x/c = 0$, where the fins dominate to that of the body alone where the fins have no effect ($x/c \approx 2.5$).

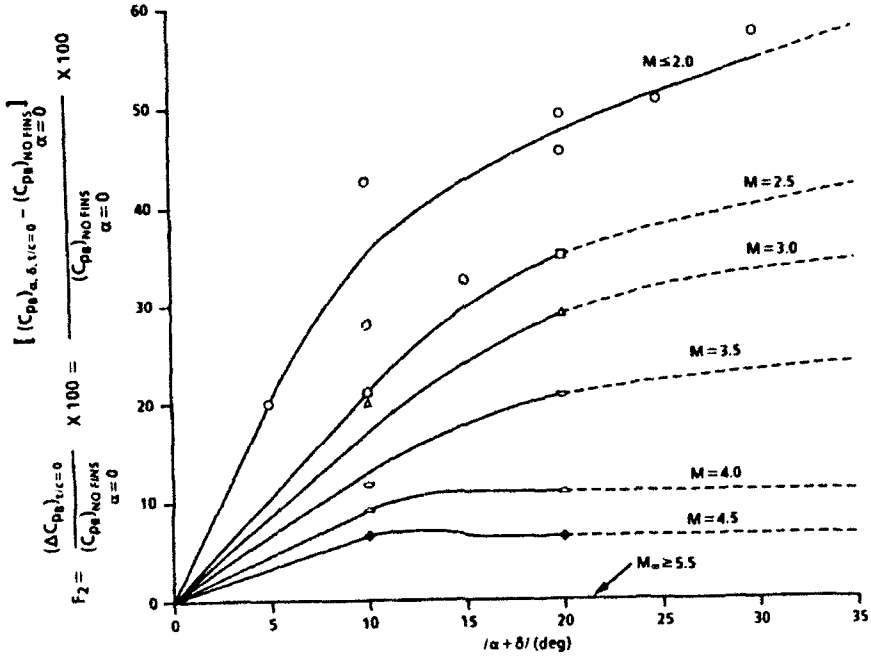

FIGURE 10. PERCENT INCREASE IN BASE PRESSURE COEFFICIENT DUE TO COMBINED EFFECTS OF ANGLE OF ATTACK AND CONTROL DEFLECTION ($t/c \approx 0$)

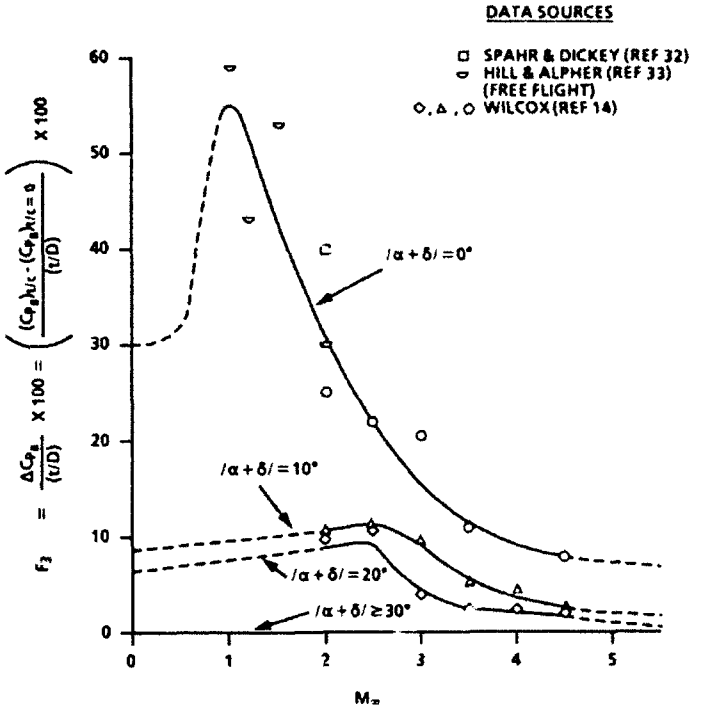

FIGURE 11. ADDITIONAL PERCENT INCREASE IN BASE PRESSURE COEFFICIENT DUE TO FIN THICKNESS AT VARIOUS VALUES OF $|\alpha + \delta|$

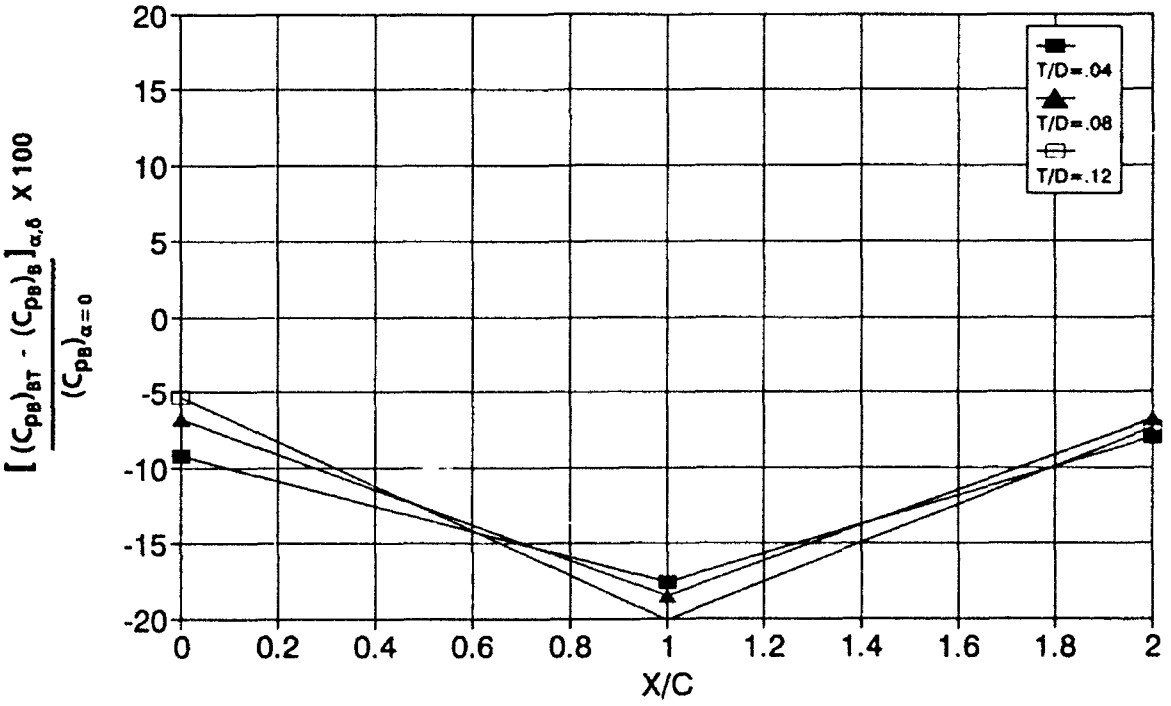

FIGURE 12. PERCENT INCREASE IN BASE PRESSURE COEFFICIENT DUE TO FIN LOCATION $|\alpha + \delta| = 10$ DEG, $M_\infty = 2.0$

2.5 BODY-ALONE NORMAL FORCE AND CENTER OF PRESSURE

The normal-force coefficient of the body alone is estimated by

$$C_N = C_{N_L} + C_{N_{NL}} \tag{22}$$

where C_{N_L} is the linear term and $C_{N_{NL}}$ the nonlinear term. The linear term is predicted in AP81 by either SOSET, Second-Order Van Dyke combined with MNT, or empirical depending on the Mach number range (see References 2, 7, or 9 for details). The nonlinear term is estimated by the Allen-Perkins viscous crossflow theory.[34] No changes were made in the linear term of Equation 22 in AP93 from AP81. Three changes in the nonlinear term of Equation 22 were made for the AP93.

The nonlinear term of Equation 22 according to Reference 34 is

$$C_{N_{NL}} = \eta C_{dc} \sin^2\alpha \frac{A_p}{A_{ref}} \tag{23}$$

The first change from AP81 is in the value of η. AP81 used an incompressible value of η with no account of compressibility effects. Reference 35 clearly showed a compressibility effect. This effect is shown in Figure 13a along with the line drawn to represent the data. This line is defined as

$$\eta = \left(\frac{1-\eta_o}{1.8}\right) M_N + \eta_o \quad \text{for } M_N \le 1.8 \tag{24}$$

$$\eta = 1 \quad \text{for } M_N > 1.8$$

where η_o is the incompressible value of η ($M_N = 0$) given in Reference 2 and used in AP81.

The second change is in the value of the crossflow drag coefficient used. This value was changed to allow the effect of transition on the body surface to impact the value chosen. This impacts the value of C_{dc} for M_N values of 0.5 and less. Also, the value of C_{dc} is slightly lower for $0.6 \le M_N \le 2.2$ than that used in AP81. This is based on the large NASA Tri-Service Database.[36] The new value of C_{dc} used in AP93 is given in Figure 13b. If the flow on the body is a combination of laminar and turbulent (which is the case for most conditions), a value somewhere in between the two values on the Figure 13b curve for $M_N \le 0.5$ will be computed. If X_L defines the length of laminar flow on the body and X_T is the total length, then for $M_N \le 0.5$,

$$C_{dc} = 1.2 - \left(\frac{X_L}{X_T}\right) 0.8 \tag{25}$$

Thus, if $X_L = 0$ so the flow over the body is fully turbulent, a value of $C_{dc} = 1.2$ will be computed, whereas a value of 0.4 will be picked if the flow is fully laminar.

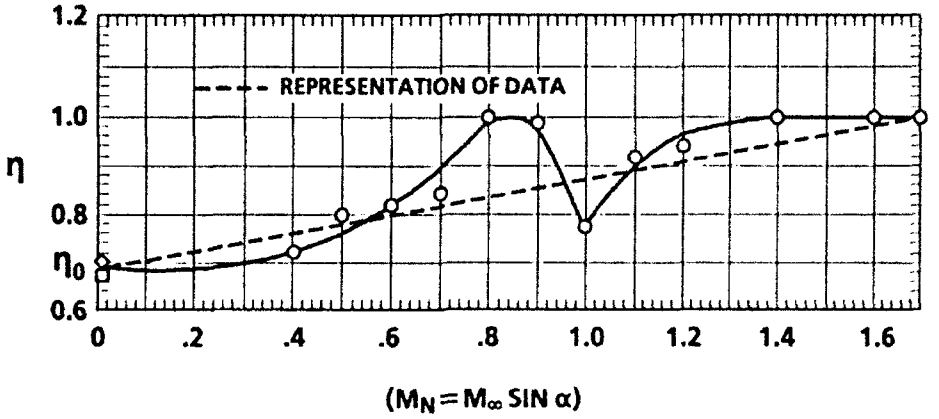

FIGURE 13a. COMPRESSIBILITY EFFECTS ON CROSSFLOW DRAG PROPORTIONALITY FACTOR

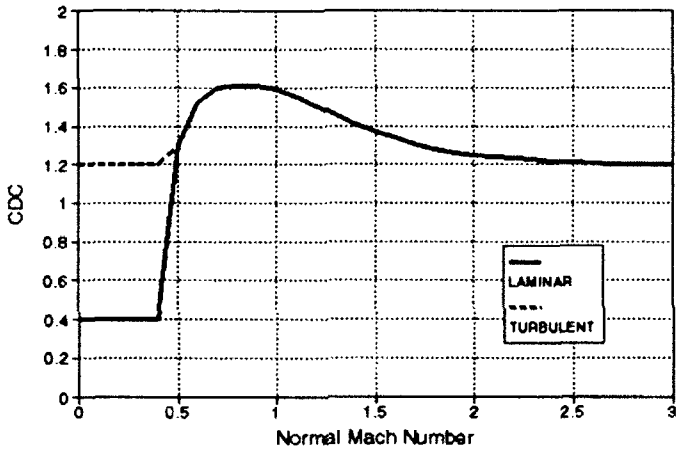

FIGURE 13b. CROSSFLOW DRAG COEFFICIENT FOR AN OGIVF-CYLINDER CONFIGURATION

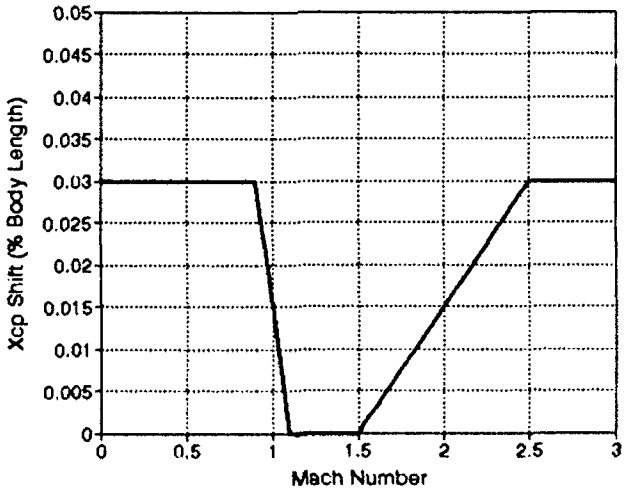

FIGURE 13c. CENTER OF-PRESSURE SHIFT IN BODY-ALONE NORMAL FORCE FOR $\alpha \geq 10$ DEG

The third change made in AP93 was in the center-of-pressure location. AP81 used a weighted average of the normal force center of pressure of the linear term and nonlinear term, where the nonlinear term X_{cp} was at the centroid of the planform area in the crossflow plane and the X_{cp} of the linear term was computed theoretically or empirically. Both these values were held constant as angle of attack increased, the only change being from the changing values of the normal-force terms of Equation 22. In numerical experiments using the database of Reference 36, it was found that the assumption of a constant value of center of pressure with angle of attack was not completely correct. It is suspected that as angle of attack increases, the center of pressure of the linear term of Equation 22 changes and can no longer be assumed to be constant. An empirical way to represent this change with Mach number is given in Figure 13c. This change is effective for $\alpha \geq 10$ deg. Between $\alpha = 0$ and 10 deg, the correction is implemented in a linear fashion between zero at $\alpha = 0$ to its full value at $\alpha = 10$ deg.

Figure 14 is an example of the normal-force and center-of-pressure comparisons of the AP81, AP93, and experimental data. The data are from Reference 36, which is for a 12.33-caliber tangent-ogive cylinder configuration with a 3.0-caliber nose. The improvements made in AP93 give significantly better results on both C_N and X_{cp} as a function of angle of attack.

2.6 WING-ALONE LINEAR NORMAL FORCE AND CENTER OF PRESSURE FOR LOW-ASPECT RATIO WINGS

The AP81 gives reasonably accurate wing-alone linear normal-force coefficients if the aspect ratio is one or greater. However, as the aspect ratio gets small, similar to what would be obtained on dorsal-like lifting surfaces, the linear theory gives values of $(C_{N_\alpha})_{\alpha=0}$, which are too high. This is because the AP81 neglects Mach lines that intersect opposite wing tips. This assumption becomes increasingly invalid as the aspect ratio gets small. To remedy this, the Evvard[37] and Krasilshchikova[38] methods for low-aspect ratio wings were implemented in the AP93. The $(C_{N_\alpha})_{\alpha=0}$ is still slightly higher than experimental data; however, it is believed this is due to neglecting thickness effects. For the details of this effort, interested readers are referred to Reference 12.

A second change was also made in the linear part of the wing-alone lift. This had to do with center-of-pressure prediction. When the linear theory or lifting surface theory said the center of pressure was further forward on the wing than 15 percent (or 10 percent of the chord subsonically), the AP93 puts a limit at these values. This limit, in effect, brings into the center-of-pressure considerations the real viscous effects, which are neglected in the linearized inviscid theories.

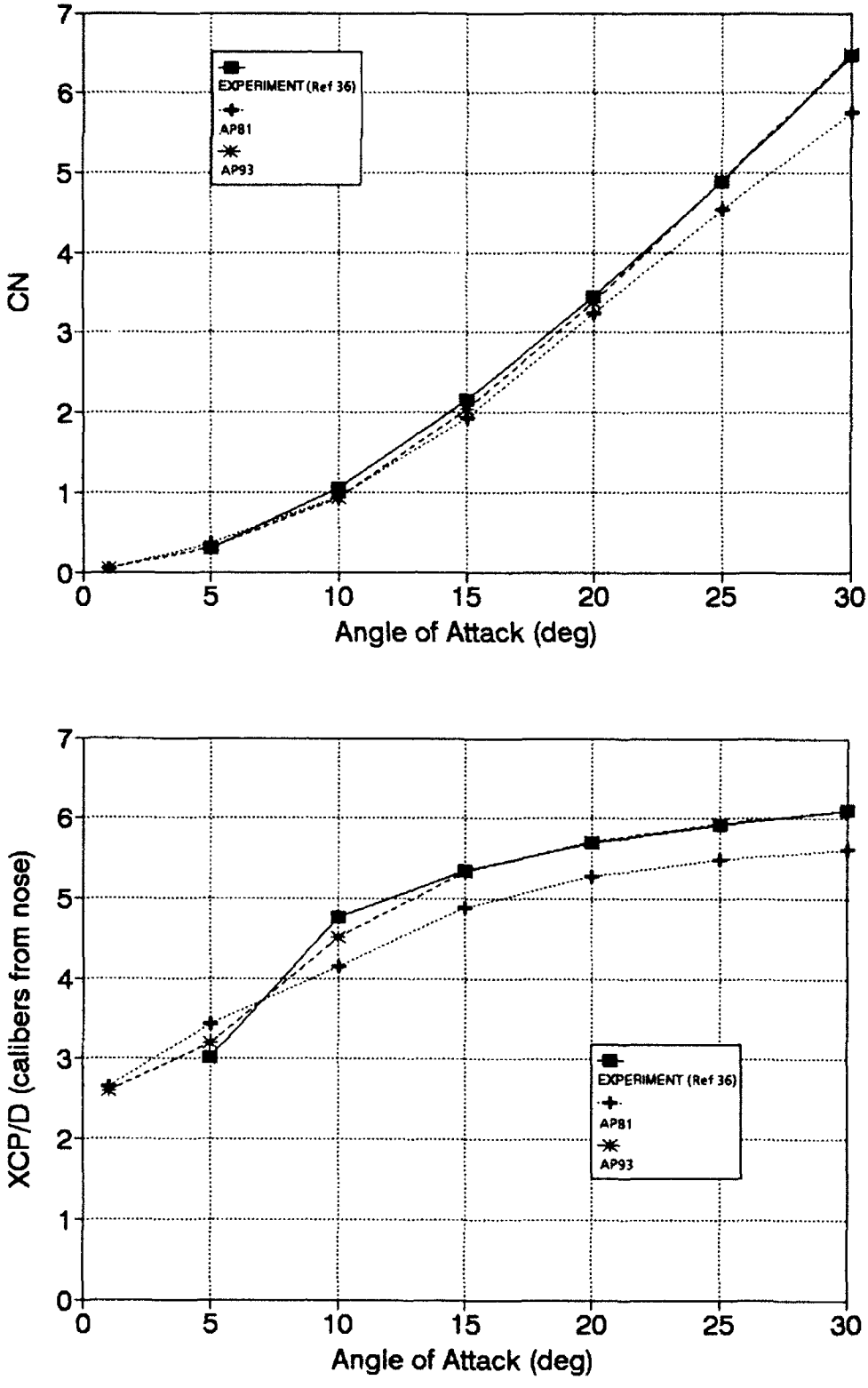

FIGURE 14. BODY-ALONE NORMAL-FORCE COEFFICIENT AND CENTER OF PRESSURE ($M_\infty = 3.5$)

2.7 WING-ALONE NONLINEAR NORMAL FORCE AND CENTER OF PRESSURE

One of the major reasons the AP81 gave poor results at $\alpha > 10$ deg for many missile configurations was failure to include nonlinearities in the wing lift. Using the databases of References 39 and 40, a semiempirical method was developed for the nonlinear wing-alone normal-force term[12,13] analogous to the body-alone Equations 22 and 23; i.e., the nonlinear term of wing-alone lift can be defined as

$$C_{N_{NL}} = f(M_N, AR, \lambda)\left(\frac{A_p}{A_{ref}}\right)\sin^2\alpha \tag{26}$$

Here, $f(M_N, AR, \lambda)$ is analogous to the $\eta\, C_{dc}$ of the body alone in Equation 23. Since the total wing-alone normal force is known for a given AR, M_∞, λ, and α from References 39 and 40, the linear value of lift is known from the 3-D thin-wing theory or lifting surface theory from AP81 (modified according to Section 2.6); the nonlinear normal force of the wing alone is

$$C_{N_{NL}}(M_N, AR, \lambda) = C_N(M_N, AR, \lambda) - C_{N_L}(M_N, AR, \lambda) \tag{27}$$

Using the data of References 39 and 40, Equation 27 values were generated and a parameter k_1 defined as

$$k_1 = \frac{C_{N_{NL}}(M_N, AR, \lambda)}{\sin^2\alpha} \tag{28}$$

was generated. Tables of k_1 for both high and low Mach numbers are given in Tables 2 and 3. The total wing-alone normal force in AP93 is therefore

$$C_{N_w} = C_{N_L} + k_1 \sin^2\alpha \frac{A_w}{A_{ref}} \tag{29}$$

The second term of Equation 29 was neglected in AP81.

The center of pressure of the wing-alone lift was assumed to vary quadratically between its linear theory value at $\alpha = 0$ to the centroid of the planform area (adjusted for thickness effects) at $\alpha = 60$ deg.

Defining the center of pressure of the wing-alone linear term as A and the center of pressure of the nonlinear term as B (both in percent of mean geometric chord), then the center of pressure of the wing lift is

$$(X_{cp})_w = A + \frac{1}{36}|\alpha_w|(B-A| + \frac{1}{5400}\alpha_w^2|A-B| \tag{30}$$

TABLE 2. VALUES OF k_1 FOR LOW MACH NUMBERS

AR ≤ 0.5; $M_\infty < 4.0$

λ/M_∞	0.0	0.5	1.0	1.5	2.0	2.5	3.0	3.5	4.0	4.5
0.0	1.55	1.57	1.60	1.60	1.51	1.25	0.92	0.56	0.29	0.16
0.5	2.84	2.90	2.82	2.30	1.35	1.00	0.80	0.64	0.47	0.33
1.0	2.37	2.45	2.43	2.31	1.50	1.05	0.90	0.75	0.61	0.48

AR = 1.0; $M_\infty < 3.5$

λ/M_∞	0.0	0.5	1.0	1.5	2.0	2.5	3.0	3.5	4.0	4.5
0.0	1.32	1.48	1.46	0.99	0.40	0.22	0.12	0.09	0.09	0.11
0.5	2.44	2.45	1.85	0.70	0.31	0.19	0.20	0.26	0.36	0.43
1.0	1.20	1.22	1.10	0.50	0.45	0.50	0.65	0.78	0.88	0.94

AR ≥ 2.0; $M_\infty < 3.5$

λ/M_∞	0.0	0.5	1.0	1.5	2.0	2.5	3.0	3.5	4.0	4.5
0.0	-1.80	-1.84	-1.95	-1.50	-0.20	0.00	0.10	0.20	0.25	0.30
0.5	-1.80	-1.84	-1.95	-1.50	-0.20	0.30	0.41	0.60	0.72	0.80
1.0	-1.45	-1.47	-1.35	-0.70	0.20	0.60	0.83	0.98	1.09	1.15

FIGURE 3. VALUES OF k_1 FOR HIGHER MACH NUMBERS

AR ≤ 0.5; $M_\infty \geq 4.0$

$\lambda/M_\infty \sin\alpha$	0.0	0.5	1.0	1.5	2.0	2.5	3.0	3.5	4.0	4.5	5.0	5.5	6.0
0.0	-1.60	-0.98	0.23	0.55	0.71	0.82	0.89	0.92	0.95	0.95	0.95	0.95	0.95
0.5	-0.87	-0.24	0.33	0.60	0.73	0.82	0.89	0.92	0.95	0.95	0.95	0.95	0.95
1.0	-0.31	0.09	0.46	0.68	0.78	0.87	0.91	0.93	0.95	0.95	0.95	0.95	0.95

AR = 1.0; $M_\infty \geq 3.5$

$\lambda/M_\infty \sin\alpha$	0.0	0.5	1.0	1.5	2.0	2.5	3.0	3.5	4.0	4.5	5.0	5.5	6.0
0.0	-0.39	-0.39	-0.29	0.06	0.29	0.48	0.60	0.69	0.75	0.81	0.86	0.91	0.94
0.5	0.14	0.17	0.29	0.46	0.63	0.76	0.85	0.90	0.93	0.95	0.95	0.95	0.95
1.0	0.30	0.50	0.86	0.93	0.94	0.95	0.95	0.95	0.95	0.95	0.95	0.95	0.95

AR ≥ 2.0; $M_\infty \geq 3.5$

$\lambda/M_\infty \sin\alpha$	0.0	0.5	1.0	1.5	2.0	2.5	3.0	3.5	4.0	4.5	5.0	5.5	6.0
0.0	-0.25	-0.05	0.20	0.50	0.80	0.95	0.95	0.95	0.95	0.95	0.95	0.95	0.95
0.5	0.02	0.29	0.80	0.98	0.98	0.97	0.97	0.96	0.95	0.95	0.95	0.95	0.95
1.0	0.66	1.02	1.15	1.18	1.15	1.09	1.02	0.96	0.95	0.95	0.95	0.95	0.95

α_w in Equation 30 is the total angle of attack in degrees on the wing. Figure 15 gives an example of the AP93 methodology compared to AP81 and experimental data. This particular case shows significant improvement in the wing-alone normal force of the AP93 versus AP81 when compared to the experiment. However, no improvement in center of pressure is obtained because $\lambda = 0$ and the centroid of the planform area are the same as experimental data suggest.

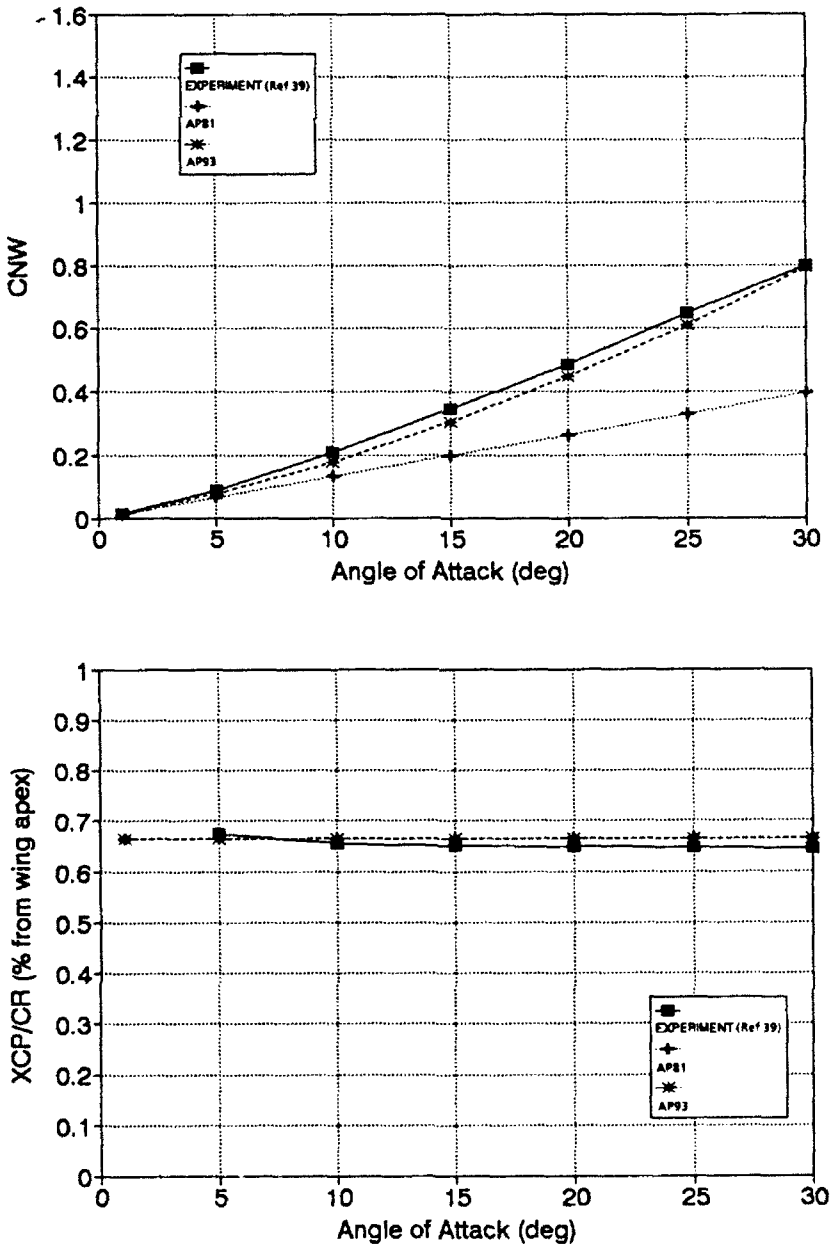

FIGURE 15. WING-ALONE NORMAL-FORCE COEFFICIENT AND CENTER OF PRESSURE ($AR = 0.5, \lambda = 0.0, M_\infty = 1.6$)

2.8 WING-BODY AND BODY-WING NONLINEAR INTERFERENCE FACTORS DUE TO ANGLE OF ATTACK

The total configuration normal-force coefficient at a given angle of attack, control deflection, and Mach number is[41]

$$C_N = C_{N_B} + \left[\left(K_{W(B)} + K_{B(W)}\right)\alpha + \left(k_{W(B)} + k_{B(W)}\right)\delta_W\right]\left(C_{N_\alpha}\right)_W + \left[\left(K_{T(B)} + K_{B(T)}\right)\alpha + \left(k_{T(B)} + k_{B(T)}\right)\delta_T\right]\left(C_{N_\alpha}\right)_T + C_{N_{T(V)}} \quad (31)$$

The first term in Equation 31 is the normal force of the body alone including the linear and nonlinear components; the second term is the contribution of the wing (or canard) including interference effects and control deflection; the third term is the contribution of the tail including interference effects and control deflection; and the last term is the negative downwash effect on the tail due to wing shed or body shed vortices. The K's represent the interference of the configuration with respect to angle of attack, and the k's represent the interference with respect to control deflection. Each of these interference factors is estimated in the AP81 by slender body or linear theory.[3] As such, they are independent of angle of attack. Estimating the change in these parameters with angle of attack is desired. To do this, Reference 12 made use of the large database of References 36, 39, and 40.

The work of Reference 12 found that the wing-body interference factor had the qualitative behavior as shown in Figure 16. At low angles of attack, slender-body theory appeared to be a good estimate of $K_{W(B)}$. This estimate was adjusted slightly for $M_\infty \leq 1.5$ by an amount $\Delta K_{W(B)}$. At some angle of attack defined as α_c, $K_{W(B)}$ seemed to decrease in a nearly linear fashion. The rate of this decrease was a function of Mach number—the higher the Mach number, the larger the rate of decrease. At some point defined as α_D, the $K_{W(B)}$ appeared to reach a minimum and remain about constant. As a result of this analysis, a mathematical model was derived to define $K_{W(B)}$ in terms of its slender-body theory value $[K_{W(B)}]_{SB}$ and an empirical correction derived from the databases of References 36, 39, and 40. This model given in Figure 16 is

$$K_{W(B)} = \left|K_{W(B)}\right|_{SB} + \left|\Delta K_{W(B)}\right|_{\alpha=0}\left(\frac{r/s}{0.5}\right) \text{ for } \alpha \leq \alpha_c$$

$$K_{W(B)} = \left|K_{W(B)}\right|_{SB} + \left\{\left|\Delta K_{W(B)}\right|_{\alpha=0} + \frac{dK_{W(B)}}{d\alpha}(\alpha - \alpha_c)\right\}\frac{r/s}{0.5} \text{ for } \alpha_c \leq \alpha \leq \alpha_D \quad (32)$$

$$K_{W(B)} = \left|K_{W(B)}\right|_{SB} + \left\{\left|\Delta K_{W(B)}\right|_{\alpha=0} + \frac{dK_{W(B)}}{d\alpha}(\alpha_D - \alpha_c)\right\}\left(\frac{r/s}{0.5}\right) \text{ for } \alpha > \alpha_D$$

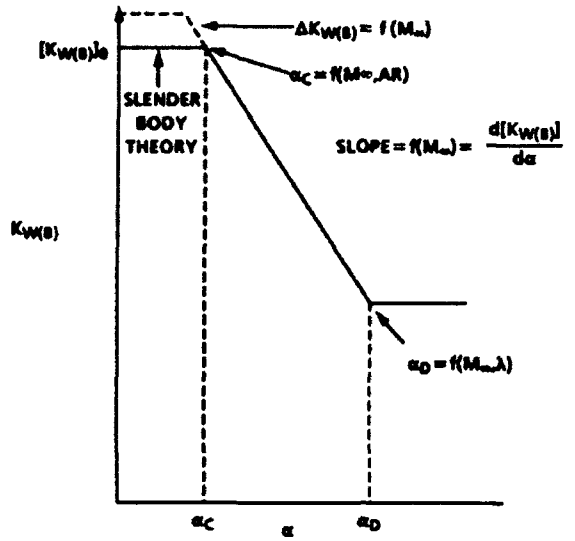

GENERAL EQUATION:

$$K_{W(B)} = \left[K_{W(B)}\right]_{SB} + \left[\Delta K_{W(B)}\right]_{\alpha=0} \frac{r/s}{0.5} \quad \text{for } \alpha \le \alpha_c$$

$$K_{W(B)} = \left[K_{W(B)}\right]_{SB} + \left[\Delta K_{W(B)}\right]_{\alpha=0} \frac{r/s}{0.5} + \left(\frac{dK_{W(B)}}{d\alpha}\right) \frac{(\alpha - \alpha_c)(r/s)}{0.5} \quad \text{for } \alpha_c \le \alpha \le \alpha_D$$

$$K_{W(B)} = \left[K_{W(B)}\right]_{SB} + \left\{\left[\Delta K_{W(B)}\right]_{\alpha=0} + \frac{dK_{W(B)}}{d\alpha}(\alpha_D - \alpha_c)\right\}\left(\frac{r/s}{0.5}\right) \quad \text{for } \alpha > \alpha_D$$

FIGURE 16. QUALITATIVE BEHAVIOR OF WING-BODY INTERFERENCE FACTOR AS A FUNCTION OF ANGLE OF ATTACK

The empirical corrections to $K_{W(B)}$ are also in a form that can be defined mathematically as opposed to a table lookup procedure. These equations for

$$\left[\Delta K_{W(B)}\right]_{\alpha=0}, \quad \frac{dK_{W(B)}}{d\alpha}, \quad \alpha_c, \text{ and } \alpha_D$$

are

$$\underline{\left[\Delta K_{W(B)}\right]_{\alpha=0}}$$

$$\left[\Delta K_{W(B)}\right]_{\alpha=0} = 0.22 \qquad \text{for } M_\infty \le 1.0$$

$$\left[\Delta K_{W(B)}\right]_{\alpha=0} = -0.44\left[M_\infty - 1.5\right] \qquad \text{for } 1.0 < M_\infty \le 1.5 \qquad (33)$$

$$\left[\Delta K_{W(B)}\right]_{\alpha=0} = 0 \qquad \text{for } M_\infty > 1.5$$

$$\underline{d\left[K_{W(B)}\right] / d\alpha}$$

$$\frac{d\left[K_{W(B)}\right]}{d\alpha} = -(0.00283M_{\infty} + 0.025) \tag{34}$$

$$\underline{\alpha_c}$$

$\underline{M \leq 2.0}$

$$\alpha_c = 12.5 - 1.06\,M_{\infty} - 2.59\,M_{\infty}^2 \qquad \text{for } AR \leq 0.5$$

$$\alpha_c = 12.5 - 6.25\,M_{\infty} \qquad \text{for } AR = 1.0$$

$$\alpha_c = 4.5 + 2.25\,M_{\infty} - 2.25\,M_{\infty}^2 \qquad \text{for } AR \geq 2.0 \tag{35}$$

$\underline{M_{\infty} > 2.0}$
$\alpha_c = 0$

$$\underline{\alpha_D}$$

$$\alpha_D = 33.3 - 8.19\,M_{\infty} + 0.82\,M_{\infty}^2 \qquad \text{for } \lambda = 0$$

$$\alpha_D = 25.3 - 6.62\,M_{\infty} + 0.66\,M_{\infty}^2 \qquad \text{for } \lambda = 1.0 \tag{36}$$

$$\alpha_D = [\alpha_D]_{\lambda=1.0} + \lambda\left[(\alpha_D)_{\lambda=0} - (\alpha_D)_{\lambda=1.0}\right] \qquad \text{for } 0 < \lambda < 1.0$$

The semiempirical model for $K_{B(W)}$ was also defined in terms of its slender body or linear theory value, plus a correction due to nonlinearities associated with angle of attack. The mathematical model for $K_{B(W)}$ was defined as[12]

$$K_{B(W)} = \left|K_{B(W)}\right|_{\substack{SB \\ LT}} + \frac{r/s}{0.5}\left\{\left|\Delta K_{B(W)}\right|_{\alpha=0} + \frac{d\left|K_{B(W)}\right|}{d\alpha}|\alpha|\right\} \tag{37}$$

Unfortunately, a mathematical model for $[\Delta K_{B(W)}]_{\alpha=0}$ and $d[K_{B(W)}]/d\alpha$ were difficult to define because of the variability of the constants as a function of the parameters of interest. As a result, a three-parameter table lookup for these two parameters is used in AP93 based on the data in Table 4. The parameters in the table lookup include M_∞, λ, and AR. Linear interpolation is used.

TABLE 4. DATA FOR BODY-WING NONLINEAR SEMIEMPIRCAL INTERFERENCE MODEL

Data for $[\Delta K_{B(W)}]_{\alpha=0}$

Aspect Ratio	Taper Ratio	Mach Number ≤0.6	0.8	1.2	1.5	2.0	2.5	3.0	3.5	≥4.5
≤0.25	0,0.5, 1.0	-0.1	-0.1	0.5	0.6	0.7	0.8	0.7	0.5	0.3
0.5	0.5	-0.28	-0.1	0.13	0.11	0.05	-0.02	-0.06	0	0
1.0	0.5	-0.26	-0.2	0.15	0.21	0.15	0	0	0	0
≥2.0	0.5	-0.13	-0.04	0.12	0.43	-0.16	0	0.37	-0.08	-0.16
0.5	0	-0.3	-0.06	0.26	0.28	0.17	0.12	0.14	0	0
≥2.0	0	-0.2	-0.1	0.12	0.52	0.12	0.15	0.22	-0.06	-0.22
0.5	1.0	-0.16	0.08	0.26	0.14	-0.12	0	-0.05	-0.10	0
≥2.0	1.0	-0.2	-0.1	0.12	0.45	-0.02	0.11	0.28	-0.17	-0.3

Data for $d[K_{B(W)}]/d\alpha$

Aspect Ratio	Taper Ratio	Mach Number ≤0.6	0.8	1.2	1.5	2.0	2.5	3.0	3.5	≥4.5
≤0.25	0,0.5, 1.0	0.018	0.013	-0.010	-0.023	-0.013	-0.022	-0.031	-0.025	-0.031
0.5	0.5	0.019	0.010	-0.008	-0.010	-0.013	-0.013	-0.013	-0.012	-0.012
1.0	0.5	0.013	0.010	-0.007	-0.013	-0.020	-0.017	-0.012	-0.012	-0.012
≥2.0	0.5	0.010	0.011	0	-0.013	-0.010	-0.017	-0.040	-0.012	-0.012
0.5	0	0.033	0.022	0	-0.007	-0.010	-0.008	-0.014	-0.012	-0.012
≥2.0	0	0.010	0.010	-0.007	-0.020	-0.011	-0.020	-0.023	-0.012	-0.012
0.5	1.0	0.019	0	-0.019	-0.010	-0.007	-0.013	-0.014	-0.012	-0.012
≥2.0	1.0	0.010	0.01	-0.007	-0.017	0	-0.017	-0.026	-0.012	-0.012

In Equations 32 and 36, the factor

$$\frac{r/s}{0.5}$$

appears. This is because the database of Reference 36 is based on $r/s = 0.5$, and Reference 41 indicates the aerodynamics vary linearly with r/s. This assumption is inherent in the semiempirical models for $K_{W(B)}$ and $K_{B(W)}$.

In examining cases where r/s is small, it was found that at high angles of attack, the wing-alone solution was not recovered properly through the Equations 32 and 37 process. To remedy this situation, the AP93 nonlinear interference factors were blended into those predicted by slender-body or linear theory as r/s became small. The specific equations used to do this are

For $r/s \geq 0.25$

$$K_{W(B)} = \left| K_{W(B)} \right|_{AP93}$$

$$K_{B(W)} = \left| K_{B(W)} \right|_{AP93} \tag{38a}$$

For $0.05 < r/s < 0.25$

$$K_{W(B)} = \left| K_{W(B)} \right|_{SBT} - \left(\left| K_{W(B)} \right|_{SBT} - \left| K_{W(B)} \right|_{AP93} \right) (r/s - 0.05)/0.2$$

$$K_{B(W)} = \left| K_{B(W)} \right|_{\substack{SBT \\ LT}} - \left(\left| K_{B(W)} \right|_{\substack{SBT \\ LT}} - \left| K_{B(W)} \right|_{AP93} \right) (r/s - 0.05)/0.2 \tag{38b}$$

For $r/s \leq 0.05$

$$K_{W(B)} = \left| K_{W(B)} \right|_{SBT} ; K_{B(W)} = \left| K_{B(W)} \right|_{\substack{SBT \\ LT}} \tag{38c}$$

In essence, the model represented by Equations 38a through 38c uses the nonlinear interference factors for r/s values greater than 0.25; they use a blend of slender-body or linear theory and the nonlinear values of interference factors for r/s values between 0.05 and 0.25. They also use the slender-body or linear theory values for r/s values less than 0.05. Hence, when the body vanishes ($r/s = 0$), the wing-alone solution will be automatically recovered in a smoother and more accurate way.

Figure 17 is an example of the normal force on the wing in the presence of the body and the normal force on the body in the presence of the wing using the AP93 theory, the AP81 theory, and compared to experimental data. Note that

$$C_{N_{W(B)}} = C_{N_W} K_{W(B)}$$

$$C_{N_{B(W)}} = C_{N_W} K_{B(W)} \tag{39}$$

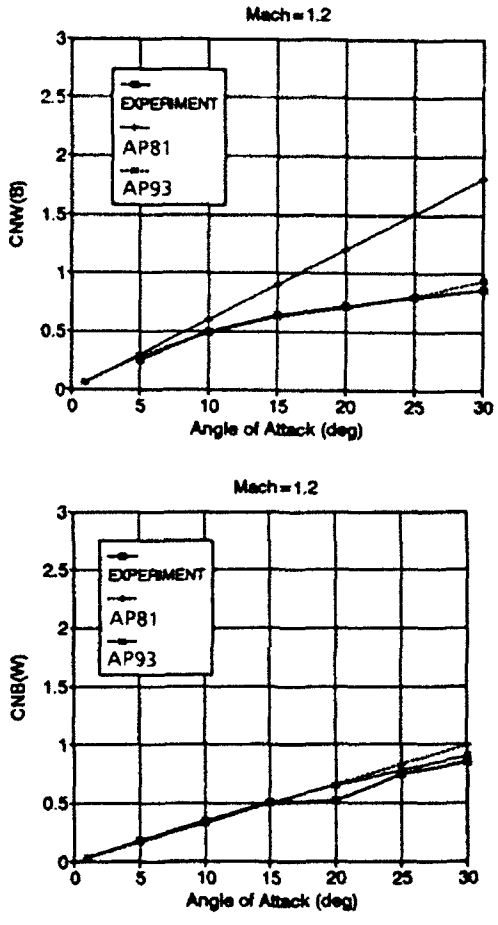

FIGURE 17. WING-BODY AND BODY-WING INTERFERENCE AS A FUNCTION OF α (AR = 2.0, λ = 0, M_∞ = 1.2)

Hence, Figure 17 is actually a representation of the normal-force coefficient on the wing and additional normal force on the body due to the wing. Thus, Equation 39 is a representation of the accuracy of not only $K_{W(B)}$ and $K_{B(W)}$, but C_{N_W} in conjunction with the interference factors. This is a more true indication of the accuracy of the code, because there are actually two of the component force terms that make up Equation 39. As seen in Figure 17, the AP93 methodology is clearly superior to the AP81 theory as angle of attack increases.

The center of pressure of the new value of normal force of the wing in the presence of the body estimated by Equation 32 is assumed to remain at the values of the wing-alone solution of AP93 given by Equation 30. The center of pressure of the additional lift on the body due to the presence of the wing is estimated the same as in AP81, which is either slender-body or linearized theory. These values are modified for short afterbodies according to Reference 3.

In exercising the AP93 on missile configurations in the transonic speed regime ($0.6 \leq M \leq 2.0$), it was found that some of the nonlinear lift associated with small aspect ratio fins ($AR \leq 1.4$) was lost due to shock-wave formation. A certain amount of linear lift loss was accounted for from an empirical approach in the AP81. This appeared to be satisfactory for the larger aspect ratio fins, where the nonlinear normal-force term with angle of attack was negative. However, when the fins have a positive nonlinear normal force due to angle of attack, some of this force appears to be lost with shock waves. This loss was estimated empirically as a function of Mach number and angle of attack for a wing that had an area-to-body reference area of about one. These data for ΔC_N losses due to compressibility effects are given in Table 5. A two parameter linear interpolation is made from Table 5 for a given M_∞ and α to compute ΔC_N. ΔC_N is further degraded for taper ratio for values of $\lambda < 0.5$. The specific equations for ΔC_N are

$$\Delta C_{N_{B(W)}} = -\left(\Delta C_N\right)\frac{A_W}{A_{ref}} \quad \text{for } \lambda \geq 0.5$$

$$\Delta C_{N_{B(W)}} = -\left(\Delta C_N\right)\left(\frac{A_W}{A_{ref}}\right)\left(\frac{\lambda}{0.5}\right) \quad \text{for } 0.1 \leq \lambda \leq 0.5 \tag{40}$$

$$\Delta C_{N_{B(W)}} = -0.2\,\Delta C_N\left(\frac{A_W}{A_{ref}}\right) \quad \text{for } \lambda \leq 0.1$$

TABLE 5. LOSS OF WING NONLINEAR NORMAL FORCE DUE TO SHOCK-WAVE EFFECTS IN TRANSONIC FLOW
$|\alpha + \delta|$ DEG

M_∞	0	5	10	15	20	25	30	35	≥40
≤0.4	0.0000	0.0000	0.0000	0.0000	0.0000	0.0000	0.0000	0.0000	0.0000
0.6	0.0000	0.0000	0.0000	0.0000	-0.0220	-0.2060	-0.6890	-0.9500	-1.300
0.8	0.0000	0.0000	0.0000	0.0000	-0.0531	-0.2200	-0.7100	-1.010	-1.400
1.2	0.0000	0.0000	-0.0093	-0.0293	-0.1651	-0.4167	-0.7629	-1.070	-1.500
1.5	0.0000	0.0000	-0.0653	-0.1111	-0.1556	-0.4444	-0.7000	-1.070	-1.500
2.0	0.0000	0.0000	-0.0076	-0.0376	-0.1502	-0.1142	-0.0951	-0.0700	-0.0500
≥2.5	0.0000	0.0000	0.0000	0.0000	0.0000	0.0000	0.0000	0.0000	0.0000

2.9 NONLINEAR WING-BODY INTERFERENCE FACTOR DUE TO CONTROL DEFLECTION

The nonlinear methodology for computing the wing-body interference due to control deflection has not been presented before. As a result, a more detailed discussion of this effort will be presented in contrast to the other new methods, which were only briefly summarized.

Initially, it was planned to use slender-body theory for the interference factors $k_{W(B)}$ and $k_{B(W)}$, as currently done in AP81. This plan was based on Reference 12 results comparing computations (using Equation 31 where all the nonlinearities are included) with experimental data at $\delta = 0$ for both body-tail and body-wing-tail or body-dorsal-tail configurations. These comparisons were good and seemed to indicate this new technology to be superior to existing engineering approaches. However, when results were examined for configurations that had control deflections on either the aft or forward lifting surface, they were found to not be as good as desired. This led to the conclusion that nonlinear interference factors due to control deflection were also required to improve the performance of AP93 when compared to experimental data.

To address this problem, the database of Reference 36 was once again employed. An attempt was made to estimate $k_{W(B)}$ based on the component measurements of this database. During these measurements, only one fin was deflected at a given set of conditions (α, M_∞, ϕ, fin geometry). Referring to Equation 31, the normal-force coefficient component resulting from a control deflection of a lifting surface is

$$\Delta C_{N_{W(B)}} = k_{W(B)} \left(C_{N_\alpha} \right)_W \delta_W \tag{41}$$

The additional normal-force coefficient on the body due to control deflection is

$$\Delta C_{N_{B(W)}} = k_{B(W)} \left(C_{N_\alpha} \right)_W \delta_W \tag{42}$$

In principal, because the database of Reference 36 was taken from wing and body independently where they were close enough to each other to get the interference effects, $k_{W(B)}$ and $k_{B(W)}$ can be determined. This was attempted with mixed success. Values of single-fin control deflection normal-force coefficients were obtained for several conditions. The $\Delta C_{N_{W(B)}}$ of Equation 41 could be readily determined by multiplying the values in the wind tunnel data by two (since only one fin was deflected) and subtracting these values for the $\Delta C_{N_{W(B)}}$ at $\delta = 0$.

It is suspected that there are several reasons for the mixed success of this approach. First of all, the area of any one fin that was deflected varied in physical size from 0.0312 to 0.0078 ft^2. This compared to a body cross-section area of 0.0490 ft^2

and a body planform area in the crossflow plane of approximately 0.7 ft^2. In other words, at zero angle of attack, where body lift and wing lift, due to angle of attack are zero, a reasonable value for the normal-force coefficient resulting from control deflection can be obtained. However, as angle of attack increases, the planform area of one fin is anywhere from 1 to 4 percent of the body planform area and it makes it difficult to get consistently accurate values resulting from control deflection. This is due to the substraction process involved in obtaining the ΔC_W due to canard deflection and the fact that there is a certain amount of experimental error in each of the measurements.

Second of all, based on comparisons with data of actual missile configurations, the effect of control deflection can increase or decrease with angle of attack, depending on the Mach number. At low supersonic and subsonic Mach numbers, the effectiveness tends to get smaller with increasing angle of attack, whereas the compressibility effects at high Mach numbers cause the opposite effect to occur. Therefore, the smaller the effect from control deflection, the harder it is to separate it out from that caused by angle of attack.

After several weeks of reducing data and attempting to develop an empirical model, it was concluded that the inconsistency of results were such that a different approach for developing a nonlinear model of interference effects due to control deflection was desired. The approach taken was to use the AP93 with the nonlinearities of wing-alone, wing-body, and body-wing interference effects due to angle of attack included, use the slender-body estimates of $k_{W(B)}$ and $k_{B(W)}$ for control deflection, and derive empirical modifications to $k_{W(B)}$ based on numerical experiments compared to actual missile data. Because $k_{W(B)}$ appears in the vortex lift on the tail due to canard or wing shed vortices, the numerical experiments were conducted with canard body-tail configurations

Referring to Equation 31, the vortex normal-force coefficient on the tail is[41]

$$C_{N_{T(V)}} = \frac{\left(C_{N_x}\right)_W \left(C_{N_x}\right)_T \left| K_{W(B)} \sin\alpha + F\, k_{W(B)} \sin\delta_W \right| i\,(s_r - r_T)\, A_W}{2\pi (AR)_T \left(f_W - r_W\right) A_{ref}} \tag{43}$$

Equation 43 has a factor F that multiplies the term due to control deflection in the wing-tail vortex lift. This factor is needed in addition to the nonlinearity for $k_{W(B)}$, partly because the negative afterbody lift due to control deflection is not presently modeled in either AP81 or AP93. This term is defined as

$$C_{N_{B(V)}} = \frac{-4\Gamma}{A_W V_\infty} \left| \frac{f_W^2 - r_W^2}{f_W} - f_T + \frac{r_T^2}{\sqrt{f_T^2 + h_T^2}} \right| \tag{44}$$

where

$$\frac{\Gamma}{V_\infty} = \frac{K_{W(B)} \sin\alpha + k_{W(B)} \sin\delta_W}{4\,(f_W - r_W)} \left(C_{N_x}\right)_W A_W$$

The main reason this term was not included in the AP81 code was that it required an estimate of f_T, which is the position of the canard shed vortex at the tail. Also, Reference 40 indicated this term was generally much smaller than that computed by Equation 43. To account for this term, a vortex tracking algorithm is needed or an empirical correction to the term in Equation 43. For angles of attack much greater than 25 or 30 deg, a vortex tracking algorithm may be needed. However, up to α of about 30 deg, an attempt will be made to develop a nonlinear model of interference effects resulting from control deflection by defining $k_{W(B)}$ as a function of angle of attack and Mach number and F as a function of Mach number.

Using References 42 through 44 and Reference 40 for low Mach number, a semiempirical nonlinear model for $k_{W(B)}$ and the parameter F were derived from numerical experiments. The mathematical model for $k_{W(B)}$ is based on slender-body theory similar to $k_{W(B)}$ and $k_{B(W)}$ and modified for angle of attack or control deflection. In general, it was found that

$$k_{W(B)} = C_1(M) \left|k_{W(B)}\right|_{SB} + C_2\left(|\alpha_W|, M_\infty\right)$$

$$F = C_3\left(M, |\alpha_W|\right) \tag{45}$$

More specifically, $k_{W(B)}$, C_1, C_2, and F are defined in Figure 18 for Mach numbers where data are available. For Mach numbers less than 0.8 and greater than 4.6, the equations derived for those conditions have been used. The current method for using the empirical estimate for $k_{W(B)}$ from Figure 1 is to linearly interpolate between Mach numbers for a given value of α, δ, and M_∞.

In examining the model in Figure 18, it has a lot of similarities to the nonlinear $K_{W(B)}$ model already discussed; i.e., at low angle of attack, slender-body theory gives a reasonable estimate of $k_{W(B)}$. However, as angle of attack increases, $k_{W(B)}$ decreases for low to supersonic Mach numbers. For higher supersonic Mach numbers, $k_{W(B)}$ actually increases at higher angles of attack, presumably due to compressibility effects. Also, for low angles of attack, a value of F near one is found for the vortex lift model, indicating again reasonable accuracy using the theory in Reference 41. However, as angle of attack is increased, F increases above one for many Mach numbers. That is, Equation 43 gives values of $C_{N_{T(V)}}$ too small due to control deflection of a forward surface. As already mentioned, this is most probably due to the neglect of the effect on the afterbody (Equation 44), which becomes more appreciable percentage wise compared to the Equation 43 results, as angle of attack increases.

$\underline{M \leq .8}$

If $|\alpha_w| \leq 24.0 \rightarrow k_{w(B)} = 1.4[k_{w(B)}]_{SB}$
If $|\alpha_w| > 24.0 \rightarrow k_{w(B)} = 1.4\,[.000794\,|\alpha_w|^2 - .0933\,|\alpha_w| + 2.71]$
$F = 1.1$

$\underline{M = 1.1}$

If $|\alpha_w| \leq 15.0 \rightarrow k_{w(B)} = 1.3[k_{w(B)}]_{SB}$
If $|\alpha_w| > 15.0 \rightarrow k_{w(B)} = 1.3\,[.00087\,|\alpha_w|^2 - .0825\,|\alpha_w| + 1.98]$
$F = 1.1$

$\underline{M = 1.5}$

If $|\alpha_w| \leq 10.0 \rightarrow k_{w(B)} = .9[k_{w(B)}]_{SB}$
If $|\alpha_w| > 10.0 \rightarrow k_{w(B)} = .9[k_{w(B)}]_{SB} - .015[|\alpha_w| - 10.0]$
If $|\alpha_w| \leq 20.0 \rightarrow F = .8$
If $|\alpha_w| > 20.0 \rightarrow F = .8 + .10[|\alpha_w| - 20.0]$

$\underline{M = 2.0}$

If $|\alpha_w| \leq 10.0 \rightarrow k_{w(B)} = .9[k_{w(B)}]_{SB}$
If $|\alpha_w| > 10.0 \rightarrow k_{w(B)} = .9[k_{w(B)}]_{SB} - .005[|\alpha_w| - 10.0]$
If $|\alpha_w| \leq 20.0 \rightarrow F = .8$
If $|\alpha_w| > 20.0 \rightarrow F = .8 + .17[|\alpha_w| - 20.0]$

$\underline{M = 2.3}$

If $|\alpha_w| \leq 20.0 \rightarrow k_{w(B)} = .9[k_{w(B)}]_{SB}$
If $|\alpha_w| > 20.0 \rightarrow k_{w(B)} = .9[k_{w(B)}]_{SB} - .005[|\alpha_w| - 20.0]$
If $|\alpha_w| \leq 30.0 \rightarrow F = .9$
If $|\alpha_w| > 30.0 \rightarrow F = .9 + .15[|\alpha_w| - 30.0]$

$\underline{M = 2.87}$

If $|\alpha_w| \leq 20.0 \rightarrow k_{w(B)} = .9[k_{w(B)}]_{SB}$
If $|\alpha_w| > 20.0 \rightarrow k_{w(B)} = .9[k_{w(B)}]_{SB} - .005[|\alpha_w| - 20.0]$
If $|\alpha_w| \leq 30.0 \rightarrow F = .9$
If $|\alpha_w| > 30.0 \rightarrow F = .9 + .17[|\alpha_w| - 30.0]$

$\underline{M = 3.95}$

$k_{w(B)} = .8[k_{w(B)}]_{SB}$
If $|\alpha_w| \leq 40.0 \rightarrow F = 0.9$
If $|\alpha_w| > 40.0 \rightarrow F = 0.9 + .4[|\alpha_w| - 40.0]$

$\underline{M \geq 4.6}$

If $|\alpha_w| \leq 20.0 \rightarrow k_{w(B)} = 0.75[k_{w(B)}]_{SB}$
If $|\alpha_w| > 20.0 \rightarrow k_{w(B)} = 0.75[k_{w(B)}]_{SB} + .01[|\alpha_w| - 20.0]$
If $|\alpha_w| \leq 35.0 \rightarrow F = .9$
If $|\alpha_w| > 35.0 \rightarrow F = .9 + .3[|\alpha_w| - 35.0]$

where $\alpha_w = \alpha + \delta$

FIGURE 18. NONLINEAR WING-BODY INTERFERENCE MODEL DUE TO CONTROL DEFLECTION

3.0 SUMMARY OF METHODS IN AP93

3.1 AP81 METHODS USED IN AP93

In picking the methods to carry forward into the AP93 code from the AP81 version, several criteria were considered: (1) is the method needed for performing aerodynamic computations, (2) have the methods been used by users or has it been basically taking up computer storage and time with little return on the investment, (3) has the AP81 method been replaced by something better in AP93, and (4) is the accuracy of the method acceptable for most engineering purposes. With these criteria in mind, a summary of the methods of AP81 that will be retained in AP93 will be given. These methods have all been well documented in References 2 through 8 so the interested reader is referred to those references for details of the methods. A brief discussion will be given in this report.

Most of the body-alone methods of AP81 will remain in AP93. The nose wave drag is currently computed at low supersonic Mach numbers by combining MNT with second-order Van Dyke.[2,46] This method, first introduced in Reference 2, remains the only engineering approach to get accurate pressure distributions and wave drag estimates on blunt bodies at low supersonic Mach numbers from $M_\infty = 1.2$ to around $M_\infty = 2$ to 3 (chosen by the user); the SOSET[47,48] combined with the improved MNT discussed earlier is used for wave drag up to about $M_\infty = 6$. Above that Mach number, the basic same approach is used but real-gas and aeroheating effects are also considered, which slightly increases the run time per Mach number.[9,10,11] At transonic speeds, the wave drag is computed by the method of Wu and Aoyoma[49] on the boattail and by a semiempirical table look-up using data generated by a Euler code[50] for the nose. Of course, no pressure drag is assumed for subsonic flow.

The skin-friction drag for both the body and wings is computed by the method of Van Driest.[51] However, options for turbulent and laminar flow are offered as discussed previously. The empirical base drag approach is retained[2] but replaced by the improved method in Section 2.0. The linearized lift and center-of-pressure estimates developed for the body alone will also be retained. They are determined by either SOSET,[47,48] Tsien first-order crossflow,[52] semiempirical,[53] Wu and Aoyoma,[49] or empirical,[2] depending on the Mach number regions. The only modification being made to this methodology is the center-of-pressure shift defined in Section 2.0. The nonlinear normal-force and center-of-pressure methods of Allen and Perkins[34] will be retained but extended as discussed in Section 2.0.

Concerning the wing and interference aerodynamic computations, all the static aerodynamic methods of References 3 and 7 will be retained. For normal-force and center-of-pressure computation, this includes lifting surface theory in subsonic flow, 3-D thin wing theory (3DTWT) in supersonic flow,[54] and an option for shock expansion strip theory[48] or 3DTWT in high supersonic or hypersonic flow.[55,56,57] For interference aerodynamics, this includes slender-body theory and linear theory,[41] and line vortex theory[41] for wing-tail interference. There is also a term estimated on the trailing edge of the fins if they are blunt, which contributes to fin base drag.[3]

Concerning dynamic derivatives, only the methods discussed in References 2 (for the body alone) and 5 (for the wing alone) will be retained. These methods include empirical for the body alone[58] and either lifting surface,[54] empirical,[59] thin wing theory,[60-66] or strip theory[48] for the wings. The main reason for decreasing the emphasis on dynamic derivatives is that they do not appear to be as important to the end users of the code as they were in the 1970's when the code was first started. This is because the code is primarily used in trim or particle aerodynamic models where static aerodynamics and not dynamic derivatives are needed. Also, guidance laws are more robust today than 20 years ago, and this decreases the need for accurate dynamic derivatives.

3.2 AP93 OVERALL METHODS SUMMARY

The methods used for computing forces and moments in the AP93 are summarized in Tables 6, 7, and 8. Note that the code can now be useful for computing aerothermal information as well as forces and moments. This means the uses of the code are now for

- Providing inputs to flight dynamics models that estimate range or miss distance
- Assessing static stability of various missile configuration
- Assessing various design parameters in terms of optimizing the configuration
- Assessing structural integrity using the loads portion of the code
- Assessing aerothermal aspects of a design using the heat transfer coefficients at high Mach numbers

As seen in Tables 6, 7, and 8, there are many methods that go into the overall makeup of a component buildup code, such as the APC. The past 20 years have shown that this type of code can be quite useful when used in preliminary or conceptual design studies to provide down selection on many configuration alternatives in a fairly accurate and cost-effective manner.

TABLE 6. AP93 METHODS FOR BODY-ALONE AERODYNAMICS

Component/ Mach Number Region	Subsonic $M_\infty < 0.8$	Transonic $0.8 \leq M_\infty < 1.2$	Low Supersonic $1.2 \leq M_\infty \leq 2.4$	High Supersonic $2.4 < M_\infty \leq 6.0$	Hypersonic $M_\infty > 6.0$
Nose Wave Drag	–	Semiempirical based on Euler Solutions	Second-Order Van Dyke plus MNT	SOSET plus IMNT	SOSET plus IMNT Modified for Real Gases
Boattail or Flare Wave Drag	–	Wu and Aoyoma	Second-Order Van Dyke	SOSET	SOSET for Real Gases
Skin Friction Drag	Van Driest II				
Base Drag	Improved Empirical Method				
Aeroheating Information	–	–	–	–	SOSET plus IMNT for Real Gases
Inviscid Lift and Pitching Moment	Empirical	Semiempirical based on Euler Solutions	Tsien First-Order Crossflow	SOSET	SOSET for Real Gases
Viscous Lift and Pitch Moment	Improved Allen and Perkins Crossflow				

TABLE 7. AP93 METHODS FOR WING-ALONE AND INTERFERENCE AERODYNAMICS

Component/ Mach Number Region	Subsonic $M_\infty < 0.8$	Transonic $0.8 \le M_\infty < 1.2$	Low Supersonic $1.2 \le M_\infty \le 2.4$	High Supersonic $2.4 < M_\infty \le 6.0$	Hypersonic $M_\infty > 6.0$
Wave Drag	–	Empirical	Linear Theory plus MNT	Shock Expansion (SE) plus MNT Along Strips	SE plus MNT for Real Gases Along Strips
Skin Friction Drag	Van Driest II				
Trailing Edge Separation Drag	Empirical				
Body Base Pressure Caused by Tail Fins	Improved Empirical				
Inviscid Lift and Pitching Moment • Linear • Nonlinear	Lifting Surface Theory Empirical	Empirical Empirical	3DTWT Empirical	3DTWT or SE Empirical	3DTWT or SE Empirical
Wing-Body, Body-Wing Interference • Linear • Nonlinear	Slender Body Theory or Linear Theory Modified for Short Afterbodies Empirical				
Wing-Body Interference due to δ • Linear • Nonlinear	Slender Body Theory Empirical				
Wing Tail Interference	Line Vortex Theory with Empirical Modifications for $k_{W(B)}$ Term and Nonlinearities				
Aeroheating	None Present				SE plus MNT for Real Gases

TABLE 8. AP93 METHODS FOR DYNAMIC DERIVATIVES

Component/Mach Number Region	Subsonic $M_\infty < 0.8$	Transonic $0.8 \le M_\infty < 1.2$	Low Supersonic $1.2 \le M_\infty \le 2.4$	High Supersonic $2.4 < M_\infty \le 6.0$	Hypersonic $M_\infty > 6.0$
Body Alone	Empirical				
Wing and Interference Roll Damping Moment	Lifting Surface Theory	Empirical	Linear Thin Wing Theory	Linear Thin Wing Theory or Strip Theory	
Wing Magnus Moment	Assumed Zero				
Wing and Interference Pitch Damping Moment	Lifting Surface Theory	Empirical	Linear Thin Wing Theory	Linear Thin Wing Theory or Strip Theory	

4.0 RESULTS AND DISCUSSION

Some results of component aerodynamics or heat transfer coefficients have already been presented during the summary of the new methods section. This section of the report will therefore focus on validation of the overall AP93 code in terms of complete missile configurations where wind tunnel data are available. Where other state-of-the-art (SOTA) aerodynamic codes have been used, these results will also be shown for comparison of the AP93. Unfortunately, funding will not permit investigating another SOTA code's performance on the example configurations unless the results are already available from calculations performed previously.

The first case considered is the body-alone configuration of Reference 31. While the base pressure information was used in the base-drag methodology for $M \leq 2.0$, no stability and control information was used in the improved body-alone method. The database used was primarily that of Reference 36. Hence, using the AP93 code on a different set of data will help validate the code's improved capability for bodies alone. Only one case is chosen from the many presented in Reference 31. The case selected is one that has a 25-percent blunt nose, is 3.58 calibers long, and has a 10-caliber afterbody. The configuration is shown in Figure 19a.

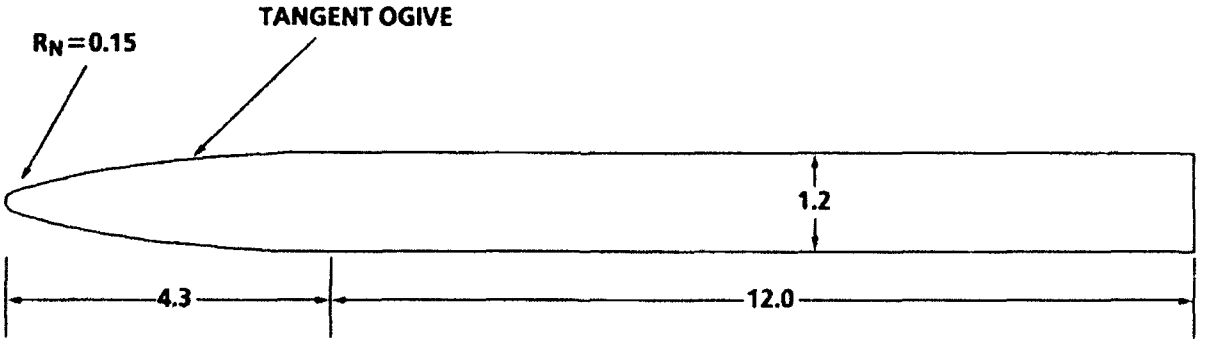

FIGURE 19a. BODY-ALONE CONFIGURATION USED IN VALIDATION PROCESS[31]

Results of the comparisons of the AP93, AP81, and experiment for the configuration of Figure 19 are given in Figures 19a through 19g in terms of normal- and axial-force coefficients and center of pressure. Results are given for Mach numbers of 0.8, 1.2, 1.5, 2.0, 3.0, and 4.0. It should be pointed out that for Mach numbers of 2.0 and greater, only the forebody axial-force coefficient is given. The reason is that no boundary layer trip was used in any of the tests, and the flow is laminar over the entire body at these Mach numbers. This means the base pressure computations could have an error built in because of the assumption of a turbulent boundary layer at the base. On the other hand, for the transonic flow experiments, the Reynolds number was high enough to ensure turbulent flow at the base without a trip. Thus, total axial-force coefficients are shown in the comparison.

In viewing the comparison of AP93 and AP81 to the data in Reference 31, it is shown that AP93 indicates improvement over AP81 at just about all conditions considered and at all Mach numbers. Experimental data were only available for angles of attack of about 15 deg, so the theoretical computations were only shown up to 20 deg. The only area where the AP93 code appears to need some improvement is in the estimation of axial force with angle of attack. The AP93 code does estimate base pressure as a function of α and has a simplified model for skin friction as well at angles of attack up to 15 deg. For supersonic flow, the wave drag is also computed as a function of α. However, it does not take into account separation regions on the body leeside, which lower the skin friction or even make it negative on some portions of the body, thus negating some of the increased base drag with angle of attack. An example of this is Figure 19b, where the base pressure and skin friction increases with angle of attack are partially offset by the flow separation on the body leeside, which is not accounted for. Other than this problem, the AP93 code appears to give improved results for the body alone over the AP81 code.

A second case considered is the canard-body-tail case shown in Figure 20a, which was taken from Reference 67. The configuration is somewhat of an extreme case for the body-alone aerodynamics because it is 100-percent blunt and is about 22.3 calibers long. The configuration tested in the wind tunnel has hangars attached to the body for aircraft carry and launch. However, tests were conducted with and without the hangars, and the results showed that C_N and C_M were unchanged but C_A was increased. The AP93 and AP81 theoretical computations are compared to the corrected data of Reference 67, where the hangars have been omitted. Results are given in Figures 20b through 20s for Mach numbers of 0.8, 1.2, 2.1, 2.86, 3.95, and 4.63 and at canard deflections of 0, 10, and 20 deg. Examining Figures 20b through 20s, it is shown that AP93 gives good agreement with experimental data at just about all conditions. Significant improvements of the AP93 over the AP81 are seen at the lower Mach numbers and at the higher Mach number, higher angle-of-attack conditions.

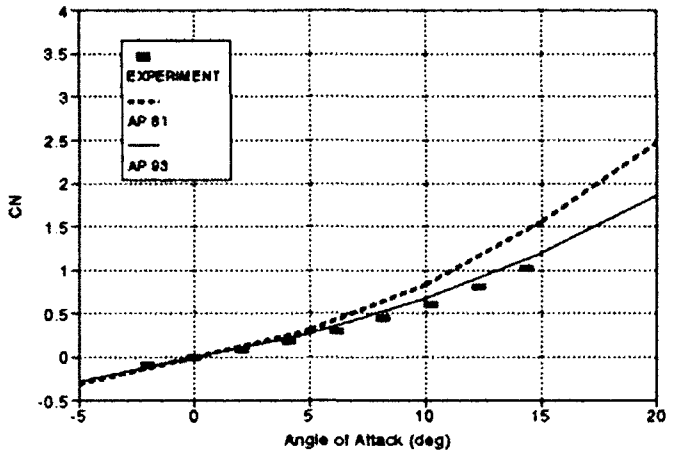

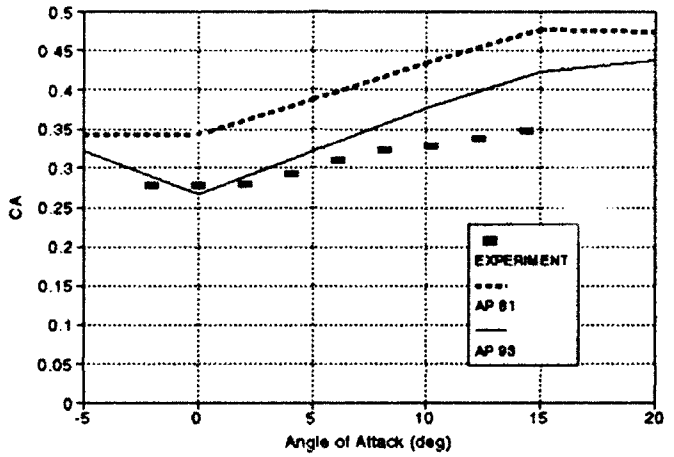

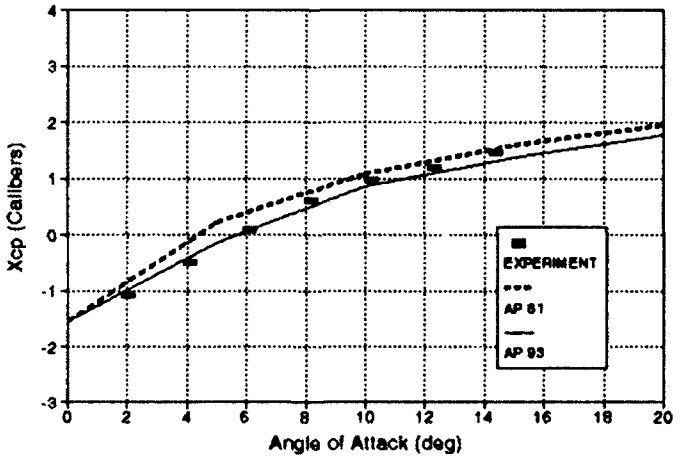

b. $M_\infty = 0.8$

FIGURE 19. NORMAL- AND AXIAL-FORCE COEFFICIENTS AND CENTER OF PRESSURE AS A FUNCTION OF ANGLE OF ATTACK FOR CONFIGURATION OF FIGURE 19a

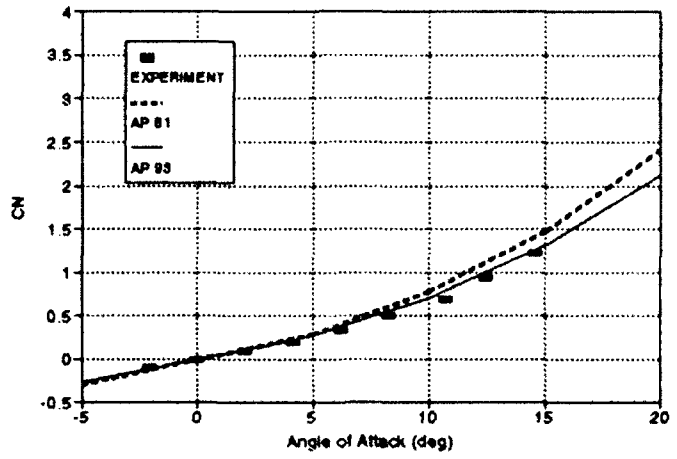

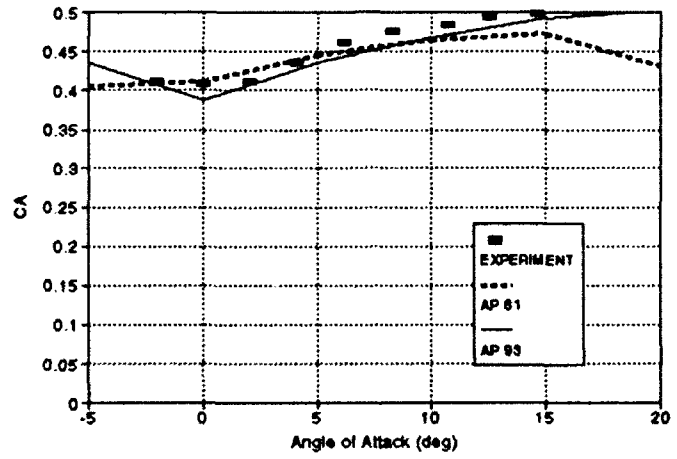

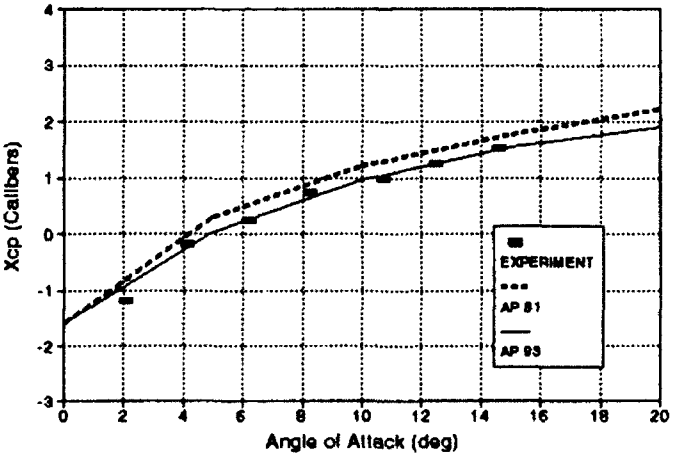

c. $M_\infty = 1.2$

FIGURE 19. NORMAL- AND AXIAL-FORCE COEFFICIENTS AND CENTER OF PRESSURE AS A FUNCTION OF ANGLE OF ATTACK FOR CONFIGURATION OF FIGURE 19a (CONTINUED)

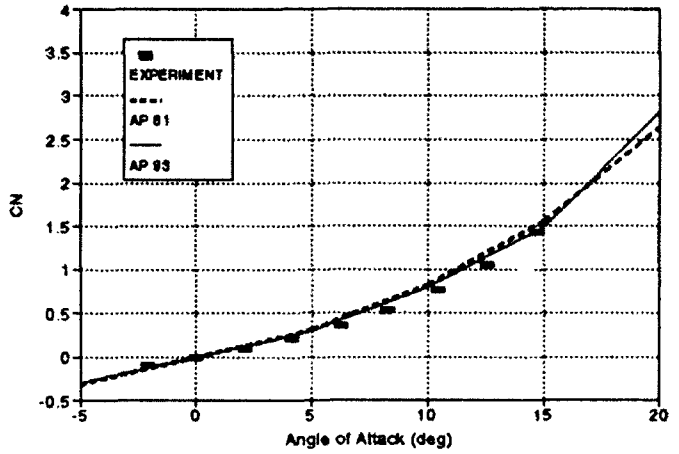

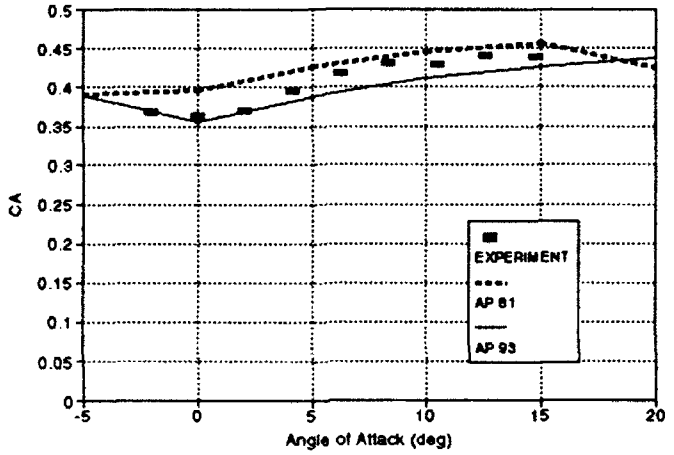

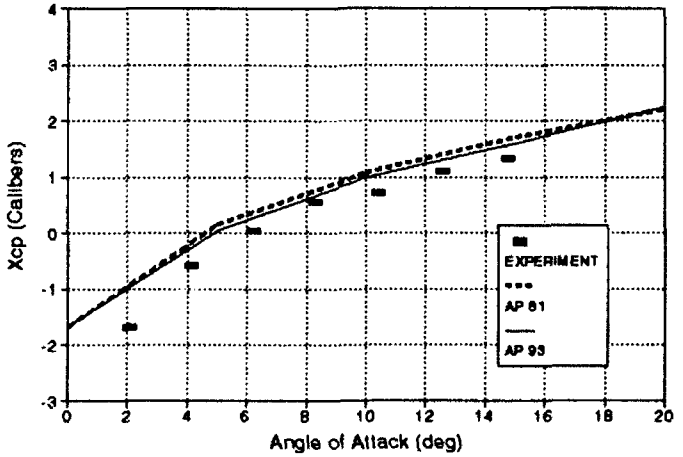

d. $M_\infty = 1.5$

FIGURE 19. NORMAL- AND AXIAL-FORCE COEFFICIENTS AND CENTER OF PRESSURE AS A FUNCTION OF ANGLE OF ATTACK FOR CONFIGURATION OF FIGURE 19a (CONTINUED)

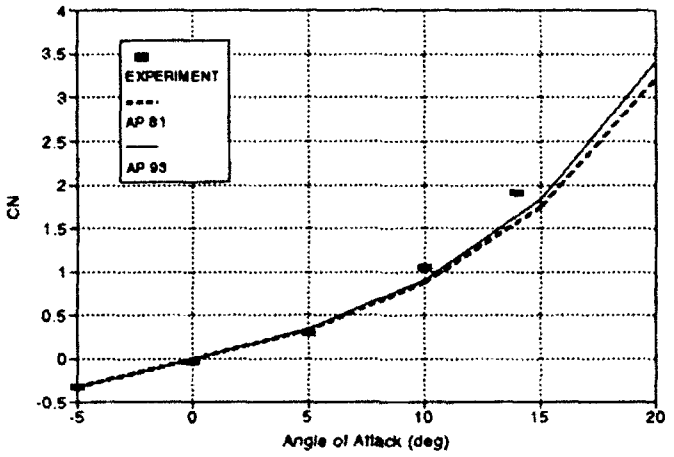

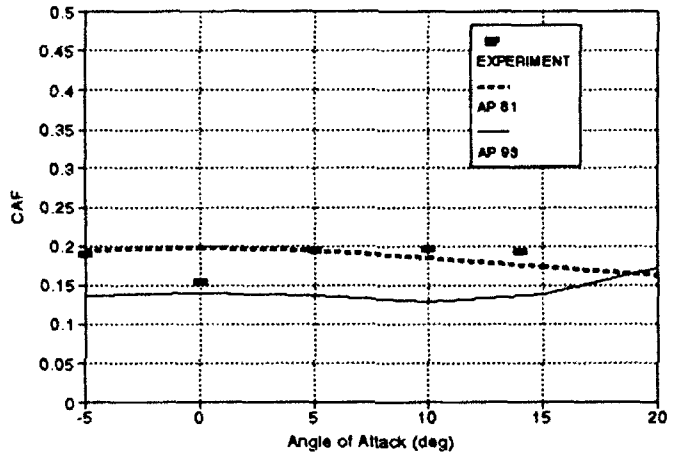

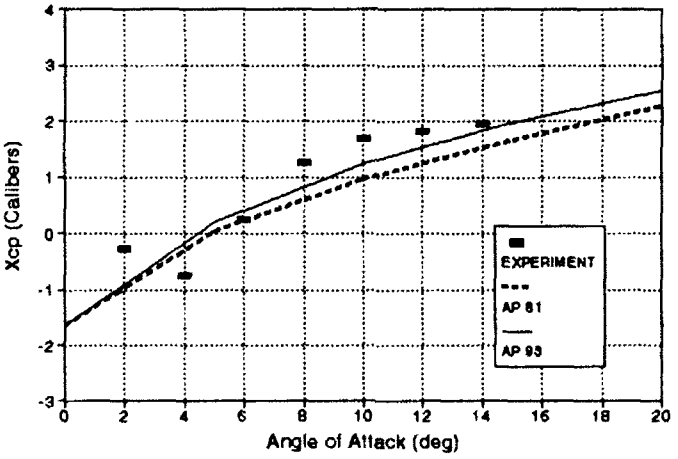

e. $M_\infty = 2.0$

FIGURE 19. NORMAL- AND AXIAL-FORCE COEFFICIENTS AND CENTER OF PRESSURE AS A FUNCTION OF ANGLE OF ATTACK FOR CONFIGURATION OF FIGURE 19a (CONTINUED)

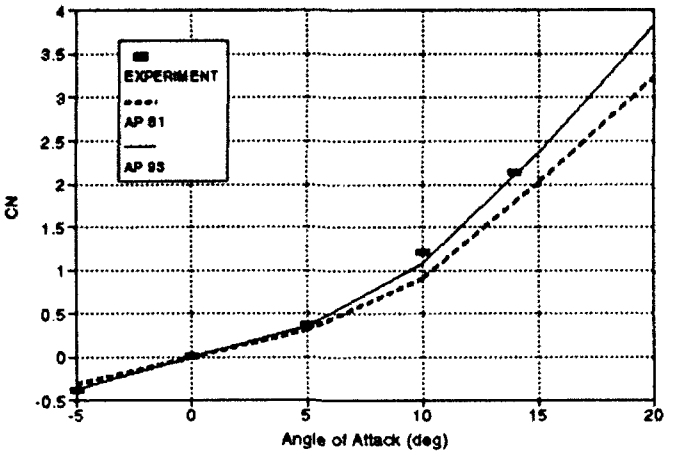

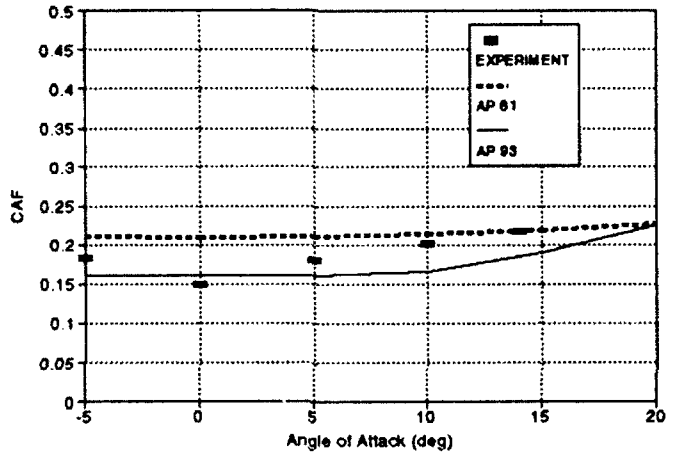

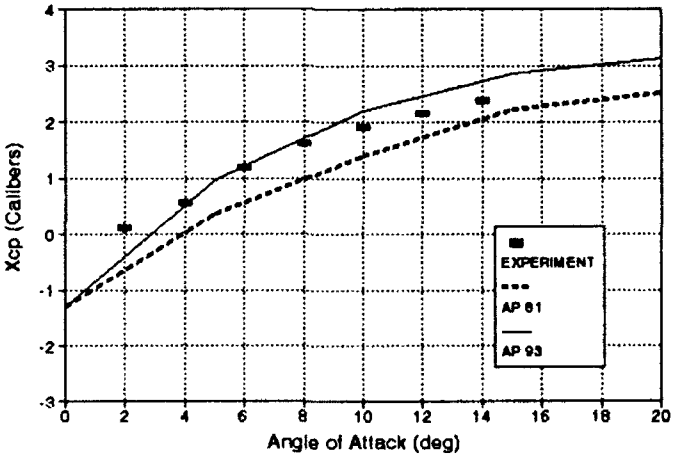

f. $M_\infty = 3.0$

FIGURE 19. NORMAL- AND AXIAL-FORCE COEFFICIENTS AND CENTER OF PRESSURE AS A FUNCTION OF ANGLE OF ATTACK FOR CONFIGURATION OF FIGURE 19a (CONTINUED)

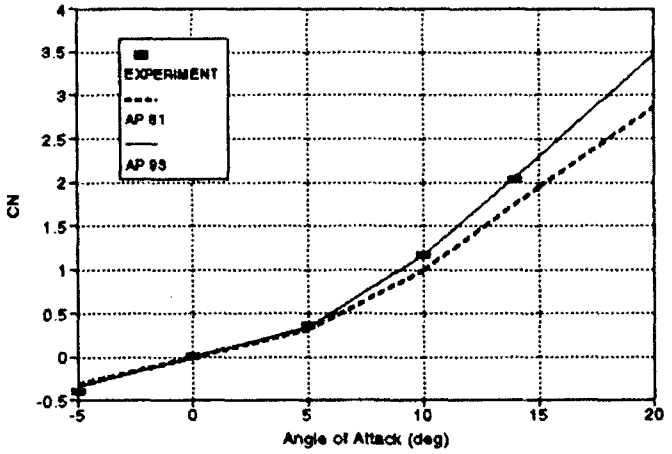

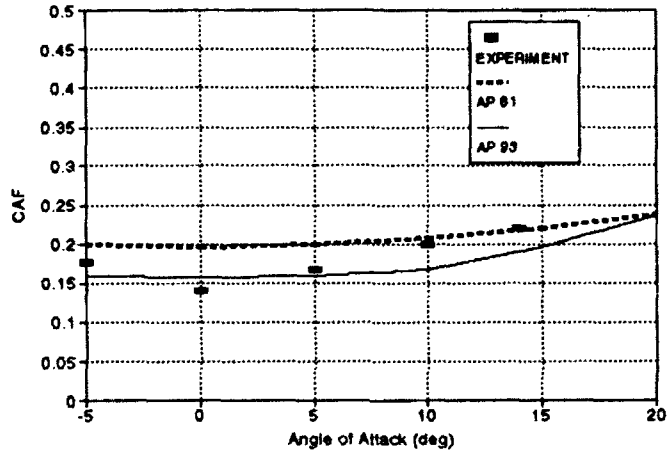

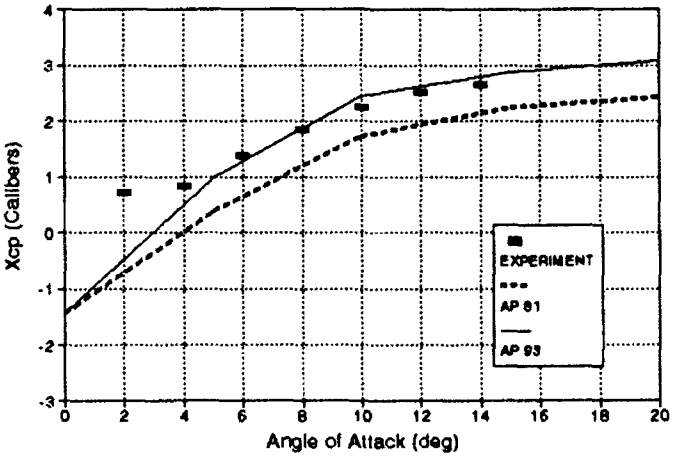

g. $M_\infty = 4.0$

FIGURE 19. NORMAL- AND AXIAL-FORCE COEFFICIENTS AND CENTER OF PRESSURE AS A FUNCTION OF ANGLE OF ATTACK FOR CONFIGURATION OF FIGURE 19a (CONTINUED)

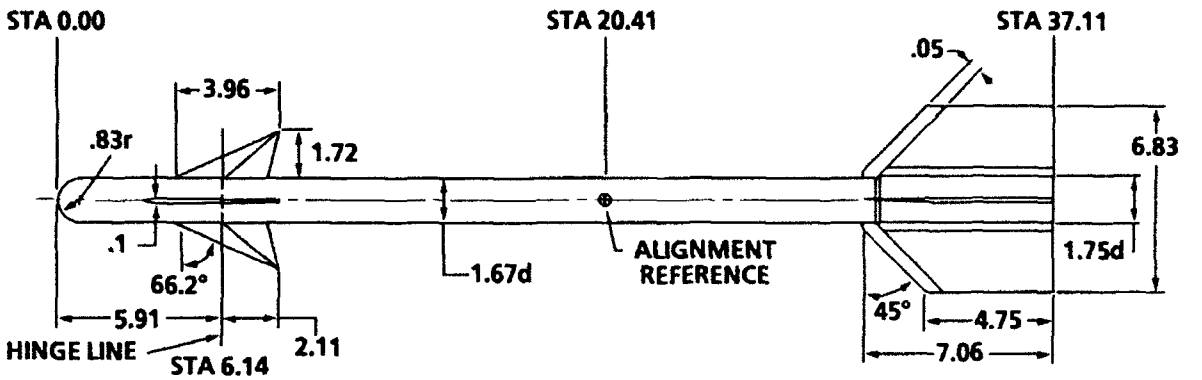

FIGURE 20a. CANARD-BODY-TAIL CONFIGURATION
USED IN VALIDATION PROCESS[67]

In analyzing why this improvement occurs at those conditions, it is noted that the aspect ratio of the tail surfaces of the configuration of Figure 20a is about 0.87 and that of the canards is about 1.7. Examining Figure 14 of Reference 12 (or Tables 2 and 3), it is seen that the nonlinearity in wing-alone lift is small for Mach numbers greater than about 1.5. As normal Mach number increases, $[M_\infty \sin(\alpha+\delta)]$ for Mach numbers greater than about 3.5 to 4.0, nonlinearity because of compressibility becomes important. The bottom line is as long as the aerodynamics are fairly linear, the AP81 gives good results up to moderate angles of attack. However, when nonlinearities are present, the AP93 shows significant improvement. This improvement is the greatest on the Figure 20a configuration at low Mach number because the nonlinear normal-force term on the canards is negative, whereas that of the tails is positive. The combination produces a strong couple in terms of the pitching moment as evidenced by Figures 20b, c, h, i, n, and o. A good nonlinear capability such as that present in the AP93 is absolutely essential to get accurate stability and control information for these cases. Just examining Figure 20b, the center of pressure of the AP81 at $\alpha = 20$ deg differs from the experimental data by -9.4 percent of the body length versus 1.3 percent for the AP93.

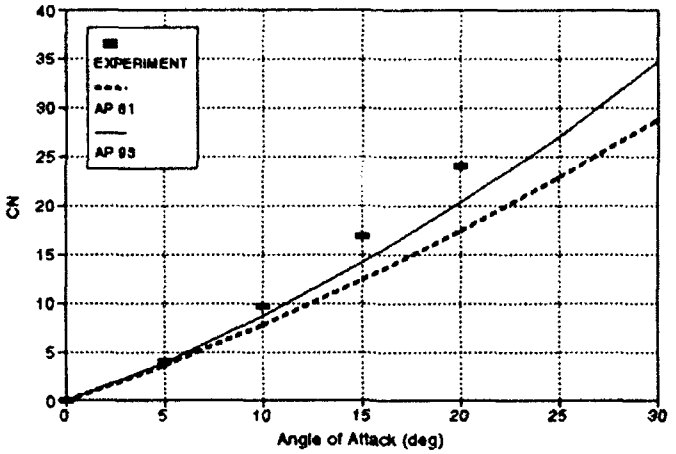

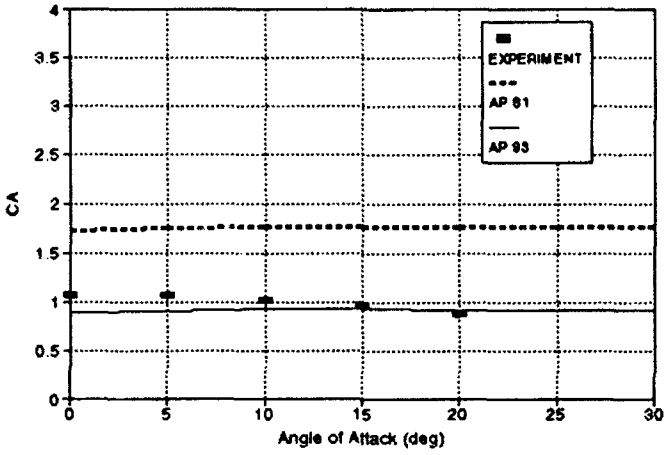

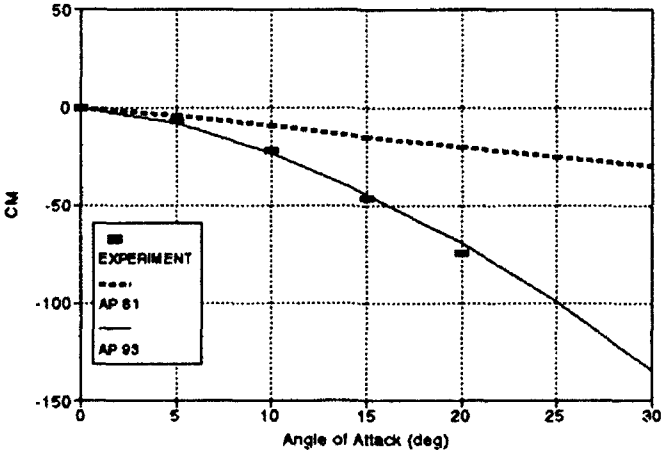

b. $M_\infty = 0.8, \delta = 0$ DEG

FIGURE 20. NORMAL- AND AXIAL-FORCE AND PITCHING MOMENT COEFFICIENTS FOR CONFIGURATION OF FIGURE 20a

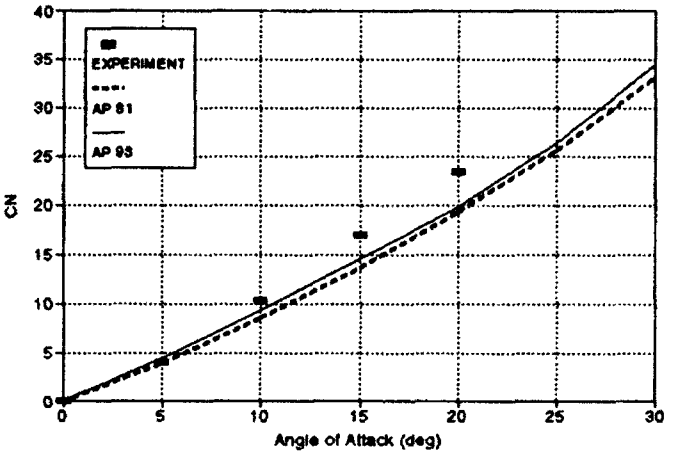

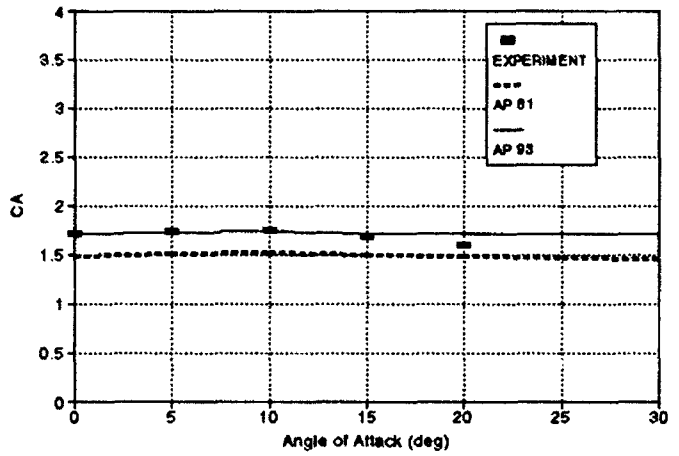

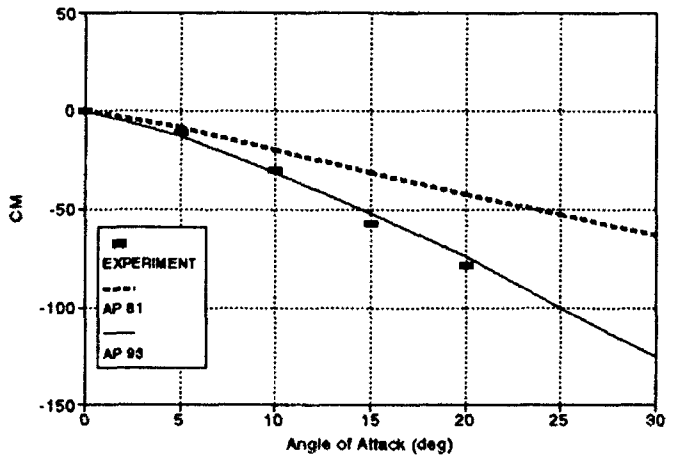

c. $M_{\infty} = 1.2, \delta = 0$ DEG

FIGURE 20. NORMAL- AND AXIAL-FORCE AND PITCHING MOMENT COEFFICIENTS FOR CONFIGURATION OF FIGURE 20a (CONTINUED)

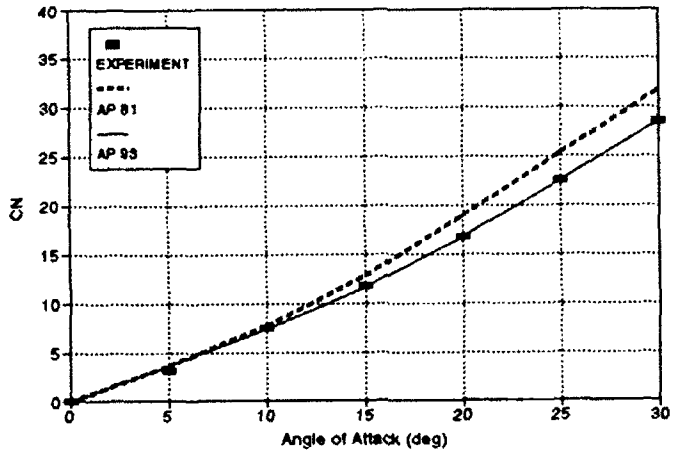

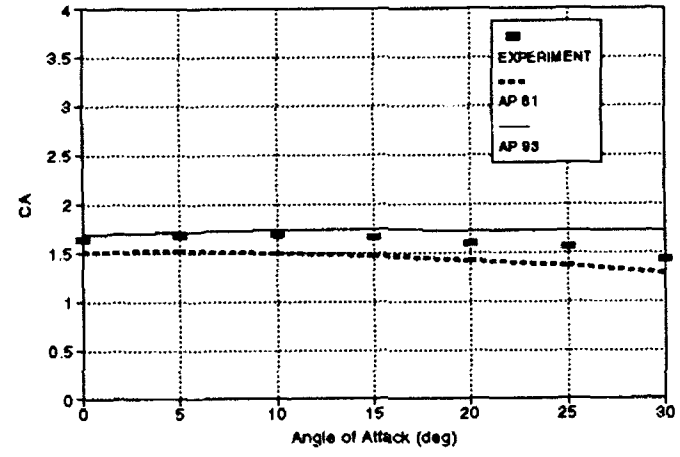

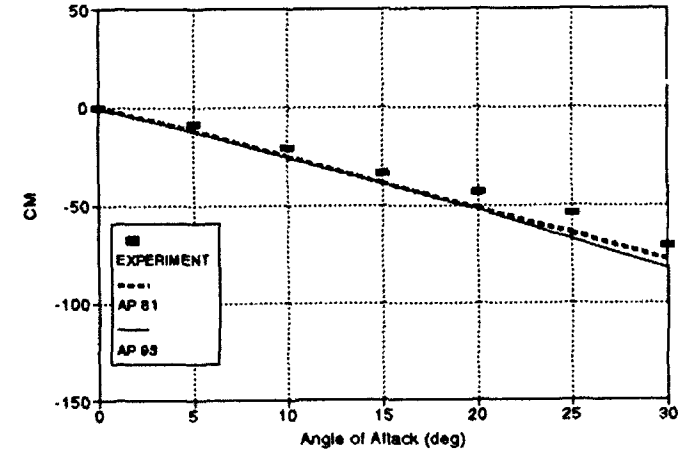

d. $M_\infty = 2.1, \delta = 0$ DEG

FIGURE 20. NORMAL- AND AXIAL-FORCE AND PITCHING MOMENT COEFFICIENTS FOR CONFIGURATION OF FIGURE 20a (CONTINUED)

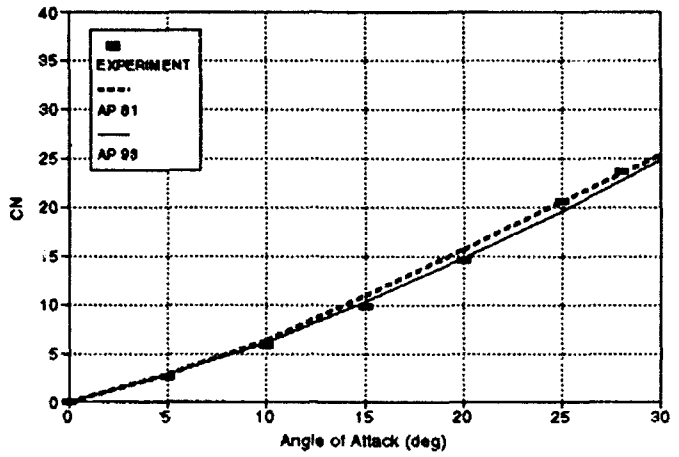

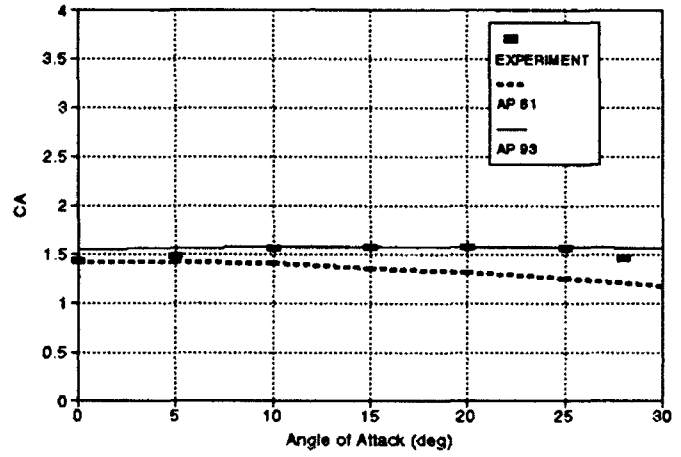

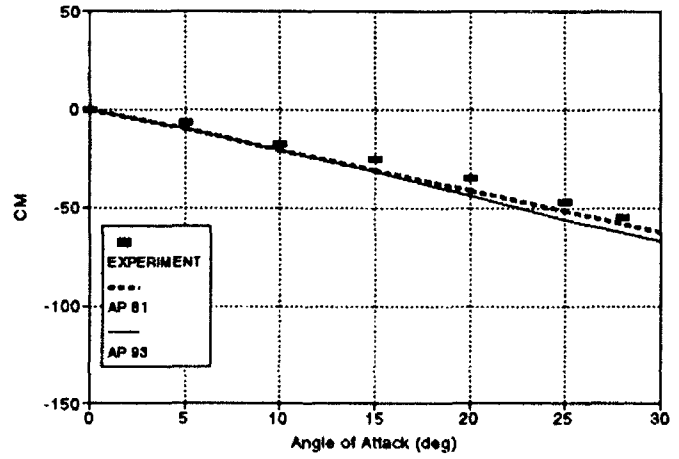

e. $M_r = 2.86, \delta = 0$ DEG

FIGURE 20. NORMAL- AND AXIAL-FORCE AND PITCHING MOMENT COEFFICIENTS FOR CONFIGURATION OF FIGURE 20a (CONTINUED)

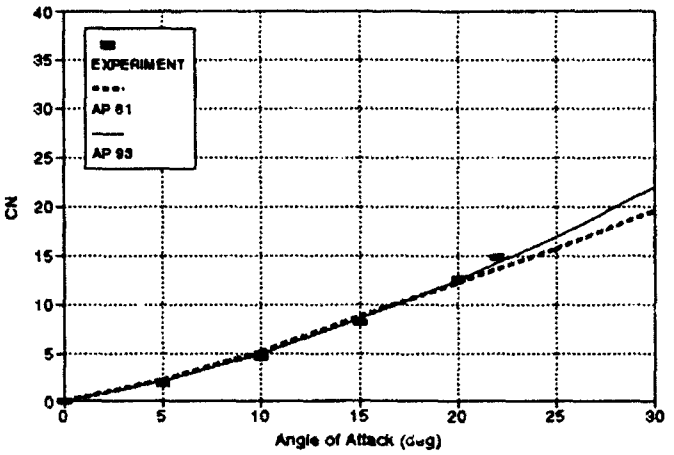

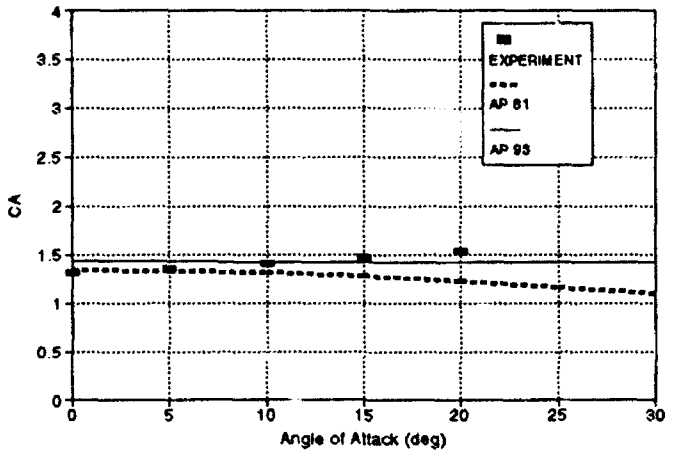

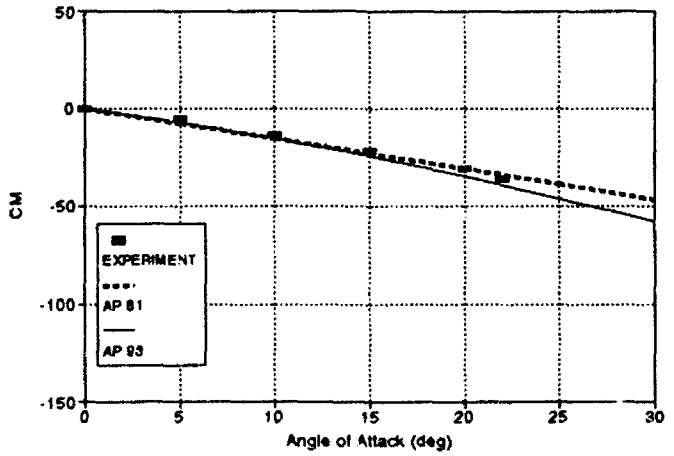

f. $M_r = 3.95, \delta = 0$ DEG

FIGURE 20. NORMAL- AND AXIAL-FORCE AND PITCHING MOMENT COEFFICIENTS FOR CONFIGURATION OF FIGURE 20a (CONTINUED)

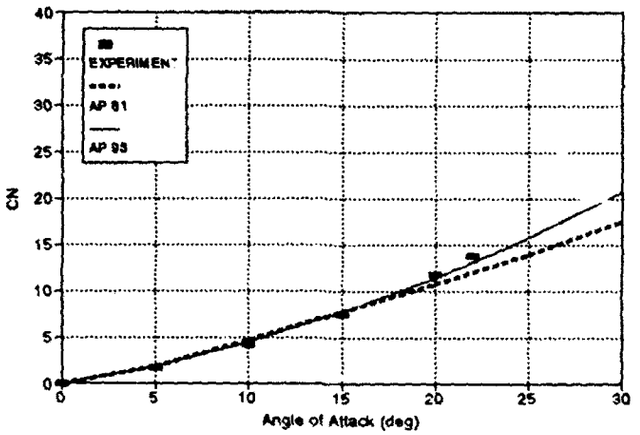

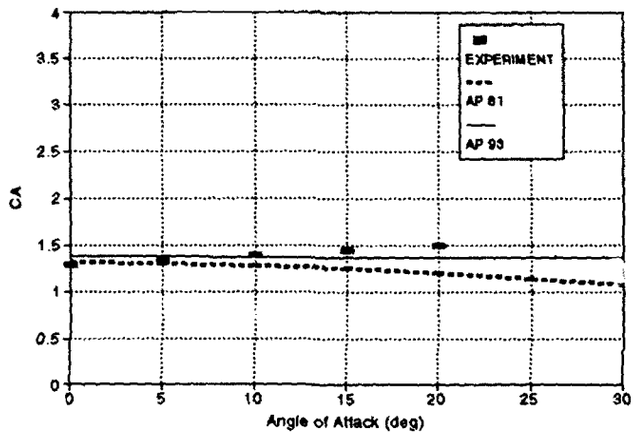

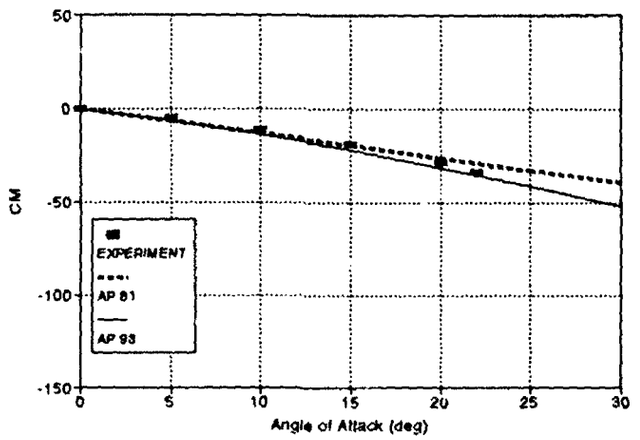

g. $M_\infty = 4.63, \delta = 0$ DEG

FIGURE 20. NORMAL- AND AXIAL-FORCE AND PITCHING MOMENT COEFFICIENTS FOR CONFIGURATION OF FIGURE 20a (CONTINUED)

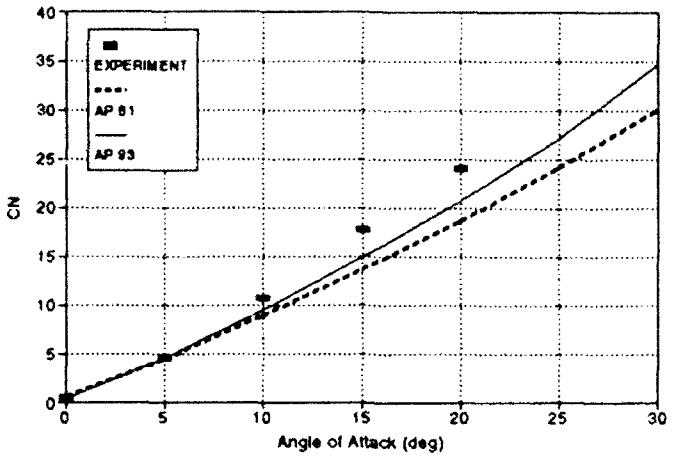

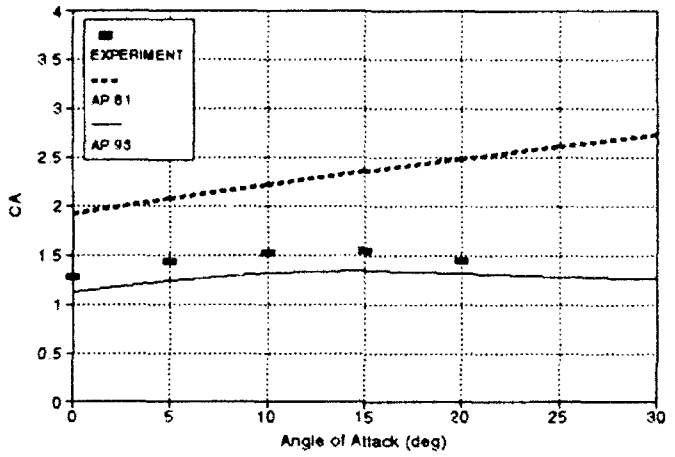

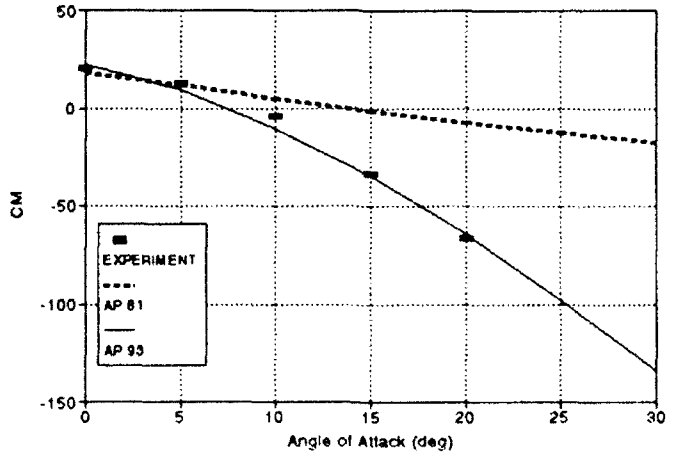

h. $M_\infty = 0.8, \delta = 10$ DEG

FIGURE 20. NORMAL- AND AXIAL-FORCE AND PITCHING MOMENT COEFFICIENTS FOR CONFIGURATION OF FIGURE 20a (CONTINUED)

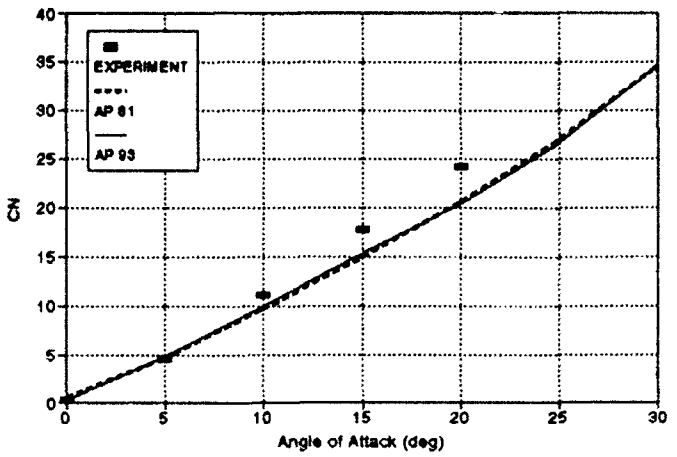

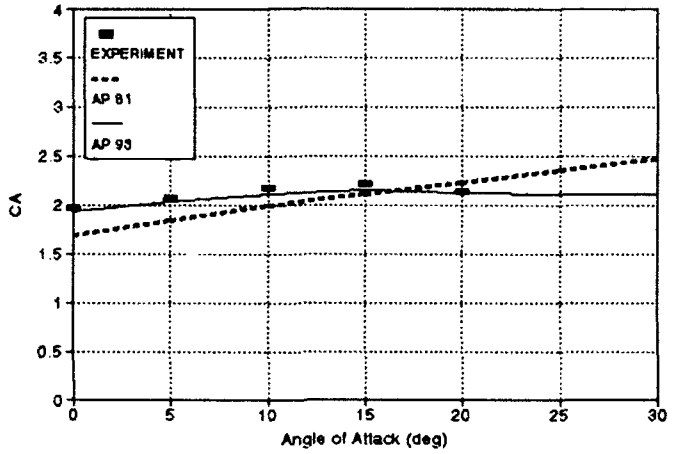

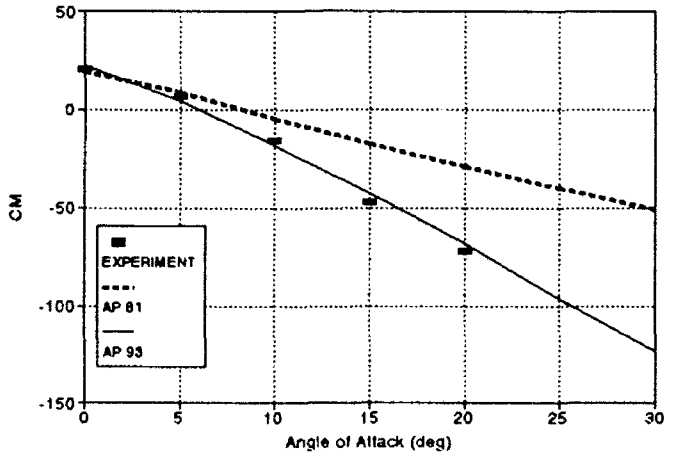

i. $M_\infty = 1.2, \delta = 10$ DEG

FIGURE 20. NORMAL- AND AXIAL-FORCE AND PITCHING MOMENT COEFFICIENTS FOR CONFIGURATION OF FIGURE 20a (CONTINUED)

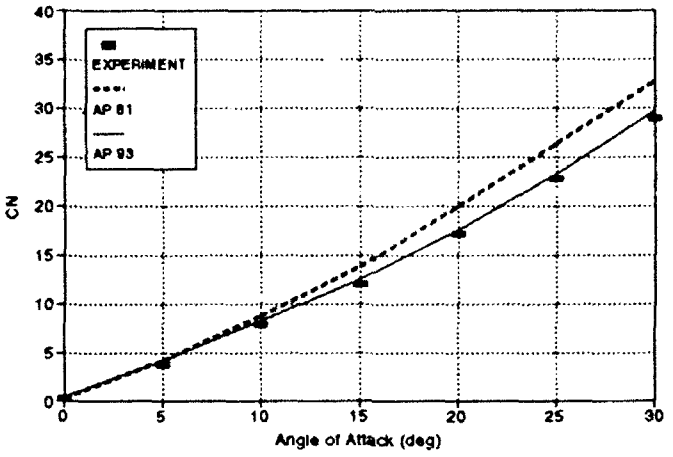

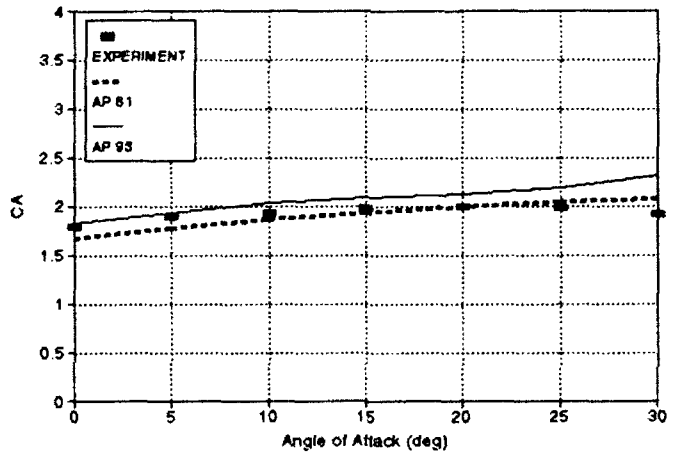

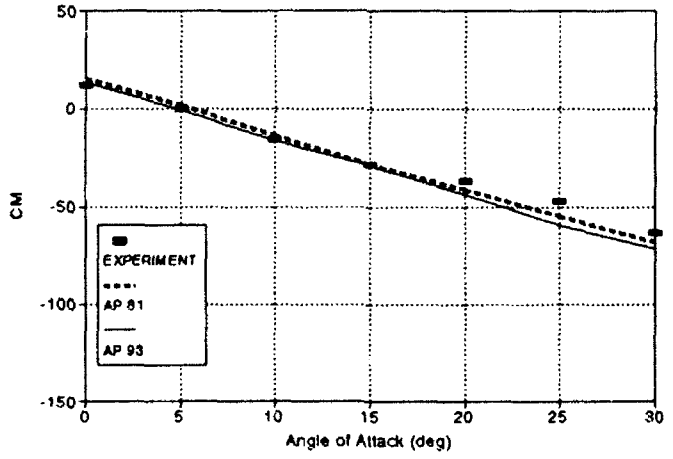

j. $M_\infty = 2.1, \delta \simeq 10$ DEG

FIGURE 20. NORMAL- AND AXIAL-FORCE AND PITCHING MOMENT COEFFICIENTS FOR CONFIGURATION OF FIGURE 20a (CONTINUED)

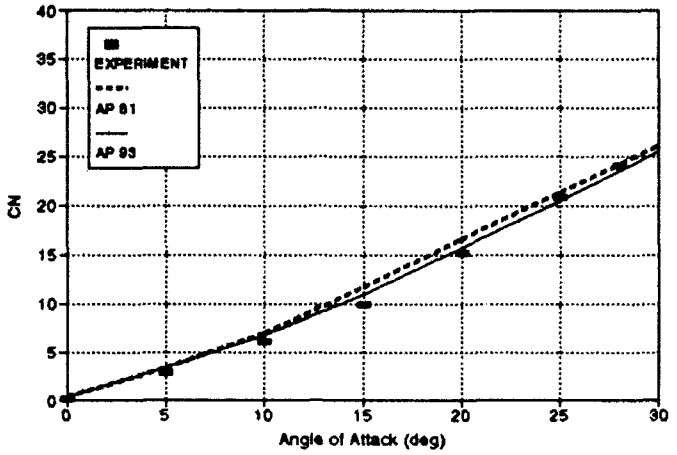

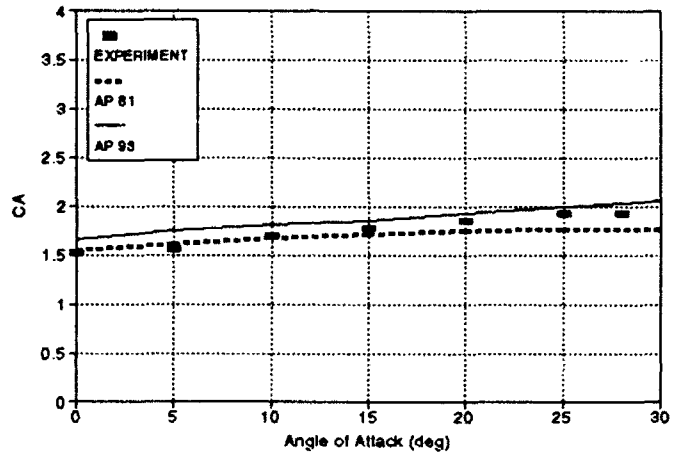

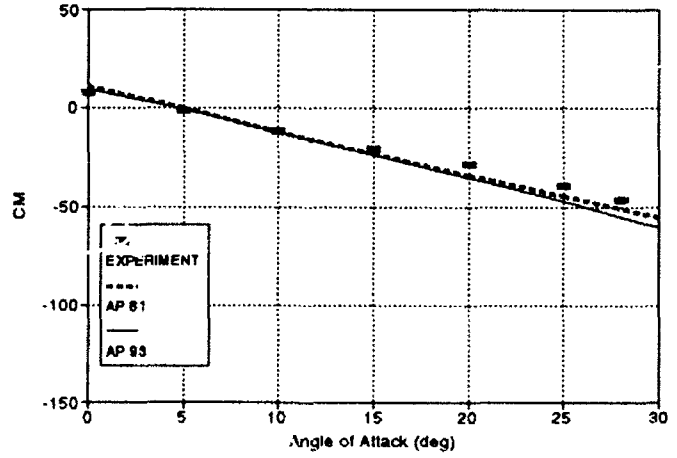

k. $M_\infty = 2.86, \delta = 10$ DEG

FIGURE 20. NORMAL- AND AXIAL-FORCE AND PITCHING MOMENT COEFFICIENTS FOR CONFIGURATION OF FIGURE 20a (CONTINUED)

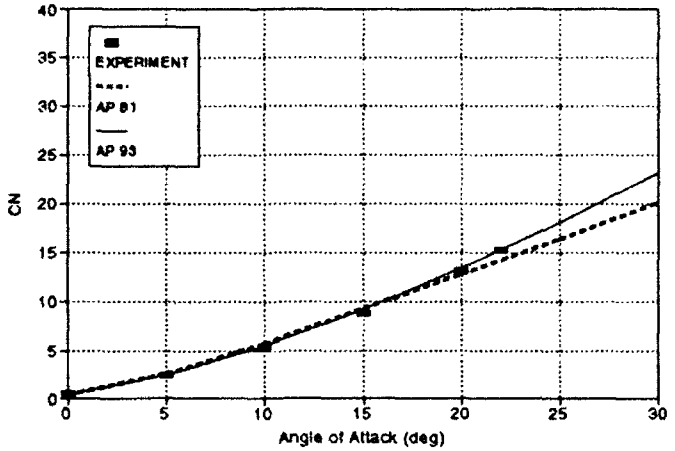

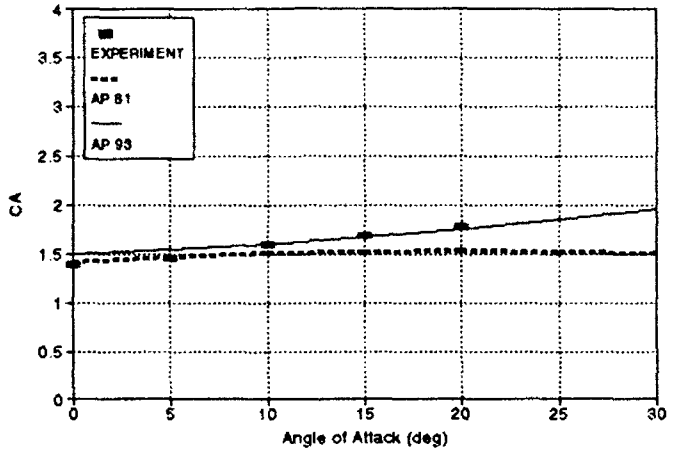

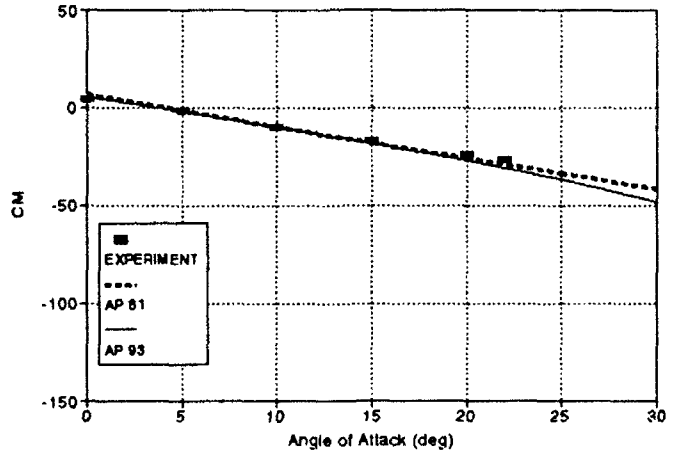

l. $M_\infty = 3.95, \delta = 10$ DEG

FIGURE 20. NORMAL- AND AXIAL-FORCE AND PITCHING MOMENT COEFFICIENTS FOR CONFIGURATION OF FIGURE 20a (CONTINUED)

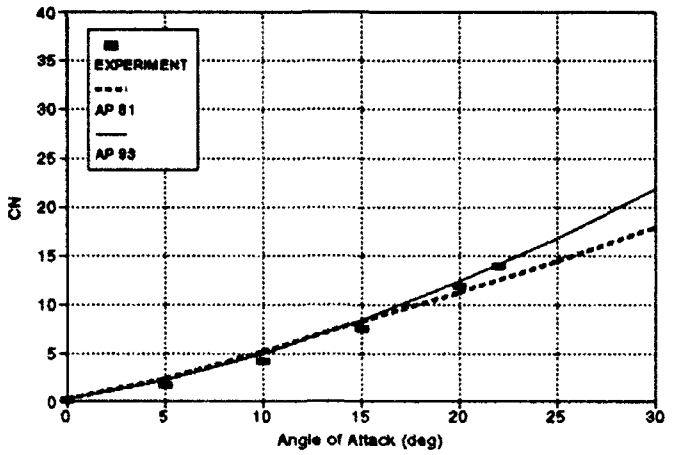

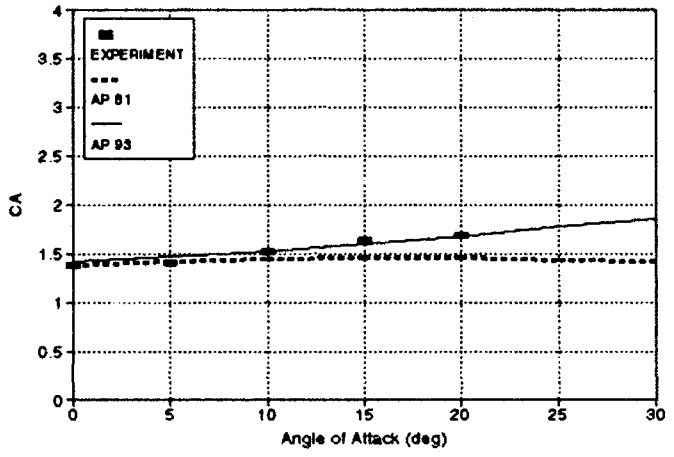

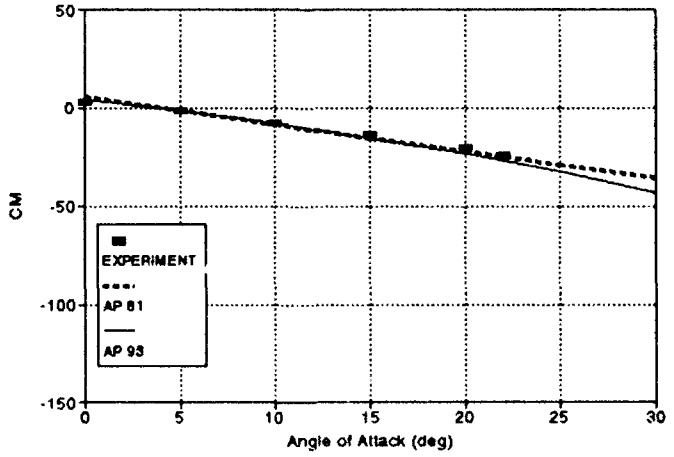

m. $M_\infty = 4.63, \delta = 10$ DEG

FIGURE 20. NORMAL- AND AXIAL-FORCE AND PITCHING MOMENT COEFFICIENTS FOR CONFIGURATION OF FIGURE 20a (CONTINUED)

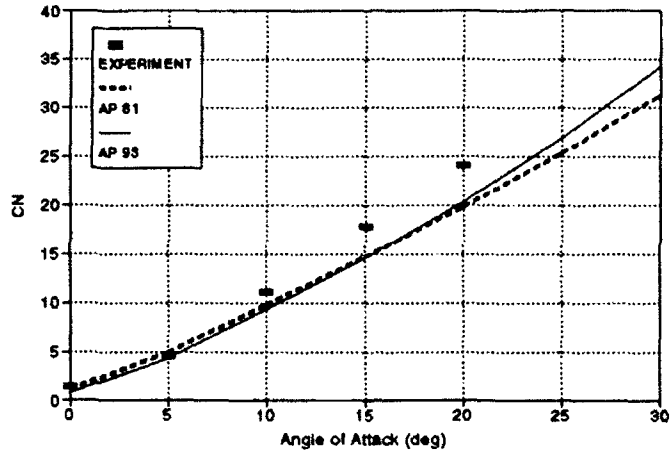

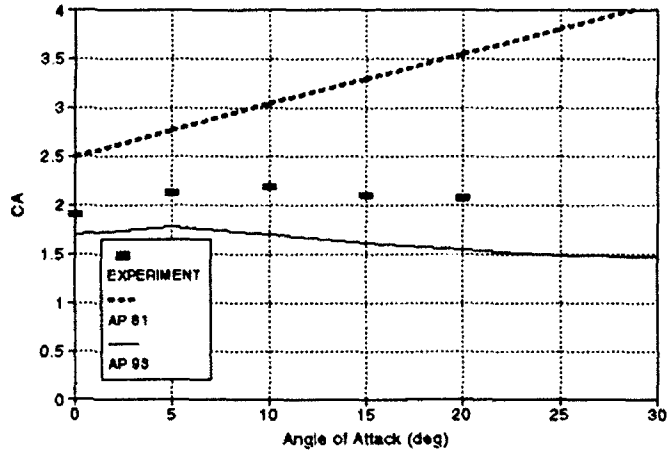

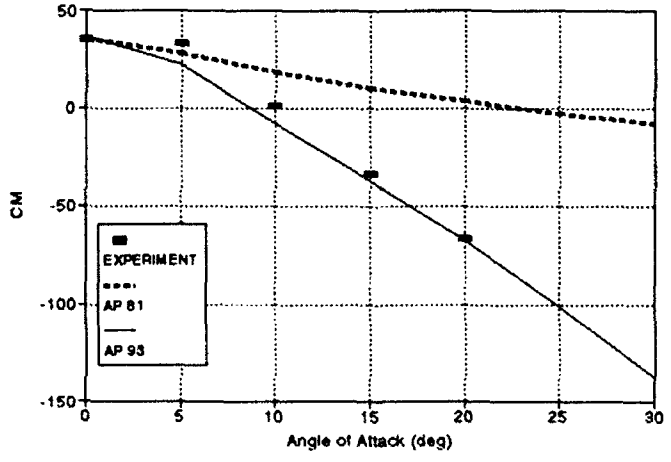

n. $M_\infty = 0.8, \delta = 20$ DEG

FIGURE 20. NORMAL- AND AXIAL-FORCE AND PITCHING MOMENT COEFFICIENTS FOR CONFIGURATION OF FIGURE 20a (CONTINUED)

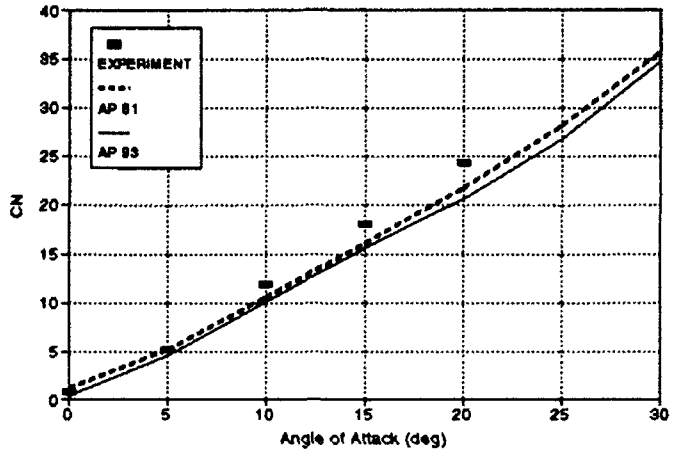

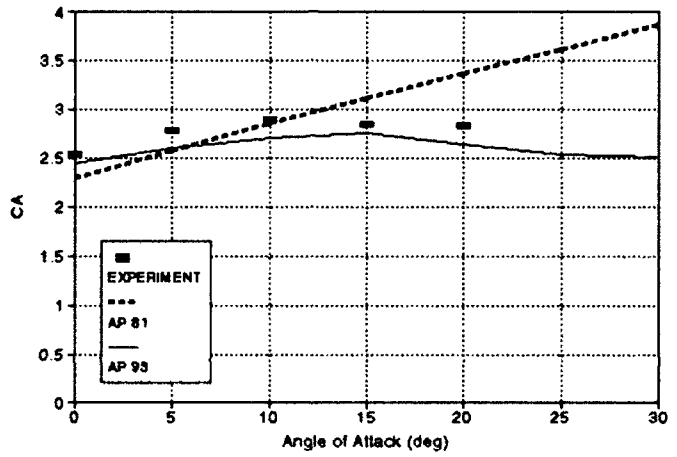

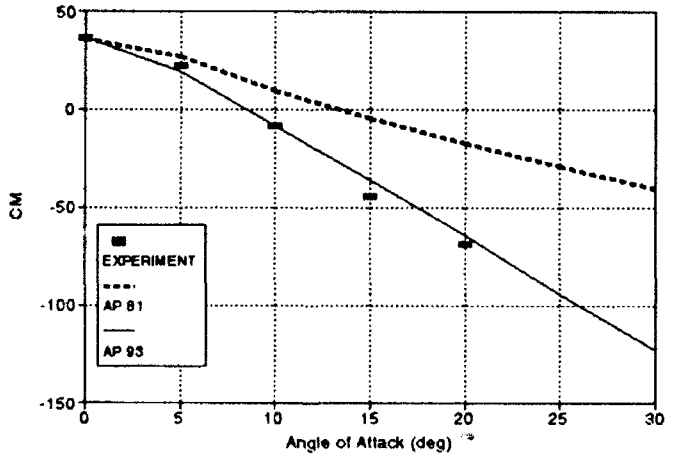

o. $M_\infty = 1.2, \delta = 20$ DEG

FIGURE 20. NORMAL- AND AXIAL-FORCE AND PITCHING MOMENT COEFFICIENTS FOR CONFIGURATION OF FIGURE 20a (CONTINUED)

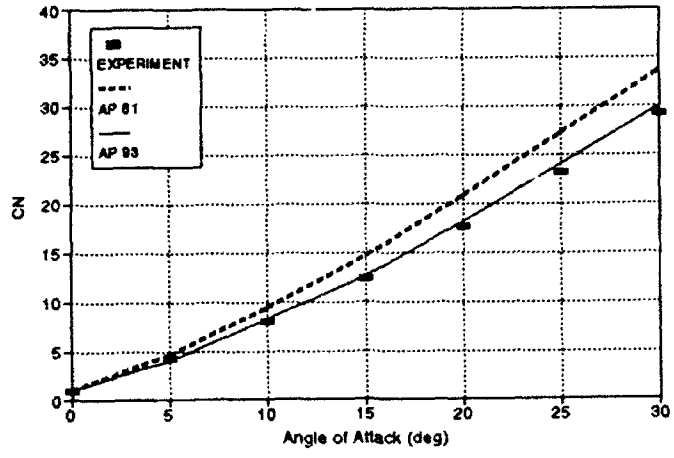

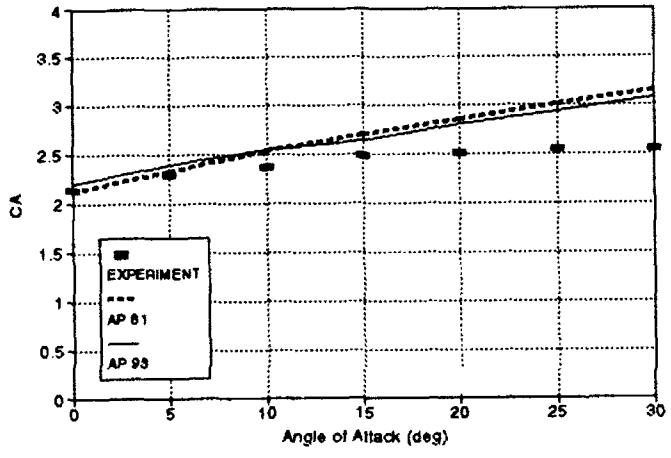

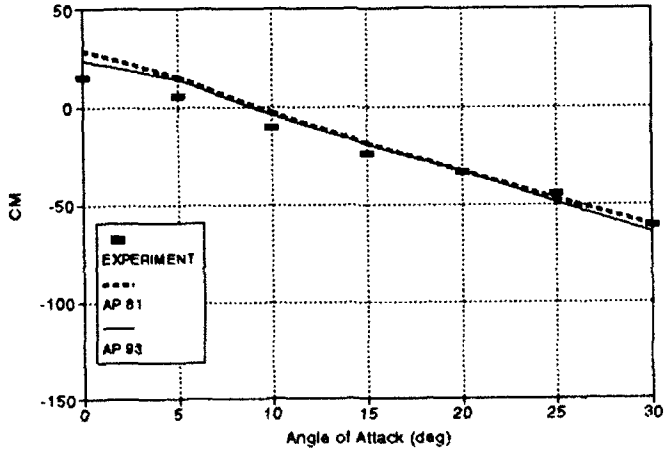

p. $M_\infty = 2.1, \delta = 20$ DEG

FIGURE 20. NORMAL- AND AXIAL-FORCE AND PITCHING MOMENT COEFFICIENTS FOR CONFIGURATION OF FIGURE 20a (CONTINUED)

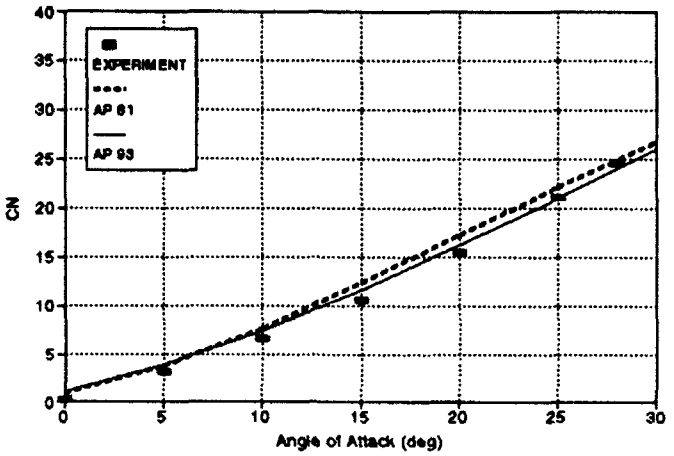

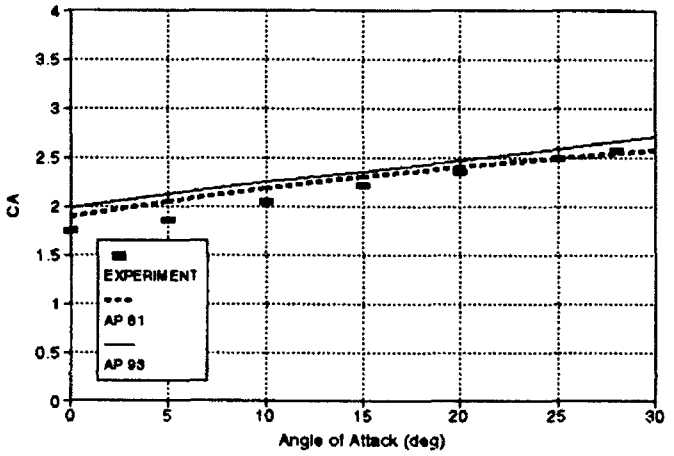

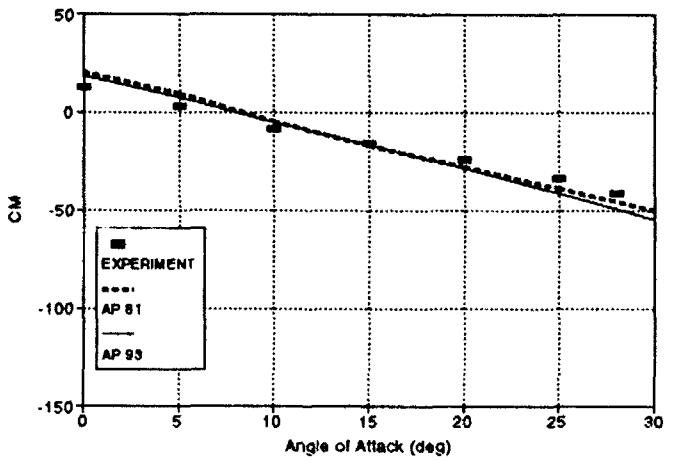

q. $M_\infty = 2.86, \delta = 20$ DEG

FIGURE 20. NORMAL- AND AXIAL-FORCE AND PITCHING MOMENT COEFFICIENTS FOR CONFIGURATION OF FIGURE 20a (CONTINUED)

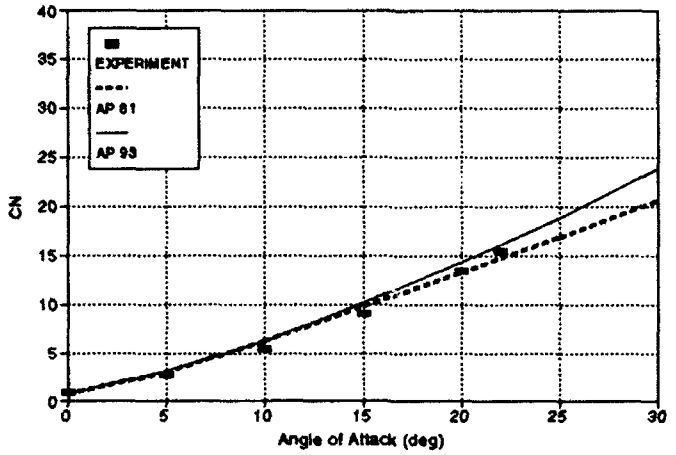

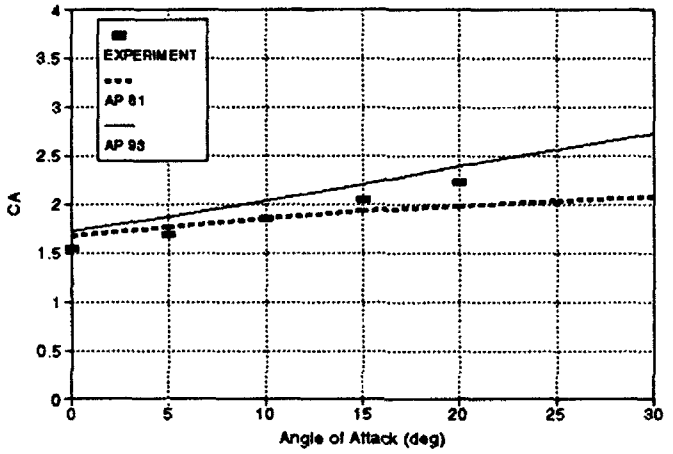

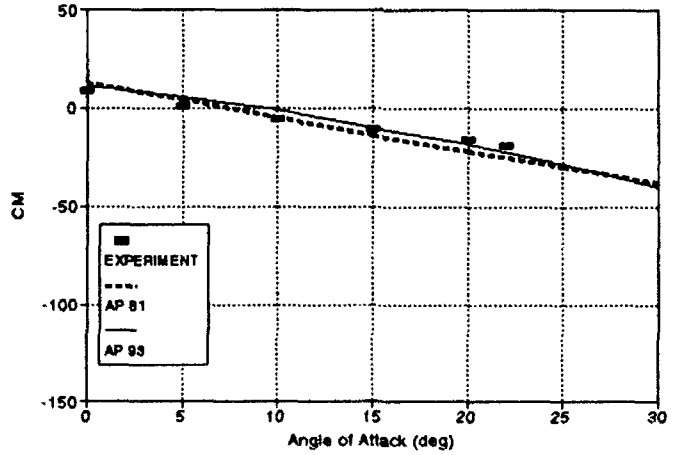

r. $M_\infty = 3.95, \delta = 20$ DEG

FIGURE 20. NORMAL- AND AXIAL-FORCE AND PITCHING MOMENT COEFFICIENTS FOR CONFIGURATION OF FIGURE 20a (CONTINUED)

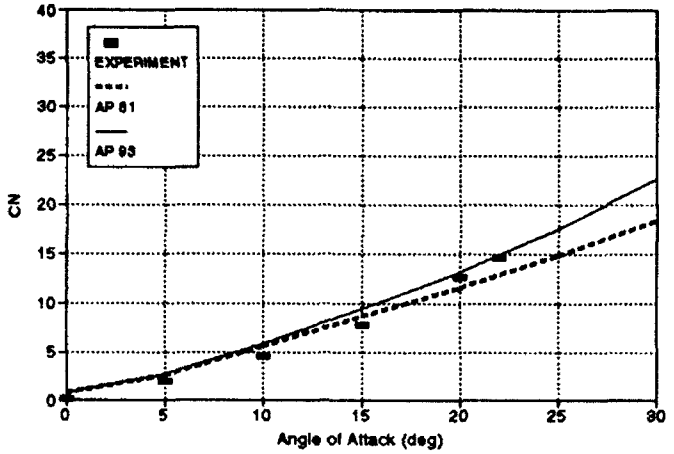

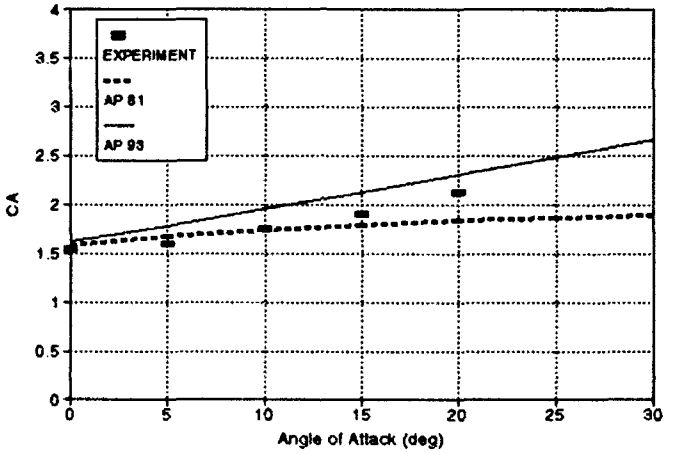

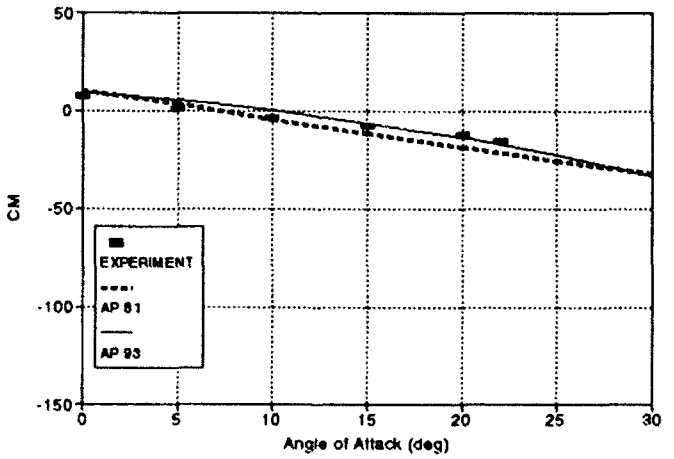

s. $M_\infty = 4.63, \delta = 20$ DEG

FIGURE 20. NORMAL- AND AXIAL-FORCE AND PITCHING MOMENT COEFFICIENTS FOR CONFIGURATION OF FIGURE 20a (CONTINUED)

A third case considered in the validation of the development of a nonlinear empirical model for $k_{W(B)}$ is a configuration tested at NASA/LRC[42,43] and is representative of the SPARROW missile. The configuration tested in Reference 43 is shown in Figure 21a. The configuration tested in Reference 42 is just like the one tested in Reference 43, except it had wiring tunnels and wave guides present. These appendages add to the normal force and pitching moment but were not accounted for in the analytical computations that are presented in Figure 21. The Reference 43 configuration did not have these appendages present and was the main set of data used for the nonlinear empirical model for $k_{W(B)}$. These results are distinguished in Figure 21 by the fact that the cases that had wave guides present are indicated.

Results of the AP81 and AP93 compared to the experiment for the case of Figure 21a are shown in Figure 21b and c. Results are presented in terms of C_N and C_M versus angle of attack for various control deflections and Mach numbers. As shown in Figure 19, the nonlinear models with and without control deflection show the AP93 code agreeing much closer to the data at all Mach numbers than the linearized approaches of AP81. On the other hand, the fact that the body-alone normal force of AP81 had the nonlinearities included makes the comparisons to experimental data better than it would be otherwise.

In examining Figure 21b, it is seen that both C_N and C_M of AP93 agree with the experiment at $\delta = 0$ and $\delta = 10$ deg for $M_\infty = 1.5$ and 2.0, respectively. C_N and C_M of the AP81 are both considerable in error as angle of attack increases above 5 to 10 deg. For $M_\infty = 2.35$, both C_N and C_M of AP93 at $\delta = 0$ and 20 deg agree with the data. Again, AP81 is in considerable error at $\alpha \geq 10$ deg, although the error is decreasing with increasing Mach number. At $M_\infty = 2.87$, both AP81 and AP93 give good results for C_N and C_M at $\delta = 0$. At $\delta = 20$ deg, C_N is also predicted quite well by both AP93 and AP81; however, C_M errors are larger for AP81 than AP93. For $M_\infty = 3.95$, AP81 gives acceptable results for C_N and C_M up to $\alpha = 15$ to 20 deg and at both $\delta = 0$ or 20 deg. The comparison with data gets worse above $\alpha = 20$ deg, whereas AP93 comparisons show good agreement at all α's and δ's. The same statements basically hold true for the $M_\infty = 4.6$ comparisons.

Figure 21c shows the comparisons of AP81 and AP93 to the data of Reference 42, which is the same configuration as that of Figure 19 except that wave guides and wiring tunnels were attached to the wind tunnel model. As already mentioned, no account was taken for these appendages in the analytical computations. Note that AP93 agrees much closer to the data than AP81 for both $M_\infty = 2.3$ and 4.6 at all values of δ. In comparing the wind tunnel data for the cases with and without appendages, it can be seen that the appendages add only a few percent to the aerodynamics.

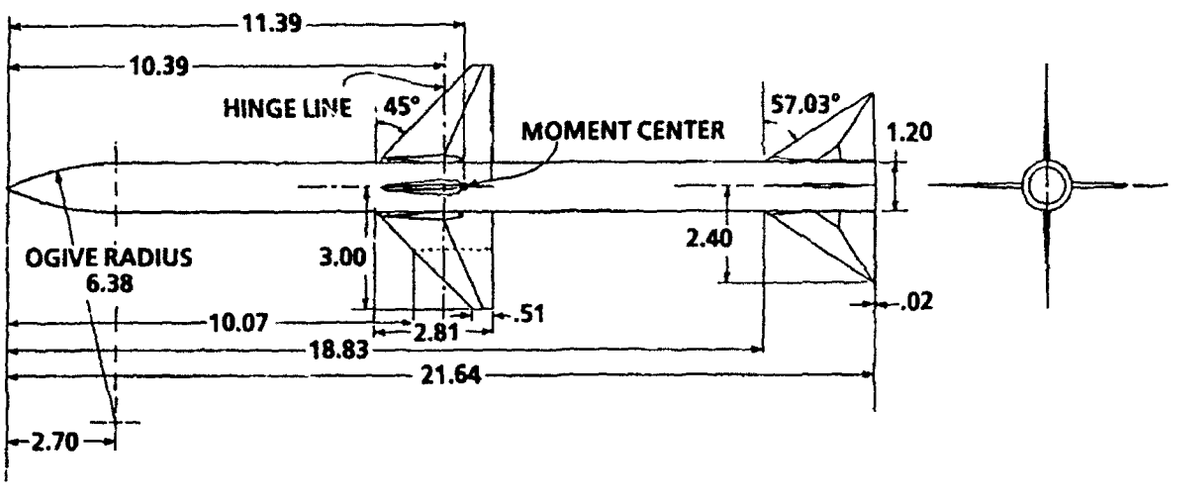

FIGURE 21a. AIR-TO-AIR MISSILE CONFIGURATION USED IN VALIDATION PROCESS[42,43]

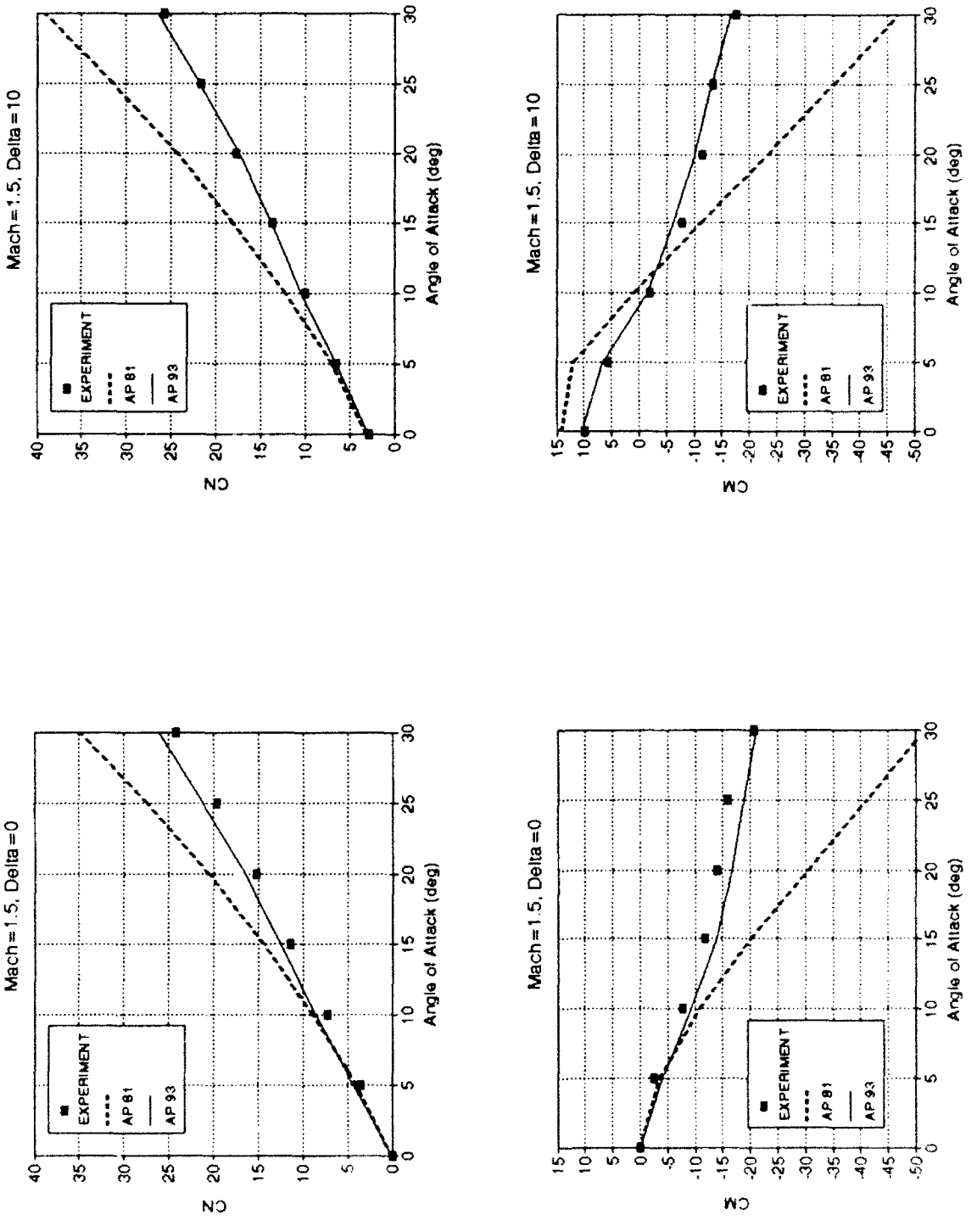

b. NO WAVE GUIDES (REFERENCE 43)

FIGURE 21. NORMAL FORCE AND PITCHING MOMENT COEFFICIENTS FOR CONFIGURATION OF FIGURE 21a FOR VARIOUS MACH NUMBERS AND CONTROL DEFLECTIONS

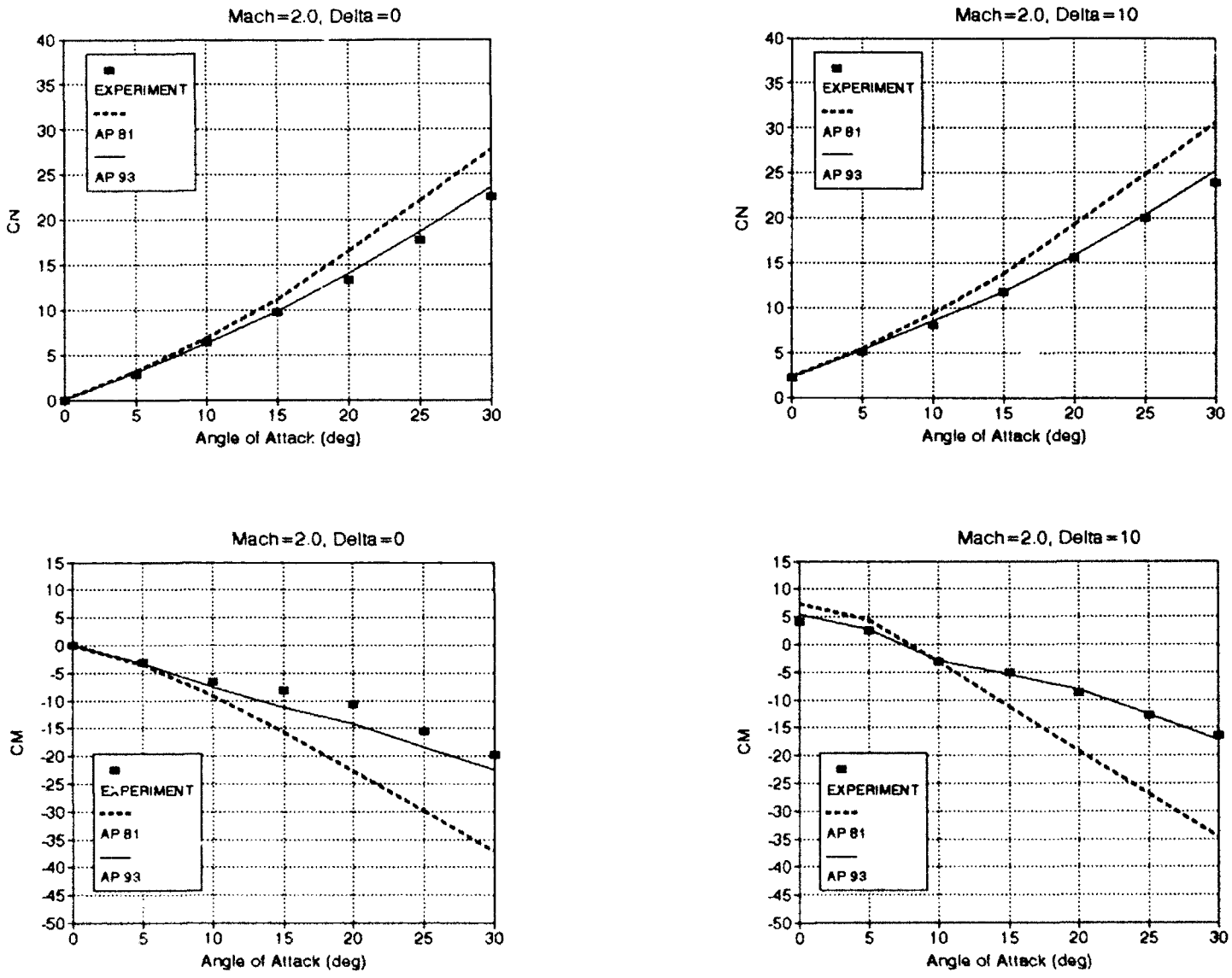

b. NO WAVE GUIDES (REFERENCE 43)

FIGURE 21. NORMAL-FORCE AND PITCHING MOMENT COEFFICIENTS FOR CONFIGURATION OF FIGURE 21a FOR VARIOUS MACH NUMBERS AND CONTROL DEFLECTIONS (CONTINUED)

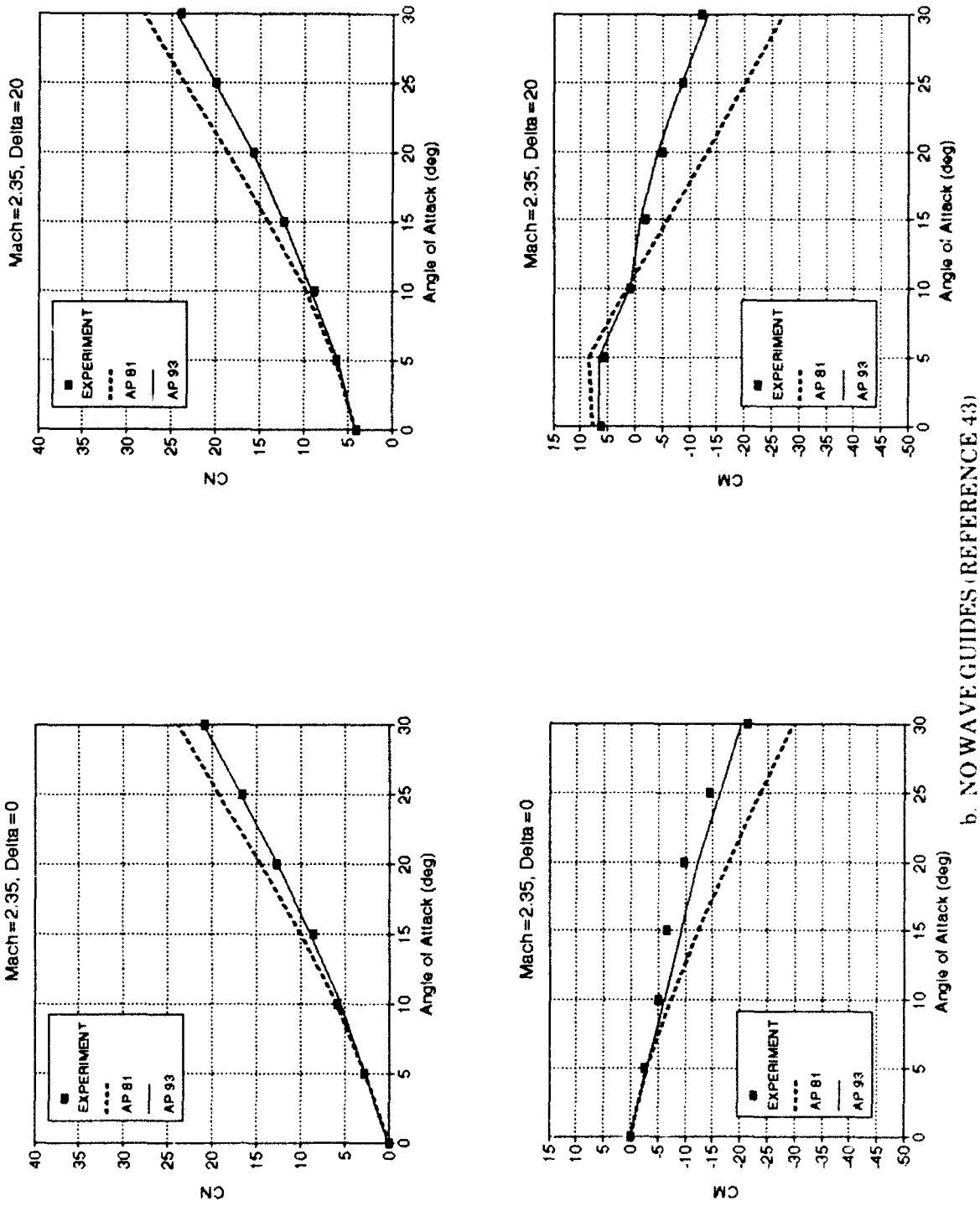

b. NO WAVE GUIDES (REFERENCE 43)

FIGURE 21. NORMAL-FORCE AND PITCHING MOMENT COEFFICIENTS FOR CONFIGURATION OF FIGURE 21a FOR VARIOUS MACH NUMBERS AND CONTROL DEFLECTIONS (CONTINUED)

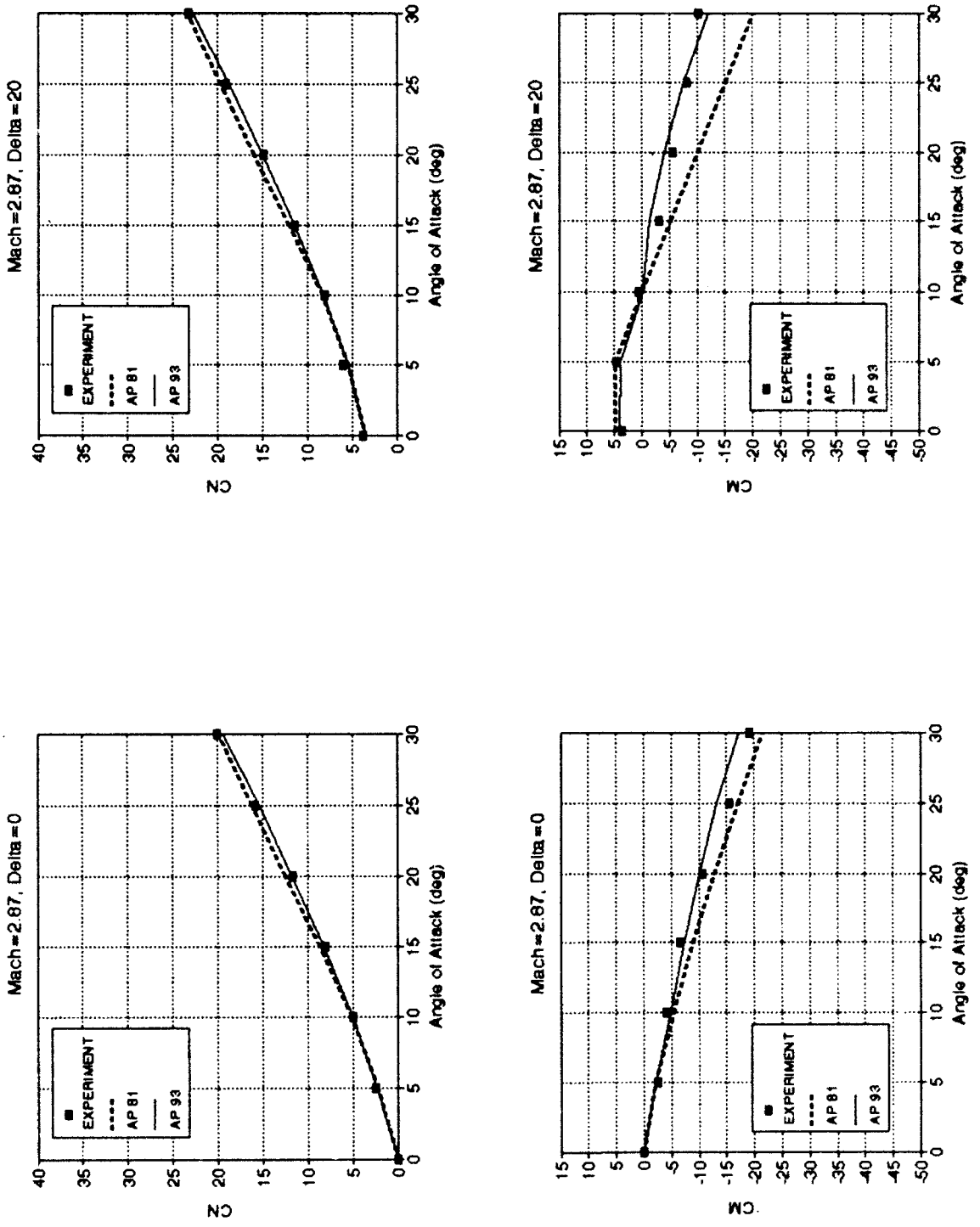

b. NO WAVE GUIDES (REFERENCE 43)

FIGURE 21. NORMAL-FORCE AND PITCHING MOMENT COEFFICIENTS FOR CONFIGURATION OF FIGURE 21a FOR VARIOUS MACH NUMBERS AND CONTROL DEFLECTIONS (CONTINUED)

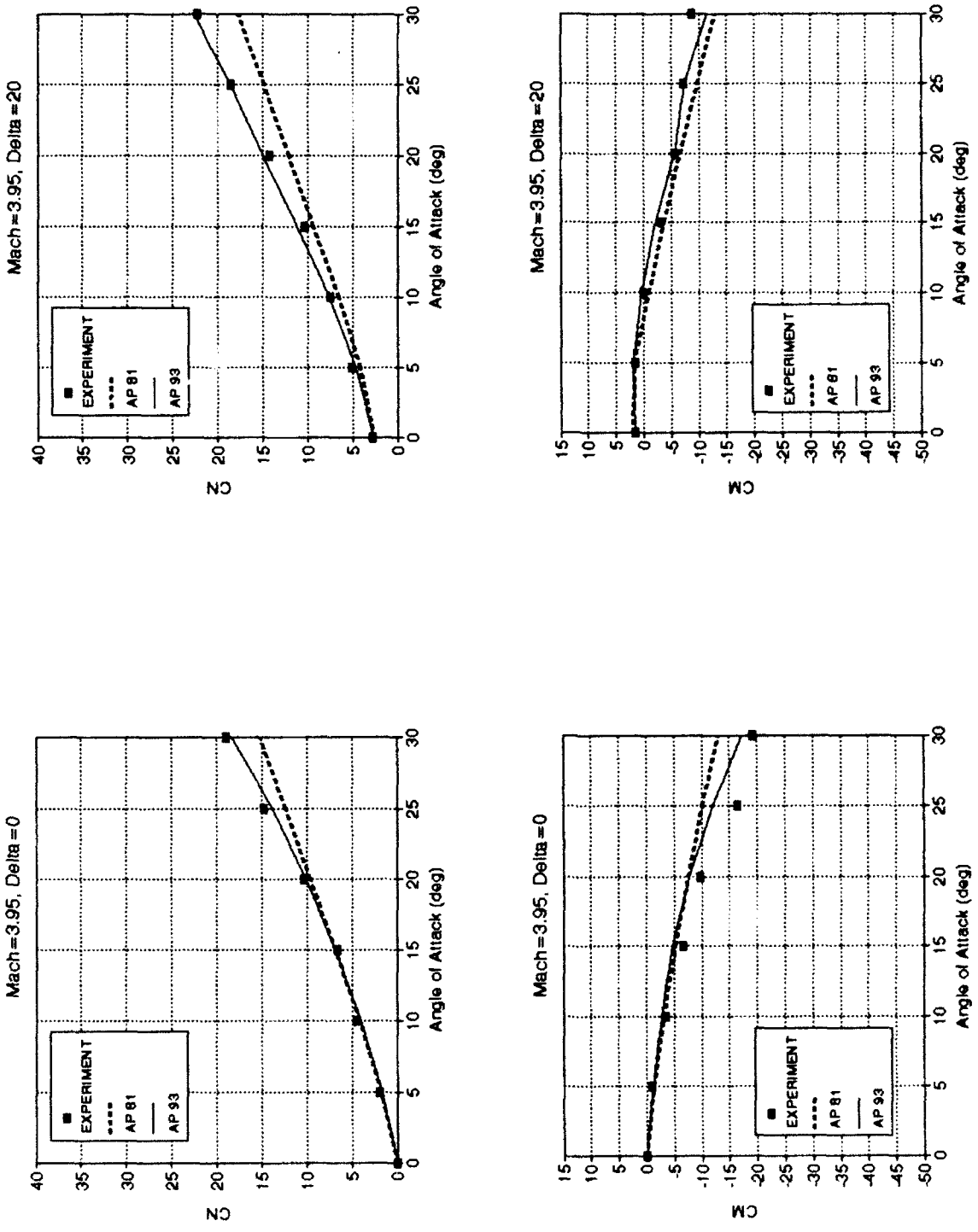

b. NO WAVE GUIDES (REFERENCE 43)

FIGURE 21. NORMAL-FORCE AND PITCHING MOMENT COEFFICIENTS FOR CONFIGURATION OF FIGURE 21a FOR VARIOUS MACH NUMBERS AND CONTROL DEFLECTIONS (CONTINUED)

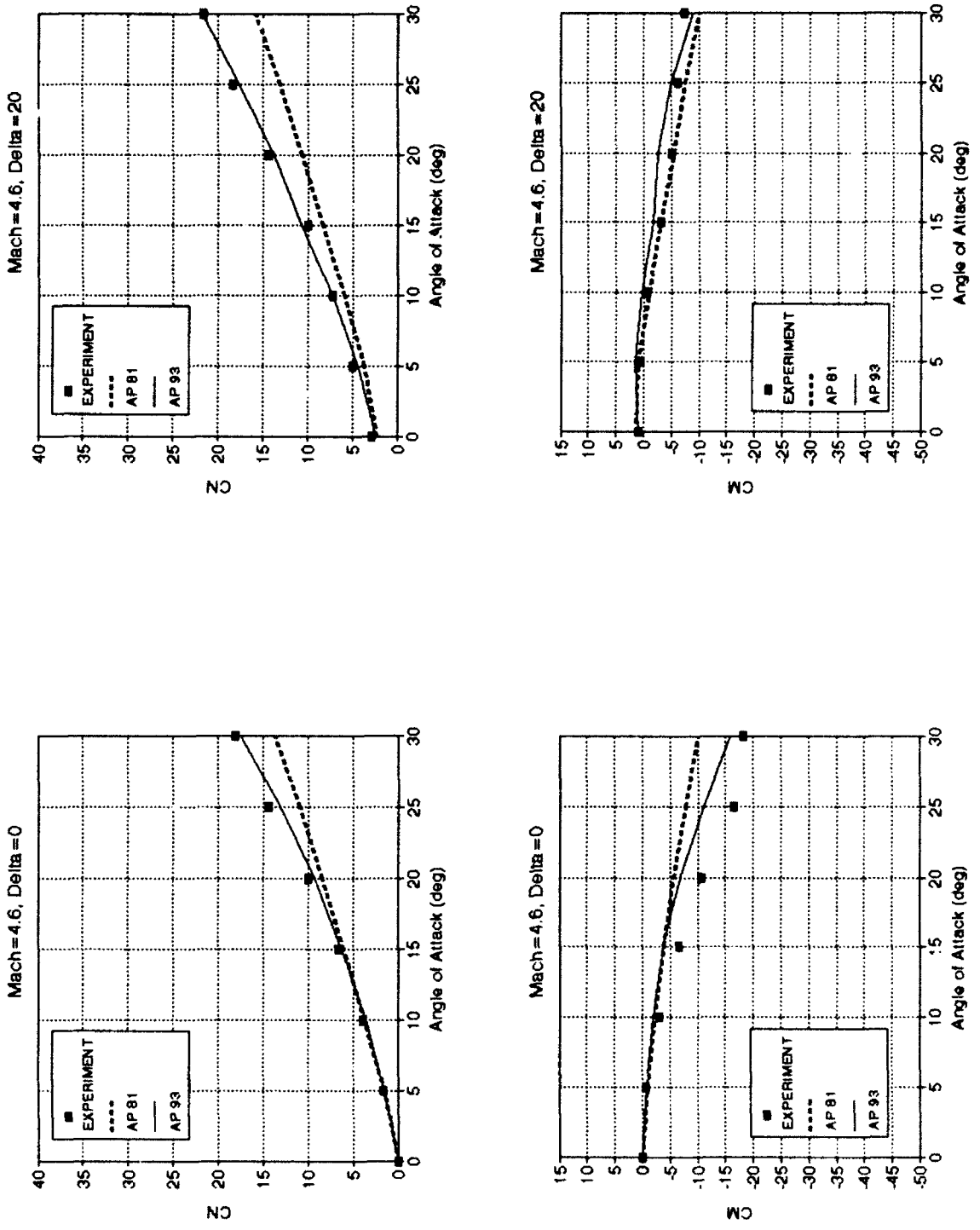

b. NO WAVE GUIDES (REFERENCE 43)

FIGURE 21. NORMAL-FORCE AND PITCHING MOMENT COEFFICIENTS FOR CONFIGURATION OF FIGURE 21a FOR VARIOUS MACH NUMBERS AND CONTROL DEFLECTIONS (CONTINUED)

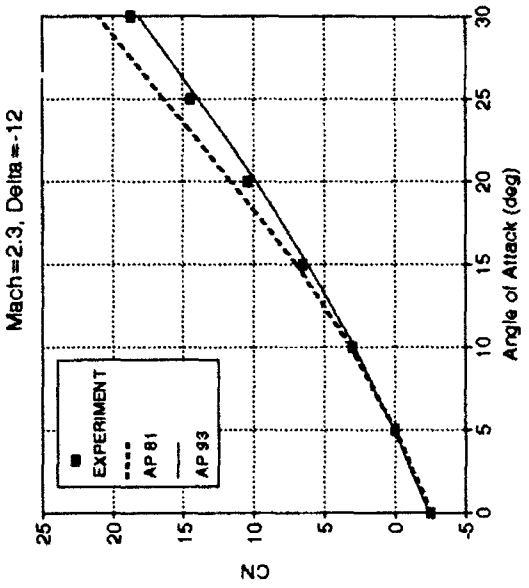

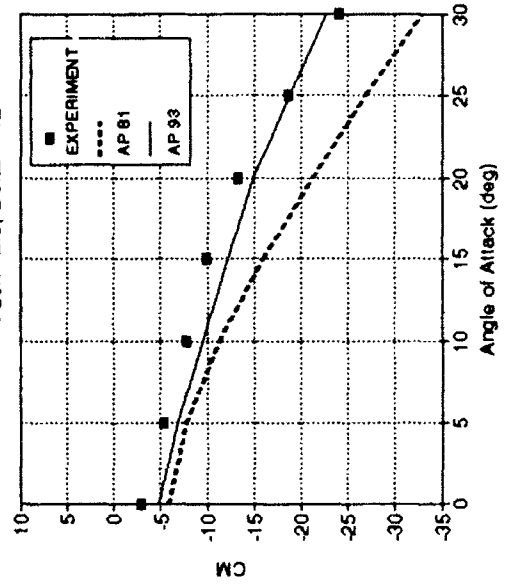

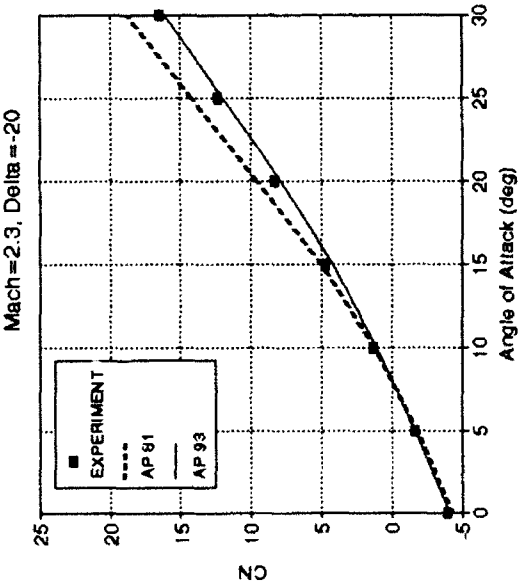

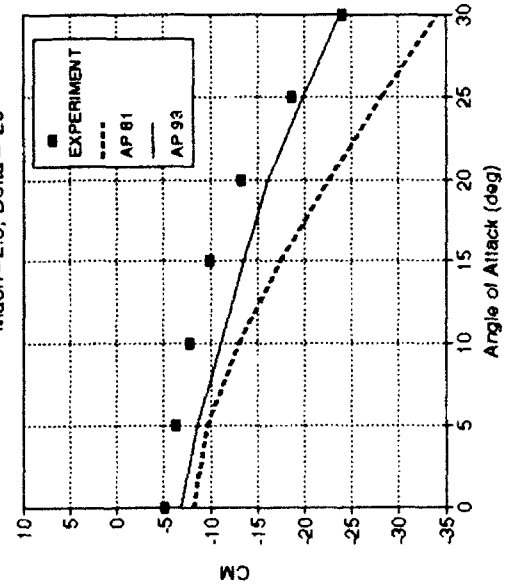

c. WITH WAVE GUIDES (REFERENCE 42)

FIGURE 21. NORMAL-FORCE AND PITCHING MOMENT COEFFICIENTS FOR CONFIGURATION OF FIGURE 21a FOR VARIOUS MACH NUMBERS AND CONTROL DEFLECTIONS

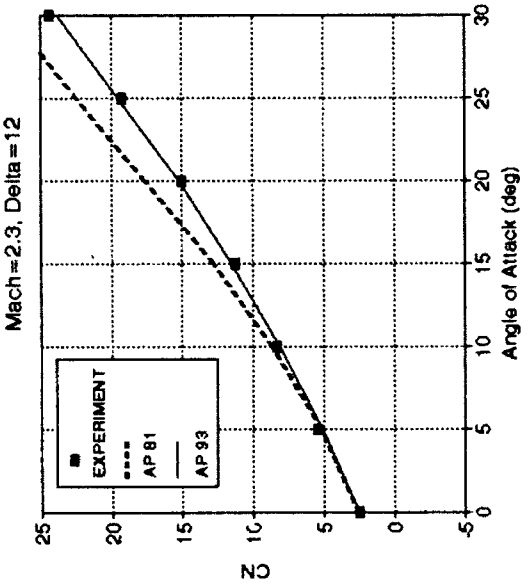

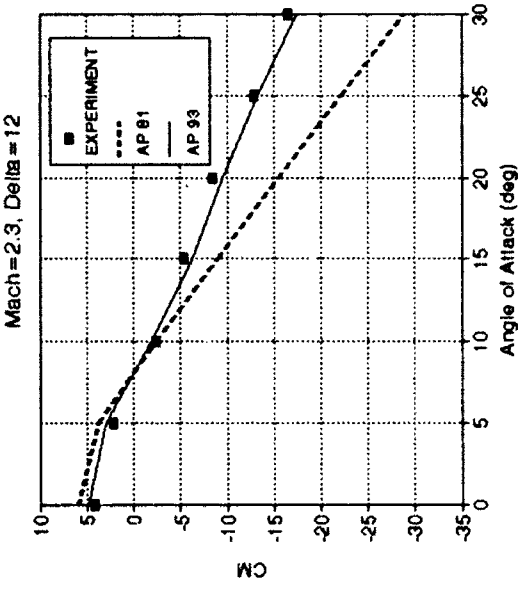

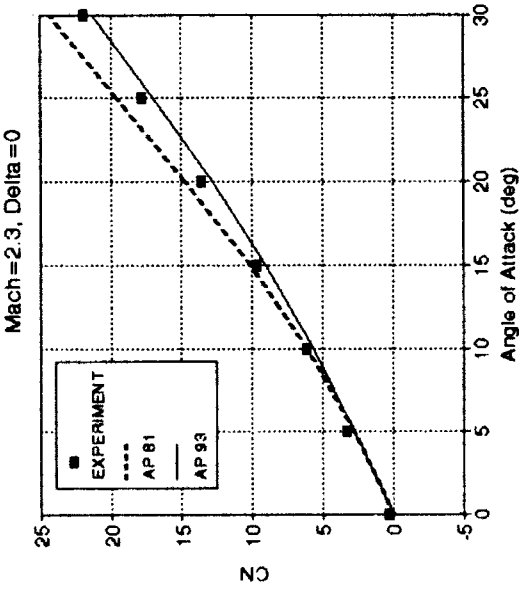

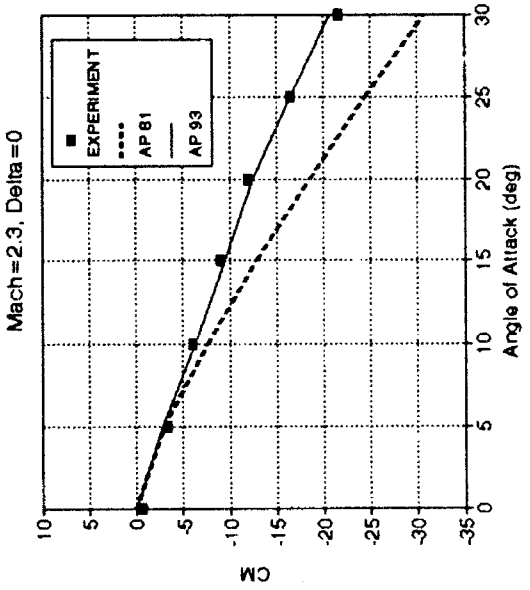

c. WITH WAVE GUIDES (REFERENCE 42)

FIGURE 21. NORMAL FORCE AND PITCHING MOMENT COEFFICIENTS FOR CONFIGURATION OF FIGURE 21a FOR VARIOUS MACH NUMBERS AND CONTROL DEFLECTIONS (CONTINUED)

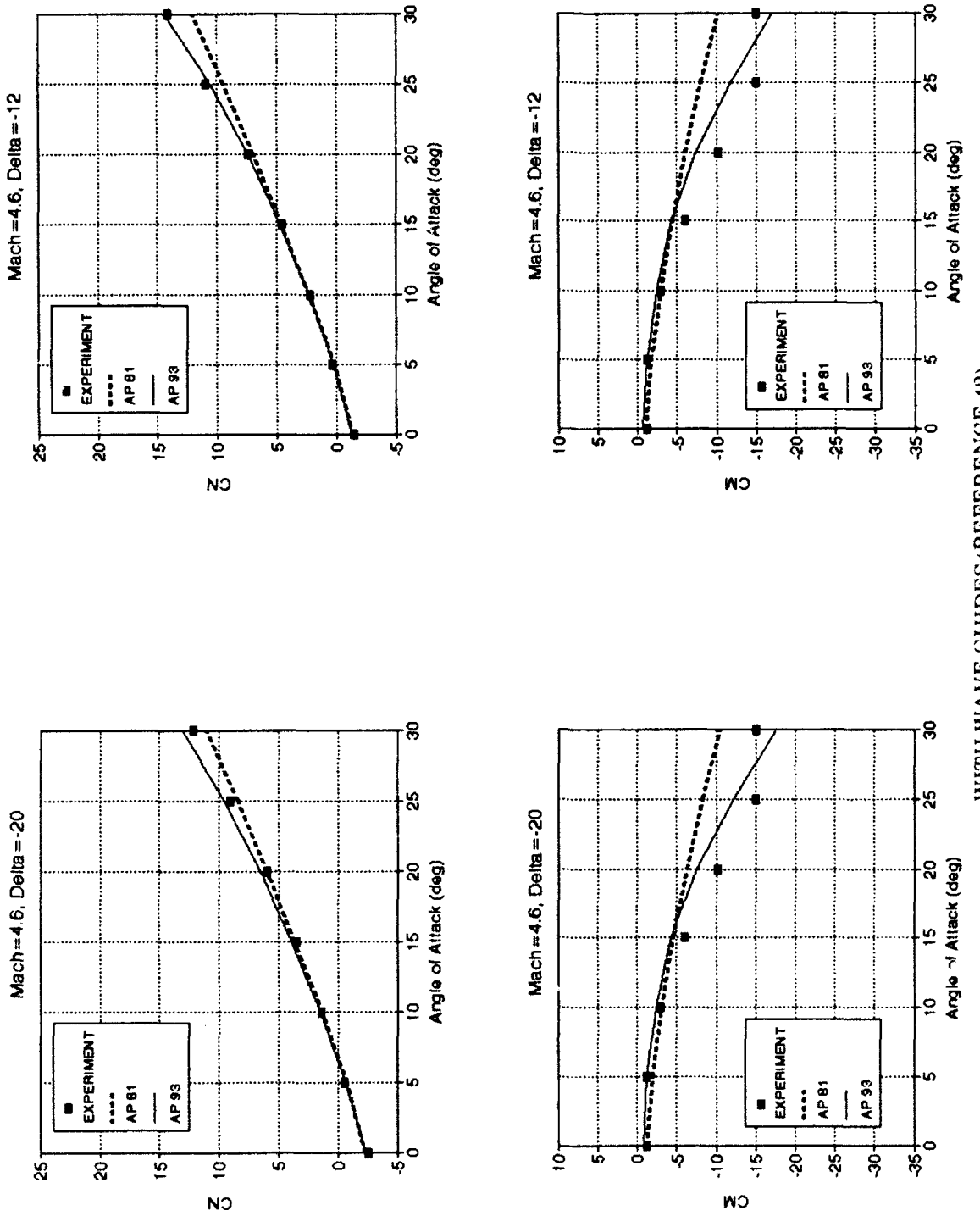

c. WITH WAVE GUIDES (REFERENCE 42)

FIGURE 21. NORMAL-FORCE AND PITCHING MOMENT COEFFICIENTS FOR CONFIGURATION OF FIGURE 21a FOR VARIOUS MACH NUMBERS AND CONTROL DEFLECTIONS (CONTINUED)

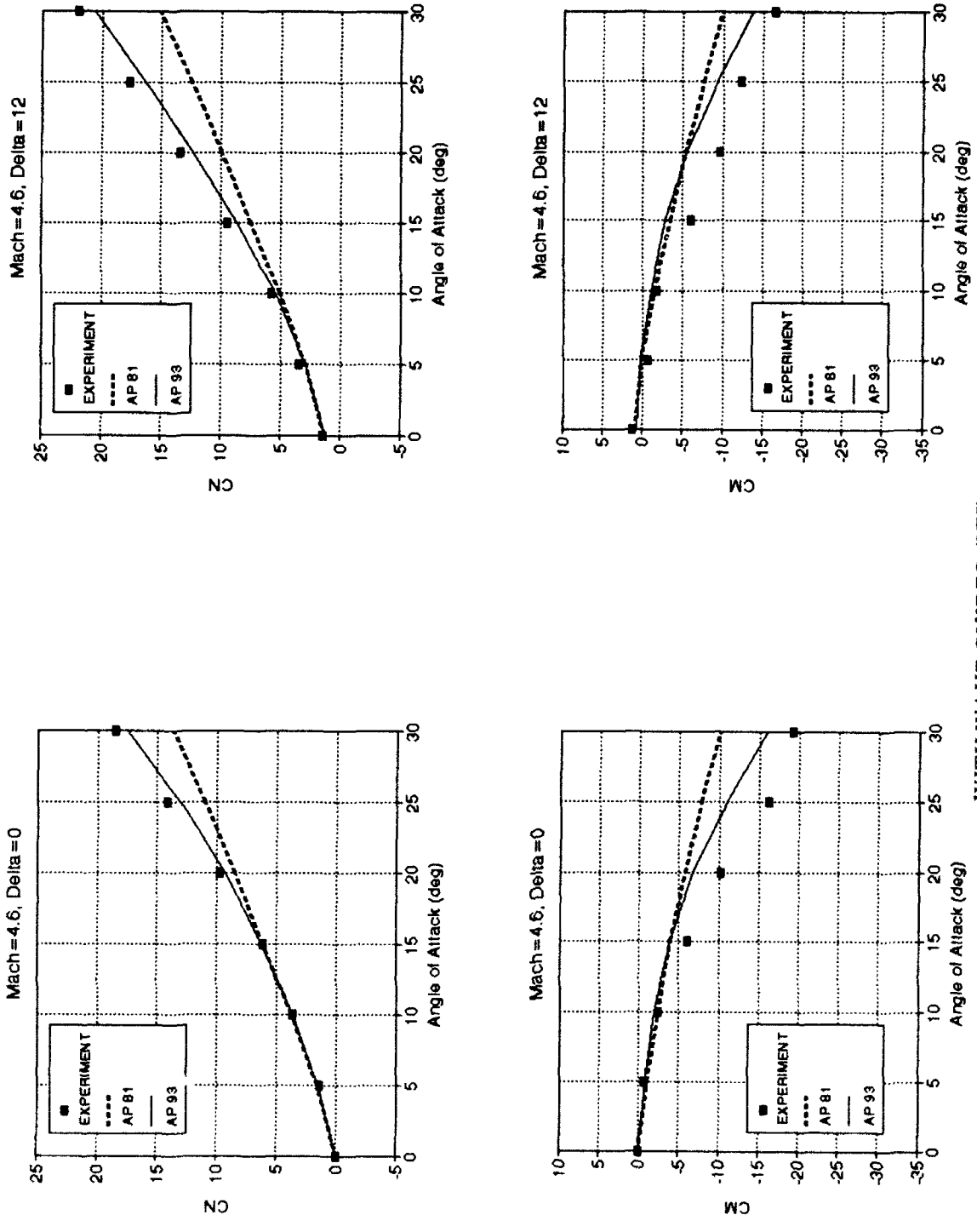

c. WITH WAVE GUIDES (REFERENCE 42)

FIGURE 21. NORMAL-FORCE AND PITCHING MOMENT COEFFICIENTS FOR CONFIGURATION OF FIGURE 21a FOR VARIOUS MACH NUMBERS AND CONTROL DEFLECTIONS (CONTINUED)

A fourth case used in the validation and development of the nonlinear $k_{W(B)}$ model is shown in Figure 22a. Note that in Figure 22a, two configurations were actually tested[44]—one that had a full-tail surface and a second that had a partial cutout removed. The APC will not handle the partial-wing configuration as it stands, so an engineering model of this wing must be created. Experience has shown that the lifting surface area, aspect ratio, span, leading edge sweep angle, and centroid of the presented area must be held constant. The chord is varied so as to meet these constraints. Hence, the configuration that represents the partial-wing results is the body canard of Figure 22a, plus the AP93 representation of the partial tail shown in the lower right of Figure 22a.

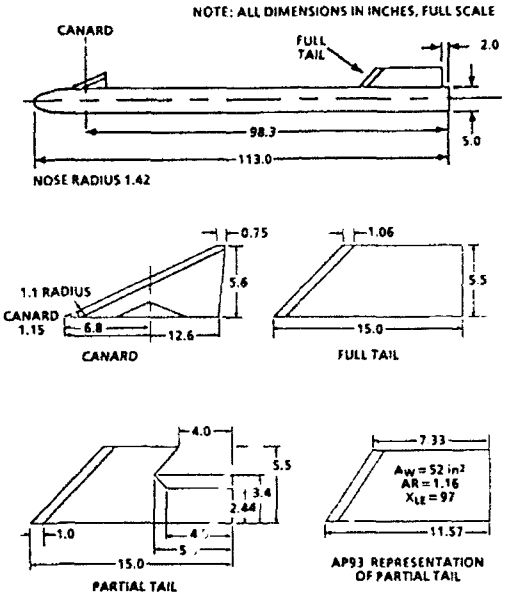

FIGURE 22a. CANARD-CONTROLLED MISSILE CONFIGURATION WITH FULL-TAIL,PARTIAL-TAIL, AND AP93 REPRESENTATION OF PARTIAL TAIL FOR USE IN VALIDATION PROCESS[44]

Figures 22b through 22d present the comparison of the AP93 with wind tunnel test data.[44] Data were only available at $M_\infty = 0.2$; however, this compliments the previous data set for the SPARROW missile in the sense that no subsonic data were available for that case. The full-tail and partial-tail results are denoted on the figure. Some results were available from Reference 44 for the Missile Datcom.[45] These results are also shown where available. As seen in the figure, the AP93 gives improved results for pitching moment and normal force for most conditions compared to the Missile Datcom. While center of pressure is not shown, the AP93 computations are generally within the goal of ± 4 percent of the body length. For example, at $\alpha = 30$ deg, $\delta = -20$ deg, x_{cp} for the data, AP93 and Missile Datcom are 5.39, 4.91, and 3.75 calibers, respectively, with respect to the moment reference point. This represents errors of 2.1 and 7.3 percent of the body length, respectively, for the AP93 and Missile Datcom codes.

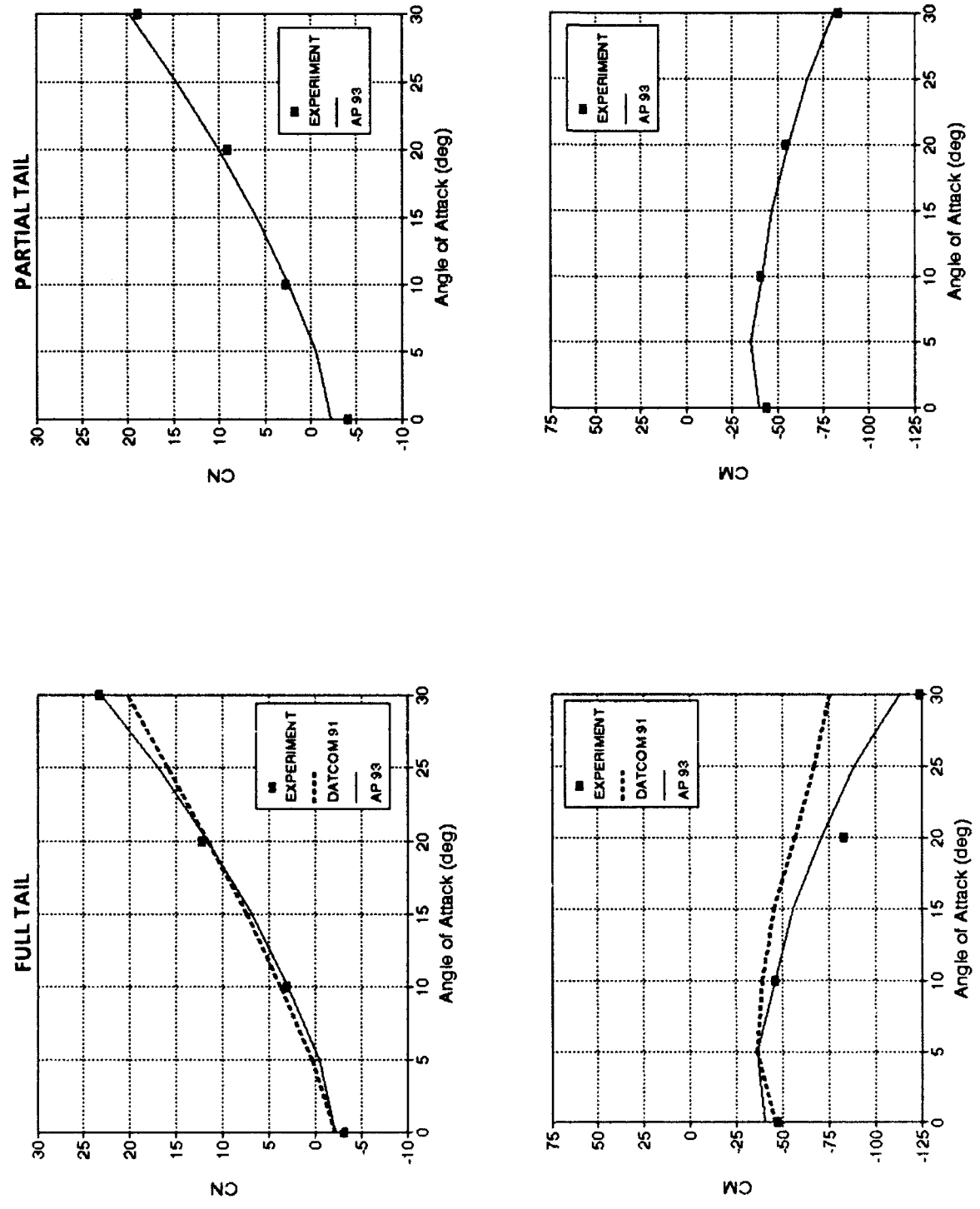

b. $M_\infty = 0.2$, $\delta_c = -20$ DEG

FIGURE 22b. COMPARISON OF AP93 TO WIND TUNNEL DATA AND MISSILE DATCOM FOR NORMAL-FORCE AND PITCHING MOMENT COEFFICIENTS OF FIGURE 22a CONFIGURATION

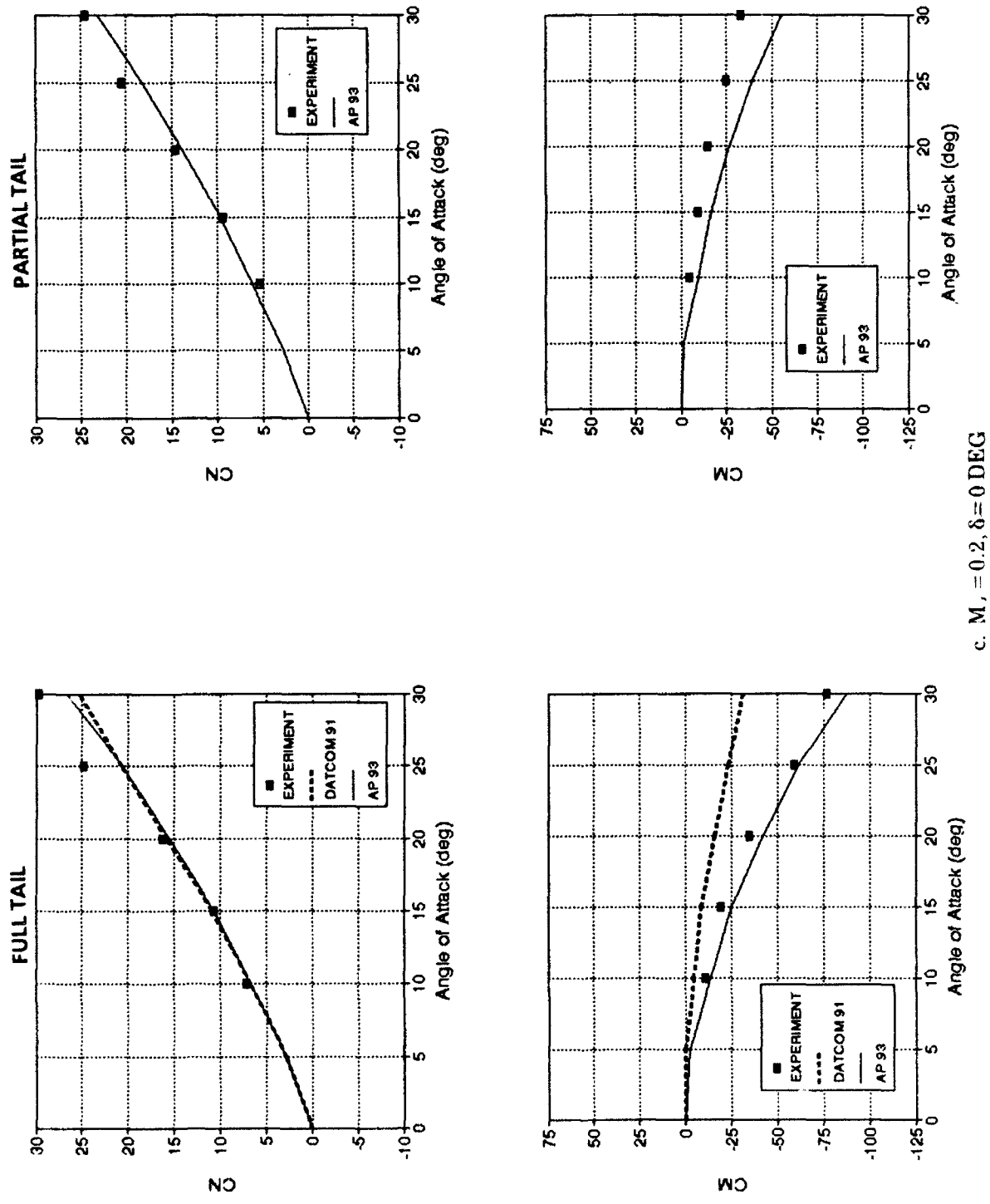

c. $M_\infty = 0.2, \delta = 0$ DEG

FIGURE 22c. COMPARISON OF AP93 TO WIND TUNNEL DATA AND MISSILE DATCOM FOR NORMAL-FORCE AND PITCHING MOMENT COEFFICIENTS OF FIGURE 22a CONFIGURATION (CONTINUED)

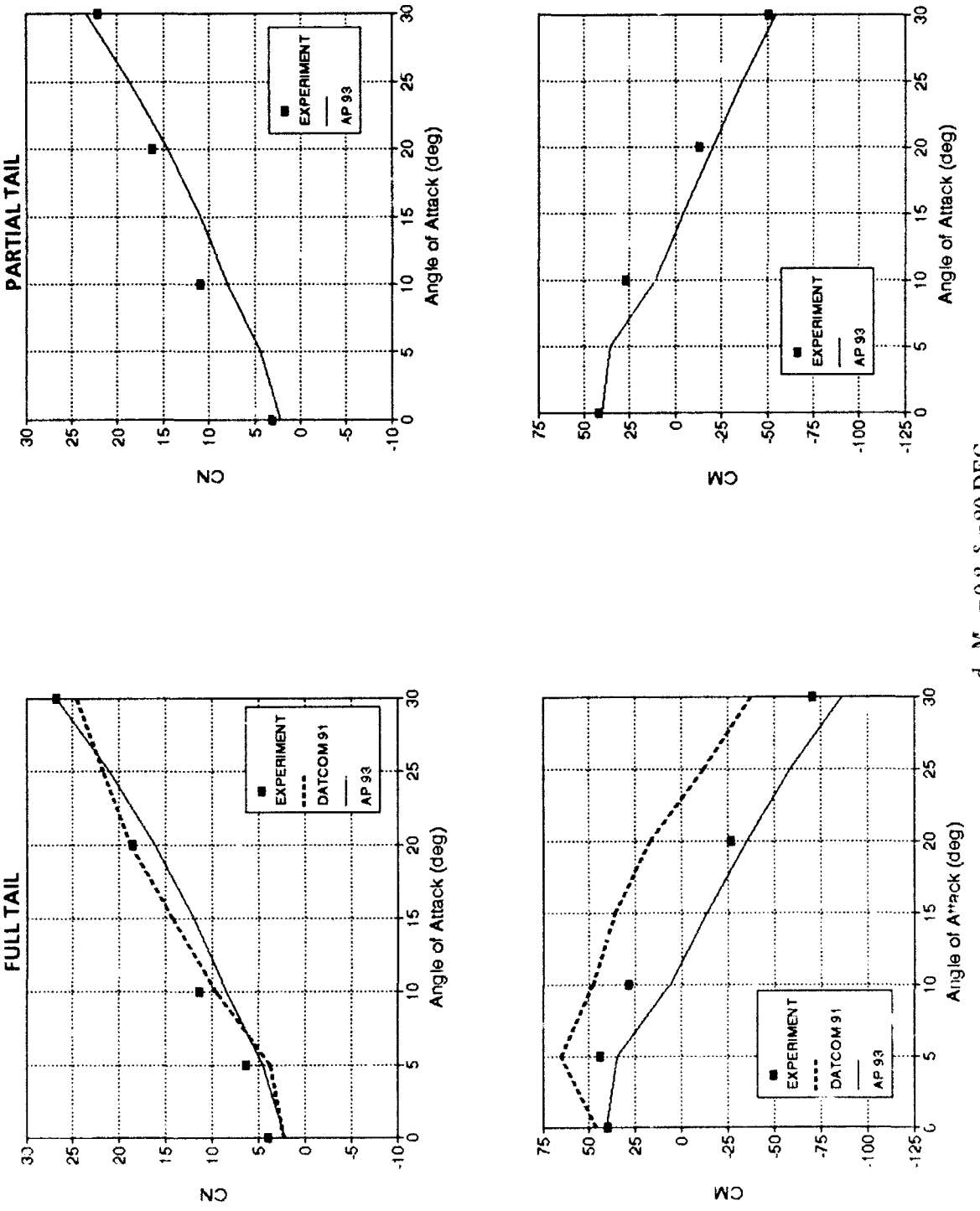

d. $M_\infty = 0.2, \delta = 20$ DEG

FIGURE 22d. COMPARISON OF AP93 TO WIND TUNNEL DATA AND MISSILE DATCOM FOR NORMAL FORCE AND PITCHING MOMENT COEFFICIENTS OF FIGURE 22a CONFIGUPATION (CONTINUED)

Two body-tail cases were considered in the validation process. The first of these is shown in Figure 23a and is taken from Reference 68. Several wing planforms were tested in Reference 68, but only one example will be shown. The body was just over 13 calibers long with a 0.54-caliber, 4-deg boattail at the rear. For these tests, a boundary layer trip was used, and data were obtained at α up to 25 deg at Mach numbers 1.6, 2.36, and 2.86 and for $\delta = 0$ and 10 deg.

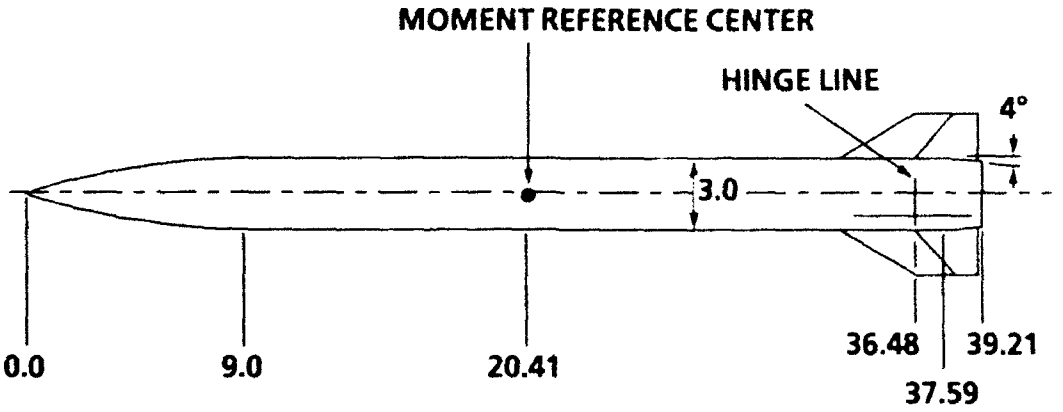

FIGURE 23a. BODY-TAIL CONFIGURATION USED IN VALIDATION PROCESS[68] (DIMENSIONS IN INCHES)

Figures 23b through 23c present the wind tunnel measurements, AP93 and AP81 for the Mach 1.6 and 2.86 cases at control deflections of 0 and 10 deg. Results are presented in terms of normal, forebody axial, and pitching moment coefficients as a function of angle of attack. The only real improvement of the AP93 code compared to the AP81 version is in pitching moment at high α and at transonic speeds. The reason for the slight improvement in the configuration is a body-tail case with a moderate aspect ratio tail surface. This type of configuration is typical of configurations where the AP81 code performed satisfactorily.

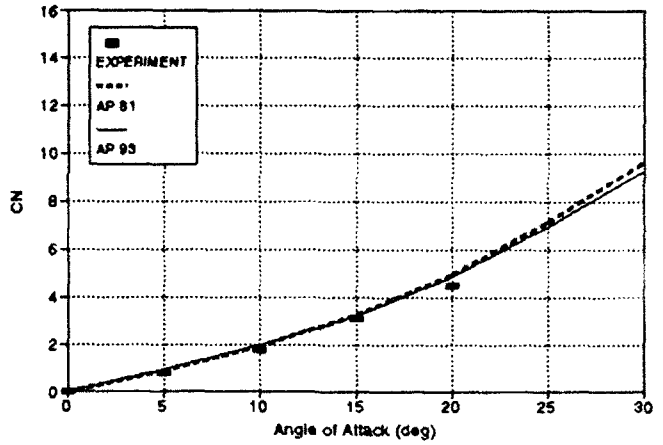

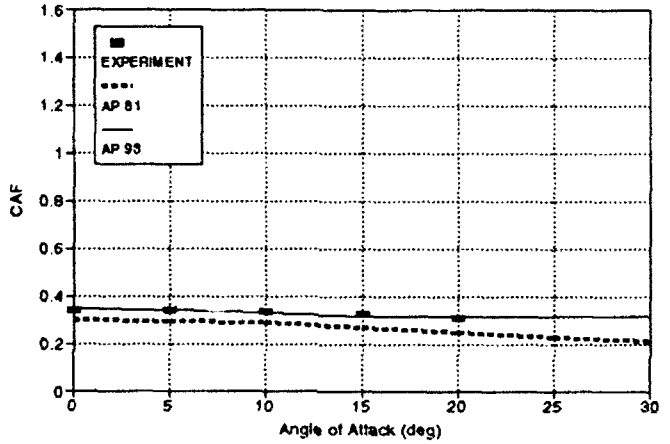

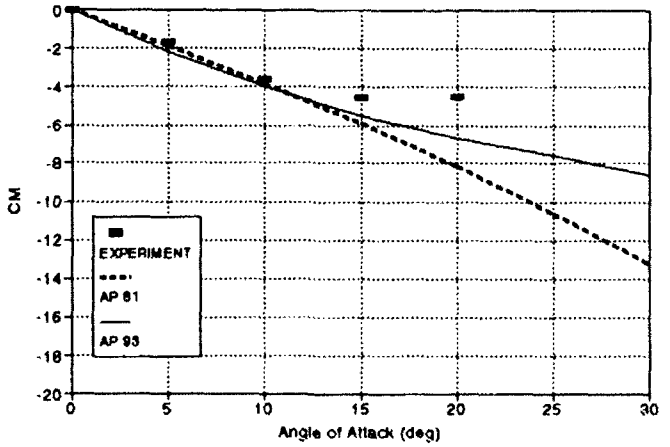

b. $M_\infty = 1.6, \delta = 0$ DEG

FIGURE 23. AERODYNAMICS OF A BODY-TAIL CONFIGURATION USED IN VALIDATION PROCESS[68]

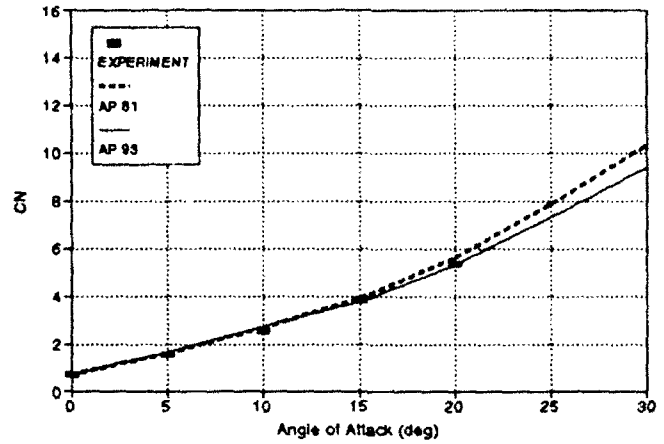

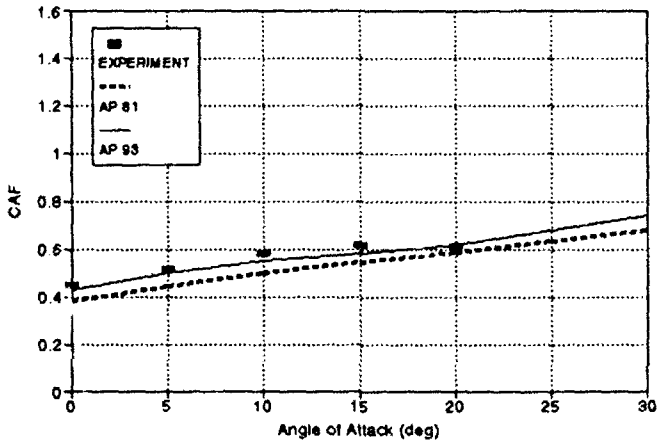

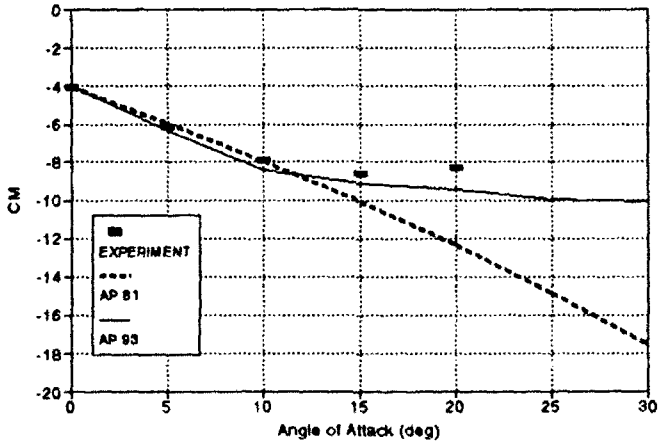

c. $M_\infty = 1.6, \delta = 10$ DEG

FIGURE 23. AERODYNAMICS OF A BODY-TAIL CONFIGURATION USED IN VALIDATION PROCESS[68] (CONTINUED)

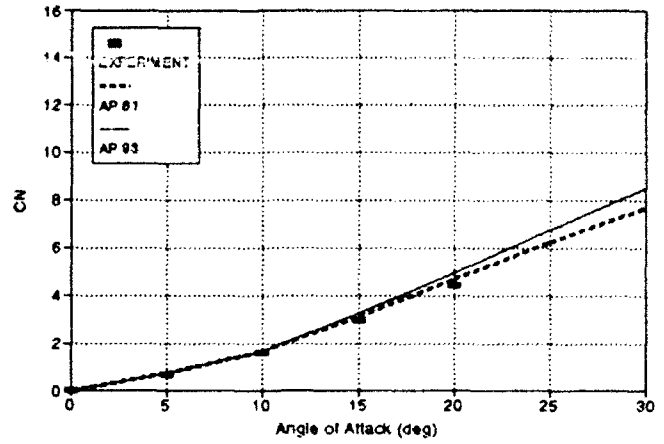

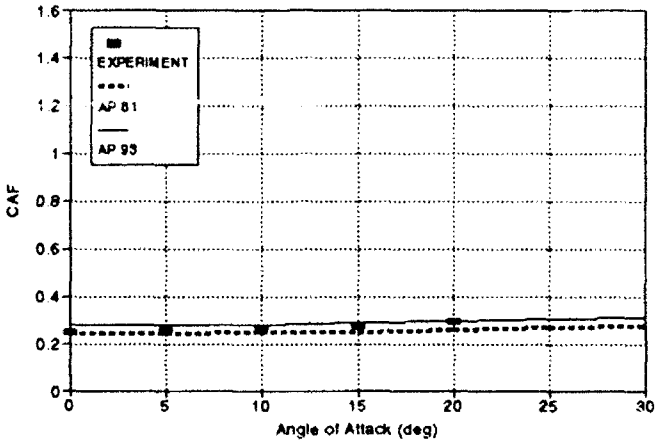

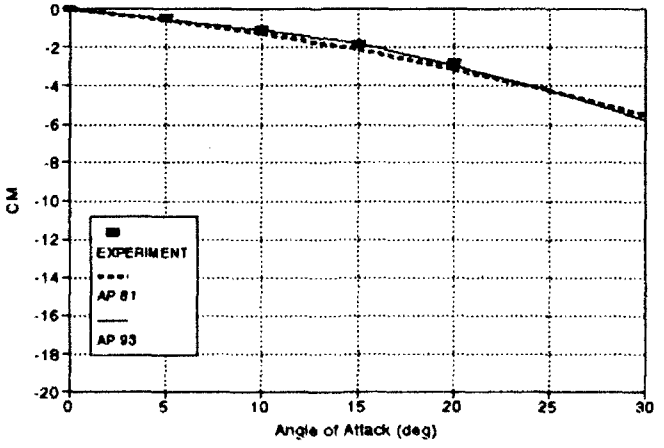

d. $M_r = 2.86, \delta = 0$ DEG

FIGURE 23. AERODYNAMICS OF A BODY-TAIL CONFIGURATION USED IN VALIDATION PROCESS[68] (CONTINUED)

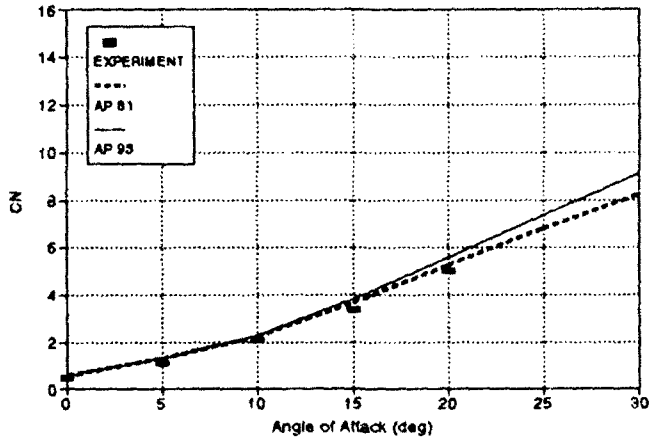

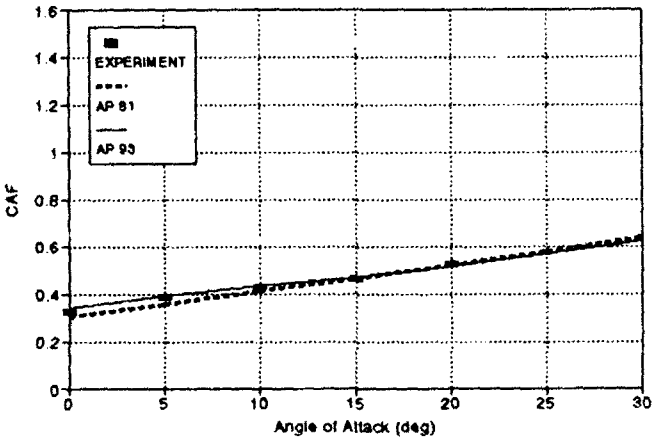

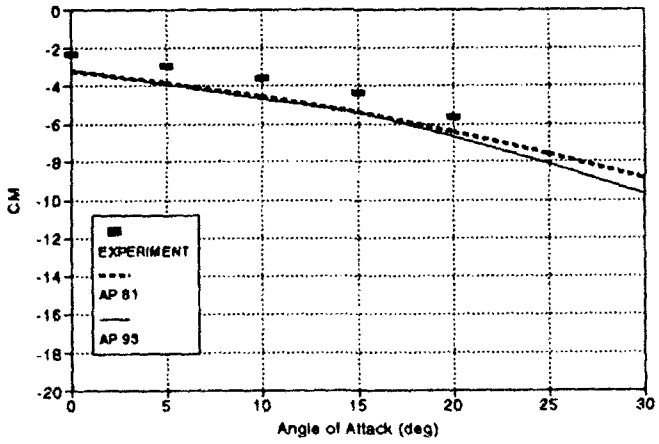

e. $M_\infty = 2.86, \delta = 10$ DEG

FIGURE 23. AERODYNAMICS OF A BODY-TAIL CONFIGURATION USED IN VALIDATION PROCESS[68] (CONTINUED)

The second body-tail configuration is shown in Figure 24a, and the wind tunnel test data along with details of the test are given in Reference 69. The configuration of Figure 24a is 10 calibers long with an aspect ratio tail of about 1.0. Again, this configuration is typical of cases where the AP81 code has performed well in the past. Results in terms of C_N and C_M as a function of α at $M_\infty = 0.6$, 0.9, and 1.3 are shown in Figure 24b for the AP93, AP81, and data. The AP93 shows some improvement over the AP81 for pitching moment at high α, but normal force is about the same. The reason for this improvement is the nonlinear lift loss methodology included in the AP93 that was not available in the AP81 code.

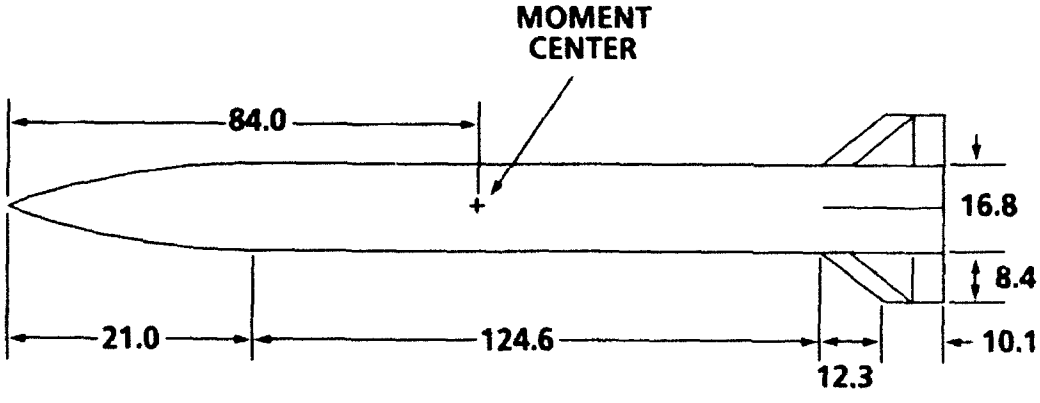

FIGURE 24a. BODY-TAIL CONFIGURATION USED IN VALIDATION PROCESS[69]
(DIMENSIONS IN INCHES, FULL SCALE)

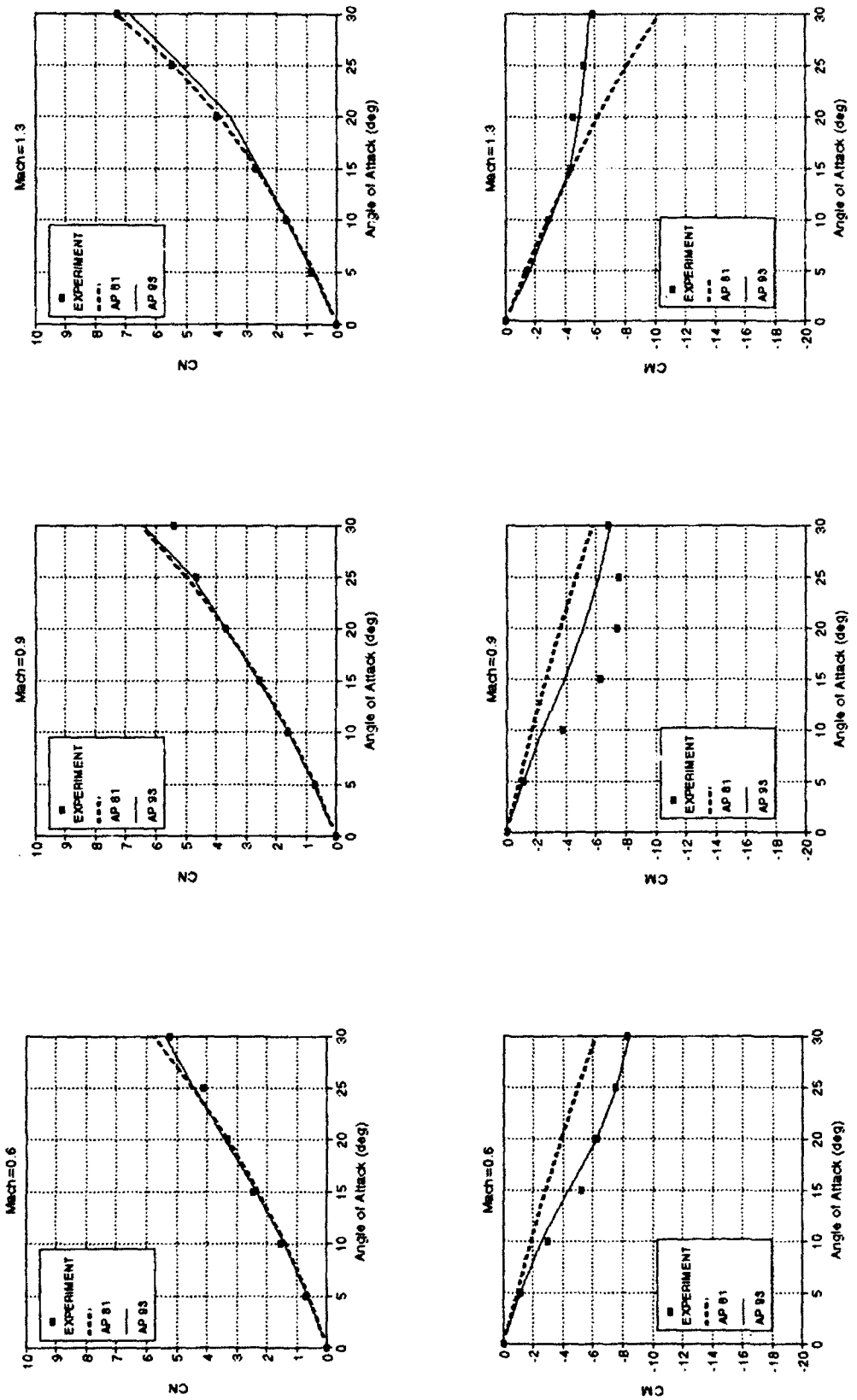

FIGURE 24b. AERODYNAMICS OF BODY-TAIL CONFIGURATION USED IN VALIDATION PROCESS[69]

The last two configurations used for the validation process are from Reference 70. These configurations feature somewhat unconventional missile fin arrangements that should help in validating the AP93. The first of these configurations is shown in Figure 25a and consists of a fairly large wing followed by a much smaller tail that is used for control. The ratio of the wing and tail planform areas to that of the body is 16.25 and 2.99, respectively. The aspect ratios of these lifting surfaces are 0.92 and 3.63, respectively, and their r/s values are 0.23 and 0.26. Example computations are shown for Mach numbers 1.61, 2.0, 2.86, 3.95, and 4.63 and at tail deflections of 0, -10 deg, and -20 deg.

Comparisons are made with AP93, AP81, and the Reference 70 wind tunnel data for lift, drag, and pitching moment coefficients in Figures 25b through 25p. For this missile configuration, the AP93 shows slight improvement in predictions over AP81. Both codes give fair to good engineering estimates of aerodynamics at all conditions considered. The area where the AP93 code still needs slight improvement is in the Mach 2.0 to 3.0 range at higher angles of attack and for AR of about one.

In attempting to analyze why this problem occurs, the wing-alone data bases of References 39 and 40 were reviewed again. The nonlinear wing-lift model of AP93 is based on the Reference 39 data for Mach numbers of 1.6 and greater and on Reference 40 data for Mach numbers of 1.2 and lower. Reference 39 data were compared with that of other data sets, including Reference 40. At Mach 2 and AR = 1.0, the Reference 39 data are up to 15 percent lower than the Reference 40 wing-alone data. It is suspected that since the Reference 39 forces and moments were not measured but integrated from pressure data, and since the wings were required to be fairly thick to house the pressure taps, that this is the reason for the difference. It is also suspected that around M = 1.5 to 2.5, the loss in lift due to thickness is larger than at other Mach numbers. In hindsight, it would have been better to develop the wing-alone nonlinear model based on an average of the two data bases. In future work, this will be done.

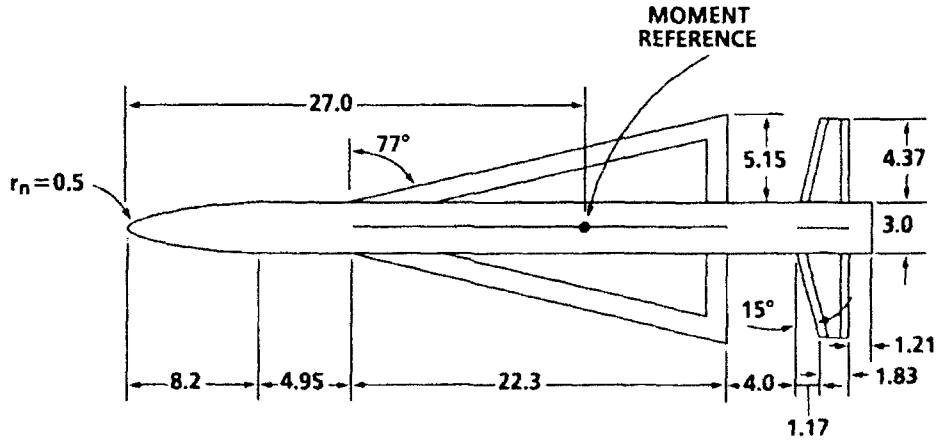

FIGURE 25a. WING-BODY-TAIL CONFIGURATION USED IN VALIDATION PROCESS[70] (DIMENSIONS IN INCHES)

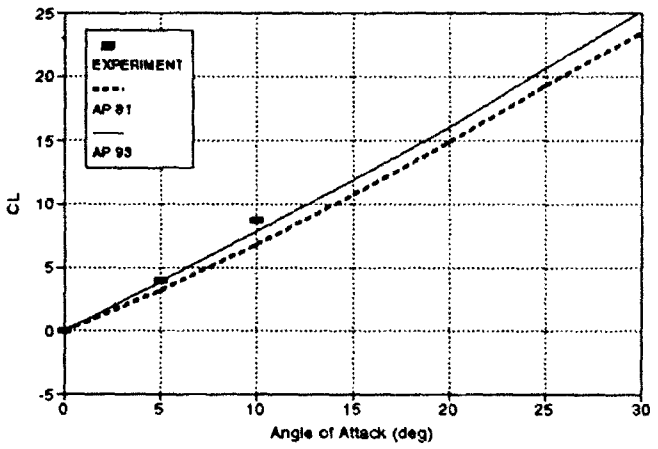

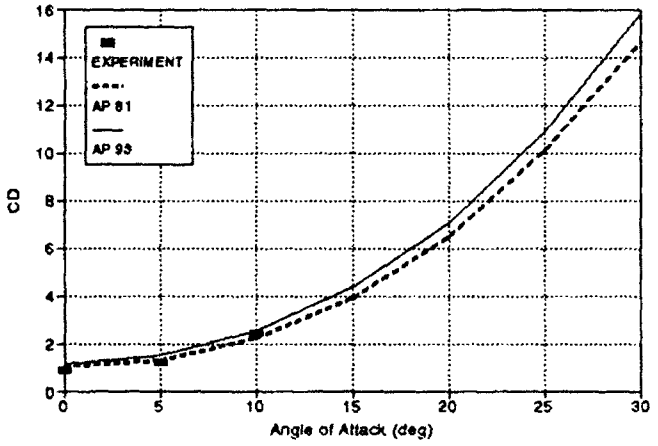

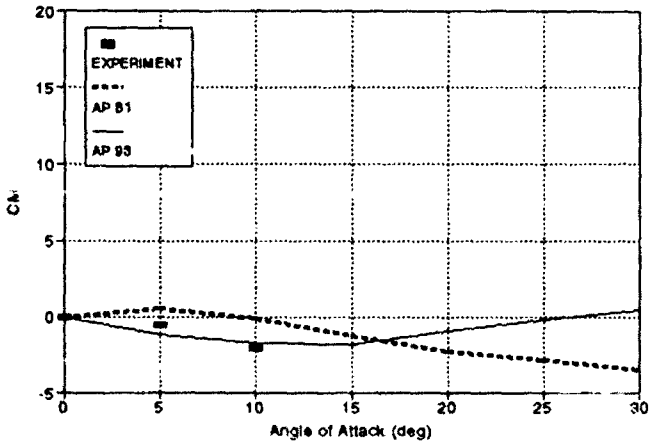

b. $M_\infty = 1.61, \delta = 0$ DEG

FIGURE 25. LIFT, DRAG, AND PITCHING MOMENT COEFFICIENTS OF A WING-BODY-TAIL CONFIGURATION USED IN VALIDATION PROCESS[70]

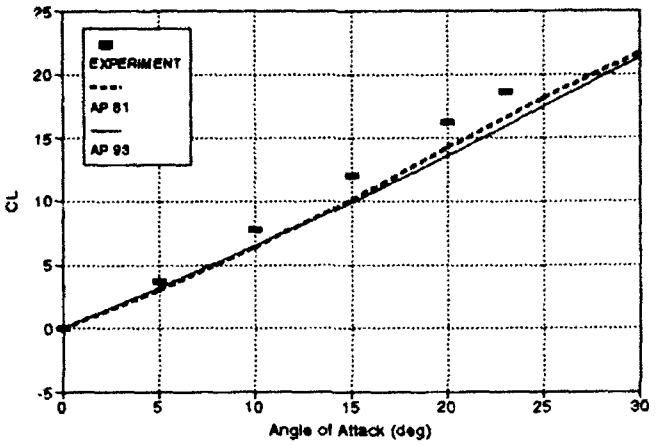

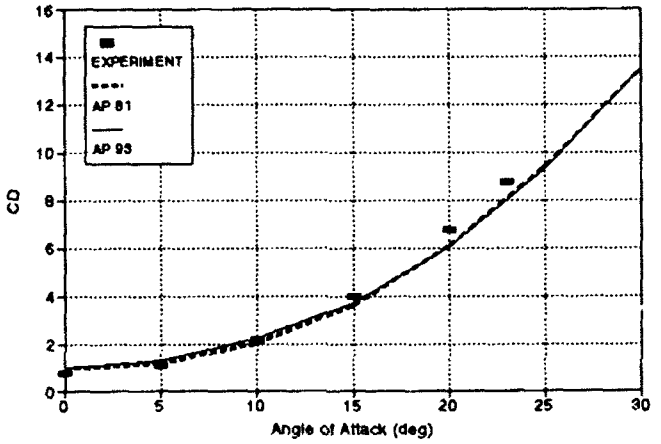

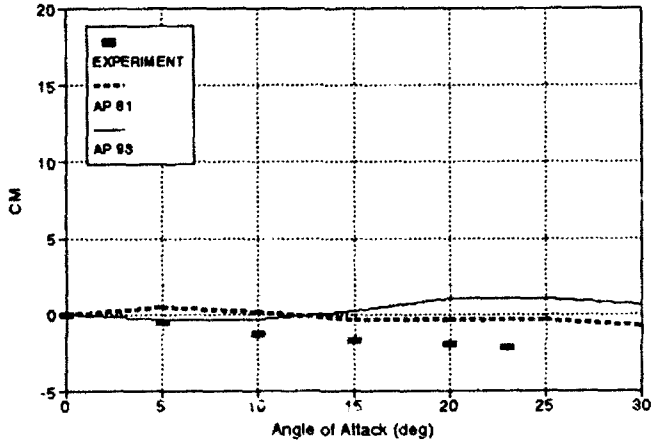

c. $M_\infty = 2.0, \delta = 0$ DEG

FIGURE 25. LIFT, DRAG, AND PITCHING MOMENT COEFFICIENTS OF A WING-BODY-TAIL CONFIGURATION USED IN VALIDATION PROCESS[70] (CONTINUED)

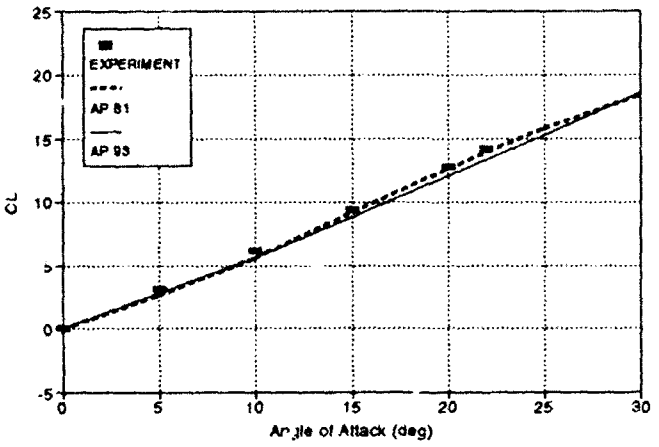

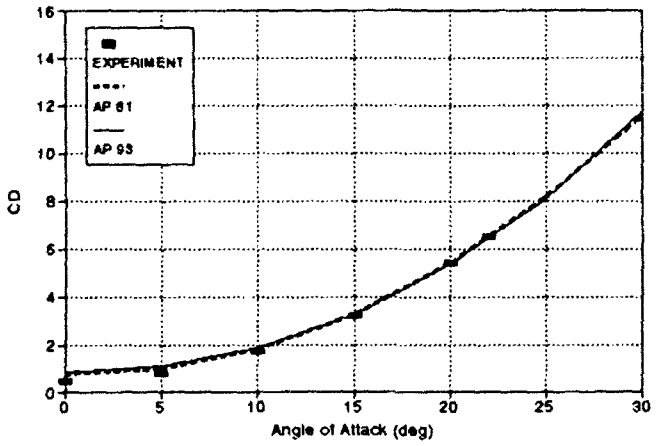

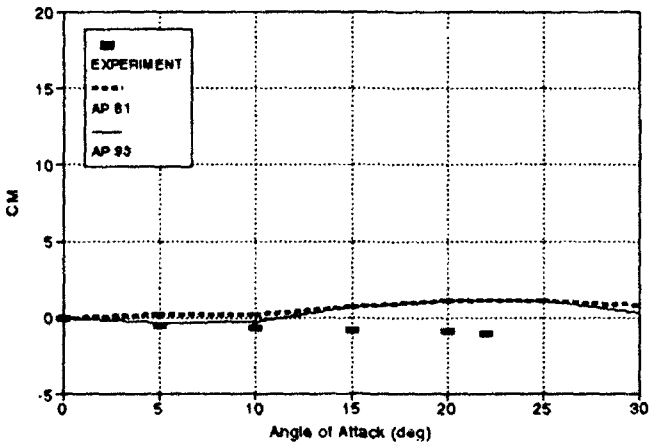

d. $M_\infty = 2.86, \delta = 0$ DEG

FIGURE 25. LIFT, DRAG, AND PITCHING MOMENT COEFFICIENTS OF A WING-BODY-TAIL CONFIGURATION USED IN VALIDATION PROCESS[70] (CONTINUED)

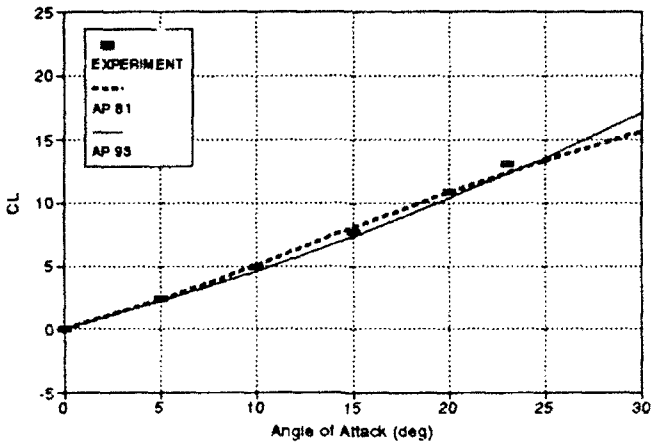

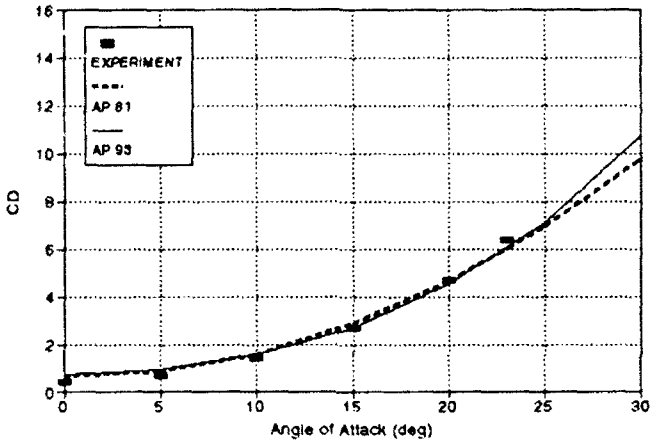

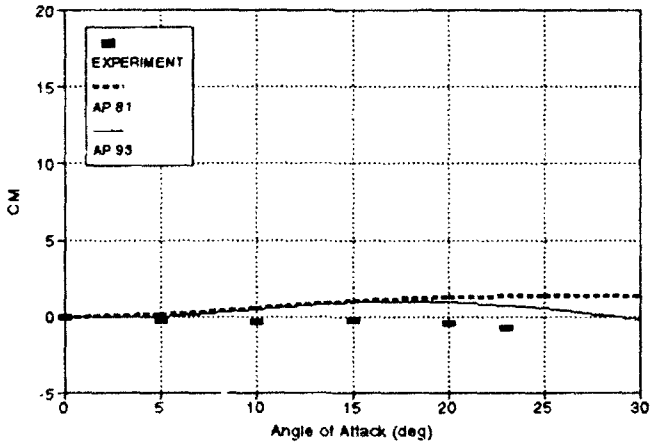

e. $M_\infty = 3.95, \delta = 0$ DEG

FIGURE 25. LIFT, DRAG, AND PITCHING MOMENT COEFFICIENTS OF A WING-BODY-TAIL CONFIGURATION USED IN VALIDATION PROCESS[70] (CONTINUED)

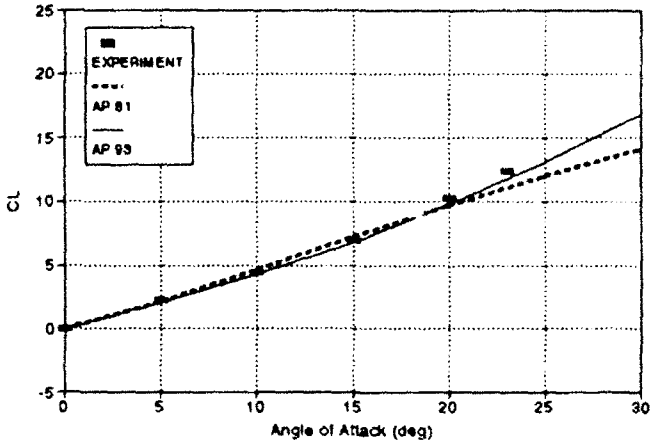

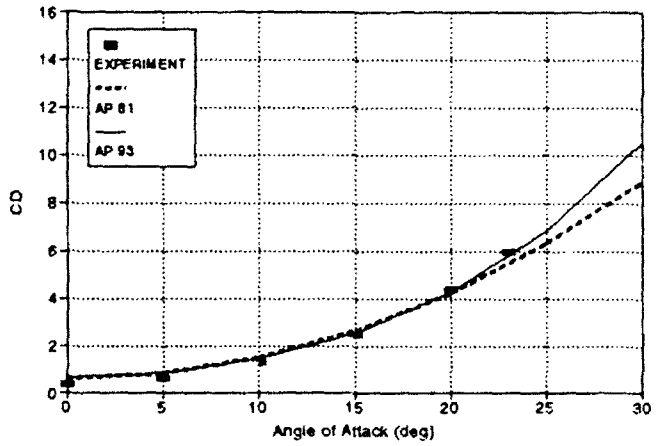

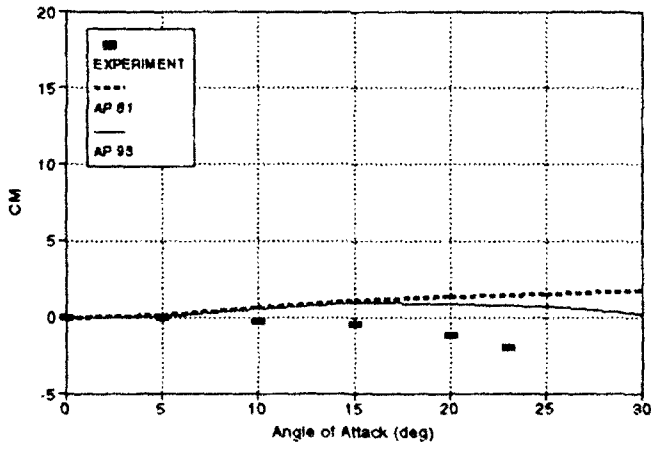

f. $M_\infty = 4.63, \delta = 0$ DEG

FIGURE 25. LIFT, DRAG, AND PITCHING MOMENT COEFFICIENTS OF A WING-BODY-TAIL CONFIGURATION USED IN VALIDATION PROCESS[70] (CONTINUED)

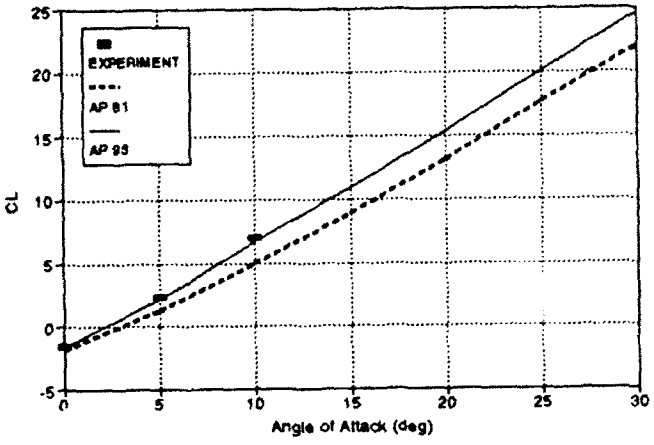

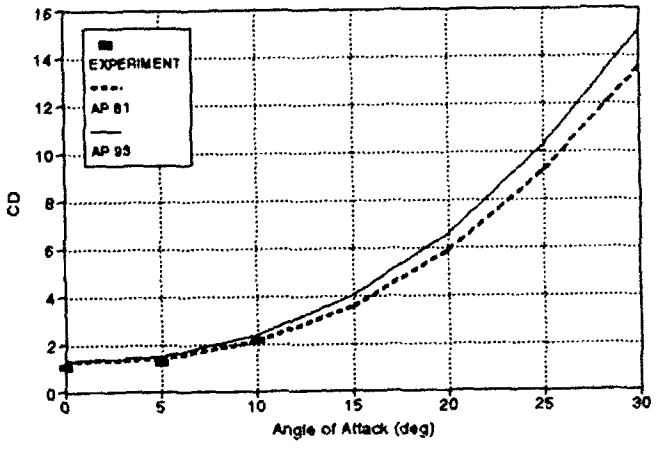

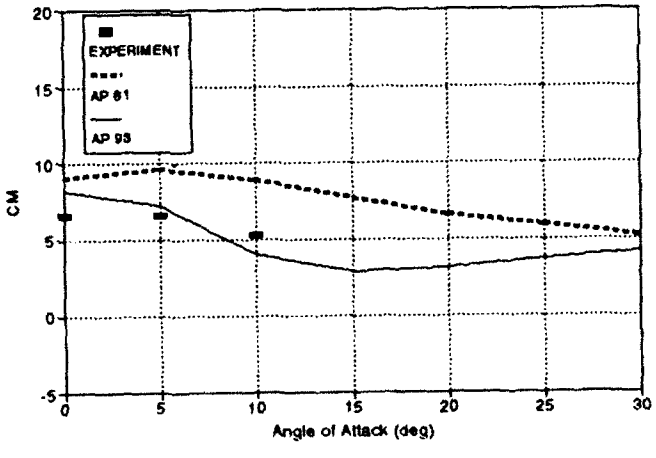

g. $M_\infty = 1.61, \delta = -10$ DEG

FIGURE 25. LIFT, DRAG, AND PITCHING MOMENT COEFFICIENTS OF A WING-BODY-TAIL CONFIGURATION USED IN VALIDATION PROCESS[70] (CONTINUED)

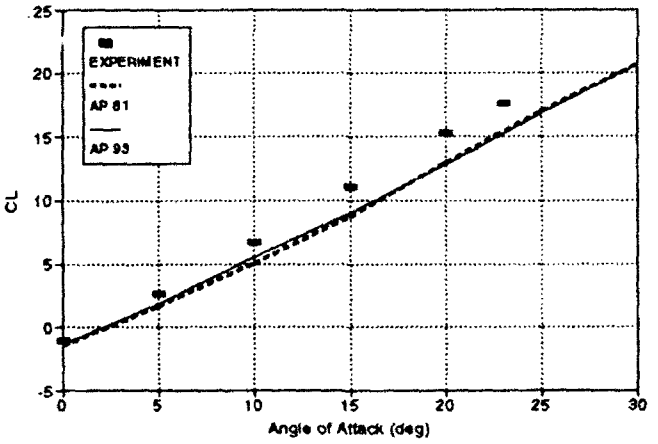

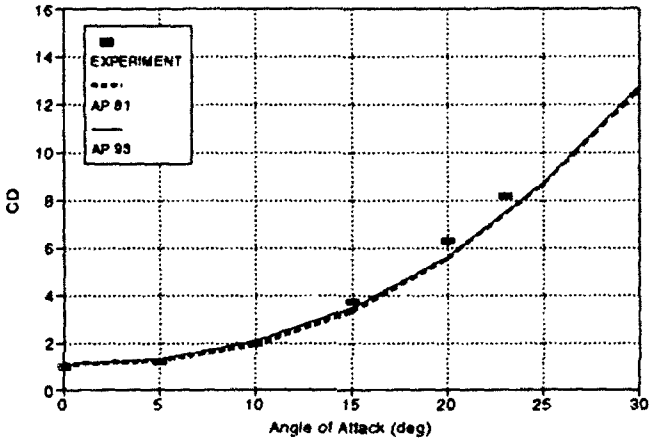

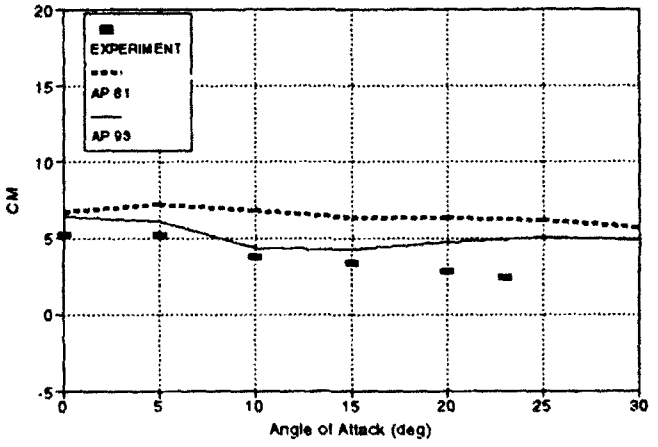

h. $M_\infty = 2.0, \delta = -10$ DEG

FIGURE 25. LIFT, DRAG, AND PITCHING MOMENT COEFFICIENTS OF A WING-BODY-TAIL CONFIGURATION USED IN VALIDATION PROCESS[70] (CONTINUED)

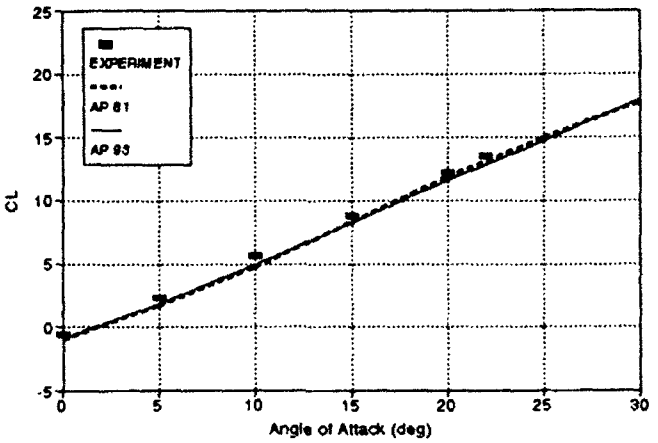

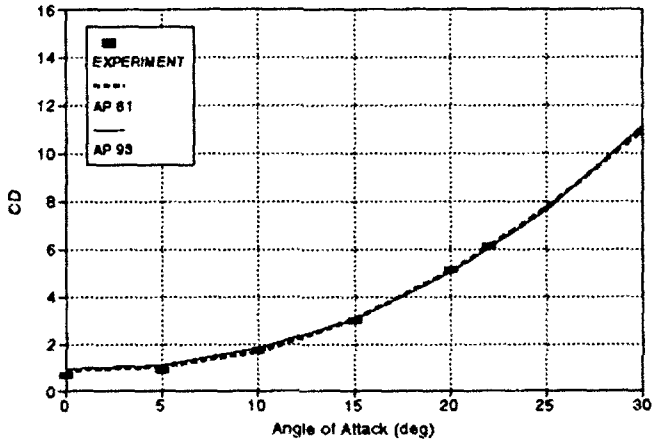

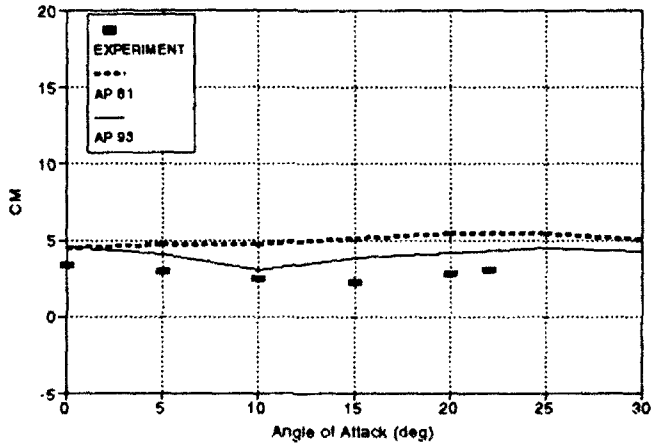

i. $M_\infty = 2.86, \delta = -10$ DEG

FIGURE 25. LIFT, DRAG, AND PITCHING MOMENT COEFFICIENTS OF A WING-BODY-TAIL CONFIGURATION USED IN VALIDATION PROCESS[70] (CONTINUED)

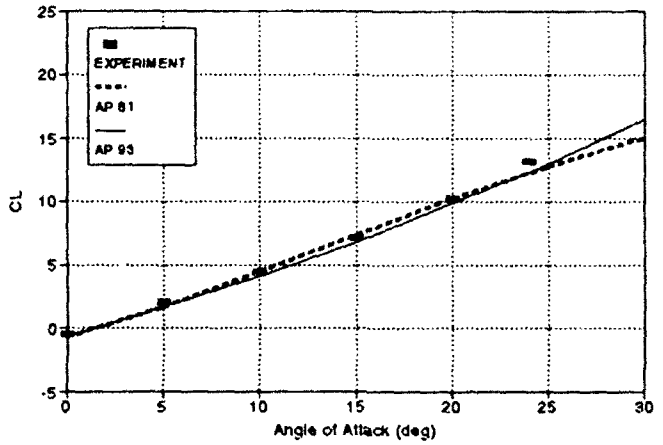

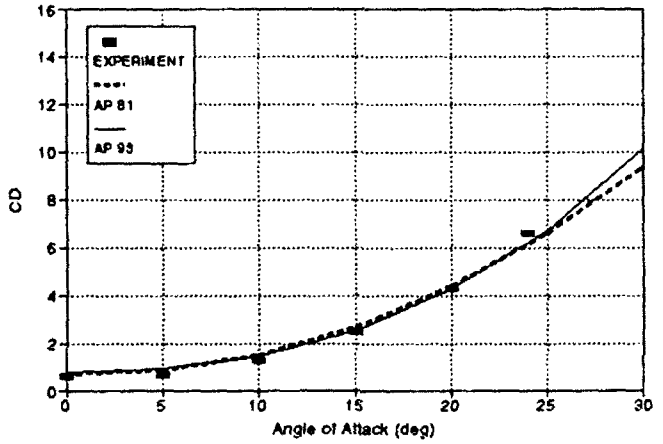

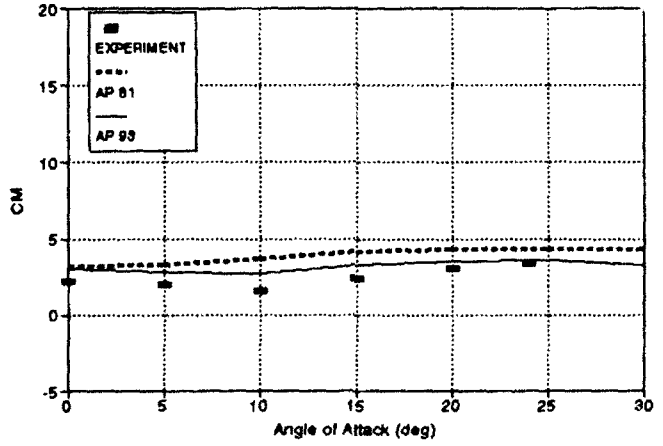

j. $M_\infty = 3.95, \delta = -10$ DEG

FIGURE 25. LIFT, DRAG, AND PITCHING MOMENT COEFFICIENTS OF A WING-BODY-TAIL CONFIGURATION USED IN VALIDATION PROCESS[70] (CONTINUED)

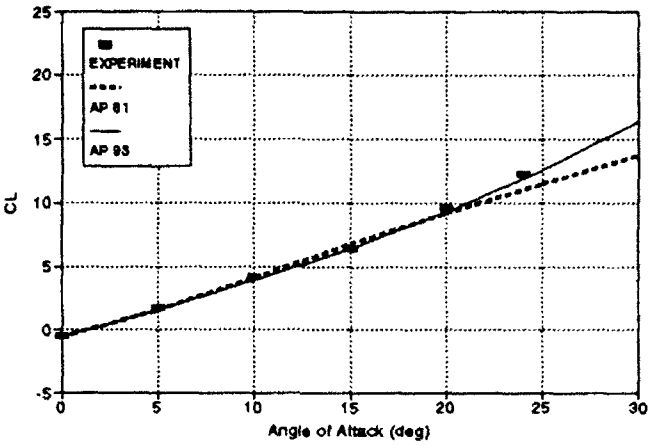

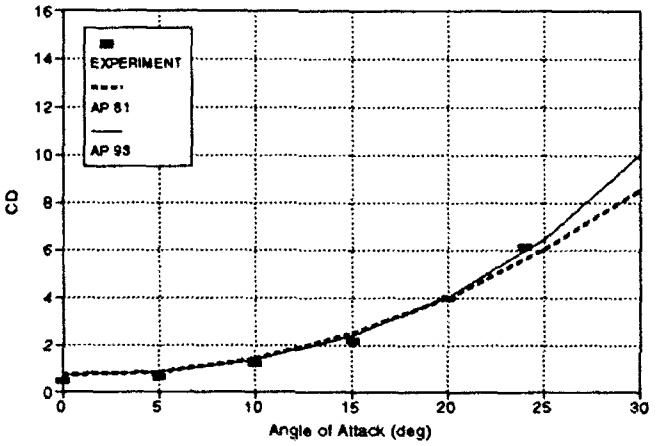

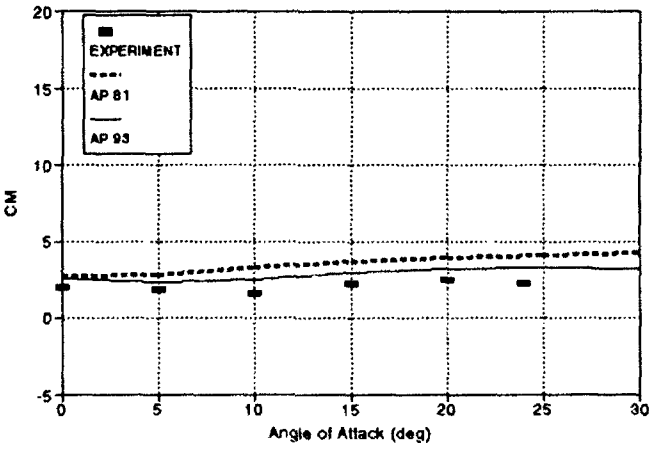

k. $M_\infty = 4.63, \delta = -10$ DEG

FIGURE 25. LIFT, DRAG, AND PITCHING MOMENT COEFFICIENTS OF A WING-BODY-TAIL CONFIGURATION USED IN VALIDATION PROCESS[70] (CONTINUED)

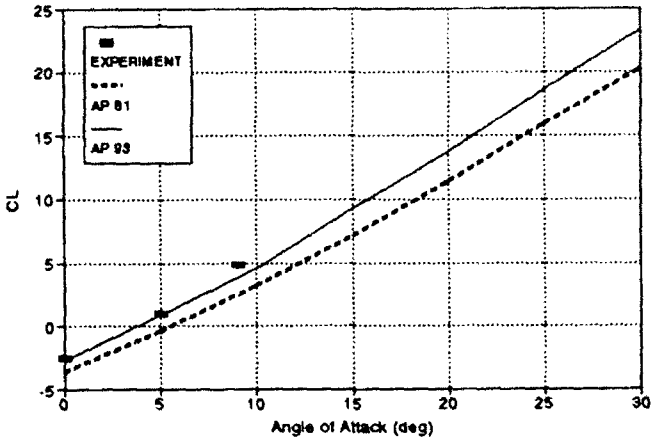

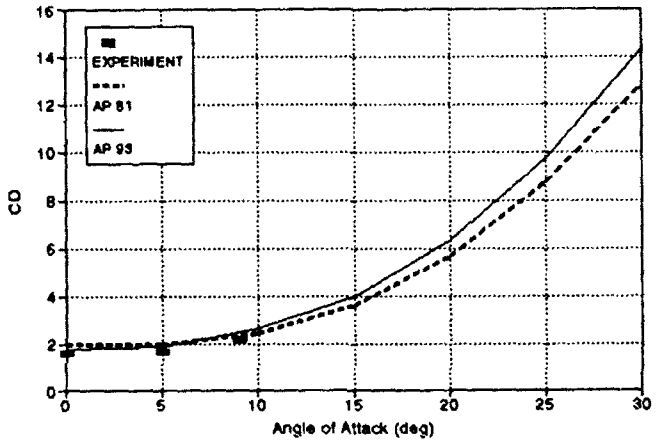

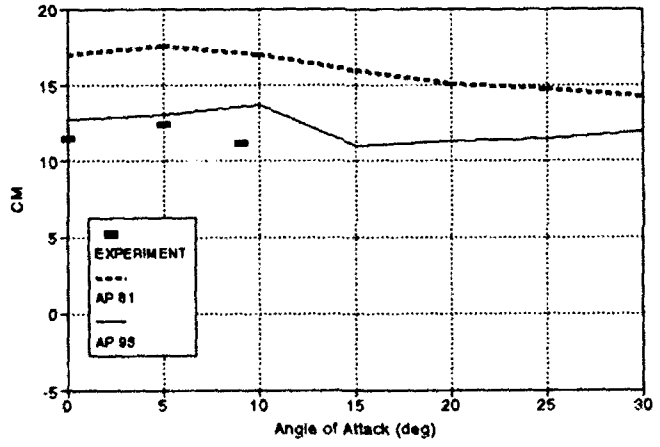

l. $M_\infty = 1.61, \delta = -20$ DEG

FIGURE 25. LIFT, DRAG, AND PITCHING MOMENT COEFFICIENTS OF A WING-BODY-TAIL CONFIGURATION USED IN VALIDATION PROCESS[70] (CONTINUED)

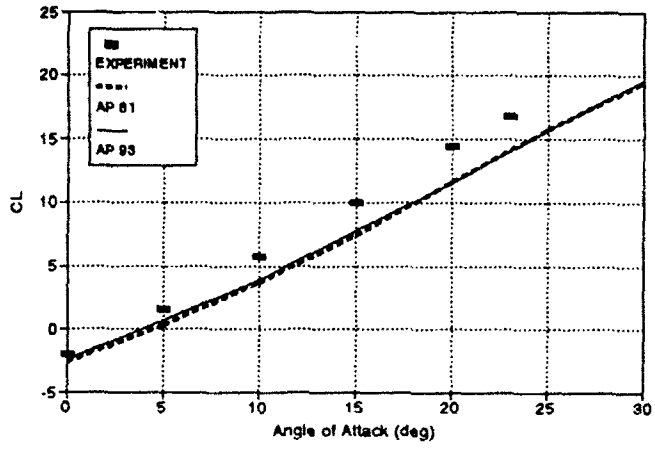

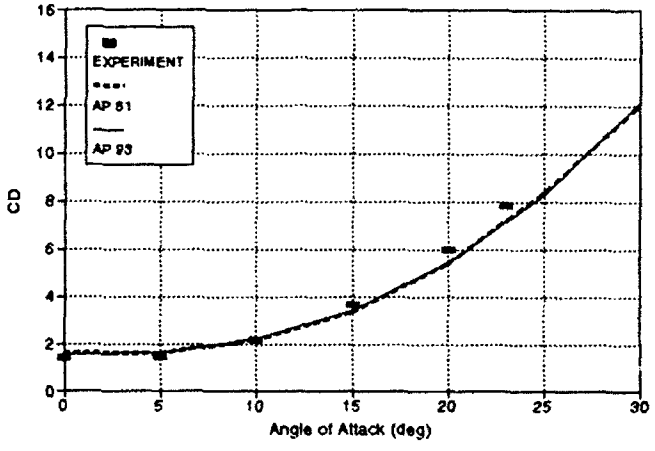

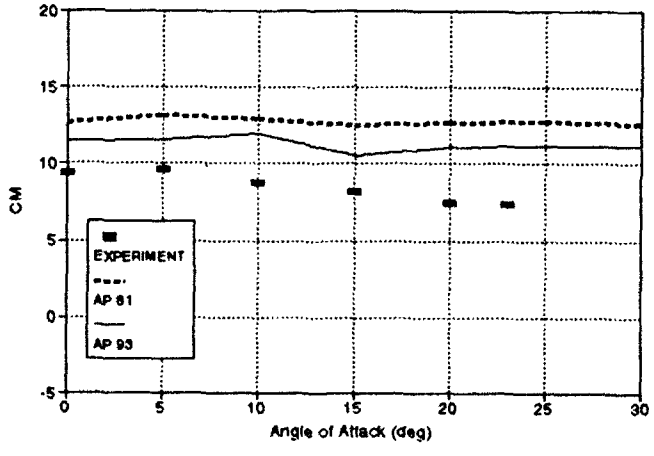

m. $M_\infty = 2.0, \delta = -20$ DEG

FIGURE 25. LIFT, DRAG, AND PITCHING MOMENT COEFFICIENTS OF A WING-BODY-TAIL CONFIGURATION USED IN VALIDATION PROCESS[70] (CONTINUED)

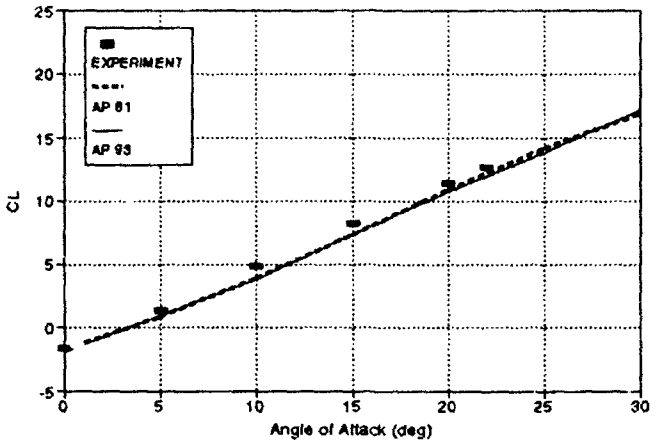

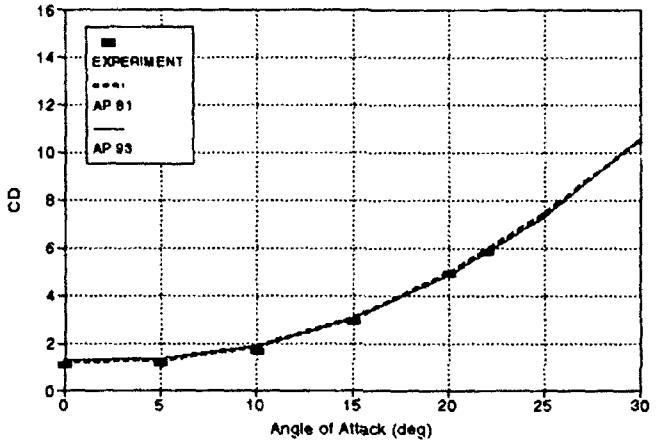

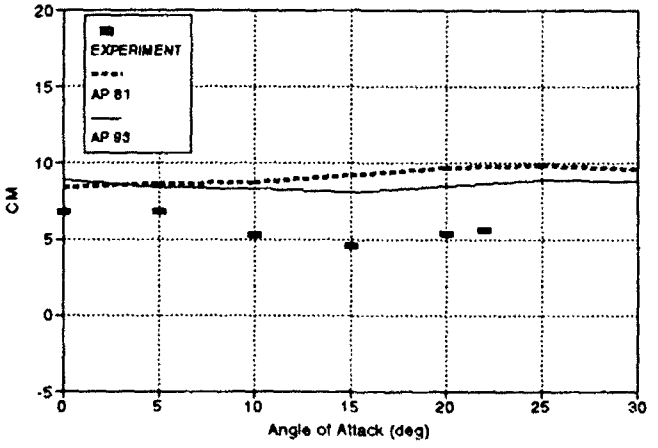

n. $M_\infty = 2.86, \delta = -20$ DEG

FIGURE 25. LIFT, DRAG, AND PITCHING MOMENT COEFFICIENTS OF A WING-BODY-TAIL CONFIGURATION USED IN VALIDATION PROCESS[70] (CONTINUED)

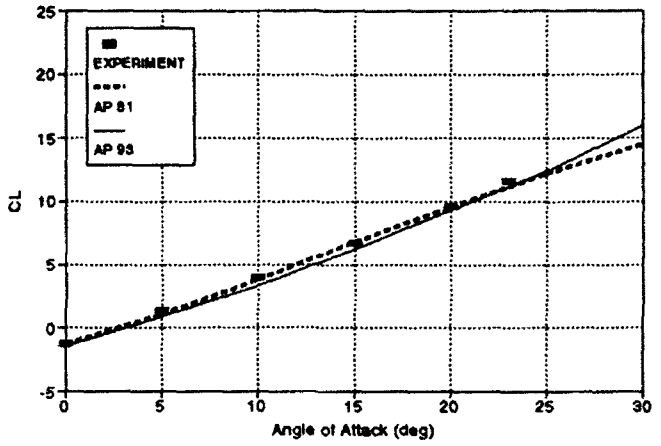

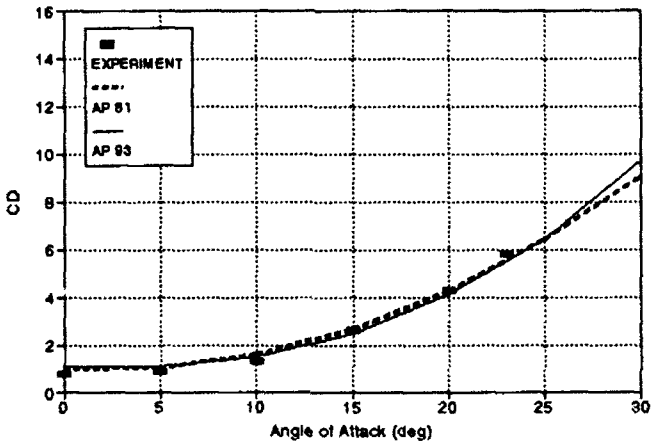

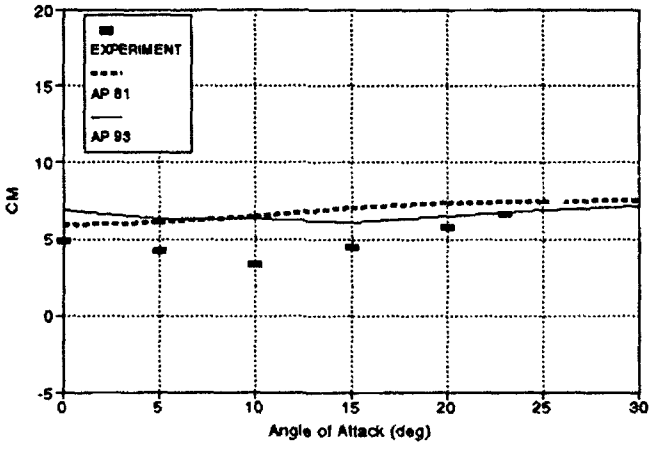

o. $M_\infty = 3.95, \delta = -20$ DEG

FIGURE 25. LIFT, DRAG, AND PITCHING MOMENT COEFFICIENTS OF A WING-BODY-TAIL CONFIGURATION USED IN VALIDATION PROCESS[70] (CONTINUED)

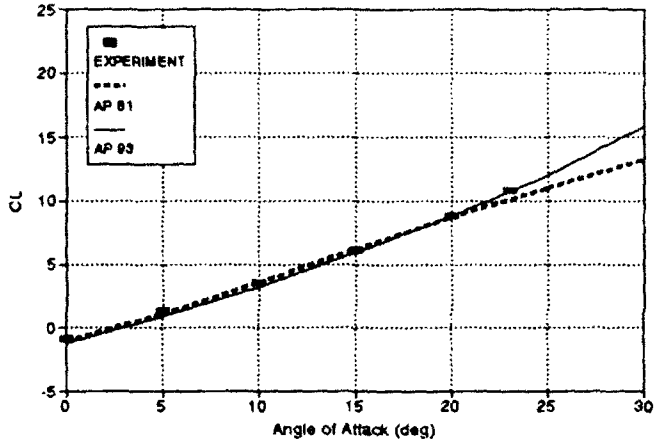

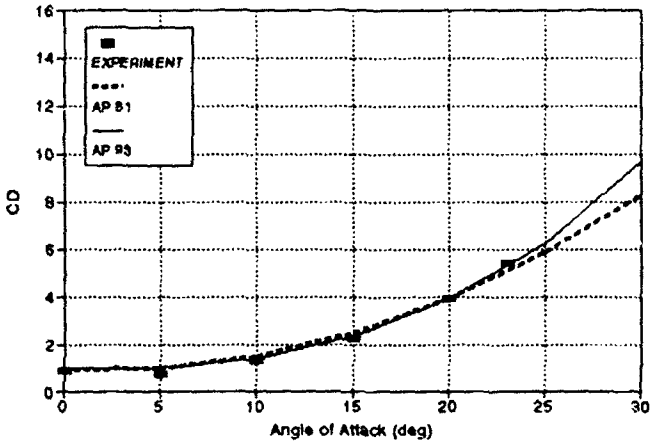

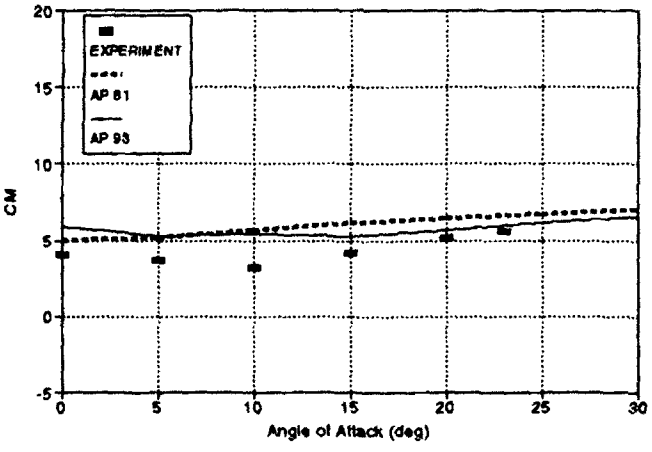

p. $M_\infty = 4.63, \delta = -20$ DEG

FIGURE 25. LIFT, DRAG, AND PITCHING MOMENT COEFFICIENTS OF A WING-BODY-TAIL CONFIGURATION USED IN VALIDATION PROCESS[70] (CONTINUED)

The final configuration considered in the validation process is the canard-wing-body configuration shown in Figure 26a. As mentioned earlier, the wind tunnel results for this configuration were also given in Reference 70. Again, results are shown for $M_\infty = 1.61$, 2.0, 2.86, 3.95, and 4.63 at control deflections of 0-, 10-, and 20-deg. Comparisons of the AP93 to the AP81 and experiment show the AP93 to be slightly superior to the AP81 at most conditions considered for the forces and moments. The greatest improvement is shown for the low Mach number (1.61) pitching moment at all control deflections. The AP81 actually is better than the AP93 at $M_\infty = 2.0$, where the linear theory actually out performs the nonlinear theory. Again, it is suspected that the previous discussion for the Figure 25a configuration also applies here. Since this has been fairly consistently true for configurations that have large lifting surfaces with low values of r/s, some adjustment in the nonlinear wing-alone lift methodology is still needed.

Reference 12 considered several cases that had low aspect ratio lifting surfaces. For configurations such as those, the AP93 shows substantial improvement in the aerodynamic estimation process. Most of the data for these type of configurations is either classified or limited distribution; therefore, no additional results are shown. However, the conclusions in that report still hold true.

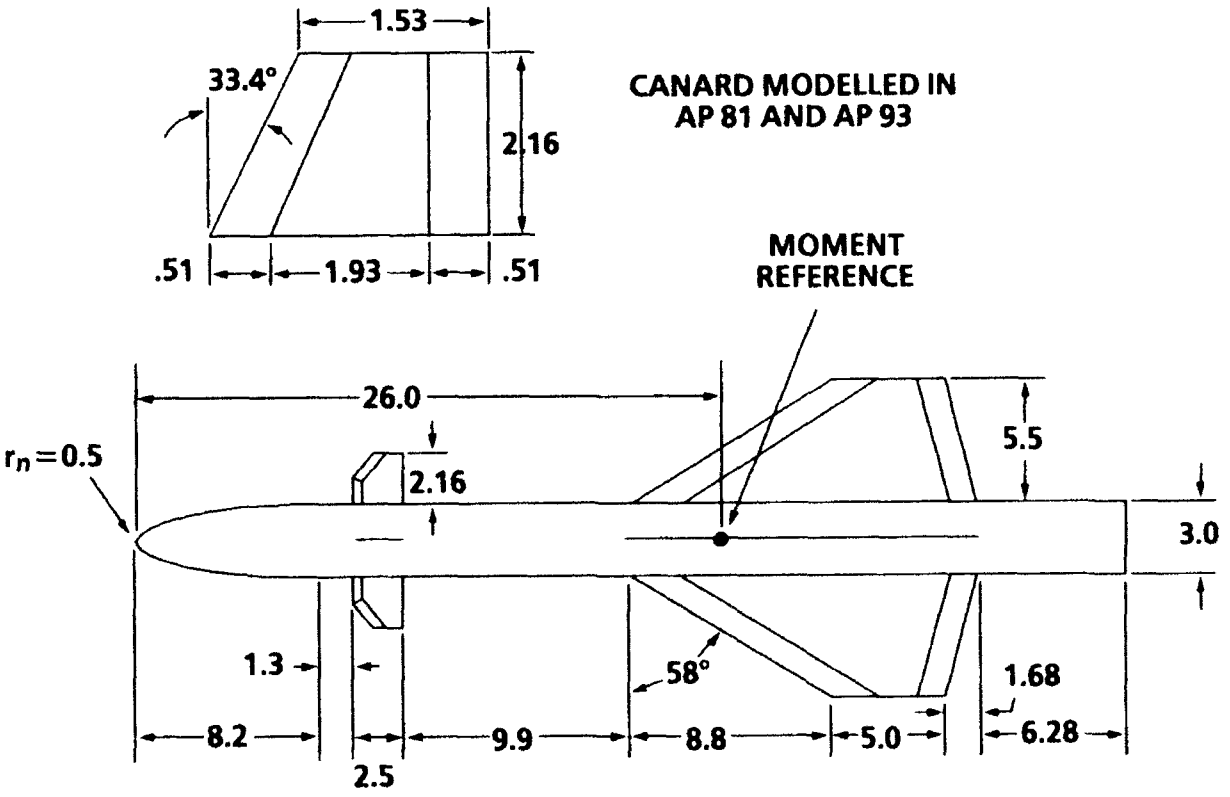

FIGURE 26a. CANARD-WING-BODY CONFIGURATION USED IN VALIDATION PROCESS[70] (DIMENSIONS IN INCHES)

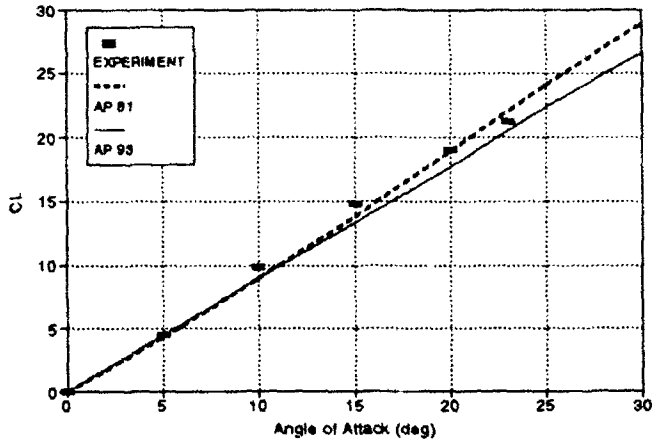

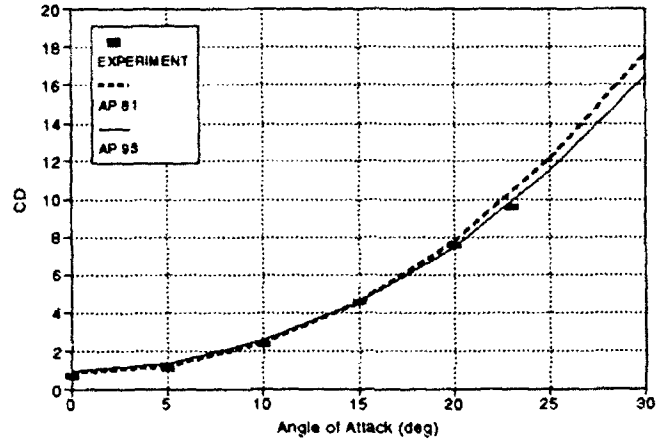

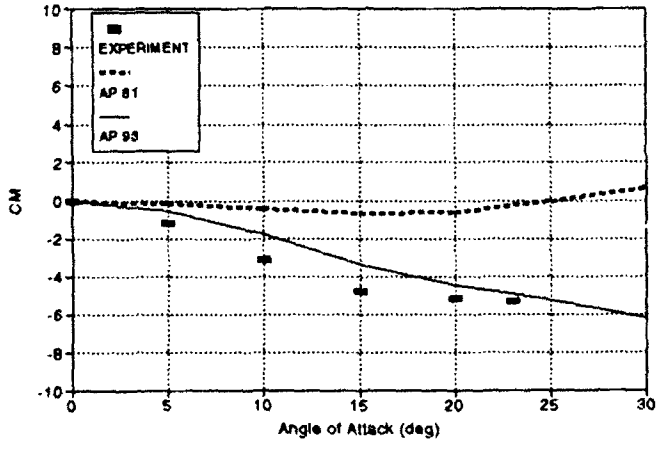

b. $M_\infty = 1.61, \delta = 0$ DEG

FIGURE 26. LIFT, DRAG, AND PITCHING MOMENT COEFFICIENTS OF A CANARD-WING-BODY CONFIGURATION USED IN VALIDATION PROCESS[70]

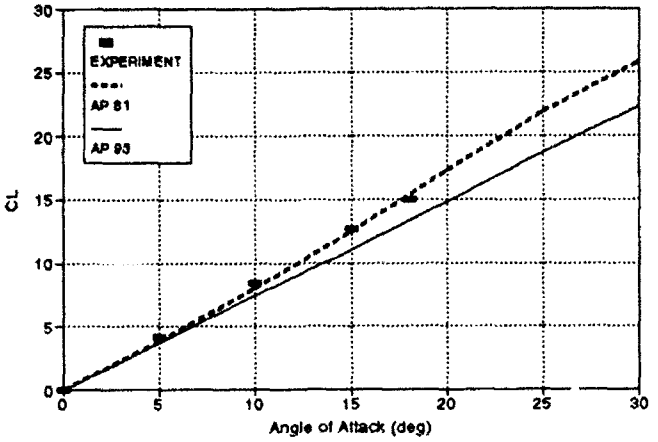

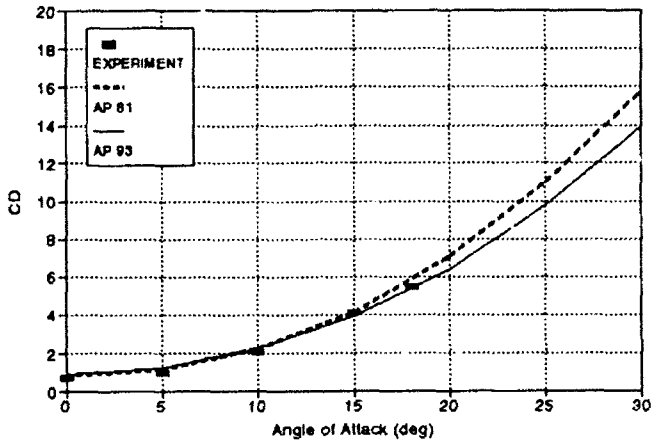

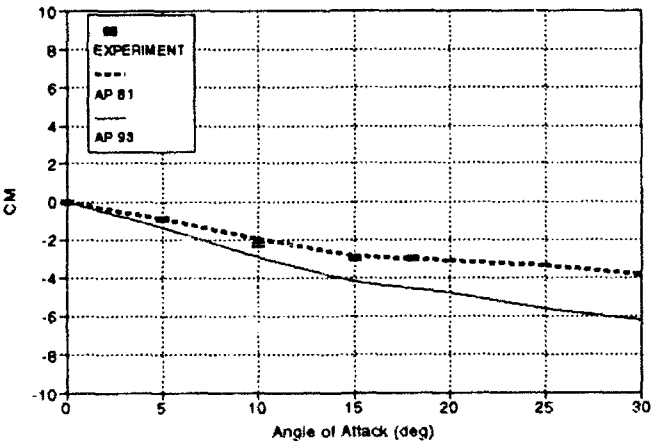

c. $M_\infty = 2.0, \delta = 0$ DEG

FIGURE 26. LIFT, DRAG, AND PITCHING MOMENT COEFFICIENTS OF A CANARD-WING-BODY CONFIGURATION USED IN VALIDATION PROCESS[70] (CONTINUED)

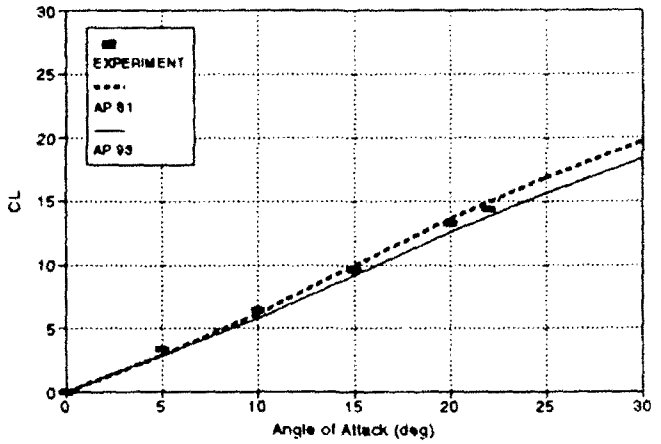

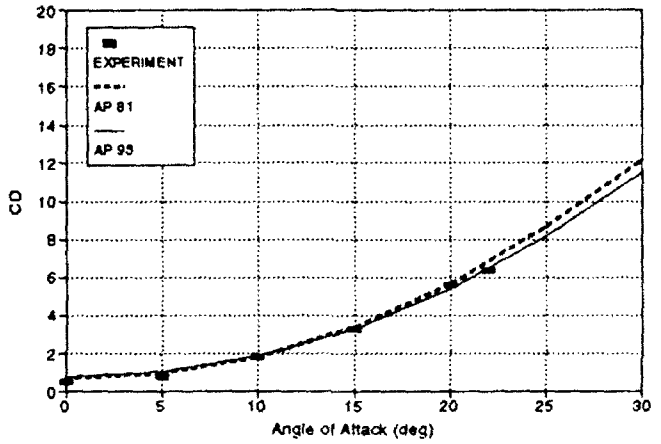

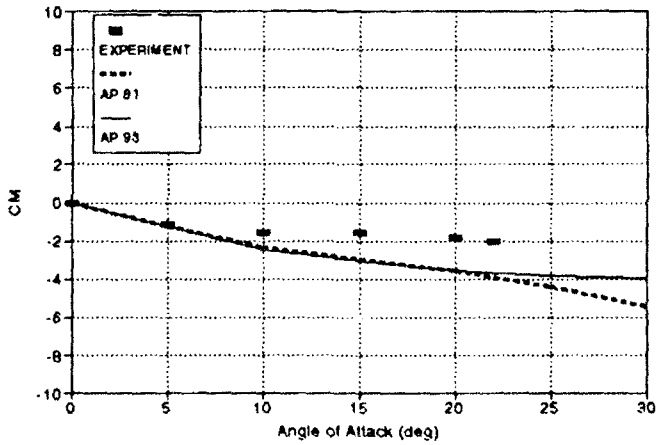

d. $M_\infty = 2.86, \delta = 0$ DEG

FIGURE 26. LIFT, DRAG, AND PITCHING MOMENT COEFFICIENTS OF A CANARD-WING-BODY CONFIGURATION USED IN VALIDATION PROCESS[70] (CONTINUED)

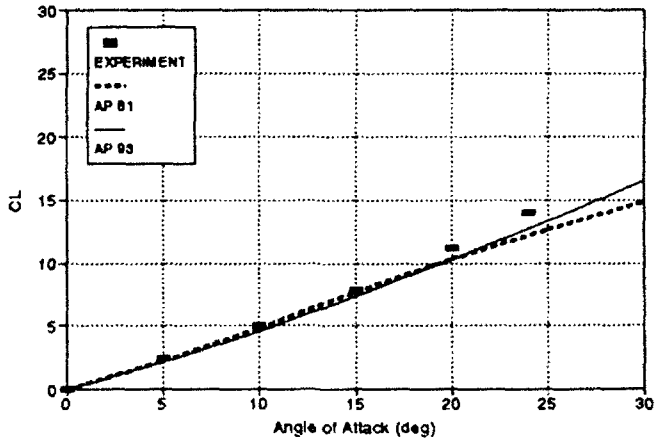

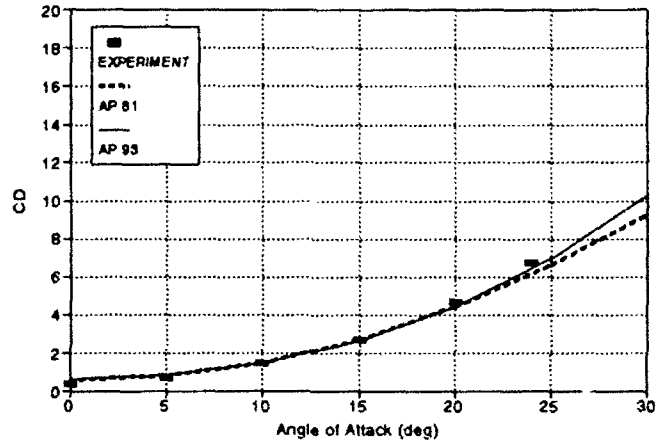

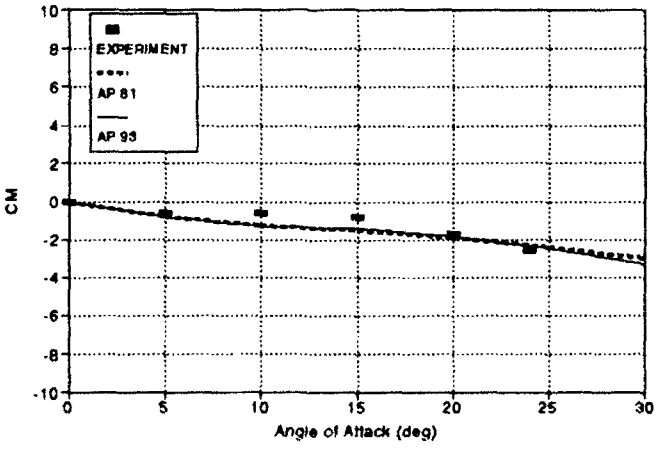

e. $M_\infty = 3.95, \delta = 0$ DEG

FIGURE 26. LIFT, DRAG, AND PITCHING MOMENT COEFFICIENTS OF A CANARD-WING-BODY CONFIGURATION USED IN VALIDATION PROCESS[70] (CONTINUED)

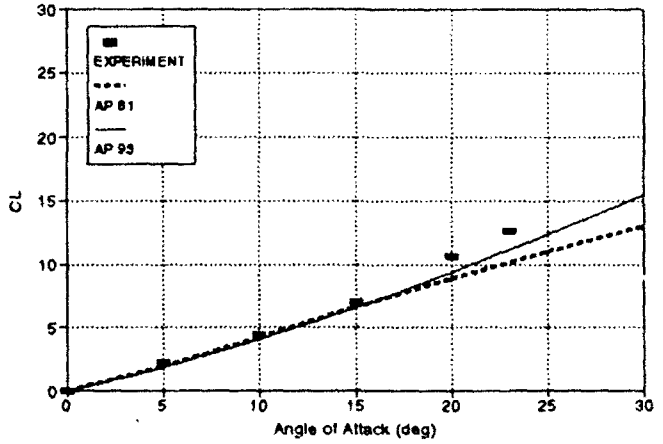

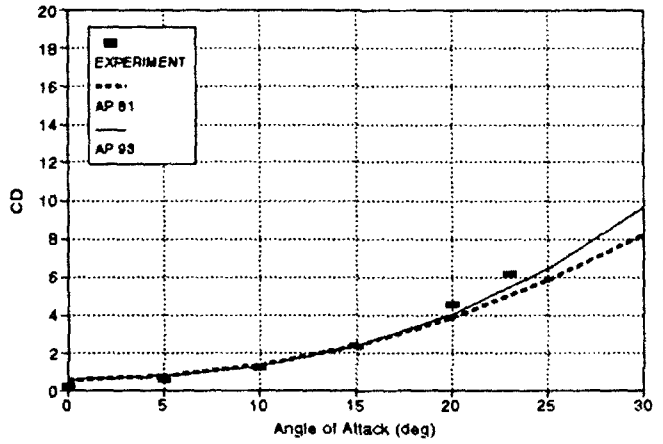

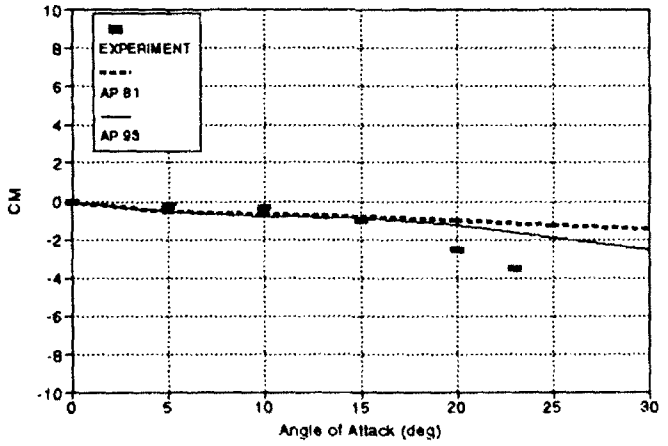

f. $M_\infty = 4.63, \delta = 0$ DEG

FIGURE 26. LIFT, DRAG, AND PITCHING MOMENT COEFFICIENTS OF A CANARD-WING-BODY CONFIGURATION USED IN VALIDATION PROCESS[70] (CONTINUED)

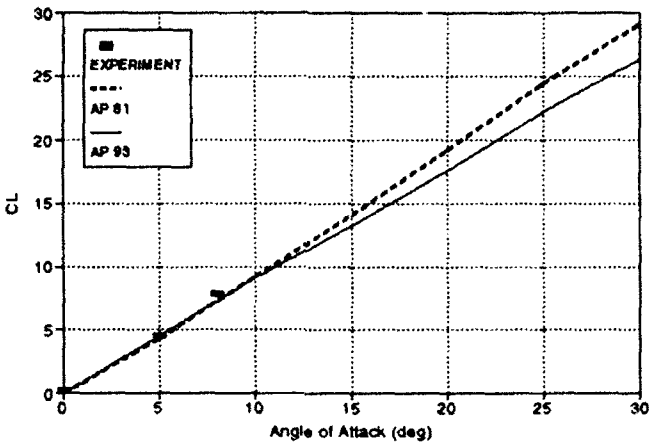

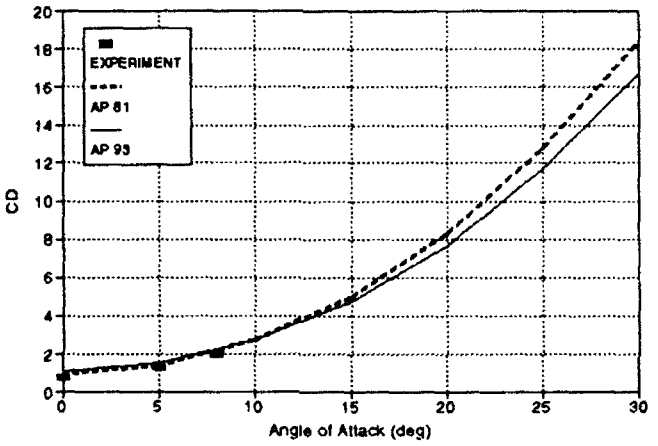

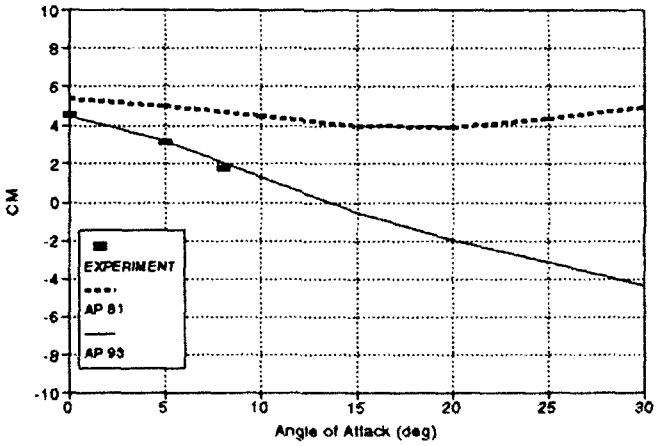

g. $M_\infty = 1.61, \delta = +10$ DEG

FIGURE 26. LIFT, DRAG, AND PITCHING MOMENT COEFFICIENTS OF A CANARD-WING-BODY CONFIGURATION USED IN VALIDATION PROCESS[70] (CONTINUED)

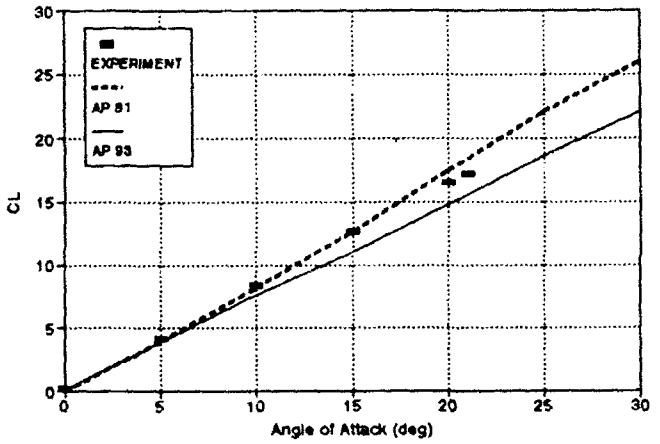

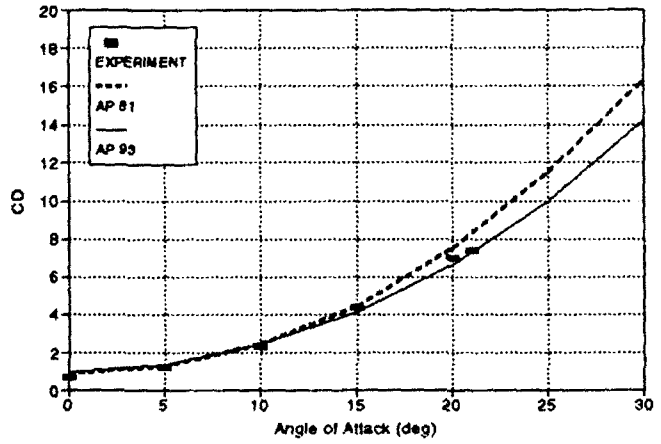

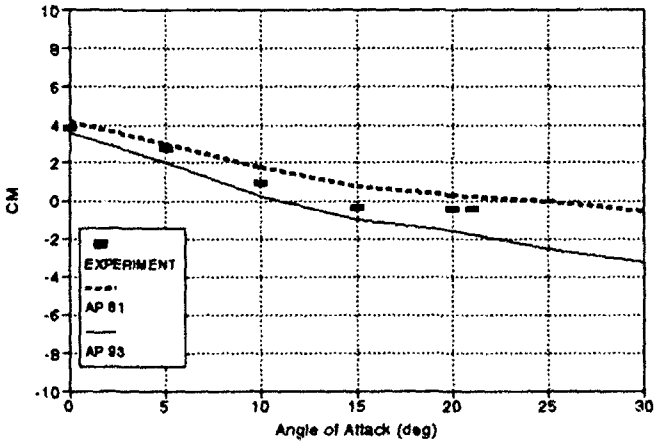

h. $M_\infty = 2.0, \delta = +10$ DEG

FIGURE 26. LIFT, DRAG, AND PITCHING MOMENT COEFFICIENTS OF A CANARD-WING-BODY CONFIGURATION USED IN VALIDATION PROCESS[70] (CONTINUED)

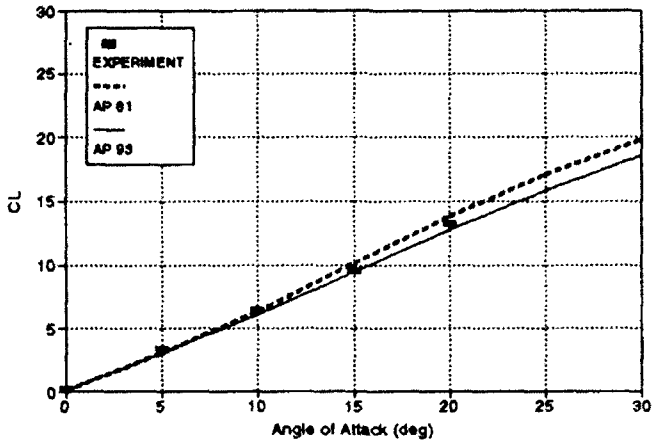

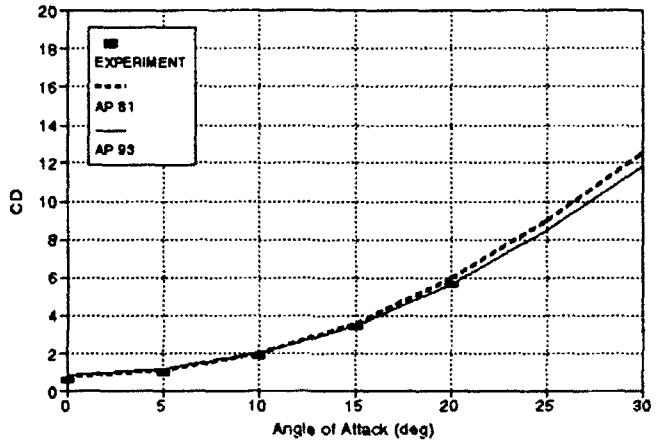

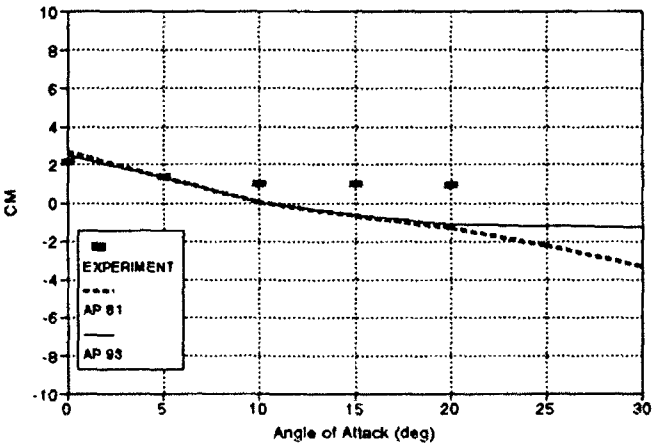

i. $M_\infty = 2.86, \delta = 10$ DEG

FIGURE 26. LIFT, DRAG, AND PITCHING MOMENT COEFFICIENTS OF A CANARD-WING-BODY CONFIGURATION USED IN VALIDATION PROCESS[70] (CONTINUED)

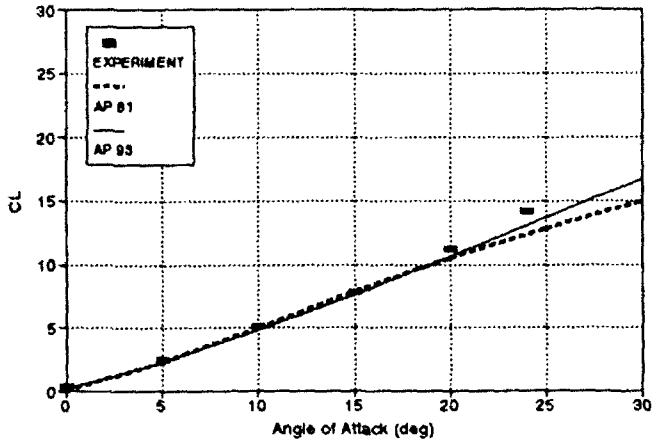

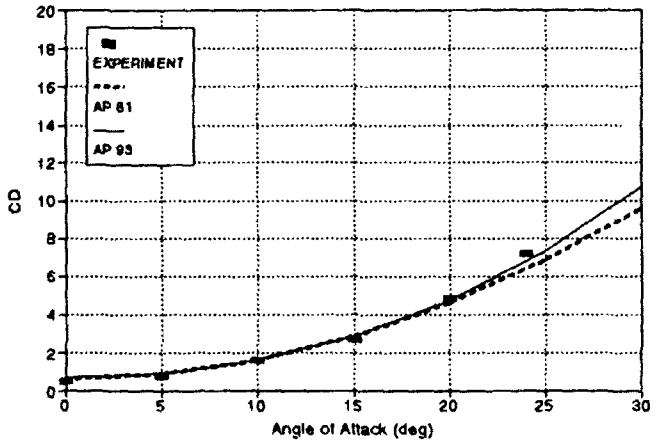

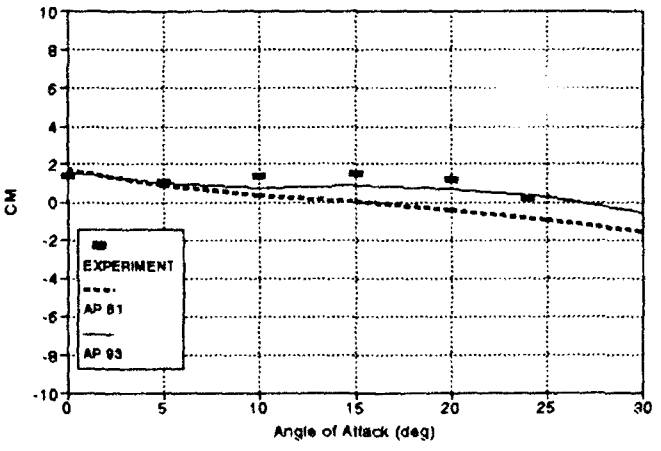

j. $M_\infty = 3.95, \delta = 10$ DEG

FIGURE 26. LIFT, DRAG, AND PITCHING MOMENT COEFFICIENTS OF A CANARD-WING-BODY CONFIGURATION USED IN VALIDATION PROCESS[70] (CONTINUED)

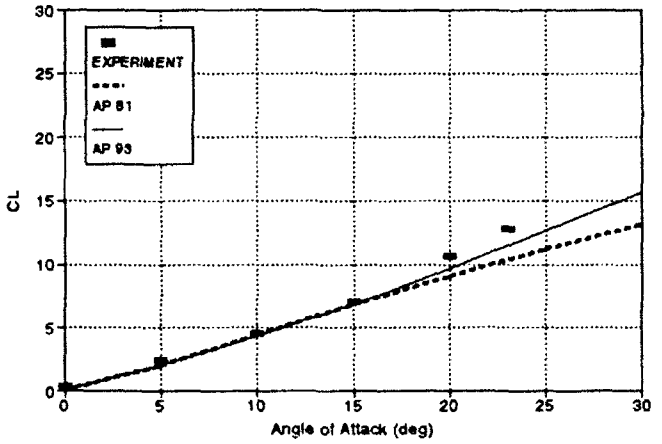

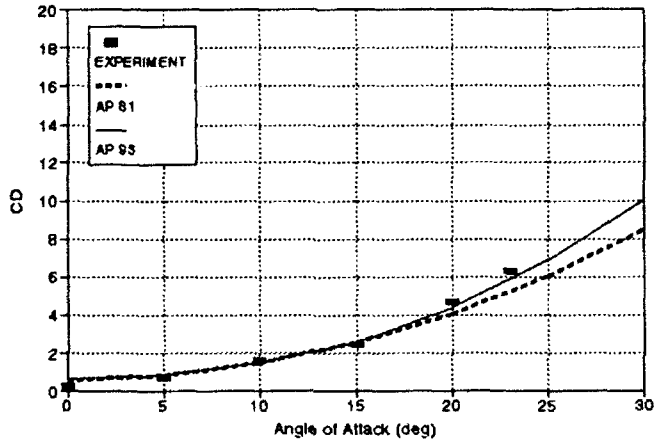

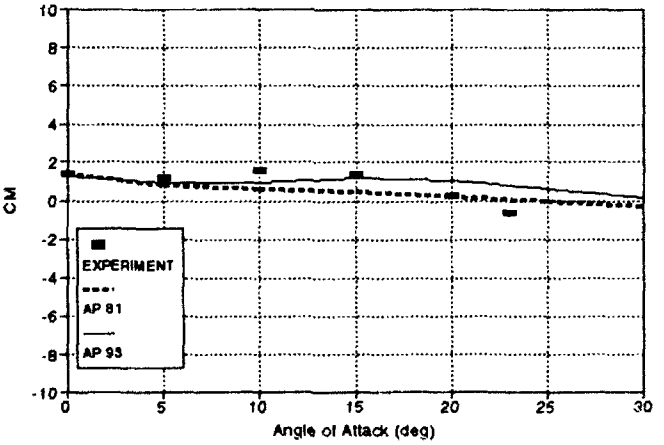

k. $M_{\infty} = 4.63, \delta = 10$ DEG

FIGURE 26. LIFT, DRAG, AND PITCHING MOMENT COEFFICIENTS OF A CANARD-WING-BODY CONFIGURATION USED IN VALIDATION PROCESS[70] (CONTINUED)

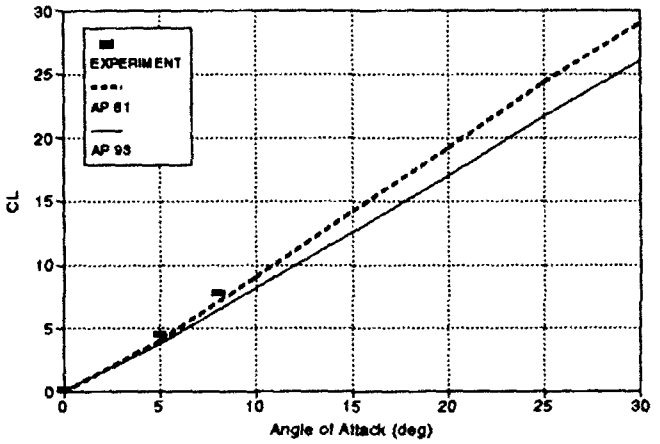

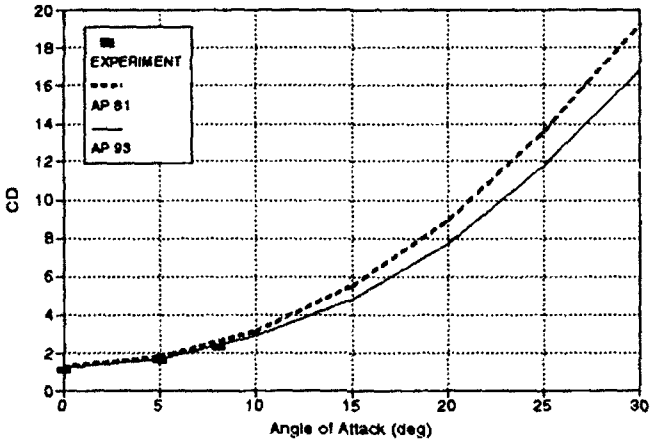

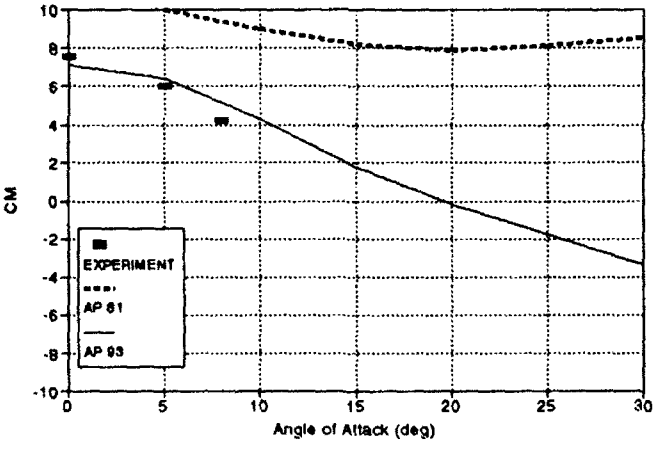

l. $M_\infty = 1.61, \delta = 20$ DEG

FIGURE 26. LIFT, DRAG, AND PITCHING MOMENT COEFFICIENTS OF A CANARD-WING-BODY CONFIGURATION USED IN VALIDATION PROCESS[70] (CONTINUED)

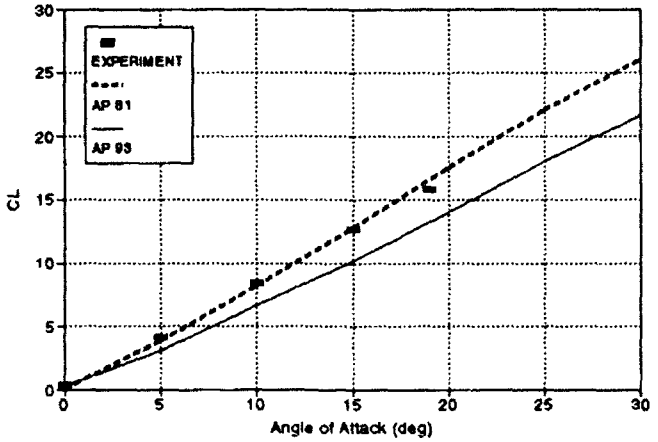

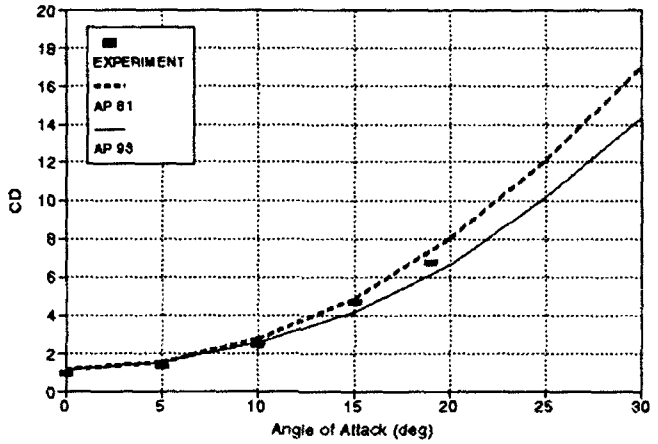

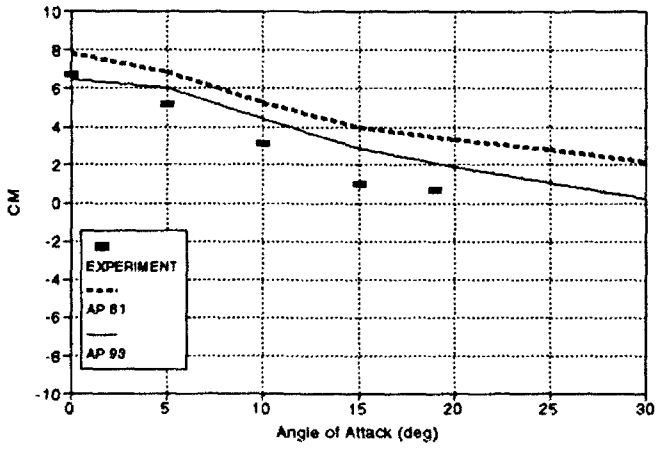

m. $M_\infty = 2.0, \delta = 20$ DEG

FIGURE 26. LIFT, DRAG, AND PITCHING MOMENT COEFFICIENTS OF A CANARD-WING-BODY CONFIGURATION USED IN VALIDATION PROCESS[70] (CONTINUED)

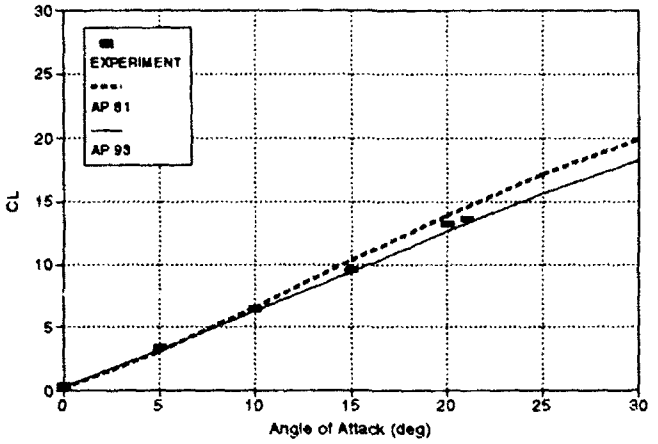

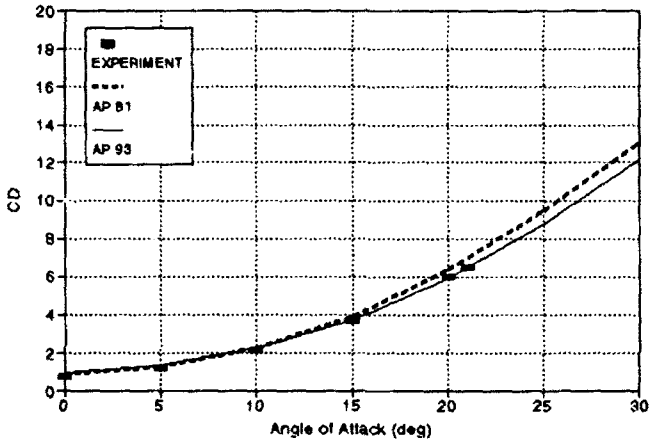

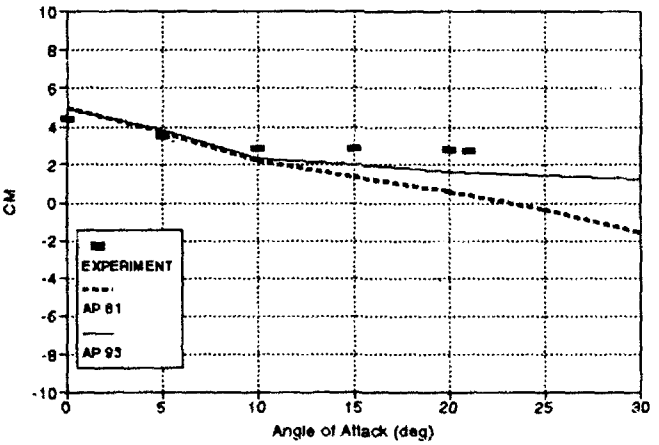

n. $M_\infty = 2.86, \delta = 20$ DEG

FIGURE 26. LIFT, DRAG, AND PITCHING MOMENT COEFFICIENTS OF A CANARD-WING-BODY CONFIGURATION USED IN VALIDATION PROCESS[70] (CONTINUED)

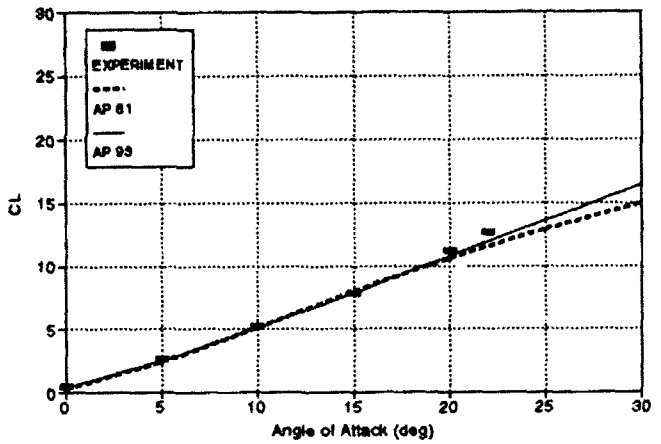

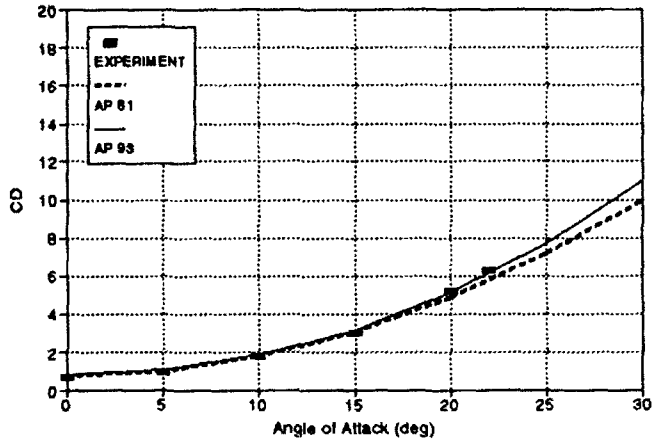

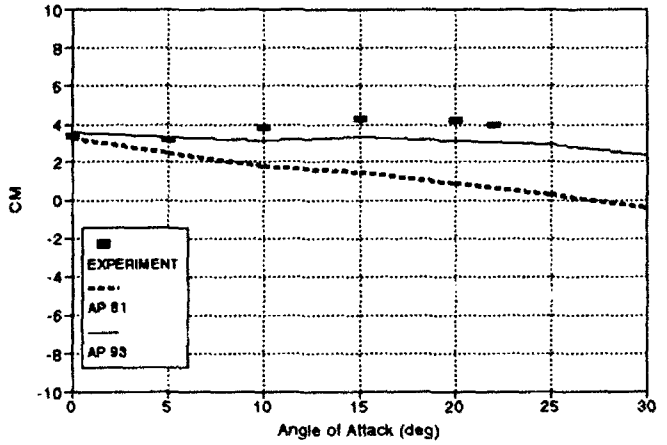

o. $M_\infty = 3.95, \delta = 20$ DEG

FIGURE 26. LIFT, DRAG, AND PITCHING MOMENT COEFFICIENTS OF A CANARD-WING-BODY CONFIGURATION USED IN VALIDATION PROCESS[70] (CONTINUED)

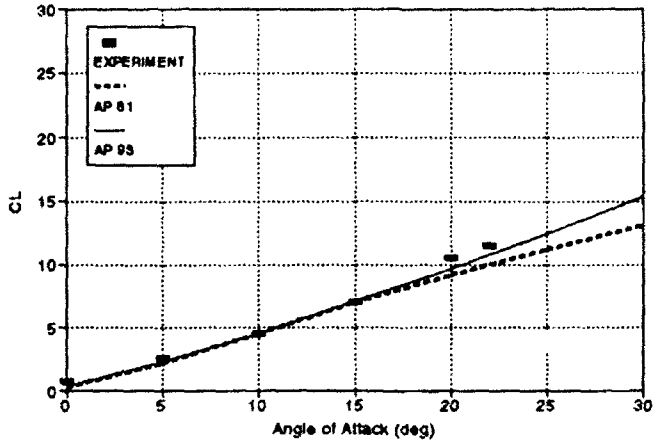

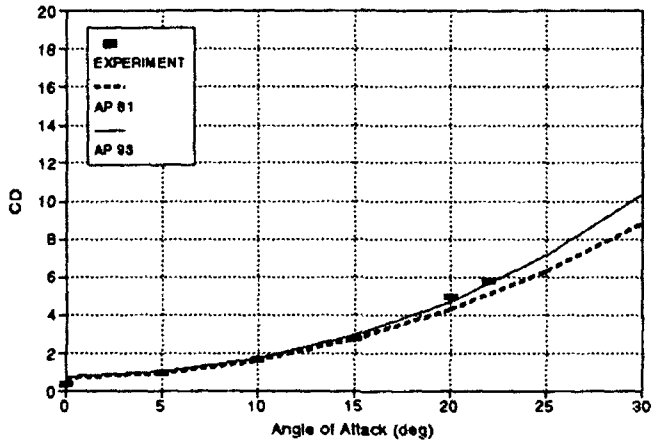

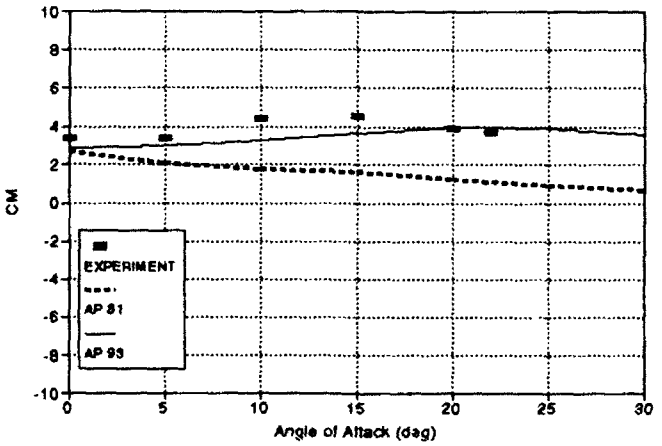

p. $M_\infty = 4.63, \delta = 20$ DEG

FIGURE 26. LIFT, DRAG, AND PITCHING MOMENT COEFFICIENTS OF A CANARD-WING-BODY CONFIGURATION USED IN VALIDATION PROCESS[70] (CONTINUED)

5.0 SUMMARY AND RECOMMENDATIONS

In summary, an improved APC (AP93) has been developed This report summarizes the methodology for the new technology previously developed and documented, presents in more detail an undocumented nonlinear method for wing-body interference due to control deflection, and compares the new AP93 code to the former APC (AP81) and experimental data.

New technology developed and summarized includes extension of the SOSET to include real-gas effects; a new engineering method to calculate heat transfer coefficients and adiabatic wall temperature; new approximate pressure prediction schemes for blunt and sharp bodies; an improved body-alone nonlinear lift prediction method; new nonlinear lift prediction methods for wing-alone, wing-body interference, body-wing interference, and wing-body interference due to control deflection; and a new base drag database to estimate the effects of angle of attack, fin location, and size, along with an improved empirical prediction model.

New capabilities of the code include the ability to calculate information to be used for conducting engineering estimates of heat transfer at high Mach numbers, the ability to use the code to get accurate estimates of nonlinear aerodynamics for low aspect ratio and low or high Mach number aerodynamics up to angles of attack of 30 deg, and improved axial-force estimations.

Comparison of the AP93 code to the AP81 version and experimental data showed the AP93 code on average reduces the errors in normal-force and center-of-pressure estimation considerably for most configurations and gives slightly improved estimates of axial-force coefficient. Comparing the AP93 code to available computations from the external literature of other SOTA codes showed the AP93 to be as good as or superior to other codes for planar aerodynamics. Regions of superiority of the AP93 code, in general, were the same weak areas of the AP81 code; i.e., lower aspect ratio, lower Mach number, higher angle of attack, pitching moments, and hypersonic Mach numbers.

The computational time of the AP93 is about the same as the AP81 version (about 1 sec per case on a CDC 995 computer). This is because many of the unused or seldom used techniques of the AP81 version were eliminated and replaced with more recent technology. There are a few new inputs, but these are minimal. In general, the AP93 has maintained the same level of computational time and ease of use (less than one-half day for an experienced user to set up a configuration for computational purposes) but is much more accurate and robust than the AP81 version. The code will be made available to legitimate requesting users at no charge to them.

While the AP93 shows substantial improvement over the AP81 code for most static aerodynamics on most configurations, there are still areas needing improvement. These include

- Refinements in the wing-alone lift curves for wings that have moderate aspect ratios
- Refinements in the nonlinear wing-body interference lift at moderate supersonic Mach numbers
- Extension of the methodology to higher angle of attack
- Extension of the methodology to the $\varnothing = 45$-deg plane in addition to the $\varnothing = 0$-deg plane

These improvements will be added as funding permits.

6.0 REFERENCES

1. Moore, F. G., *Computational Aerodynamics at NAVSWC: Past, Present, and Future*, NAVSWC TR 90-569, Oct 1990, NAVSWC, Dahlgren, VA.

2. Moore, F. G., *Body Alone Aerodynamics of Guided and Unguided Projectiles at Subsonic, Transonic, and Supersonic Mach Numbers*, NWL TR-2796, Nov 1972.

3. Moore, F. G., *Aerodynamics of Guided and Unguided Weapons: Part I–Theory and Application*, NWL TR-3018, Dec 1973.

4. Moore, F. G. and McKerley, W. C., *Aerodynamics of Guided and Unguided Weapons: Part II–Computer Program and Users Guide*, NWL TR-3036, Jan 1974.

5. Moore, F. G. and Swanson, R. C., *Aerodynamics of Tactical Weapons to Mach Number 3 and Angle of Attack 15 Degrees: Part I–Theory and Application*, NSWCDL TR-3584, Feb 1977, NSWCDL, Dahlgren, VA.

6. Swanson, R. C. and Moore, F. G., *Aerodynamics of Tactical Weapons to Mach Number 3 and Angle of Attack 15 Degrees: Part II–Computer Program and Usage*, NSWCDL TR-3600, Mar 1977, NSWCDL, Dahlgren, VA.

7. Devan, L., *Aerodynamics of Tactical Weapons to Mach Number 8 and Angle of Attack 180°: Part I, Theory and Application*, NSWC TR 80-346, Oct 1980, NSWC, Dahlgren, VA.

8. Devan, L. and Mason, L., *Aerodynamics of Tactical Weapons to Mach Number 8 and Angle of Attack 180°: Part II, Computer Program and Users Guide*, NSWC TR 81-358, Sep 81, NSWC, Dahlgren, VA.

9. Moore, F. G.; Armistead, M.; Rowles, S. H.; and DeJarnette, F. R., *Second-Order Shock-Expansion Theory Extended to Include Real Gas Effects*, NAVSWC TR 90-683, Feb 1992, NAVSWC, Dahlgren, VA.

10. Moore, F. G.; Armistead, M.; Rowles, S. H.; and DeJarnette, F. R., "A New Approximate Method for Calculating Real Gas Effects on Missile Configurations," *AIAA Paper*, No. 92-4637, Atmospheric Flight Mechanics Conference, Aug 1992 (also *Journal of Spacecraft and Rockets*, Jan–Feb 1993).

11. McInville, R. and Moore F., *Incorporation of Boundary Layer Heating Predictive Methodology into the NAVSWC Aeroprediction Code*, NSWCDD/TR-93/29, Apr 1993, NSWCDD, Dahlgren, VA.

12. Moore, F. G.; Hymer, T.; Devan, L., *New Methods for Predicting Nonlinear Lift, Center of Pressure, and Pitching Moment on Missile Configurations*, NSWCDD/TR-92/217, Jul 1992, NSWCDD, Dahlgren, VA.

13. Moore, F. G.; Devan, L.; and Hymer, T., "A New Semiempirical Method for Computing Nonlinear Angle-of-Attack Aerodynamics on Wing-Body-Tail Configurations," *AIAA Paper*, No. 93-0038, 31st Aerospace Sciences Meeting, Jan 1993.

14. Moore, F. G.; Wilcox, F.; and Hymer, T., *Improved Empirical Model for Base Drag Prediction on Missile Configurations Based on New Wind Tunnel Data*, NSWCDD/TR-92/509, Oct 1992, NSWCDD, Dahlgren, VA.

15. Moore, F. G.; Wilcox, F.; and Hymer, T., "Base Drag Prediction on Missile Configurations," *AIAA Paper*, No. 93-3629, to be presented at Atmoshperic Flight Mechanics Conference, Aug 1993, Monterey, CA.

16. Hudgins, Henry E., Jr., *Supersonic Flow About Right Circular Cones at Zero Yaw in Air at Chemical Equilibrium, Part I–Correlation of Flow Properties*, TM 1493, Picatinny Arsenal, PA, Aug 1965.

17. Wittliff, Charles E. and Curtis, James T., *Normal Shock Wave Parameters in Equilibrium Air*, Cornell Aero Lab Report, CAL-III, Nov 1961.

18. Tannehill, J. C. and Mugge, P. H., *Improved Curve Fits for the Thermodynamic Properties of Equilibrium Air Suitable for Numerical Computation using Time-Dependent Shock-Capturing Methods*, NASA CR-2470, 1974.

19. Srinivasan, S.; Tannehill, J.; and Wielmuenster, K., *Simplified Curve Fits for the Thermodynamic Properties of Equilibrium Air*, Report ISSU-ERI-AMES 86401, Eng. Research Institute, Iowa State Univ., Ames, IA, Jun 1986.

20. Morrison, A. M.; Solomon, J. M.; Ciment, M.; and Ferguson, R. E., *Handbook of Inviscid Sphere-Cone Flow Fields and Pressure Distributions: Volume I*, NSWC/WOL/TR 75-45, Dec 1975, White Oak, MD.

21. Jones, D. J., *Numerical Solutions of the Flow Field for Conical Bodies in a Supersonic Stream*, National Research Council of Canada, Report LR-507, Jul 1968.

22. Priolo, F. J.; Wardlaw, A. B., Jr.; and Kuhn, G. D., "High Temperature Effects for Missile-Type Bodies using the Euler Solver, ZEUS," *AIAA Paper*, No. 91-3259, presented at 1991 Applied Aerodynamics Conference, Baltimore, MD, 23–25 Sep 1991.

23. Anderson, J. D., *Hypersonic and High Temperature Gasdynamics*, McGraw-Hill Book Co., 1989.

24. Beckwith, I. E. and Gallagher, J. J., *Local Heat Transfer and Recovery Temperatures on a Yawed Cylinder at Mach Numbers of 4.15 and High Reynolds Numbers*, NASA Technical Report R-104, 1961.

25. Hender, D. R., *A Miniature Version of the JA70 Aerodynamic Heating Computer Program, H800 (MINIVER)*, McDonnell-Douglas Astronautics Co., Report MCD G0462, Jun 1970.

26. Eckert, E. R. G., "Engineering Relations for Heat Transfer and Friction in High-Velocity Laminar and Turbulent Boundary Layer Flow over Surfaces with Constant Pressure and Temperature," *Trans. of the ASME*, Vol. 78, No. 6, Aug 1956.

27. Eckert, E. R. G., *Survey of Boundary Layer Heat Transfer at High Velocities and High Temperatures*, WADC Technical Report 59-624, Apr 1960.

28. DeJarnette, F. R., *Calculation of Heat Transfer on Shuttle Type Configurations Including the Effects of Variable Entropy at Boundary Layer Edge*, NASA CR-112180, Oct 1972.

29. Cleary, J. W., *Effects of Angle of Attack and Bluntness on Laminar Heating Rate Distribution of a 15° Cone at a Mach Number of 10.6*, NASA TN D-5450, 1969.

30. Riley, C. J. and DeJarnette, F. R., "Engineering Aerodynamic Heating Method for Hypersonic Flow," *Journal of Spacecraft and Rockets*, Vol. 29, No. 3, May–Jun 1992.

31. Butler, C.; Sears, E.; and Pellas, S., *Aerodynamic Characteristics of 2-, 3-, and 4-caliber Tangent-Ogive Cylinders with Nose Bluffness Ratios of 0.00, 0.25, 0.50, and 0.75 at Mach Numbers from 0.6 to 4.0*, AFATL-TR-77-8, Jan 1977.

32. Spahr, J. and Dickey, R., *Effect of Tail Surfaces on the Base Drag of a Body of Revolution at Mach Numbers of 1.5 and 2.0*, NACA TN-2630, 1951.

33. Hill, F. and Alpher, R., "Base Pressures at Supersonic Velocities," *Journal of Aeronautical Sciences*, Vol. 16, No. 3, Mar 1949.

34. Allen, J. H. and Perkins, E. W., *Characteristics of Flow Over Inclined Bodies of Revolution*, NACA RM A 50L07, Mar 1951.

35. Jorgensen, L. H., *Prediction of Static Aerodynamic Characteristics for Slender Bodies Alone and with Lifting Surfaces to Very High Angles of Attack*, NASA TR R-474, Sep 1977.

36. NASA Langley Research Center Tri-Service Missile Data Base, transmitted from NASA/LRC Jerry M. Allen to NAVSWC, 5 Nov 1991 (formal documentation in process).

37. Evvard, J. C., *Use of Source Distributions for Evaluating Theoretical Aerodynamics of Thin Finite Wings at Supersonic Speeds*, NACA Report 951, 1950.

38. Krasilshchikova, E. A., "Effect of the Tip Edge on the Motion of a Wing at Supersonic Speeds," *Doklady Akademii Navk*, Vol. VIII, No. 4, 1947 (See also NACA TM 1386, 1956, for English translation.)

39. Stallings, R. L., Jr. and Lamb, Milton, "Wing-Alone Aerodynamic Characteristics for High Angles of Attack at Supersonic Speeds," *NASA Technical Paper 1889*, Jul 1981.

40. Nielsen, J. N.; Hemsch, M. J.; and Smith, C. A., *A Preliminary Method for Calculating the Aerodynamic Characteristics of Cruciform Missiles to High Angles of Attack Including Effects of Roll Angle and Control Deflections*, ONR Report CR 215-226-4F, Nov 1977.

41. Pitts, W. C.; Nielsen, J. N.; and Kaattari, G. E., *Lift and Center of Pressure of Wing-Body-Tail Combinations at Subsonic, Transonic, and Supersonic Speeds*, NACA TR 1307, 1957.

42. McKinney, R. L., *Longitudinal Stability and Control Characteristics of an Air-to-Air Missile Configuration at Mach Numbers of 2.3 and 4.6 and Angles of Attack from −45° to 90°*, NASA TM X-846, 1972.

43. Monta, W. J., *Supersonic Aerodynamic Characteristics of a Sparrow III Type Missile Model with Wing Controls and Comparison with Existing Tail-Control Results*, NASA TP 1078, Nov 1977.

44. Smith, E. H.; Hebbar, S. K.; and Platzer, M., "Aerodynamic Characteristics of a Canard-Controlled Missile at High Angles of Attack," *AIAA Paper*, No. 93-0763, presented at 31st Aerospace Sciences Meeting, Reno, NV, 11-14 Jan 1993.

45. Vukelich, S. R.; Stoy, S. L.; Burns, K. A.; Castillo, J. A.; and Moore, M. E., *Missile DATCOM Volume I–Final Report*, AFWALTR-86-3091, Air Force Wright Aeronautical Laboratory, Wright Patterson AFB, OH, Dec 1988.

46. Van Dyke, M. D., *Practical Calculation of Second-Order Supersonic Flow Past Nonlifting Bodies of Revolution*, NACA TN-2744, Jul 1952.

47. Jackson, C. M., Jr.; Sawyer, W. C.; Smith, R. S., *A Method for Determining Surface Pressures on Blunt Bodies of Revolution at Small Angles of Attack in Supersonic Flow*, NASA TN D-4865, Nov 1968.

48. DeJarnette, F. R.; Ford, C. P.; and Young, D. E., "Calculation of Pressures on Bodies at Low Angles-of-Attack in Supersonic Flow," *Journal of Spacecraft and Rockets*, Vol. 17, No. 6.

49. Wu, J. M. and Aoyoma, K., *Transonic Flow-Field Calculation Around Ogive Cylinders by Nonlinear-Linear Stretching Method*, Technical Report No. RD-TR-70-12, Apr 1970, U.S. Army Missile Command, Redstone Arsenal, AL.

50. Chaussee, D., *Improved Transonic Nose Drag Estimates for the NSWC Missile Computer Program*, NSWC/DL-TR-3030, Apr 1978.

51. Van Driest, E. R., "Turbulent Boundary Layer in Compressible Fluids," *Journal of Aeronautical Sciences*, Vol. 18, No. 3, 1951.

52. Tsien, H. S., "Supersonic Flow Over an Inclined Body of Revolution," *Journal of Aeronautical Sciences*, Vol. 5, No. 12, Oct 1938.

53. Klopfer, G. and Chausee, D., *Numerical Solution of Three-Dimensional Transonic Flows Around Axisymmetric Bodies at Angle of Attack*, NEAR TR-176, Mountain View, CA, Feb 1979.

54. Chadwick, W. R., "The Application of Non-Planar Lifting Surface Theory to the Calculation of External Store Loads," *AIAA Journal*, Vol. II, Mar 1974.

55. Ferri, Antonio, *Elements of Aerodynamics of Supersonic Flows*, MacMillan Co., New York, 1949.

56. Jones, R. T. and Cohen, D., *High Speed Wing Theory*, Princeton Aeronautical Paperbacks, No. 6, 1960.

57. Ashley, H. and Landahl, M., *Aerodynamics of Wings and Bodies*, Addison-Wesley Publishing Co., Reading, MA, 1965.

58. Whyte, R. H., *Spinner-A Computer Program for Predicting the Aerodynamic Coefficients of Spin Stabilized Projectiles*, General Electric Class 2 Reports, Aug 1969.

59. Douglas Aircraft Company, Inc., *USAF Stability and Control DATCOM*, Revisions by Wright Patterson Air Force Base, July 1963, 2 Vol.

60. Martin, J. C., and Jeffreys, I., *Span Load Distribution Resulting from Angle of Attack, Rolling, and Pitching for Tapered Sweptback Wings with Streamwise Tips*, NACA TN 2643, 1952.

61. Malvestuto, F. S., Jr.; Margolis, K.; and Ribner, H., *Theoretical Lift and Damping in Roll at Supersonic Speeds of Thin Sweptback Tapered Wings with Streamwise Tips, Subsonic Leading Edges and Supersonic Trailing Edges*, NACA TR 970, 1950.

62. Lockwood, V. E., *Effects of Sweep on the Damping-in-Roll Characteristics of Three Sweptback Wings having an Aspect Ratio of 4 at Transonic Speeds*, NACA RM L50J10, Dec 1950.

63. Bryson, A. E., "Stability Derivatives for a Slender Missile with Application to a Wing-Body Vertical Tail Configuration," *Journal of Aeronautical Sciences*, Vol. 20, No. 5, 1953.

64. Cole, I. J. and Margolis, K., *Lift and Pitching Moment at Supersonic Speeds Due to Constant Vertical Acceleration for Thin Sweptback Tapered Wings with Streamwise Tips, Supersonic Leading, and Trailing Edges*, NACA TN 3196, Jul 1954.

65. Martin, J. C.; Margolis, K.; and Jeffreys, I., *Calculation of Lift and Pitching Velocity at Supersonic Speeds for Thin Sweptback Tapered Wings with Streamwise Tips and Supersonic Leading and Trailing Edges*, NACA TN 2699, Jun 1952.

66. Malvestuto, F. S. and Hoover, D. M., *Lift and Pitching Derivatives of Thin Sweptback Tapered Wings with Streamwise Tips and Subsonic Leading Edges at Supersonic Speeds*, NACA TN 2294, Feb 1951.

67. Graves, E. and Fournier, R., *Stability and Control Characteristics at Mach Numbers from 0.2 to 4.63 of a Cruciform Air-to-Air Missile with Triangular Canard Controls and a Trapezoidal Wing*, NASA-TM-X-3070, Nov 1974.

68. Trescot, C. D., Jr.; Foster, G. V.; Babb, D. C., *Effect of Fin Planform on the Aerodynamic Characteristics of a Wingless Missile with Aft Cruciform Controls at Mach 1.6, 2.36, and 2.86*, NASA TM X-2774, Jul 1973.

69. Whoric, J. M. and Washington, E. S., *Aerodynamic Characteristics of the Air Slew Demonstrator Models at Mach Numbers from 0.6 to 1.3*, AEDC TR-76-92, Aug 1976.

70. Corlett, W. A. and Howell, D. T., *Aerodynamic Characteristics at Mach 0.60 to 4.63 of Two Cruciform Missile Models, One Having Trapezoidal Wings with Canard Controls and the Other Having Delta Wings with Tail Controls*, NASA TM X 2780, Aug 1973.

7.0 SYMBOLS AND DEFINITIONS

A_p	Planform area of the body or wing in the crossflow plane (ft^2)
A_{ref}	Reference area (maximum cross-sectional area of body if a body is present or planform area of wing if wing alone) (ft^2)
A_W	Planform area of wing in crossflow plane (ft^2)
a	Speed of sound (ft/sec)
AR	Aspect ratio = b^2/A_W
b	Wing span (not including body) (ft)
C_A	Axial force coefficient
C_M	Pitching moment coefficient (based on reference area and body diameter if body present or mean aerodynamic chord if wing alone)
C_N	Normal force coefficient $\left(\frac{\text{Normal Force}}{1/2\,\rho_\infty V_\infty^2 A_{ref}} \right)$
$C_{N_{B(V)}}$	Negative afterbody normal-force coefficient due to canard or wing shed vortices
$C_{N_{B(W)}}$	Additional normal-force coefficient on body due to presence of wing
$\Delta C_{N_{B(W)}}$	Additional normal-force coefficient on body due to a control deflection of the wing
C_{N_L}	Linear component of normal-force coefficient
$C_{N_{NL}}$	Nonlinear component of normal-force coefficient
$C_{N_{T(V)}}$	Negative normal-force coefficient component on tail due to wing or canard shed vortex

$C_{N_{W(B)}}$	Normal-force coefficient of wing in presence of body
$\Delta C_{N_{W(B)}}$	Additional normal-force coefficient of wing in presence of body due to a wing deflection
C_{N_α}	Normal-force coefficient derivative
C_p	Pressure coefficient $\left(\frac{p - p_\infty}{1/2\, \rho_\infty V_\infty^2} \right)$
C_{P_B}	Base pressure coefficient
$(C_{P_B})_{NF,\alpha}$	Base pressure coefficient with no fins present and at angle of attack
$(C_{P_B})_{\alpha,\delta,t/c,x/c}$	Base pressure coefficient with fins present of some t/c, x/c, δ, and body at some α
C_{P_o}	Stagnation pressure coefficient
c_r	Root chord (ft)
c_t	Tip chord (ft)
d	Body diameter (ft)
d_{ref}	Reference body diameter (ft)
e	Internal energy (ft^2/sec^2)
F	Dimensionless empirical factor used in tail normal-force coefficient term due to canard or wing shed vortices to approximate nonlinear effects due to a control deflection
F_1, F_2, F_3	Symbols defining parameters used in base drag empirical model
f_w, f_t	Lateral location of wing or tail vortex (measured in feet from body center line)
H	Heat transfer coefficient based on wall local temperature (ft-lb)/(ft^2-sec-°R)
H_o	Total enthalpy (ft^2/sec^2)

H_l	Heat transfer coefficient based on wall local specific enthalpy [slug/(ft^2-sec)]
h	Specific enthalpy (ft^2/sec^2)
h_{aw}	Adiabatic wall specific enthalpy (ft^2/sec^2)
h_e	Specific enthalpy at outer edge of boundary layer (ft^2/sec^2)
h_T	Height of wing or canard shed vortex at tail center of pressure (ft)
h_w	Specific enthalpy at wall (ft^2/sec^2)
h*	Reference value of specific enthalpy (ft^2/sec^2) (see Equation 16)
i	Tail interference factor
k_1	Empirical factor defined in wing-alone nonlinear normal-force coefficient term
$K_{B(W)}$	Ratio of additional body normal-force coefficient derivative due to presence of wing to wing-alone normal-force coefficient derivative at $\delta = 0$ deg
$K_{W(B)}$	Ratio of normal-force coefficient derivative of wing in presence of body to that of wing alone at $\delta = 0$ deg
$k_{B(W)}$	Ratio of additional body normal-force coefficient derivative due to presence of wing at a control deflection to that of the wing alone at $\alpha = 0$
$k_{W(B)}$	Ratio of wing normal-force coefficient derivative in presence of body due to a control deflection to that of wing alone at $\alpha \neq 0$ deg
$[k_{W(B)}]_{SB}$	Value of $k_{W(B)}$ calculated by slender-body theory at $\alpha = 0$
$\Delta K_{W(B)}$, $\Delta K_{B(W)}$	Nonlinear corrections to $K_{B(W)}$ and $K_{W(B)}$ due to higher angle of attack
l	Length (ft)
l_N	Nose length (can be in calibers or feet)
LT	Linear theory
M	Mach number = V/a

M_N	Normal Mach number to body axis = M sin α
N_l, N_t	Transformation factors used in Eckert reference enthalpy to approximate three-dimensional effects for laminar and turbulent flow (= 3 and 2, respectively)
p	Pressure (lb/ft^2)
p_c	Pressure of a cone of given half angle (lb/ft^2)
P_r	Prandtl number
$\dot{q}_w$	Heat transfer rate (ft-lb)/(ft^2-sec) at wall
$\dot{q}_{w,l}$, $\dot{q}_{w,t}$	Heat transfer rate at wall for laminar or turbulent flow, respectively
R	Gas constant [for air R = 1716 ft-lb/(slug-°R)]
Re	Reynolds number = $\frac{\rho V l}{\mu}$
$(Re)_c$	Critical Reynolds number where flow transitions from laminar to turbulent flow
Re_D	Reynolds number based on diameter of wing leading edge bluntness
r	Radius of body (ft)
r_n	Radius of nose tip (ft)
r_w, r_t	Radius of body at wing or tail locations
r/s	Ratio of body radius to wing or tail semispan plus the body radius
s	Distance along body surface in SOSET (also wing or tail semispan plus the body radius in wing-body lift methodology)
SB	Slender-body theory
T	Temperature (°R)
T_{aw}, T_o, T_w	Adiabatic wall, total, and wall temperature, respectively
t/c_r	Tail thickness to its root chord

t/d	Tail thickness to body diameter
V	Velocity (ft/sec)
V_e	Velocity at edge of boundary layer (ft/sec)
V_p	Velocity parallel to leading edge of wing (ft/sec)
x	Distance along the axis of symmetry measured positive aft of nose tip (feet or calibers)
x/c	Parameter used in base drag methodology to represent the number of chord lengths from the base (measured positive upstream of base)
x_{cp}	Center of pressure (in feet or calibers from some reference point that can be specified)
x_L, x_T	Laminar and turbulent flow lengths on body (ft)
Z	Compressibility factor
α	Angle of attack (degrees)
α_c	Angle of attack where wing-body interference factor starts decreasing from its slender-body theory value (degrees)
α_D	Angle of attack where the wing-body interference factor reaches a minimum (degrees)
α_W, α_T	Local angle of attack of wing or tail ($\alpha + \delta_W$ or $\alpha + \delta_T$, respectively, in degrees)
δ	Control deflection degrees
δ_{eq}	Angle between a tangent to the body surface at a given point and the velocity vector (degrees)
δ_W, δ_T	Deflection of wing or tail surfaces (degrees), positive leading edge up
ϕ	Circumferential position around body where $\phi = 0$ is leeward plane (degrees)
λ	Taper ratio of a lifting surface $= c_t/c_r$

η	Parameter used in SOSET and also used in viscous crossflow theory for nonlinear body normal force (in this context, it is the normal force of a circular cylinder of given length-to-diameter ratio to that of a cylinder of infinite length)
η_o	Value of η in viscous crossflow theory for $M_N = 0$
μ_o, μ^*	Viscosity coefficient at stagnation or reference conditions, respectively (slug/ft-sec)
ρ, ρ_o, ρ^*	Density of air at local, stagnation, or reference conditions, respectively (slugs/ft^3)
γ	Specific heat ratio
θ	Local body slope at a given point (degrees)
Λ	Leading edge sweep angle of wing or tail (degrees)
∞	Free-stream conditions
2-D	Two dimensional
3-D	Three dimensional
3DTWT	3-D thin wing theory
AP81	Aeroprediction 1981
AP93	Aeroprediction 1993
APC	Aeroprediction code
GSET	Generalized shock-expansion theory
IMNT	Improved modified Newtonian theory
MNT	Modified Newtonian theory
NASA/LRC	National Aeronautics and Space Administration/Langley Research Center
NSWCDD	Naval Surface Warfare Center, Dahlgren Division
SE	Shock expansion
SOSET	Second-order shock-expansion theory
SOTA	State of the art

DISTRIBUTION

	Copies
ATTN CODE 21 (ZIMET)	1
CODE 213 (SIEGEL)	1
OFFICE OF NAVAL RESEARCH	
800 N QUINCY ST BCT #1	
ARLINGTON VA 22217-5000	
ATTN CODE 1132F (LEKOUDIS)	1
CODE 12 (WOOD)	1
CODE 121 (HANSEN)	1
CODE 1215 (FEIN)	1
CHIEF OF NAVAL RESEARCH	
BALLSTON TOWER 1	
800 N QUINCY ST BCT #1	
ARLINGTON VA 22217-5660	
ATTN CODE C2771 (SMITH)	1
CODE C2891 (PORTER)	1
CODE C2892 (STRUTZ)	1
CODE C2892 (HALTER)	1
CODE C2892 (GLEASON)	1
CODE C2894 (VAN DYKEN)	1
CODE C29B10	1
TECHNICAL LIBRARY	1
COMMANDER	
NAVAL AIR WARFARE CENTER	
WEAPONS DIVISION	
CHINA LAKE CA 93555-6001	
ATTN TECHNICAL LIBRARY	1
COMMANDER	
NAVAL SEA SYSTEMS COMMAND	
2531 NATIONAL CENTER BLDG 3	
WASHINGTON DC 20362-5160	
ATTN AIR 53012D (JOHNSON)	1
RM 904 JP2	
TECHNICAL LIBRARY	1
COMMANDER	
NAVAL AIR SYSTEMS COMMAND	
1421 JEFFERSON PLAZA BLDG 2	
WASHINGTON DC 20361-5120	

	Copies
ATTN C KLEIN	1
TECHNICAL LIBRARY	1
COMMANDER	
NAVAL AIR WARFARE CENTER	
WEAPONS DIVISION	
POINT MUGU CA 93042-5000	
ATTN T C TAI	1
M J MALIA	1
TECHNICAL LIBRARY	1
COMMANDER	
NAVAL SHIP RESEARCH AND	
DEVELOPMENT CENTER	
WASHINGTON DC 20034	
ATTN R M HOWARD	1
TECHNICAL LIBRARY	1
SUPERINTENDENT	
US NAVAL POSTGRADUATE SCHOOL	
MONTEREY CA 93943-5000	
ATTN S GREENHALGH	1
C REITZ	1
TECHNICAL LIBRARY	1
COMMANDING OFFICER	
NAVAL AIR WARFARE CENTER	
AIRCRAFT DIVISION WARMINSTER	
WARMINSTER PA 18974-5000	
ATTN HEAD WEAPONS DEPT	1
HEAD SCIENCE DEPT	1
SUPERINTENDENT	
US NAVAL ACADEMY	
ANNAPOLIS MD 21402	
ATTN M KRUMINS	1
TECHNICAL LIBRARY	1
OFFICER IN CHARGE	
NAVAL INTELLIGENCE SUPPORT CENTER	
4301 SUITLAND RD	
WASHINGTON DC 20390	

DISTRIBUTION (CONTINUED)

	Copies
ATTN CODE 30 (CHILDERS) CHIEF OF NAVAL RESEARCH NAVY SDI 2211 JEFFERSON DAVIS HWY RM 810 CP5 ALEXANDRIA VA 22217	1
ATTN DIAG DT 4T (PAUL MURAD) DEFENSE INTELLIGENCE AGENCY WASHINGTON DC 20546	2
ATTN CODE 50255 (WAGGONER) COMMANDER CRANE DIVISION NAVAL SURFACE WARFARE CENTER CRANE IN 47522-5000	1
ATTN CODE 5252P (KRAUSE) TECHNICAL LIRRARY COMMANDER INDIAN HEAD DIVISION NAVAL SURFACE WARFARE CENTER INDIAN HEAD MD 20640-5000	1 1
ATTN TECHNICAL LIBRARY COMMANDING GENERAL MARINE CORPS COMBAT DEVELOPMENT COMMAND QUANTICO VA 22134-5000	1
ATTN M TAUBER TECHNICAL LIBRARY AFATL (ADLRA) (DLGC) EGLIN AFB FL 32542-5000	1 1
ATTN K COBB E SEARS L E LIJEWSKI C COTTRELL TECHNICAL LIBRARY EGLIN AIR FORCE BASE FL 32542	1 1 1 1 1
ATTN TECHNICAL LIBRARY USAF ACADEMY COLORADO SPRINGS CO 80912	1
ATTN TECHNICAL LIBRARY NASA WASHINGTON DC 20546	1
ATTN G KURYLOWICH D SHEREDA J JENKINS R SAMUELS TECHNICAL LIBRARY COMMANDING OFFICER AFSC WRIGHT PATTERSON AFB OH 45433	1 1 1 1 1
ATTN TECHNICAL LIBRARY ADVANCED RESEARCH PROJECTS AGENCY DEPARTMENT OF DEFENSE WASHINGTON DC 20305	1
ATTN J USSELTON W B BAKER JR TECHNICAL LIBRARY ARNOLD ENGINEERING DEVELOPMENT CENTER USAF TULLAHOMA TN 37389	1 1 1
ATTN M TAUBER TECHNICAL LIBRARY NASA AMES RESEARCH CENTER MOFFETT CA 94035-1099	1 1
ATTN C SCOTT D CURRY NASA JOHNSON SPACE CENTER HOUSTON TX 77058	1 1
ATTN W C SAWYER B HENDERSON D MILLER J ALLEN F WILCOX TECHNICAL LIBRARY NASA LANGLEY RESEARCH CENTER HAMPTON VA 23365	1 1 1 1 1 2
ATTN BILL WALKER DAVE WASHINGTON COMMANDING GENERAL AMSI RD SI AT REDSTONE ARSENAL AL 35898	1 1

DISTRIBUTION (CONTINUED)

	Copies
ATTN H HUDGINS	1
G FRIEDMAN	1
TECHNICAL LIBRARY	1
COMMANDING GENERAL	
ARRADCOM	
PICATINNY ARSENAL	
DOVER NJ 07801	
ATTN C H MURPHY	1
R M MCCOY	1
W STUREK	1
C NIETUBICZ	1
A MIKHAIL	1
P PLOSTINS	1
TECHNICAL LIBRARY	1
COMMANDING GENERAL	
BALLISTIC RESEARCH LABORATORY	
ABERDEEN PROVING GROUND	
MD 21005	
ATTN CODE TNC (BLACKLEDGE)	1
CDR AL KOREJO	1
DIRECTOR	
INTERCEPTOR TECHNOLOGY	
STRATEGIC DEFENSE INITIATIVE	
THE PENTAGON	
WASHINGTON DC 20350	
ATTN SFAE SD ASP	1
SFAE SD HED	1
DEPUTY COMMANDER	
US ARMY STRATEGIC DEFENSE COMMAND	
PO BOX 1500	
HUNTSVILLE AL 35807-3801	
ATTN PROF J A SCHETZ	1
VIRGINIA POLYTECHNIC AND	
STATE UNIVERSITY	
DEPT OF AEROSPACE ENGINEERING	
BLACKSBURG VA 24060	
ATTN F R DEJARNETTE	1
NORTH CAROLINA STATE UNIVERSITY	
DEPT OF MECHANICAL AND	
AEROSPACE ENGINEERING	
BOX 7921	
RALEIGH NC 27695	

	Copies
ATTN J M WU	1
C BALASUBRAMAYAN	1
TECHNICAL LIBRARY	1
THE UNIVERSITY OF TENNESSEE	
SPACE INSTITUTE	
TULLAHOMA TN 37388	
ATTN R NELSON	1
TECHNICAL LIBRARY	1
UNIVERSITY OF NOTRE DAME	
DEPT OF AEROSPACE AND	
MECHANICAL ENGINEERING	
BOX 537	
NOTRE DAME IN 46556	
ATTN E LUCERO	1
L TISSERAND	1
D FROSTBUTTER	1
TECHNICAL LIBRARY	1
APPLIED PHYSICS LABORATORY	
JOHNS HOPKINS UNIVERSITY	
JOHNS HOPKINS RD	
LAUREL MD 20723-6099	
ATTN D G MILLER	1
TECHNICAL LIBRARY	1
LAWRENCE LIVERMORE NATIONAL LABORATORY	
EARTH SCIENCES DIVISION	
UNIVERSITY OF CALIFORNIA	
PO BOX 808	
LIVERMORE CA 94550	
ATTN F PRILLMAN	1
W B BROOKS	1
R STANCIL	1
VOUGHT CORPORATION	
PO BOX 5907	
DALLAS TX 75222	
ATTN TECHNICAL LIBRARY	1
HUGHES AIRCRAFT COMPANY	
MISSILE SYSTEMS SECTOR	
PO BOX 7928	
CANOGA PARK CA 91304-7928	

DISTRIBUTION (CONTINUED)

	Copies
ATTN WALTER RUTLEDGE (1635)	1
R LAFARGE	1
R EISLER	1
TECHNICAL LIBRARY	1
SANDIA NATIONAL LABORATORY	
PO BOX 5800	
ALBUQUERQUE NM 87185-5800	
ATTN TECHNICAL LIBRARY	1
MARTIN MARIETTA AEROSPACE	
PO BOX 5837	
ORLANDO FL 32805	
ATTN B OMILIAN	1
CAL SPAN ADVANCED	
TECHNOLOGY CENTER	
PO BOX 400	
BUFFALO NY 14225	
ATTN R CAVAGE	1
ADVANCED SYSTEMS DESIGN	
DEPT 113 407 (GB14)	
ROCKWELL	
NORTH AMERICAN AIRCRAFT	
OPERATIONS	
PO BOX 92098	
LOS ANGELES CA 90009	
ATTN G H RAPP	1
MOTOROLA INC	
MISSILE SYSTEMS OPERATIONS	
8201 E McDOWELL RD	
PO BOX 1417	
SCOTTSDALE AZ 85252	
ATTN R WYRICK	1
BOEING COMPUTER SERVICES INC	
PO BOX 24346	
SEATTLE WA 98124	
ATTN WAYNE CHRISTENSON	1
DWIGHT WARNER	1
MN 11 2920	
ALLIANT TECHSYSTEMS INC	
600 SECOND ST NE	
HOPKINS MN 55343	

	Copies
ATTN J XERIKOS	1
N CAMPBELL	1
TECHNICAL LIBRARY	1
MCDONNELL DOUGLAS ASTRONAUTICS	
CO (WEST)	
5301 BOLSA AVE	
HUNTINGTON BEACH CA 92647	
ATTN M DILLENIUS	1
NIELSEN ENGINEERING AND	
RESEARCH INC	
510 CLYDE AVE	
MOUNTAIN VIEW CA 95043	
ATTN J WILLIAMS	1
S VUKELICH	1
J FIVEL	1
R GERBSCH (CODE 1111041)	1
TECHNICAL LIBRARY	1
MCDONNELL DOUGLAS ASTRONAUTICS	
CO (EAST)	
BOX 516	
ST LOUIS MO 63166-0516	
ATTN DR M FINK	1
UNITED TECHNOLOGIES	
NORDEN SYSTEMS	
MAIL STOP K041	
NORWALK CT 06856	
ATTN T LUNDY	1
D ANDREWS	1
TECHNICAL LIBRARY	1
LOCKHEED MISSILES AND SPACE	
CO INC	
PO BOX 1103	
HUNTSVILLE AL 35807	
ATTN L E ERICSSON	1
P REDING	1
G CHRUSCIEL	1
TECHNICAL LIBRARY	1
LOCKHEED MISSILES AND SPACE	
CO INC	
PO BOX 504	
SUNNYVALE CA 94086	

DISTRIBUTION (CONTINUED)

	Copies
ATTN M WAREHAM RAYTHEON MISSILE SYSTEMS 50 APPLE HILL DR STOP T2SA9 TEWKSBURY MA 01876-0901	1
ATTN LLOYD PRATT AEROJET TACTICAL SYSTEMS CO PO BOX 13400 SACRAMENTO CA 95813	1
ATTN KURT HIVELY GENERAL DYNAMICS CONVAIR PO BOX 85357 SAN DIEGO CA 92138	1
ATTN SAM BLACK GOODYEAR AEROSPACE CORP 1210 MASSILLON RD AKRON OH 44315	1
ATTN W NORDGREN 721 GOULD INC OSD 18901 EUCLID AVE CLEVELAND OH 44117	1
ATTN DR Y C SHEN AEROJET ELECTRO SYSTEMS CO PO BOX 296 III AZUSA CA 91702	1
ATTN PETROS KYPRIOS TEXAS INSTRUMENTS INC PO BOX 405 MAIL STOP 3408 LOUISVILLE TX 75067	1
ATTN GERMAN MILITARY REP US OA GMR TRAFFIC AND TRANSPORTATION DIVISION 10 SERVICE RD DULLES INTERNATIONAL AP WASHINGTON DC 20041	1
ATTN DORIA GLADSTONE BATTELLE MEMORIAL INSTITUTE COLUMBUS DIVISION 505 KING AVE COLUMBUS OH 43201-2693	1
ATTN DR T P SHIVANANDA TRW ONE SPACE PARK REDONDO BEACH CA 90278	1
ATTN K C LEE ACCUREX CORP PO BOX 7040 520 CLYDE AVE MOUNTAIN VIEW CA 94039	1
ATTN A CHABOKI FMC CORPORATION 1300 S SECOND ST PO BOX 59043 MINNEAPOLIS MN 55459-0043	1
ATTN L FRENCH TRACOR AEROSPACE AUSTIN INC 6500 TRACO LANE AUSTIN TX 87825	1
ATTN ASO LO IS ISRAEL AIR FORCE LIAISON OFFICER 700 ROBBINS AVE PHILADELPHIA PA 19111	1
ATTN W J CLARK DYNA EAST CORPORATION 3132 MARKET ST PHILADELPHIA PA 19104	1
ATTN D SCHMITZ CHAMBERLAIN MANUFACTURING CORP R AND D DIVISION PO BOX 2545 WATERLOO IA 50704-2545	1
ATTN BRIAN WALKUP HERCULES AEROSPACE PRODUCT CO ALLEGHANY BALLISTIC LAB ROCKET CENTER WV 26726	1

DISTRIBUTION (CONTINUED)

	Copies
ATTN ASSISTANT DEFENSE COOPERATION ATTACHE EMBASSY OF SPAIN WASHINGTON DC 20016	1
ATTN J FORKOIS KAMAN SCIENCES CORP 1500 GARDEN OF THE GODS RD PO BOX 7463 COLORADO SPRINGS CO 80933	1
ATTN M R D ANGELO MIT LINCOLN LABORATORY LEXINTON NA 02173-0073	1
ATTN M S MILLER DYNETICS INC PO DRAWER B HUNTSVILLE AL 35814-5050	1
ATTN H A MCELROY GENERAL DEFENSE CORP PO BOX 127 RED LION PA 17356	1
ATTN R SEPLAK BRUNSWICK CORP DEFENSE DIVISION 3333 HARBOR BLVD COSTA MESA CA 92628-2009	1
ATTN J W MCDONALD GENERAL RESEARCH CORP ADVANCED TECHNOLOGY INC 5383 HOLLISTER AVE PO BOX 6770 SANTA BARBARA CA 93160-6770	1
ATTN CAROL BUTLER OTI INTERNATIONAL 60 2ND ST SUITE 301 PO BOX 37 SHALIMAR FL 32579	1
ATTN ARMAMENT SYSTEMS DEPT GENERAL ELECTRIC CO BURLINGTON VT 05401	1
ATTN DR T LIN TRW ELECTRONICS AND DEFENSE SECTOR BLDG 527/RM 706 PO BOX 1310 SAN BERNADINO CA 92402	1
ATTN B S PRATS AIRTHERMOPHYSICS GENERAL ELECTRIC CO 3198 CHESTNUT ST PHILADELPHIA PA 19104	1
ATTN G VINCENT SPARTA INC 4301 CORPORATE DR HUNTSVILLE AL 35805	1
ATTN D P FORSMO TECHNICAL LIBRARY RAYTHEON COMPANY MISSILE SYSTEMS DIVISION HARTWELL RD BEDFORD MA 01730	1 1
ATTN S PEARLSING P GIRAGOSIAN RAYTHEON COMPANY SPENCER LABORATORY BOX SL7162 BURLINGTON MA 01803	1 1
ATTN NEILL S SMITH ARAP 1950 OLD GALLOWS RD SUITE 302 VIENNA VA 22180	1
ATTN DR SHIVANANDA TRW BMD PO BOX 1310 SAN BERNADINO CA 92402-1313	1
ATTN T R PEPITONE AEROSPACE TECHNOLOGY INC PO BOX 1809 DAHLGREN VA 22448	1

DISTRIBUTION (CONTINUED)

	Copies
ATTN WILLIAM FACINELLI ALLIED SIGNAL PO BOX 22200 MS 1230 21E TEMPE AZ 85285	1
ATTN ERIC MOORE LOCKHEED SANDERS MAILSTOP MER 24-1281 PO BOX 868 NASHUA, NH 03061	1
ATTN CDR R TEMPEST BRITISH NAVY STAFF WASHINGTON DC 20008	1
ATTN J EVANS DREV PO BOX 8800 COURCELETTE PQ CANADA GOA 1RO	1
ATTN DENNIS BROWN NATIONAL AERONAUTICAL ESTAB NATIONAL RESEARCH COUNCIL MONTREAL RD OTTAWA ON CANADA K1A0R6	1
ATTN H G KNOCHE DR GREGORIOU MESSERSCHMIDT BOLKOW BLOHM GMBH UNTERNEHMENSBEREICH APPARATE MUNCHEN 80 POSTFACH 801149 BAYERN FED REP OF GERMANY (DFR)	1 1
ATTN DR DONALD SPRING AEROSPACE ENGINEERING DEPT AUBURN UNIVERSITY AL 36849-5338	1
ATTN BOB WHYTE ARROW TECH ASSOCIATES INC 1233 SHELBURNE RD D8 SO BURLINGTON VT 05403	1
ATTN FU HO LING 1300 30TH ST APT E2 31 BOULDER CO 80303	1
ATTN PROF H F NELSON DEPT OF MECH AND AERO ENG UNIVERSITY OF MISSOURI ROLLA ROLLA MO 65401	1
DEFENSE TECHNICAL INFORMATION CENTER CAMERON STATION ALEXANDRIA VA 22304-6145	12
ATTN GIFT AND EXCHANGE DIVISION LIBRARY OF CONGRESS WASHINGTON DC 20540	4
GIDEP OPERATIONS OFFICE CORONA CA 91720	1
DEFENSE PRINTING SERVICE WASHINGTON NAVY YARD WASHINGTON DC 20374	1
ATTN ROBERT ENGLAR GEORGIA TECH RESEARCH INSTITUTE AEROSPACE SCIENCE AND TECHNOLOGY LAB ATLANTA GA 30332	1
ATTN JUAN AMENABAR SAIC 1700 N MOORE ST STE 1820 ARLINGTON VA 22209	1
INTERNAL DISTRIBUTION	
C	1
D	1
D1	1
D2	1
D4	1
A	1
B	1
B51 (ARMISTEAD)	1
E	1
E231	3
E232	2
E281 (GARNER)	1
F	1
G	1
G02	1

DISTRIBUTION (CONTINUED)

	Copies
G04	10
G05	1
G06	1
G07	1
G20	1
G205	1
G23	1
G23 (CHADWICK)	1
G23 (DEVAN)	1
G23 (GRAFF)	1
G23 (HARDY)	1
G23 (HYMER)	1
G23 (McINVILLE)	1
G23 (ROWLES)	1
G23 (WEISEL)	1
G30	1
G40	1
G50	1
G60	1
G80	1
G90	1
GHO	1
GH3	1
K	1
K10	1
K20	1
K204	1
N	1
N74 (GIDEP)	1
R	1
R44	1
R44 (PRIOLO)	1
R44 (HSIEH)	1
R44 (WARDLAW)	1

REPORT DOCUMENTATION PAGE

Form Approved
OMB No 0704-0188

1. AGENCY USE ONLY (Leave blank)	2. REPORT DATE	3. REPORT TYPE AND DATES COVERED
	May 1993	

4. TITLE AND SUBTITLE
Improved Aeroprediction Code: Part I-Summary of New Methods and Comparison with Experiment

5. FUNDING NUMBERS

6. AUTHOR(S)
Frank G. Moore, Tom Hymer, and Roy McInville

7. PERFORMING ORGANIZATION NAME(S) AND ADDRESS(ES)
Naval Surface Warfare Center
Dahlgren Division (Code G04)
Dahlgren, VA 22448-5000

8. PERFORMING ORGANIZATION REPORT NUMBER
NSWCDD/TR-93/91

9. SPONSORING/MONITORING AGENCY NAME(S) AND

10. SPONSORING/MONITORING AGENCY REPORT NUMBER

11. SUPPLEMENTARY NOTES

12a. DISTRIBUTION/AVAILABILITY
Approved for public release; distribution is unlimited.

12b. DISTRIBUTION CODE

13. ABSTRACT *(Maximum 200 words)*

A new and improved version of the Naval Surface Warfare Center, Dahlgren Division aeroprediction code (AP93) has been developed. The new code contains new technology that allows planar aerodynamics of axisymmetric solid rocket-type weapons to be computed accurately over the entire Mach number range and for angles of attack to 30 deg. New technology developed and included in the AP93 includes a new engineering method to compute aeroheating information at a high Mach number; extension of the second-order shock-expansion theory to include real-gas effects, including several new pressure prediction techniques; an improved body-alone nonlinear normal-force method; new methods for computing nonlinear wing alone, wing body, and body wing due to angle of attack, and wing body due to control deflection aerodynamics; and a new base-drag database and improved empirical base-drag estimation technique.

Comparison of the AP93 code to the former aeroprediction code (AP81) and experimental data on many configurations and test conditions showed the following: the AP93 code reduces the normal-force and center-of-pressure errors of the AP81 code considerably for most configurations; the AP93 code is more robust in terms of accuracy over a broad range of Mach numbers, angles of attack, and configuration geometries; the AP93 code gave slightly improved axial-force coefficients; computational time and ease of use were about the same.

Comparison of the AP93 code to available computations of other state-of-the-art codes shows the AP93 to be as good or superior to these codes for planar aerodynamics. The new code and associated technology will be available for transition to legitimate requesting users by September 1993 at no charge to the user.

14. SUBJECT TERMS	15. NUMBER OF PAGES
aeroprediction code (AP93), planar aerodynamics, high Mach number	159
	16. PRICE CODE

17. SECURITY CLASSIFICATION OF REPORT	18. SECURITY CLASSIFICATION OF THIS PAGE	19. SECURITY CLASSIFICATION OF ABSTRACT	20. LIMITATION OF ABSTRACT
UNCLASSIFIED	UNCLASSIFIED	UNCLASSIFIED	UL

GENERAL INSTRUCTIONS FOR COMPLETING SF 298

The Report Documentation Page (RDP) is used in announcing and cataloging reports. It is important that this information be consistent with the rest of the report, particularly the cover and its title page. Instructions for filling in each block of the form follow. It is important to ***stay within the lines*** to meet ***optical scanning requirements***.

Block 1. Agency Use Only *(Leave blank)*.

Block 2. Report Date. Full publication date including day, month, and year, if available (e.g. 1 Jan 88). Must cite at least the year.

Block 3. Type of Report and Dates Covered. State whether report is interim, final, etc. If applicable, enter inclusive report dates (e.g. 10 Jun 87 - 30 Jun 88).

Block 4. Title and Subtitle. A title is taken from the part of the report that provides the most meaningful and complete information. When a report is prepared in more than one volume, repeat the primary title, add volume number, and include subtitle for the specific volume. On classified documents enter the title classification in parentheses.

Block 5. Funding Numbers. To include contract and grant numbers; may include program element number(s), project number(s), task number(s), and work unit number(s). Use the following labels:

C	- Contract	**PR**	- Project
G	- Grant	**TA**	- Task
PE	- Program Element	**WU**	- Work Unit Accession No.

BLOCK 6. Author(s). Name(s) of person(s) responsible for writing the report, performing the research, or credited with the content of the report. If editor or compiler, this should follow the name(s).

Block 7. Performing Organization Name(s) and address(es). Self-explanatory.

Block 8. Performing Organization Report Number. Enter the unique alphanumeric report number(s) assigned by the organization performing the report.

Block 9. Sponsoring/Monitoring Agency Name(s) and Address(es). Self-explanatory.

Block 10. Sponsoring/Monitoring Agency Report Number. *(If Known)*

Block 11. Supplementary Notes. Enter information not included elsewhere such as: Prepared in cooperation with...; Trans. of...; To be published in.... When a report is revised, include a statement whether the new report supersedes or supplements the older report.

Block 12a. Distribution/Availability Statement. Denotes public availability or limitations. Cite any availability to the public. Enter additional limitations or special markings in all capitals (e.g. NOFORN, REL, ITAR).

DOD	- See DoDD 5230.24, "Distribution Statements on Technical Documents."
DOE	- See authorities.
NASA	- See Handbook NHB 2200.2
NTIS	- Leave blank

Block 12b. Distribution Code.

DOD	- Leave blank.
DOE	- Enter DOE distribution categories from the Standard Distribution for Unclassified Scientific and Technical Reports.
NASA	- Leave blank.
NTIS	- Leave blank.

Block 13. Abstract. Include a brief ***(Maximum 200 words)*** factual summary of the most significant information contained in the report.

Block 14. Subject Terms. Keywords or phrases identifying major subjects in the report.

Block 15. Number of Pages. Enter the total number of pages.

Block 16. Price Code. Enter appropriate price code ***(NTIS only)***

Block 17.-19. Security Classifications. Self-explanatory. Enter U.S. Security Classification in accordance with U.S. Security Regulations (i.e., UNCLASSIFIED). If form contains classified information, stamp classification on the top and bottom of this page.

Block 20. Limitation of Abstract. This block must be completed to assign a limitation to the abstract. Enter either UL (unlimited or SAR (same as report). An entry in this block is necessary if the abstract is to be limited. If blank, the abstract is assumed to be unlimited.